The Synthesis of Dendrimer and Their Application for Drug Delivery and as Haemoglobin Model for Artificial Blood

Khaled Tahir Elhmiadi

A dissertation submitted in partial fulfilment of the requirements for the degree of

Doctor of Philosophy

Supervisor: Dr: Lance J Twyman

April 2024

Department of Chemistry

The University of Sheffield

Sheffield, S3 7HF

England

Acknowledgements

I am grateful to Dr. Lance Twyman for his exceptional support and guidance throughout my research and writing process. His supervision was instrumental to my PhD study.

It is essential to admit the invaluable support and friendship provided by my colleagues within our research group, Special thanks and appreciation go to Dr Reyad, Dr Abdulfatah, Dr Abdullah, Dr Enas, Abdullatif, Nayef, and Chen for their friendship and encouragement. I am grateful to Amal, Leema, Manar, Ohoud, and Nada, who have supported me during this journey.

With a heavy heart, I wish my father could have been here to witness this moment; his absence is deeply felt. I send all my love to my mother, brothers, and little sister for their endless support and strength throughout this journey.

Finally, I must express my reflective gratitude to my wife. Thank you for your unwavering love and support. I deeply appreciate the great patience you have shown during the most challenging times.

Abstract

Dendrimers are a class of highly branched, tree-like macromolecules that have garnered significant interest due to their unique structure and potential applications in various scientific fields. This section overviews dendrimers, their synthesis, properties, and applications. Dendrimers are characterised by a central core, from which dendritic branches radiate outwards in successive layers or generations, leading to a spherical structure. The terminal functionalities on the surface of dendrimers play a crucial role in defining their properties, such as solubility, shape, and viscosity.

The study extends into the creation of artificial blood intended to mimic natural haemoglobin structures using a biomimetic approach involving branched polymers. It focuses on the development of artificial/synthetic blood as a volume expander in emergencies utilizing soluble PAMAM dendritic polymers. The research explores porphyrin core substituents within dendritic polymers with molecular weights between 8k and 9k Da, essential for controlling the polymer's molecular weight. Using ester-amide as the monomer, a water-soluble dendritic polymer system was synthesized. The encapsulation of various porphyrin core variants was achieved using water-soluble PAMAM dendrimers ranging from G 0.5 to G 3.5. This porphyrin-dendrimer approach replaces previous systems, providing a water-tolerant and exceptionally stable alternative for developing artificial blood systems.

The study aimed to investigate the use of hyperbranched polymers HBP as alternatives to dendrimers for drug delivery systems. The study found that HBPs can be used to achieve similar levels of encapsulation and stability as dendrimers but with the advantage of being less expensive and easier to synthesize. The study focused on amido-amine dendrimers and HBPs and found that the second generation of neutral PAMAM dendrimers G2.5 OH was the most effective in encapsulating Ibuprofen and a lead anti-cancer compound F73. However, the study also noted that the dendrimer formed large aggregates at high concentrations, which reduced the amount of drug that could be encapsulated.

The study also found that the zinc-metalated porphyrin could be encapsulated 100% better than the corresponding free base porphyrin due to the strong coordination bond between the zinc porphyrin and the internal amines within the dendrimer. The study

concluded that HBPs and dendrimers with similar functional group connectivity are equally suitable for use as efficient drug delivery systems, and the choice between the two may come down to factors such as cost or therapeutic regulations.

Keywords** Artificial Blood, Porphyrin, PAMAM Dendrimer, Dendrons, Hyperbranched Polymer, Liposomes, Drug Delivery.

Abbreviations

1. *^{13}C NMR** – Carbon Nuclear Magnetic Resonance Spectrometry

2. **^{1}H NMR** – Proton Nuclear Magnetic Resonance Spectrometry

3. **CMC** – Critical Micelle Concentration

4. **D** – Doublet

5. **DA** – Dalton

6. **DD** – Doublet of doublets

7. **DCM** – Dichloromethane

8. **DLS** – Dynamic Light Scattering

9. **DMF** – Dimethylformamide

10. **D6-DMSO** – Deuterated Dimethyl Sulphoxide

11. **EDA** – Ethylene Diamine

12. **Ɛ** – Extinction Coefficient

13. **ES-MS** – Electrospray Ionisation Mass Spectrometry

14. **$FeCl_2$** – Iron II Chloride

15. **FT-IR** – Fourier Transform Infrared Spectrophotometry

16. **G** – Generation

17. **GPC** – Gel Permeation Chromatography

18. **HBP** – Hyperbranched Polymer

19. **HBPAMAM** – Hyperbranched PAMAM

20. **MA** – Methyl Acrylate

21. **M** – Multiplet

22. **Mn** – Number Average Molecular Weight

23. **MW** – Molecular Weight

24. **Mw** – Weight Average Molecular Weight

25. **NMR Abbreviations**

26. **O** – Ortho

27. **OH** – Hydroxyl

28. **P** – Para

29. **PDT** – Photo Dynamic Therapy

30. **PD** – Polydispersity

31. **Q** – Quartet

32. **S** – Singlet

33. **T** – Triplet

34. **THF** – Tetrahydrofuran

35. **THPP** – Tetrakis 3.5 di hydroxy phenyl porphyrin

36. **TMPP** – Tetrakis 3,5 methoxyphenyl porphyrin

37. **TPP** – Tetra phenyl porphyrin

38. **TRIS** – Tris hydroxymethyl amino methane

39. **UV/Vis** – Ultraviolet-Visible Light Spectrophotometry

40. **ZnTHPP** – Zinc tetra hydroxy phenyl porphyrin

Contents

Chapter 1

1 Introduction

1.1 Dendrimers.

Dendrimers, a subset of dendritic polymers, represent a unique class of highly branched, tree-like macromolecules. The term 'dendrimer' derives from the Greek words 'dendri' tree-like and 'meros' part. This nomenclature reflects their branched, tree-like structure. Dendrimers were first introduced and discussed by Tomalia et al., with Polyamidoamines PAMAM dendrimers being among the earliest examples [1].

The structure of a dendrimer is defined by its dendritic branches, which radiate out from a central core. As each new 'generation' of branches is added, the dendrimer grows in complexity, leading to an increase in the width of its internal globular structure[2]. The size of dendrimers typically ranges from 1 to 10 nanometres, placing them firmly in the nanoscale domain[3]. This nanosized is critical to their functionality, as it provides a high surface-area-to-volume ratio, which is ideal for interactions at the molecular and cellular level[4]. The nanosized also allows dendrimers to easily penetrate biological membranes, making them particularly effective in biomedical applications such as targeted drug delivery and gene therapy[5].

Another critical aspect of dendrimers is their terminal functionalities, which are located on the surface of the macromolecule. These terminal groups play a significant role in defining the properties of the dendrimer, such as its solubility, shape, stability, flexibility, and viscosity [5,6]. The nature and type of these terminal groups can be varied, allowing for a wide range of possible polymeric properties.

Dendrons, another key component, are the individual branched structures that link the dendritic segments to the core. The design and synthesis of dendrimers, including the determination of their molecular weight, involve precise control over the addition of

each generation of dendrons, ensuring the development of a well-defined and structured macromolecule[7]. In material science, dendrimers play a pivotal role in developing advanced coatings and functionalized surfaces. Their nanoscale structure enables the creation of materials with unique properties, such as hydrophobicity, anti-corrosive properties, or electrical conductivity[8]. Dendrimers are also used to fabricate nanocomposites and nanofibers, which find applications in electronics, optics, and catalysis. For instance, dendrimer-based nanocomposites can enhance the performance of light-emitting diodes (LEDs) or serve as efficient catalysts in chemical reactions[9].

In environmental science, the unique architecture of dendrimers lends itself to applications in pollutant removal and water treatment[10]. Their high density of surface functional groups allows them to chelate heavy metals, such as lead or mercury, and bind with organic pollutants, such as dyes or pesticides[11]. These interactions facilitate the efficient removal of contaminants from water sources, contributing to environmental remediation efforts. Additionally, dendrimers are explored for use in sensors that detect pollutants at trace levels, further underscoring their utility in sustainable technologies[12].

Dendrimer synthesis typically follows a hierarchical assembly process, beginning with a core molecule that forms the foundation. Monomers, the basic building blocks, are added repetitively to this core, creating successive layers or generations that increase the dendrimer's size and complexity [13]. The process involves coupling reactions to attach these monomers, followed by de-protection steps to prepare for subsequent layers[14]. The synthesis culminates with the addition of terminal groups to the outermost layer, which can be tailored to impart specific properties such as solubility, reactivity, or molecular binding capabilities [6]. This precise, step-by-step construction

allows for the creation of dendrimers with highly specific sizes, shapes, and functionalities, making them versatile tools in various scientific fields as shown in Scheme 1.1.

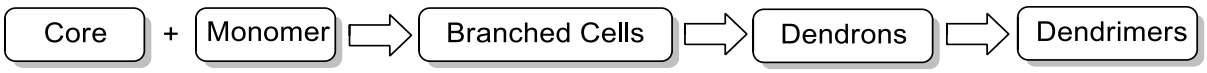

Scheme 1.1 The structure elements of the dendrimer synthases.

1.2 The Synthesis of Dendrimers.

The structure of a dendrimer, as illustrated in Figure 1.1, highlights their main three components: the central core, the end of terminal groups and the repeating branching units[15]. The core serves as the foundational element from which the dendrimer grows. The branching units, added repetitively, extend outward from this core in successive layers or generations, increasing the complexity and size of the dendrimer [13].

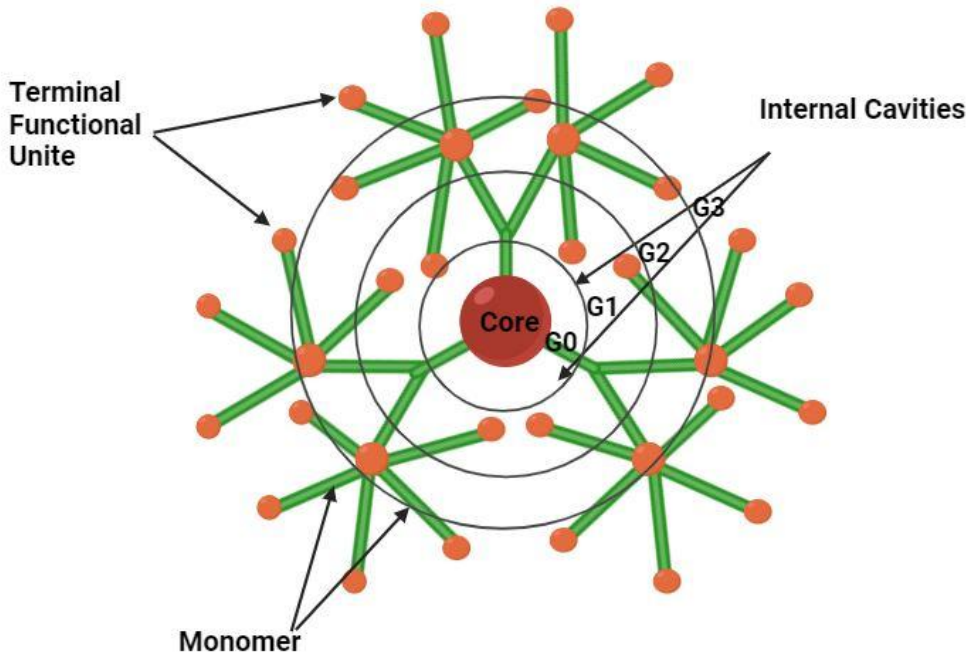

Figure 1.1: The Structure of Dendrimer scaffold: based on components.

The terminal end groups, located on the outermost layer, define the dendrimer's surface properties and functionalities [16]. Dendrimer synthesis, a complex and expansive subject, can be broadly discussed in terms of its synthetic methodologies [17]. These methods are primarily classified into two categories: divergent and convergent approaches.

The choice between these approaches depends on the specific goals and desired characteristics of the dendrimer. The divergent approach starts from the core and builds outward, layer by layer[18].

while the convergent method starts with the synthesis of the end groups and works inwards and towards the core. Each approach offers distinct advantages and challenges, influencing the final structure, size, and functionality of the dendrimer, making dendrimer synthesis a highly versatile and customizable process in materials science and nanotechnology [19].

1.2.1 Divergent Approach.

Previous research, particularly those studies focusing on divergently synthesized dendrimers, has made significant strides in this field[20]. According to Vogtle, one of the earliest reports on dendrimer development demonstrated the successful preparation of dendrimer-like structures, albeit with lower molecular weights compared to typical dendrimers[21]. These early versions of dendrimers, corresponding to the structures shown in Figure 1.2, placed the base for future advancements in dendrimer synthesis [22].

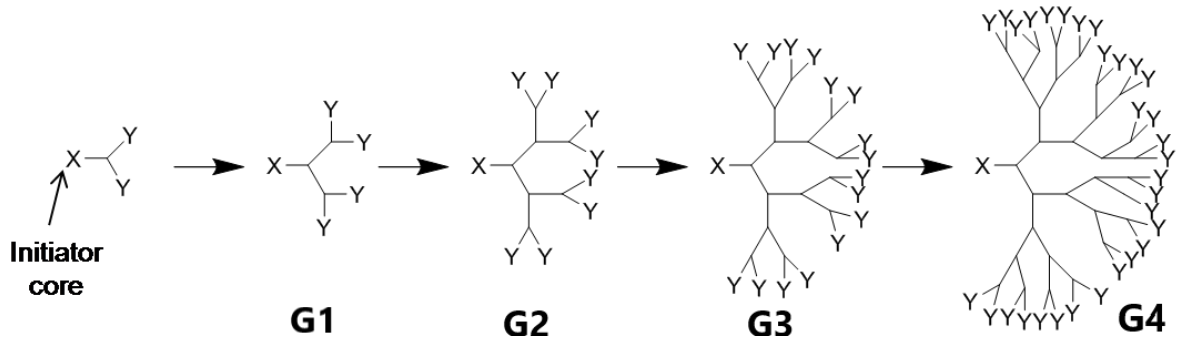

Figure 1.2: The divergent synthesis of Dendrimers.

https://www.researchgate.net/figure/Divergent-synthesis-of-dendrimer_fig1_282829598

In the divergent synthesis methodology, the method is characterized by its step-by-step construction, starting from the core, and expanding outward, making it a fundamental approach in dendrimer synthesis[23]. The process begins with core reactive site C. These sites are specially designed to form dendritic branches F through a series of reactions. Each step involves coupling these core sites with another reactive terminal functionality, as depicted in Figure 1.3, which allows for the controlled growth of the dendrimer, ranching outward from the core [24]. This outward progression of synthesis adds successive layers or generations of branches, expanding the dendrimer's size and complexity with each step. The divergent approach is notable for its ability to create highly branched, well-defined structures, which can be tailored for specific applications in various fields, including drug delivery, catalysis, and materials science[13,25].

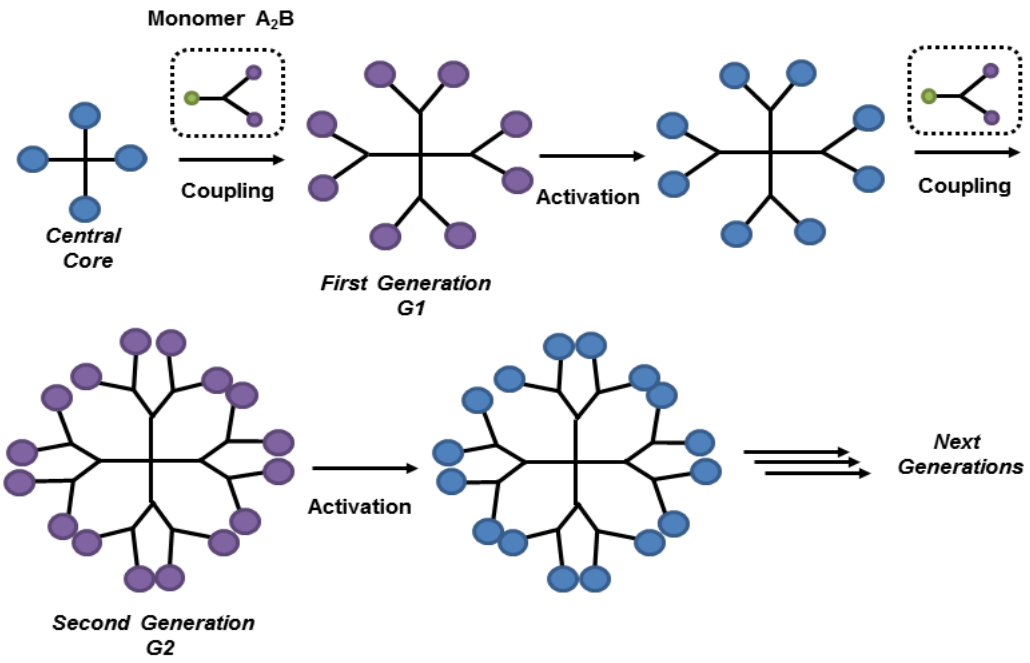

Figure 1.3; The steps processes of divergent synthesis Merging and activation for each dendrimer generation.

https://www.researchgate.net/figure/Divergent-synthesis-of-dendrimer_fig1_282829598

Divergent methods are particularly advantageous for synthesizing macromolecules with high molecular weights, and they allow for the automation of repetitive synthesis steps [26]. This technique has been successfully applied in the creation of POPAM and PAMAM dendrimers. However, one challenge with this approach is achieving complete reactivity with the intended number of terminal functional groups. As the dendrimer grows and each generation becomes exponentially larger, it becomes increasingly difficult to ensure that every terminal group reacts as intended[27]. This can lead to defects in surface functionality, resulting in dendrimers with imperfect structures. Furthermore, the similarity in structure between perfect and imperfect dendrimers makes the purification process challenging, as it is difficult to separate reacted dendrimers from those with incomplete reactions or structural anomalies. This

highlights the delicate balance required in dendrimer synthesis to achieve the desired structural precision and functionality [28].

1.2.2 Convergent Approach.

The convergent approach in dendrimer synthesis, which is essentially the opposite of the divergent approach, begins at the periphery and progresses inward towards the centre[29]. The method, as shown in Figure 1.4, involves synthesizing the outermost parts of the dendrimer first, known as dendrons. These dendrons are the functionalized components of the dendrimer, each equipped with a reactive terminal group. Once synthesized, these dendrons are then methodically connected to a multifunctional core unit [19,26].

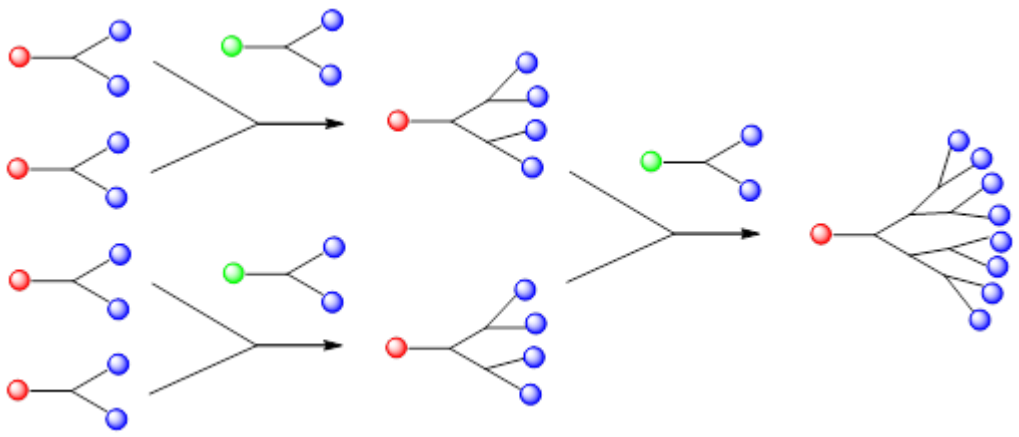

Figure 1.4: The convergent synthesis Diagram for Dendron assembly

This outside-to-inside approach is distinct in that it allows for greater control over the surface chemistry and functionality of the dendrimer. By first constructing the outer layers and then linking them to the core, the convergent method can produce dendrimers with highly specific surface properties[8]. This strategy is particularly beneficial when precise control over the dendrimer's surface characteristics is crucial, such as in targeted drug delivery applications[30]. The convergent method, however,

can be more challenging in terms of synthesizing larger dendrimers, as the synthesis and subsequent coupling of large dendrons to the core can become increasingly complex with each generation [31].

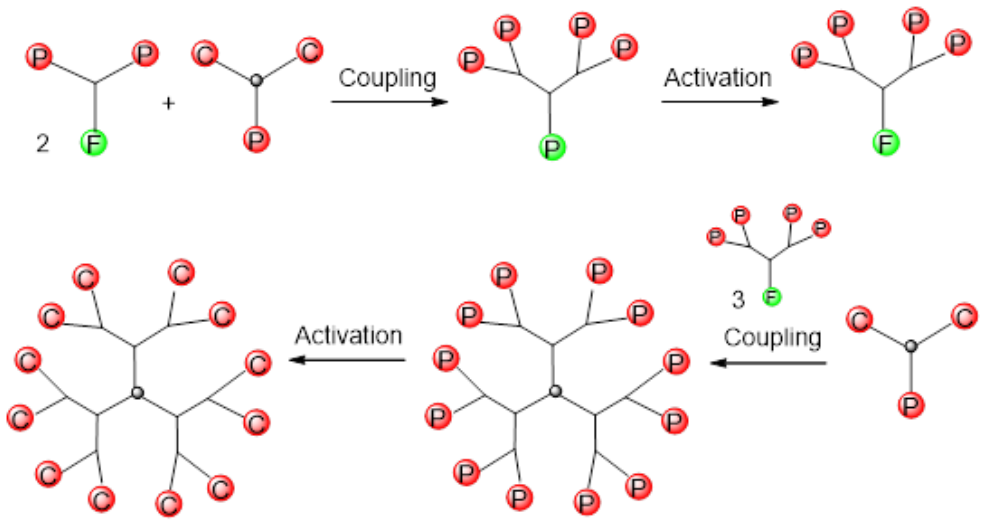

Figure 1.5: A self-assembly system of dendrimers based on convergent dendrons.

In the convergent synthesis of dendrimers, the process begins with the formation of a first-generation dendron[32]. This is achieved by coupling two protected linkage groups P each with an active functional terminal group F, to a branching unit that contains two active coupling sites C and a protected or inactive functional group P [19]. In this arrangement, the two active sites C are linked to one inactive functional unit P. To progress to the next generation, the protected group P of the first-generation dendron is activated, allowing for further coupling and the formation of a higher generation dendron Figure 1.5. This process is repeated with an oligo-functional core to produce dendrimers of higher generations[31,33].

One advantage of the convergent method is the smaller number of reactive terminal groups involved in each reaction step, which increases the likelihood of producing dendrimers with perfect terminal functionalities. This contrasts with the divergent

strategy, where there is a higher risk of defective terminal groups at the dendrimer's surface due to the exponential increase in the number of reactive sites with each generation [34].

Moreover, in the convergent approach, the molar quantities of reactants must be precisely controlled, with no large excess of branching units allowed. This precision is crucial because of the expressive mass variation among the smaller monomer branching units and the considerable dendrons, making it easier to identify any side products that form during the reaction[35]. However, as the dendrimer grows, steric hindrance near the periphery may restrict further growth. This makes the convergent approach more suitable for the synthesis of lower-generation dendrimers, as opposed to those with long-chain, high-generation structures. The method's ability to control the surface chemistry of the dendrimer makes more accurately it an effective strategy for creating specific and well-defined lower-generation dendrimers [28,36].

1.3 Dendrimer Properties.

The development of dendrimers leads to the creation of nanoscale devices that are specifically tailored for various applications. Dendrimers consist of several key architectural components: a core, interior repeating branches units, and terminal functional groups, each playing a distinct role. The shape, size, directionality, and multiplicity of the dendrimer are covalently determined by attaching branching units to the core [37,38].

The type and size of the internal compartment are dictated by the degree of amplification of the interior branching units Table 1.1. With each generation, the density and degree of amplification vary, creating void spaces that can accommodate

guest and host molecules[39]. The bulky, globular structure of dendrimers makes them particularly advantageous for encapsulating molecules such as iron porphyrin, either through non-covalent means or by covalently functionalizing the core linkage [40].

Terminal functional groups are also crucial, serving multiple purposes. Upon activation, these end groups can be used as a platform for further amplification of the branching units, laying the foundation for new generational growth[41,42]. Depending on the dendrimer's generation, its structure can be flexible, semi-flexible, or rigid. As the dendrimer reaches higher generational levels, its exterior surface tends to become more congested and rigid, enhancing its surface functionalities [43]. This allows dendrimers to control the movement of host molecules in or out of their supramolecular structure, making them highly adaptable for various nanoscale applications[44].

The dendrimer’s size, shape, and flexibility are governed by its core, interior branched units, and terminal functional groups[41]. There is a proportional linear relationship between the dendrimer's size and its generational growth. With each new generation, the terminal features increase exponentially, and the level of steric hindrance is dynamically determined at each generational level[20]. Lower-generation dendrimers usually possess a weaker structure, allowing direct contact with solvents within their interior. In contrast, higher-generation dendrimers exhibit better steric hindrance, wider internal compartments, and increased rigidity, influenced by the shape and directionality of the chosen core. This structural complexity and versatility make dendrimers dynamic and adaptable for a wide range of applications [43,45].

1.3.1 Solubility.

Dendrimers, known for their unique branching architecture, exhibit solubility characteristics influenced by several factors including their chemical structure,

generation, pH, and temperature[46]. The nature of terminal groups on these dendrimers determines their affinity for water or organic solvents, with hydrophilic groups enhancing water solubility and hydrophobic groups favouring organic solvents [47]. Higher generation dendrimers, featuring more surface groups, generally show increased solubility, although extremely high generations may lead to reduced solubility due to steric hindrance. Additionally, solubility can be pH-dependent, particularly for dendrimers with ionizable groups, and is also influenced by temperature changes. These solubility properties, coupled with their distinctive structure, render PAMAM dendrimers particularly useful in diverse fields such as drug delivery, catalysis, and nanotechnology[48,49].

1.3.2 Viscosity.

The viscosity of dendrimer solutions, a key aspect in their application across various fields, is influenced by factors such as molecular weight, concentration, temperature, solvent type, and dendrimer architecture. As the generation and hence the molecular weight of a dendrimer increases, the viscosity typically rises due to enhanced molecular interactions and branch entanglement [50]. Concentration plays a crucial role, with higher concentrations leading to increased viscosity because of closer molecular proximity and more significant intermolecular forces. Temperature also impacts viscosity, as higher temperatures tend to reduce it by providing dendrimer molecules with more energy to overcome these forces[51]. The choice of solvent can significantly affect viscosity, with solvents that strongly interact with dendrimers increasing viscosity and those with weaker interactions or better solubility reducing it. Additionally, the internal structure and surface functionality of dendrimers can alter their interaction with

solvents, further influencing viscosity[52]. These viscosity characteristics are essential in various applications, including drug delivery, where they affect drug release rates, and in material science, where they impact the processing and properties of nanocomposites and coatings [33,53].

1.4 Monodispersity.

The convergent strategy in dendrimer synthesis is particularly effective in producing homogeneous molecular structures, mainly because it allows for the purification of the dendrimer at each step of the synthesis process[54]. This approach significantly reduces the chances of cumulative defects being carried through to the final product. Each generation of the dendrimer can be purified to ensure uniformity and consistency in its structure before proceeding to the next step, minimizing imperfections [55].

On the other hand, dendrimers synthesized using the divergent method have demonstrated the ability to achieve high levels of Monodispersity, maintaining consistent molecular masses across the molecules. This is particularly noteworthy at higher generations, where densely packed regions within the dendrimer structure are more prevalent [56]. Despite the increased complexity at these higher generations, the molecular weight distribution of the dendrimers remains remarkably narrow. This indicates a high degree of uniformity in the size of the dendrimers, even though the actual experimental masses may differ significantly from their theoretical values[57]. This consistency in molecular mass, despite the inherent challenges of the divergent method at higher generations, underscores the effectiveness of this approach in creating uniform dendrimer structures, especially for applications where precise molecular sizing is crucial[25,58].

1.5 Unimolecular Internal Structure Assembly.

The behaviour and characteristics of the dendrimer series vary significantly based on their scaffolding, which is largely determined by the chosen core[59]. The core plays a crucial role in defining the size, shape, and directionality of the internal branching units and the peripheral functionalities of the dendrimer[60]. As the number of layers or generations in the dendrimer increases, so does the steric hindrance and rigidity of the structure. This change in physical properties affects the dendrimer's ability to encapsulate or interact with guest molecules [61].

Different generations of dendrimers exhibit varying levels of container properties, or their ability to host guest molecules within their structure. Lower-generation dendrimers often have more accessible internal spaces for guest molecules compared to higher-generation dendrimers[51]. This increased accessibility is due to their less rigid and less crowded internal structure. In contrast, higher-generation dendrimers, with their increased steric hindrance and rigidity, can restrict the entry and movement of guest molecules within their structure[62].

For instance, in the case of Polyamidoamines PAMAM dendrimers, the container properties in the earlier generations are not as clearly defined or effective as in later generations[3]. This is because the internal structure of early-generation PAMAM dendrimers is less dense, offering fewer binding sites and less defined cavities for guest molecules [63]. As the dendrimer grows and complexity with each generation, its ability to encapsulate or interact with guests becomes more pronounced, making the higher generations more effective for applications requiring specific container properties. This variability across generations is a key aspect of dendrimer design,

influencing their suitability for different applications in fields such as drug delivery, catalysis, and material science[64].

1.6 Dendrimers and their Applications.

Dendrimers have gained significant popularity as mimics of globular proteins, primarily due to their controlled structure and nanoscale dimensions[3]. Their symmetrical structure and hydrodynamic behaviours make them highly suitable for modelling artificial proteins. The unique architectural features of dendrimers, including their well-defined, symmetric macromolecular structures, enable them to replicate the essential characteristics of natural globular proteins [65,66]. The versatility of dendrimers extends to a wide range of applications, where they serve as replacements or analogues for globular proteins. In gene therapy, dendrimers offer a means of delivering genetic material into cells, leveraging their ability to encapsulate and protect nucleic acids. In the realm of protein mimicry, dendrimers are used to imitate the functional aspects of proteins, such as binding specific molecules or participating in biochemical processes [67].

Dendrimers are also employed in light-harvesting applications, where their ability to organize multiple light-absorbing units at the nanoscale is advantageous. This property is critical in the development of efficient and compact systems for capturing and utilizing solar energy[3]. Furthermore, in the field of catalysis, dendrimers function as enzyme-like catalysts. Their defined structure allows for the precise positioning of catalytic sites, enhancing the specificity and efficiency of catalytic reactions, much like natural enzymes [17,68].

Dendrimers can be easily functionalized, enabling the attachment of heme or porphyrin molecules essential for oxygen binding and release. Additionally, their internal cavities offer an ideal environment for encapsulating heme mimics, thus stabilizing the oxygen-binding site[3]. The design flexibility of dendrimers facilitates the optimization of oxygen-binding properties and the potential to mimic haemoglobin's allosteric responses to environmental changes. Moreover, their biocompatibility makes them suitable for biomedical applications, particularly in developing artificial oxygen carriers that emulate the functions of natural haemoglobin[69].

The application of dendrimers as globular protein substitutes in these diverse fields highlights their potential to advance various scientific and technological areas. Their design flexibility, coupled with their ability to mimic the structural and functional attributes of proteins, positions dendrimers as valuable tools in nanotechnology, biomedicine, and materials science [70].

Chapter 2

2 Artificial Blood.

2.1 Introduction.

Blood, a crucial connective tissue, plays a multifaceted role in human physiology, encompassing the transport of gases, nutrients, and hormones, as well as the removal of waste products. It consists of red blood cells erythrocytes, white blood cells leukocytes, platelets thrombocytes, and plasma [71]. Red blood cells, rich in haemoglobin, are vital for transporting oxygen from the lungs to body tissues and returning carbon dioxide to the lungs[72]. White blood cells form the cornerstone of the immune system, combating infections and foreign bodies. Platelets, essential for blood clotting, aggregate at wound sites to form clots, preventing excessive bleeding. The plasma, constituting about 55% of blood volume, is primarily water but contains dissolved proteins, electrolytes, and hormones, serving as the transportation medium for various substances throughout the body[73].

In humans, the average blood volume is approximately 5.5 litres, with a composition of about 45% red blood cells and 55% plasma [74,75]. This composition contributes to blood's viscosity and colour. The exploration of artificial blood originated from the need to mimic these complex functions, especially critical in transfusion medicine where natural blood availability might be limited. Blood's role extends beyond oxygen delivery and waste removal; it's integral to maintaining homeostasis and overall health, underscoring the significance of each component in its intricate network of functions [76].

However, it's important to note that artificial blood cannot completely replicate the varieties of physiological functions carried out by human blood[77]. While it can be

instrumental in increasing blood volume and transporting respiratory gases (oxygen and carbon dioxide) throughout the body, it cannot perform all the functions of natural blood. This includes aspects like immune responses, detailed coagulation mechanisms, and the transport of various nutrients and hormones[78,79].

This is where the potential use of artificial blood or blood substitutes becomes particularly compelling [80]. The concept of using a blood substitute in such critical situations is driven by the need to quickly restore blood volume and improve oxygenation, especially when conventional blood transfusions are not an option[81].

In situations of massive bleeding, particularly following trauma, the use of blood substitutes primarily aims to stabilize the patient by maintaining circulatory volume and ensuring adequate oxygenation of tissues until they can be transported to a facility where full medical care, including real blood transfusions, can be provide [79]. The development and implementation of effective blood substitutes in emergency medical services could mark a significant advancement in trauma care and emergency medicine, potentially saving countless lives in situations where immediate access to blood transfusions is not possible[82].

The term "blood substitute" can indeed be somewhat misleading when referring to products currently in development that primarily address the transport of respiratory gases like oxygen and carbon dioxide[7583]. Research into artificial blood has intensified, driven by the discovery of haemoglobin structures and the need for alternatives to traditional transfusions due to immune sensitization and infection risks. [7984].

On the other hand, the safety of blood transfusions has been a significant concern, particularly following the HIV outbreak in 1981. This led to the development of more

stringent screening procedures [85]. Despite these improvements, the demand for blood continues to outpace the supply, partly due to public awareness issues and the high volume of blood needed for major surgeries [86,87]. The scientific interest in blood substitutes has intensified since the discovery of haemoglobin and myoglobin structures by Perutz and Kendrew in 1959, Research is now exploring a range of products derived from natural sources like perfluorocarbons and synthetic materials[88].

2.1.1 The Main challenges.

. The complexity of blood is further highlighted by the blood typing phenomena, which are based on proteins present in the cell membranes [89]. These proteins are recognized by the immune system, necessitating compatibility between donor and recipient blood types for safe transfusions [90].

scientists aim to develop a liquid that can efficiently transport oxygen, akin to the function of natural red blood cells [91]. Thus, these products are more aptly described as oxygen carriers rather than true artificial blood. Blood group discovery in the 19th century significantly advanced our understanding of blood compatibility, yet the global supply of blood, especially in developing countries, remains a challenge [92,93].

Historically, blood transfusions were fraught with complications, mainly due to a lack of understanding about agglutination [94]. Early attempts to use haemoglobin extracts often led to severe adverse reactions, including acute renal failure, which threatened to halt the development of blood transfusion practices. More recently, fears regarding the transmission of diseases such as variant Creutzfeldt-Jakob disease have arisen [95,96].

2.1.2 Blood Substitute Models.

Synthetic blood substitutes, commonly referred to as "oxygen carriers," [97]. These substitutes primarily focus on mimicking the oxygen-carrying capacity of haemoglobin in red blood cells[98,99]. Additionally, they incorporate antioxidant functions to protect tissues from oxidative damage. However, unlike natural blood, these synthetic carriers lack the complexity of real blood, as they do not contain cells, antibodies, or coagulation factors, limiting their ability to reproduce the full spectrum of blood's functions [100,101]. Their primary role is to restore lost blood volume and maintain oxygen transport. Despite their critical utility in such situations, these oxygen carriers are not comprehensive substitutes for blood, emphasizing the need for continued research and development in this field to more closely replicate the multifaceted nature of blood [102].

2.1.3 The Structure Haemoglobins.

Haemoglobin, a key molecule in red blood cells responsible for transporting oxygen from the lungs to other body tissues, is not only vital for physiological functions but also central to artificial blood research [103]. This pigment, found in the blood of vertebrates and responsible for the red colour of cells, contains the prosthetic group Fe^{II} protoporphyrin IX, a common feature in various eukaryotes[104]. In humans, there are several types of haemoglobins HBs, each consisting of two distinct pairs of globin chains associated with heme groups, essential for oxygen binding [105].

Leveraging haemoglobin’s innate ability to covalently bind oxygen unlike perfluorocarbon PFC products, which dissolve oxygen haemoglobin-based artificial blood products offer significant advantages, such as obviating the need for blood

typing, as they are not confined within a membrane-like whole blood. However, the direct use of raw haemoglobin in these applications is impractical [106]. Haemoglobin tends to degrade into smaller, potentially toxic compounds in the body and faces issues with stability in solution [103]. This challenge has led to various strategies in artificial blood research to modify the haemoglobin molecule, addressing these stability and degradation concerns, while maintaining its crucial oxygen-carrying function[107]. The diversity in human haemoglobins, each variant tailored for specific physiological needs, further underscores the complexity and potential of haemoglobin in medical and research applications [108]. Haemoglobin, a vital component of vertebrate blood responsible for oxygen transport, exhibits diverse forms in adult humans. The primary form of haemoglobin in adults is known as Major HbA (α2, β2), which constitutes most of the haemoglobin in the bloodstream. Additionally, there is a secondary type, Hb A2 (α2,δ2), accounting for about 2.5% of the total haemoglobin [109].

Recent research has shed light on the composition of Haemoglobin F Hb F, another form of haemoglobin predominantly found in foetuses but also present in minor amounts in adults. HbF is characterized by a mix of molecular species with the formulas (α2γ2136glY) and (α2γ2136ala). The molecular weight of adult haemoglobin is approximately 64k Daltons, indicative of its size and complexity [110,111].

Structurally, haemoglobin in the adult blood is composed of two types of globin subunits, α and β, arranged in a tetrameric structure as seen in Figure 2.1. This arrangement is crucial for its function in oxygen transport and delivery throughout the body[112]. The intricate structure and varying types of haemoglobin, each tailored for specific physiological roles, underscore the protein's complexity and its significance in

both natural physiological processes and in medical applications like artificial blood development [111].

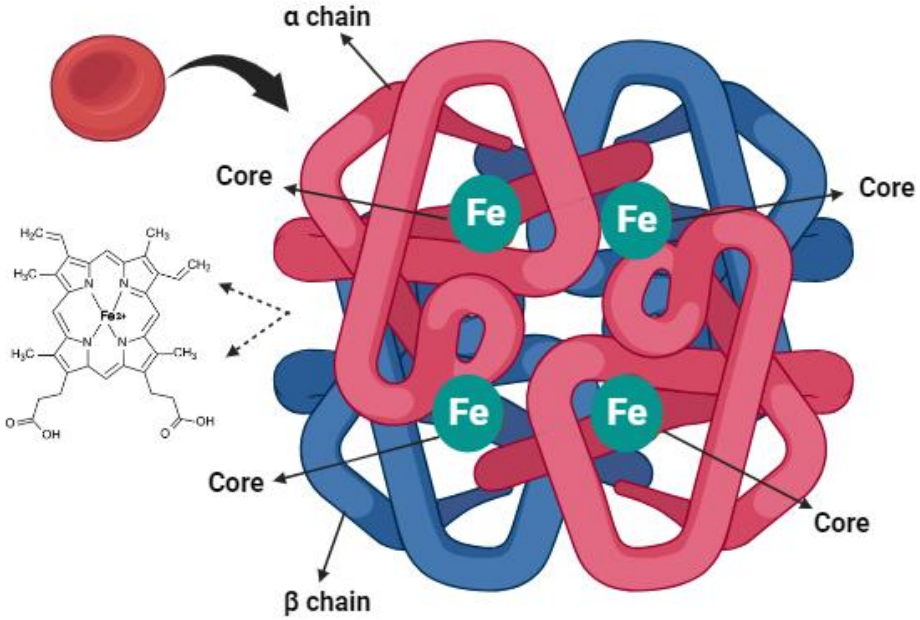

Figure 2.1: Tetrameric haemoglobin protein containing four globin subunits.

In the globin polypeptide chains of haemoglobin, each chain contains either 141 or 146 amino acids, depending on the specific globin subunit. Each of these globin chains is associated with a heme unit, which is embedded within the globular structure of the peptide [109]. The heme unit is characterized by an iron core at the centre of a porphyrin ring, specifically the ninth in the series. This iron core can bind a single oxygen molecule[113].

The structure of the heme is further stabilized by its interaction with the surrounding globin polypeptide. It is attached to the larger globin macrocycles through non-covalent ligation [84]. A critical aspect of this structure is the formation of a penta-coordinate bond between the iron core and the imidazole group of the proximal histidine residue, known

as His F8. This bond is essential for the function of haemoglobin The imidazole group of the proximal histidine in haemoglobin plays a critical role in maintaining the structure and function of the protein[114]. It directly coordinates with the central iron Fe^{II} atom of the heme group, stabilizing the heme-iron complex and enabling efficient and reversible oxygen binding. This interaction prevents iron oxidation and displacement from the heme plane, ensuring proper oxygen transport. Additionally, the imidazole group transmits conformational changes during oxygen binding, facilitating haemoglobin's cooperative binding mechanism. It also contributes to the Bohr effect by influencing oxygen affinity in response to pH changes[115]. Overall, the proximal histidine's imidazole group is essential for haemoglobin's stability, oxygen-binding capacity, and regulatory functions. Additionally, the iron core is held in place by four planar ligands that are part of the porphyrin ring structure, with nitrogen atoms centrally positioned within the ring. This complex arrangement allows for the efficient binding and release of oxygen, a key function of haemoglobin in oxygen transport within the body [116].

2.1.4 The Environmental Modification of Haemoglobin and Their Oxygen Binding Process of

Upon entering the bloodstream, oxygen molecules bind to heme groups within haemoglobin. Each haemoglobin molecule can carry a maximum of four oxygen molecules when fully saturated [117].

The release of oxygen from haemoglobin is influenced by several environmental factors that trigger a conformational change in the protein[118]. These factors include partial oxygen pressure pO_2, pH levels, temperature, and partial carbon dioxide pressure pCO_2. Additionally, the allosteric effector 2,3-diphosphoglycerate DPG plays

a crucial role in facilitating the transition from a high to a lower oxygen affinity state by reducing haemoglobin's affinity for oxygen, thus aiding in oxygen offloading [119]. During oxygen dissociation from the globin chain, CO_2 binds to it, forming carbamate-haemoglobin, which is then carried back to the lungs. It's worth noting that only about 20% of CO_2 in the blood is transported in this manner [120].

The processes of oxygenation and deoxygenation, where haemoglobin binds and releases oxygen, lead to the formation of two states of haemoglobin: oxy-haemoglobin and deoxyhaemoglobin. Crystal structure studies have described these states as the taut (T) and relaxed (R) states[111] . In the T state, the core metal Iron is in a five-coordinated high spin state and positioned below the porphyrin plane, with the binding of histidine to the imidazole proximal contributing to this non-planar position. Upon forming an oxygen adduct, the metal moves back into the porphyrin plane, transitioning to a six-coordinated low-spin state [121]. This dynamic structural change is fundamental to haemoglobin's ability to effectively bind and release oxygen, crucial for its role in transporting oxygen and CO_2 between the lungs and tissues as shown in Figure 3.2.

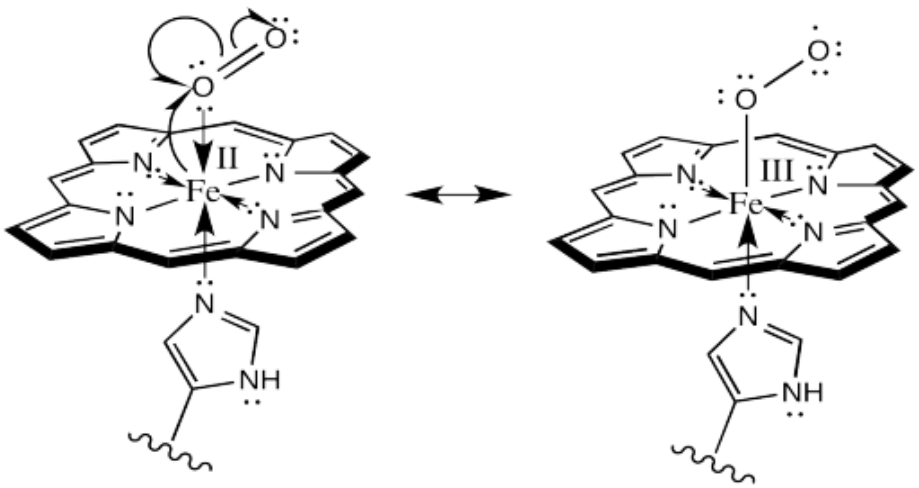

https://www.researchgate.net/figure/Chemical-structure-of-a-oxygenated-heme-and-b-deoxygenated-heme_fig2_343882652

Figure 2.2: The structure of heme following oxygenation.

The binding of oxygen to the heme group in haemoglobin induces significant structural changes in the polypeptide chain, primarily through the movement of a histidine residue towards the porphyrin plane [122]. This movement is triggered by the binding of oxygen to the iron Fe^{II} in the porphyrin, the active centre of the heme group. As the globin chains shift, they form a hydrophobic cavity at the distal end of the heme, creating an optimal environment for oxygen binding[123]. This structural rearrangement is crucial for the binding of oxygen. The van der Waals forces within the distal planar cavity provide a polar environment, facilitating the reversible binding of oxygen [124]. This is further enhanced by the presence of a highly polar group near the coordination site, contributing to the appropriate spatial arrangement for oxygen binding. The unique bond geometry, characterized by a slight tilt of the bound oxygen, helps in maintaining its electronic character, enabling strong yet reversible binding to the heme [125].

Molecular studies of oxyhaemoglobin have shown that it is stabilized by medium-strength hydrogen bonds. Typically, a bond angle of approximately 120 degrees is observed between the iron and oxygen molecules [126]. However, this angle is not absolute and can vary due to steric constraints within the pocket of the heme group [127]. These constraints affect the significance of the bond angle, underscoring the complex and dynamic nature of oxygen binding in haemoglobin[128]. This intricate mechanism allows haemoglobin to effectively capture, transport, and release oxygen, which is essential for cellular respiration and the overall oxygenation of the body's tissues [129].

2.1.5 Haemoglobin based products.

. Haemoglobin-based products offer an advantage in blood transfusions as they don't contain membranes, eliminating the issue of blood typing [130]. However, there are challenges in using raw haemoglobin for artificial blood [131]. In its natural, unmodified form, haemoglobin is prone to breaking down into smaller, potentially toxic compounds within the body [132]. Additionally, haemoglobin faces stability issues when in solution, as it does not remain stable in organic solutions.

To address these problems, various strategies are employed to modify and stabilize haemoglobin. These include recombinant DNA technology to produce modified proteins and chemical cross-linking of molecules[133]. Approaches such as encapsulating haemoglobin in nanoparticles, polymersomes, or liposomes, and creating stabilized, polymerized, or conjugated haemoglobin solutions have been explored [134]. Conjugation of haemoglobin increases its molecular size and reduces its antigenicity, resulting in slower removal from circulation and lower visibility to the immune system. These conjugated haemoglobins exhibit high oncotic pressure, making them potent plasma volume expanders [102].

Furthermore, intramolecularly linked haemoglobins maintain a reasonable molecular weight but are chemically cross-linked to prevent dissociation into dimers or monomers, enhancing stability and solubility in solutions. These modifications aim to create artificial blood products that can carry oxygen more efficiently than natural red blood cells, potentially revolutionizing medical treatments for blood loss and transfusion[135].

2.1.6 Cross-linked Haemoglobins.

The key challenge in developing haemoglobin-based artificial blood is to modify the haemoglobin molecule to overcome these drawbacks [136]. This modification involves either chemically cross-linking haemoglobin molecules or employing recombinant DNA technology to create altered proteins[137]. Various methods have been explored to stabilize haemoglobin in artificial blood, including encapsulation within Modified Liposomes, nanoparticles, and polymersomes. Other strategies include creating stabilized, polymerized, and conjugated haemoglobin solutions. Each of these approaches aims to maintain the functional integrity of haemoglobin while ensuring its stability and safety for medical use [138].

In the realm of haemoglobin-based therapeutics, there are primarily two categories of cross-linked haemoglobin intramolecular and intermolecular cross-linked haemoglobin [139]. Intramolecular cross-linking is designed to decrease the oxygen affinity of haemoglobin and prevent its dissociation into smaller units. This is achieved by creating chemical bridges within the haemoglobin molecule, particularly between the amino acids of its dimers, resulting in the formation of smaller, stabilized molecules[140]. While intramolecular cross-linked haemoglobin presents a promising avenue for medical treatments, its application in clinical settings has encountered challenges. A notable example is HemAssist-31, a cross-linked haemoglobin product developed by the US Army. Despite its potential, (HemAssist-31) was withdrawn from the market following Phase III trials that reported an unexpectedly high mortality rate among participants. This adverse outcome was attributed to the relatively small size of the intramolecular cross-linked haemoglobin molecules[141]. Their small size facilitated the leakage of haemoglobin from blood vessels into surrounding tissues. This leakage led

to the accumulation of haemoglobin outside the vascular system, causing toxicity and various side effects [142].

This state highlights the complex balance between modifying haemoglobin to enhance its therapeutic potential and ensuring its safety and efficacy in medical treatments [143]. The experience with (HemAssist-31) underscores the need for careful consideration of the molecular size and properties of modified haemoglobin products in the development of safe and effective artificial blood substitutes[144].

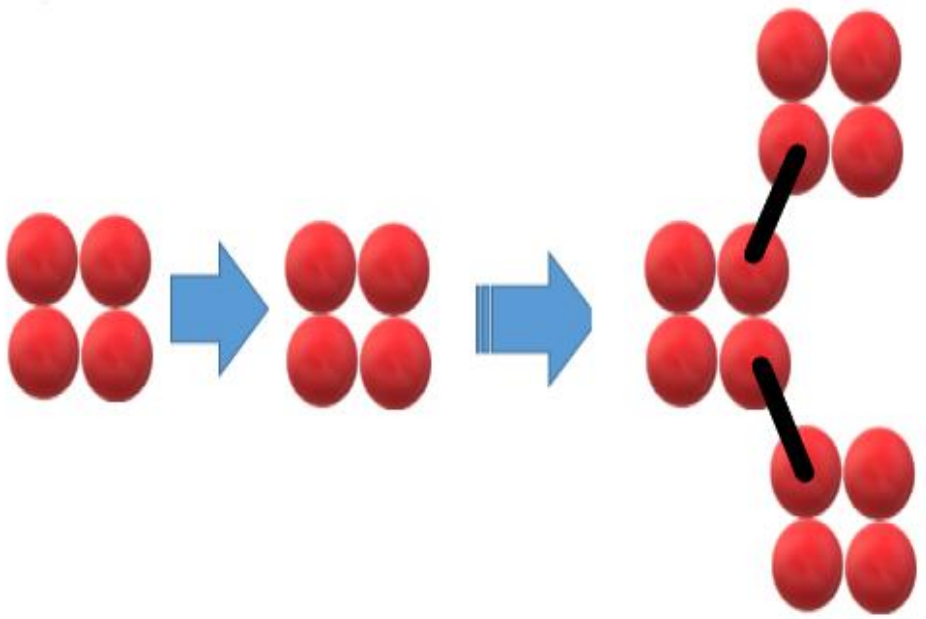

Figure 2.3: Intermolecular-cross-linked Hb

Intermolecular cross-linking in haemoglobin involves the formation of links between two or more haemoglobin units, leading to their oligomerization[143] *Figure 2.3*. This process is aimed at reducing oncotic pressure and increasing the molecular size to slow down metabolism by the body. A commonly used reagent for this purpose is glutaraldehyde, which can form an unsaturated polymer with aldehyde groups that

react with the amino acids in haemoglobin[145]. However, a major challenge with this process is the potential formation of toxic glutaraldehyde if the Schiff bases, which are generated during the reaction, are not fully reduced, leading to depolymerization [146]. To mitigate this issue and enhance the properties of haemoglobin, the molecules can be modified with functionalised dendritic polymer encapsulated within modified Liposomes. This modification increases both the size and hydrophilicity of the haemoglobin molecules, improving their suitability for therapeutic applications [147].

2.1.7 The Prevention of Heme Autoxidation.

During the autoxidation process, oxygen reacts with heme units at the centre of Fe^{II} core porphyrins[148]. This reaction involves the formation of μ-oxo dimers, which originate from the rotational decay of μ-peroxo dimers and the oxidation of Fe^{IV} atoms in a rapid bimolecular redox reaction[149] Figure 2.4. In natural systems, this leads to the formation of a six-coordinate O_2, Fe^{III}, and Imidazole adducts, particularly during irreversible autoxidation. When oxygen reacts with the iron core, it is approximately (4.4 Angstroms) away from the core, a distance that hinders further oxygen binding mechanisms [150].

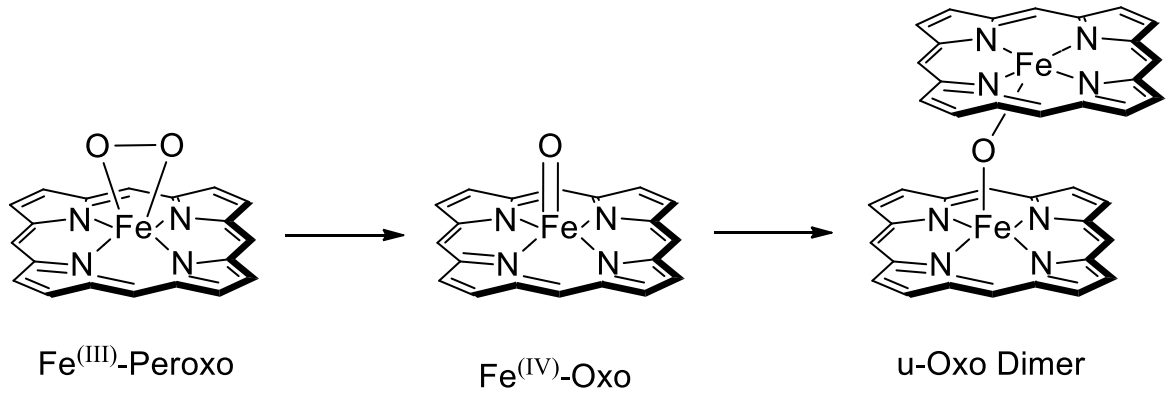

https://www.researchgate.net/figure/Scheme-1-Formation-of-a-N-bridged-high-valent-diiron-oxo-complex-from-FeIII-FeIV_fig1_275364943

Figure 2.4: The μ-oxo dimer formation from the decaying peroxo species of Fe^{III}.

Moreover, the globin structure surrounding each heme unit plays a crucial role in ensuring the reversible binding of oxygen to heme, thereby preventing oxygen loss and waste. Haemoglobin is designed with tiny holes that facilitate this reversible binding process [151]. However, when oxygen is introduced into the iron core at room temperature, it leads to irreversible autoxidation. The steric nature of this tertiary protein protects against oxidative damage to the heme units, underscoring the intricate design and functionality of haemoglobin in oxygen transport and protection [152].

Frequent studies have indicated that the stability of natural haemoglobin within the body surpasses that of free haemoglobin when tested outside the body, or in vivo [153]. A key observation in these studies is the rapid autoxidation of simple, non-hindered Fe^{II} porphyrins, which occurs even at low temperatures. Interestingly, this autoxidation process is not significantly impacted by the temperatures found within the human body[148]. Furthermore, research has revealed that the reversibility and stoichiometry of oxygen binding to iron-containing porphyrin solutions are influenced by the presence of ligand hindrance. This suggests that the structure and surrounding environment of the haemoglobin molecule play a crucial role in its ability to bind oxygen effectively and maintain its stability[154]. These findings highlight the complexity of haemoglobin's functionality and the importance of its molecular environment in determining its behaviour and efficiency in oxygen transport [155,156].

2.1.8 The Haemoglobin Mimicry in the cells.

Researchers have embarked on projects to replicate or synthesize the functions of the polypeptide chains that envelope the heme units in haemoglobin, driven by the scarcity of raw haemoglobin and the intricacies associated with its modification. In pursuit of viable alternatives, the potential of dendrimers has come into focus [126,150]. These

synthetic, branched molecules are gaining attention for their ability to be engineered to mirror the shapes and sizes of natural heme-containing proteins, thus closely emulating the structure of haemoglobin. This approach offers a promising pathway to create haemoglobin-like functionalities, circumventing the limitations of direct haemoglobin sourcing and complex modification processes [157]. One of the primary goals of this research is to develop a method for reversible oxygen bonding, coordinating to how natural haemoglobin operates. This approach would ideally replicate the oxygen-carrying capacity of haemoglobin, which is crucial for its role in transporting oxygen throughout the body [158]. While there has been success in creating a reversible oxygen bonding mechanism, the synthesis of such dendrimer-based structures poses significant challenges. These challenges include replicating the intricate and finely tuned environment of natural haemoglobin, which is essential for its stability and functionality. Despite these difficulties, the exploration of dendrimers for this purpose is a testament to the ongoing efforts to innovate in the field of synthetic blood substitutes and haemoglobin-like materials [159].

2.1.9 Liposomes

The preparation of liposomes involves the combination of Di phospholipids [61], which consists of a hydrophilic (polar) block and a hydrophobic (non-polar) block, as illustrated in Figure 2.5. By copolymerizing two or three monomer blocks, di- or tri-block amphiphilic copolymers can be produced. These copolymers exhibit contrasting behaviours within the same molecule, identical to the amphiphilic nature of surfactants in soaps [160].

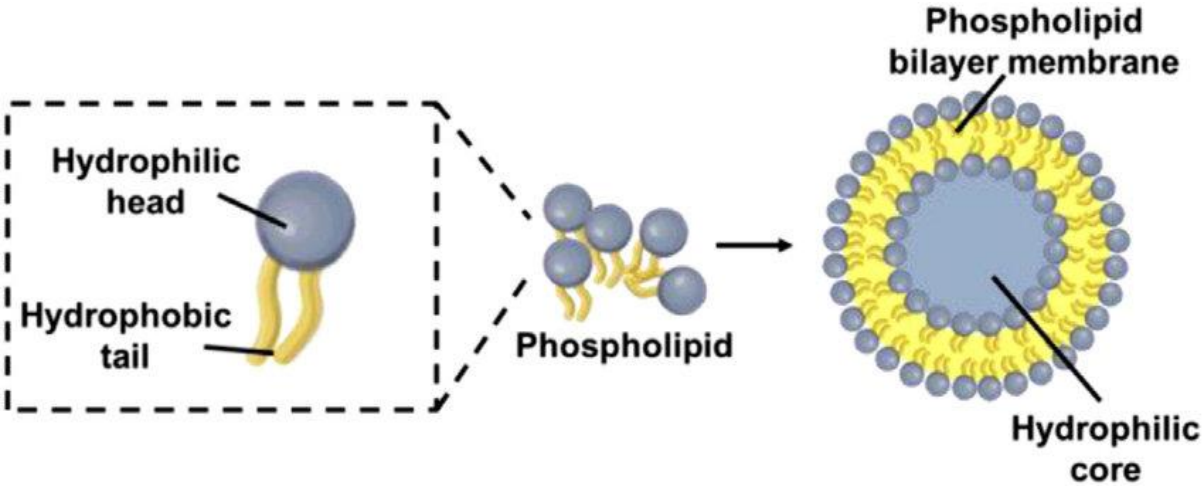

Figure 2.5: The structure of liposomes.

On the other hand, the key properties of these lipids are their ability to self-assemble in solutions, forming structures like liposomes or vesicles. This self-assembly results from non-covalent forces such as hydrogen bonding, electronic forces, van der Waals forces, and the hydrophobic effect [161]. These interaction forces are crucial in driving the reversible and spontaneous aggregation of these molecules in solution, leading to an equilibrium state. The formation of these various structures depends on the balance of hydrophilic and hydrophobic segments within the liposomes, and this ability to form organized, self-assembled structures particularly useful in applications like drug delivery and nanotechnology[65].

2.1.10 liposome Properties

liposome formed when amphiphilic molecules like surfactants reach the critical micelle concentration in a solvent and exhibit unique properties crucial for various applications [162]. Their structure, typically spherical but variable in shape, consists of hydrophobic

tails facing inward and hydrophilic heads outward, enabling them to solubilize hydrophobic compounds within their core [163]. This solubilization and encapsulation efficiency is vital in pharmaceuticals for enhancing the bioavailability of poorly water-soluble drugs [164]. liposomes are dynamic, with their stability influenced by environmental factors such as temperature, pH, and ionic strength, and they possess the ability to adsorb at interfaces, reducing surface tension, which is essential in detergency [165,166]. Additionally, some liposomes exhibit distinctive optical and electrical properties, making them useful in nanotechnology, while their biocompatibility and toxicity are key considerations in biomedical applications [167]. Overall, the versatility of liposome from their formation and structural adaptability to their functional properties, makes them invaluable in fields ranging from drug delivery to materials science [168,169]

.

2.2 Aims and Objectives

Polymers, with their customisable structures and properties, offer a promising pathway for mimicking the natural functions of heme proteins [167]. They can be engineered to provide a protective environment for the heme groups, thereby preventing oxidative damage and maintaining efficient oxygen transport. Polymers are characterized by their multifaceted structural features, which include a polyfunctional core and numerous branching units terminated with functional end groups [170]. These end groups act as foundational building blocks. The distinct structural uniformity of these polymers, combined with their multifunctional surfaces and internal cavities, makes them highly applicable in pharmaceutical and biomedical research contexts [171] . *Figure 2.6*.

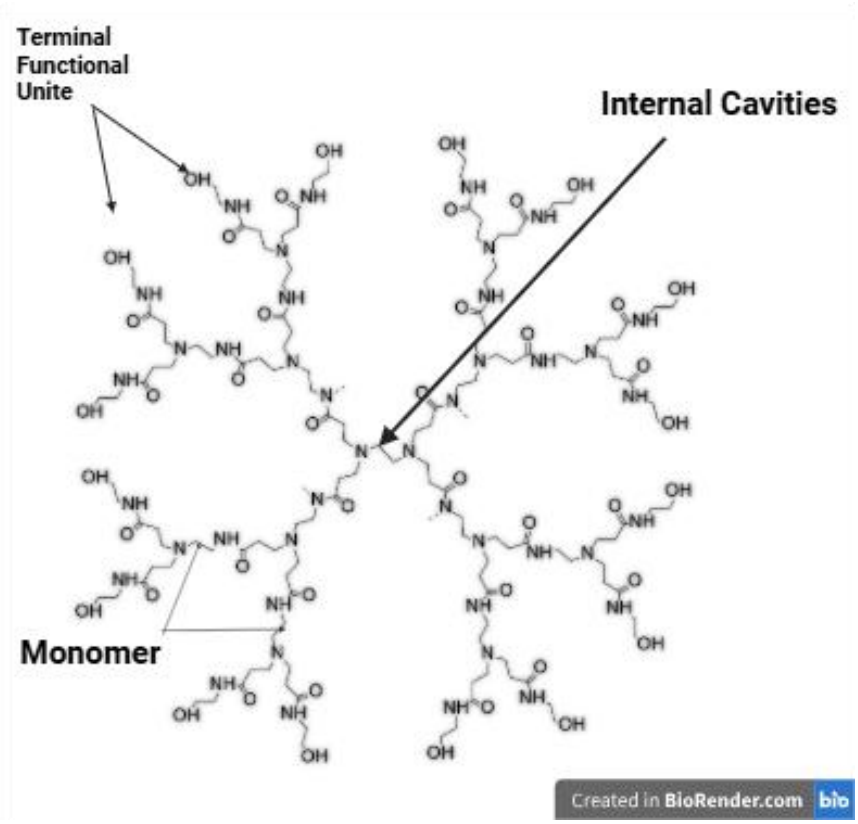

Figure 2.6 Polymeric System Structure

Furthermore, polymers can also attend as a core matrix in which active molecules are embedded, providing a unique mechanism for drug delivery and controlled release in therapeutic applications [172]. This versatility in encapsulation and modification underscores the significance of polymers in the development of advanced drug delivery systems and biomaterials[173].

2.2.1 The Structure Porphyrin and Their Substituents

The iron atom in haemoglobin is integrated into a porphyrin ring structure, known as heme. This encapsulation is essential to maintain the iron atom's oxidation state between Fe^{II} and Fe^{III}, which is crucial for reversible oxygen binding [153174].

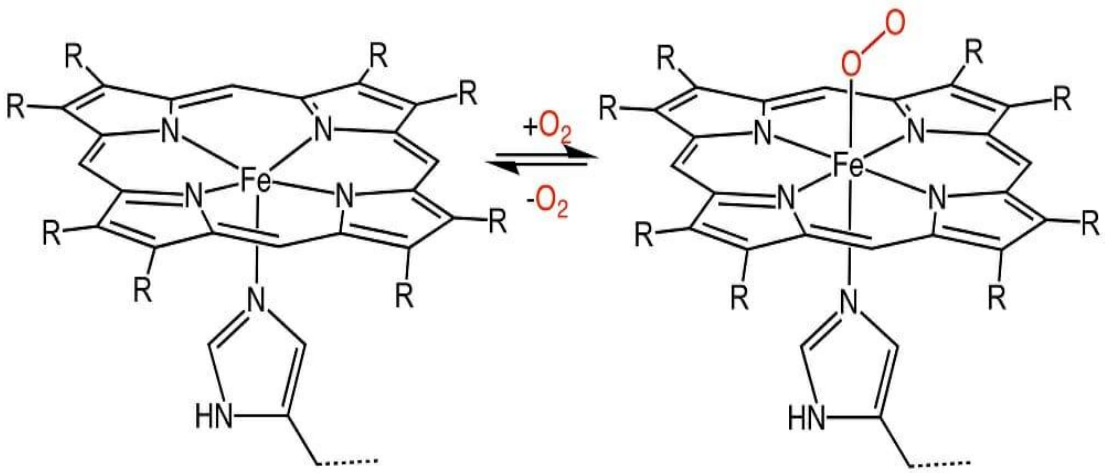

https://www.researchgate.net/figure/Chemical-structure-of-a-oxygenated-heme-and-b-deoxygenated-heme_fig2_343882651

Figure 2.7 Porphyrin structure depends on the oxygenation.

Our strategy involves the synthesis of a bulky polymer that encapsulates the porphyrin core for several reasons, the hydrophobic encapsulation of porphyrins in dendritic structures enhances their stability and solubility, protects them from degradation, and facilitates targeted drug delivery while minimizing toxicity and immunogenicity [175]. This approach is crucial for optimizing the effectiveness and safety of porphyrin-based applications in biomedicine. This encapsulation is gained by initiating polymerization from a functionalised porphyrin core, leading to the growth of polymer chains. This process creates steric hindrance around the active site of the porphyrin, effectively protecting the porphyrin from aquatic influences[176].

We propose a dendrimer with OH terminal groups for our haemoglobin model. The OH groups can be added to the end of the dendrimer with terminal ester groups, followed by the addition of ethanolamine to give the desired OH-terminated dendrimer. A series of different generation dendrimers will be constructed, which allows for different levels of hydrophobicity within the dendrimer's interior.

The internal amine groups of these dendrimers will coordinate with the iron in the porphyrin cores. It is expected that the largest dendrimer system, with the most hydrophobic, will exhibit the highest oxidative stability of the iron, enabling the optimum ability to reversibly bind oxygen across multiple cycles *Figure 2.9*.

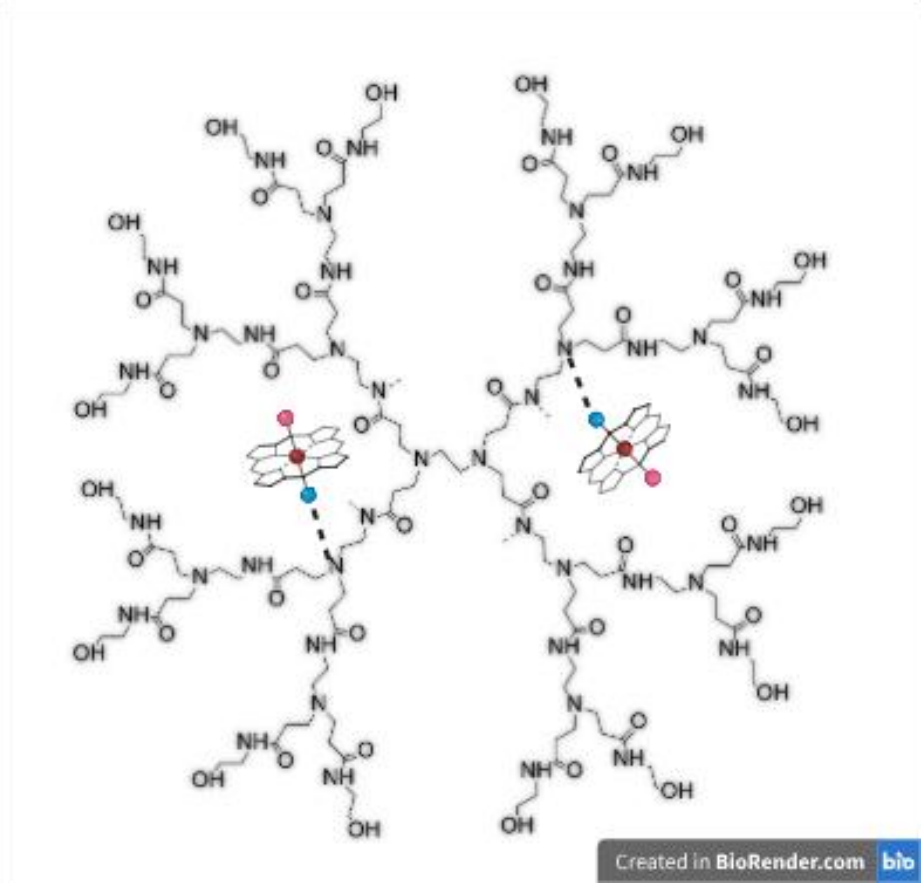

Figure 2.9 Encapsulation of Water-Soluble PAMAM Dendrimer with Iron-Cored Porphyrin through Non-Covalent Interactions.

2.2.2 The Encapsulation of Metalated Porphyrin-Cored Dendritic Polymer System within Liposomes.

The final phase of the study will focus on encapsulating a porphyrin within a dendrimer and then encapsulating the dendrimer within the aqueous phase of a liposome.

Dendrimers, being small, pose a risk of leaking from the vascular system into surrounding tissues, which can lead to toxicity. This leakage occurs because the size

of dendrimers is often smaller than the pores in the vascular system, allowing them to escape the bloodstream [177]. liposomes remain within the bloodstream, which can be designed to release their contents at controlled rates or in response to specific triggers to maintain the optimal oxygen levels in the body. Liposomes are composed of phospholipids [178].

This approach aims to significantly improve the stability and functionality of the dendritic polymer system, making it a more viable candidate for artificial oxygen carriers. The integration of these two technologies could make a significant step forward in the development of artificial blood substitutes [179]. Figure 2.10

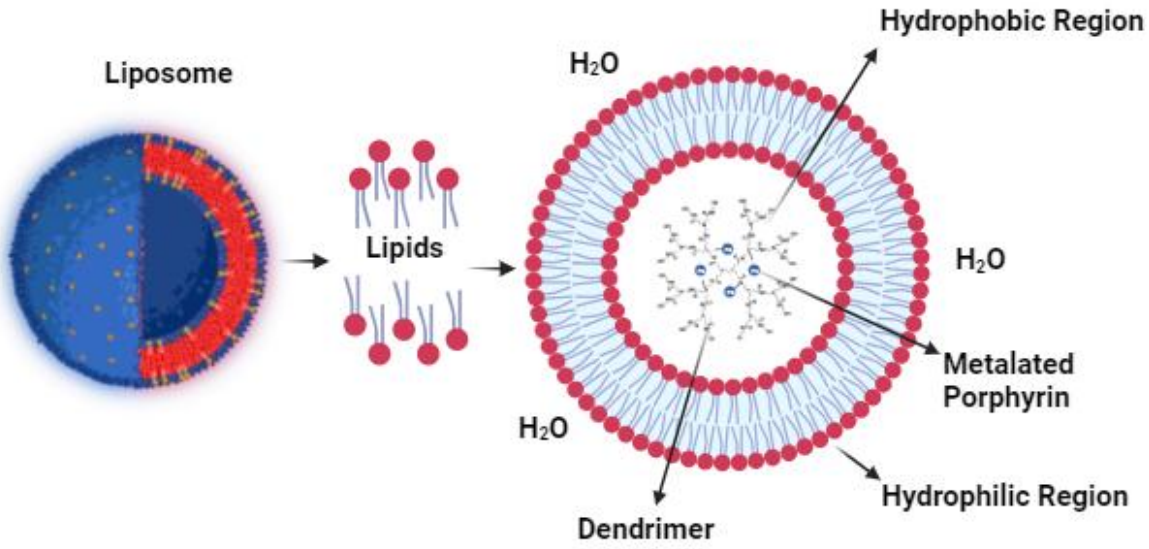

Figure: 2.10 Encapsulating dendritic polymers in liposome within a hydrophilic environment.

2.3 Result and Discussion.

2.3.1 The Synthesis of Polyamidoamines PAMAM.

The synthesis of PAMAM Polyamidoamines dendrimers was conducted with a divergent method, known for its integrity and systematic nature. Michael's Addition reaction forms the base of the process, where a core molecule EDA ethylenediamine reacts with methyl acrylate to produce half-generation dendrimers with ester-terminated groups, followed by an amidation reaction, where the ester-terminated dendrimers react further with EDA, leading to full-generation dendrimers with amine-terminated groups. The Twyman research group has extensively explored the synthesis of PAMAM dendrimers using the divergent approach [98].

2.3.1.1 The Synthesis of PAMAM Dendrimers.

The divergent method was used for the synthesis of Polyamidoamines PAMAM dendrimers, ranging from generation 0.5G to 3.5G and containing 4 to 32 terminal groups. This approach was first developed by Tomalia, et al, in 1985. The process involves an iterative sequence of two reactions starting with a Michael addition followed by an amidation process [98]. The Half-generation dendrimers with ester terminal groups result from the initial step of a two-step synthesis process, the first step involving a 1,4 Michael addition as presented in *Figure* 2.11, these dendrimers have reactive terminal groups and display an intermediate stage in the dendrimer's development. The full-generation dendrimers are achieved subsequently in the second synthesis step (amidation reaction), which caps the dendrimer with the anticipated surface functional groups. The 1.4 Michael addition reaction step utilises alpha-beta unsaturated carbonyl compounds. The presence of these carbonyl groups

leads to electron withdrawal, creating resonance-stabilized structures. This effect generates a partial positive charge (delta positive) on the alpha carbon atom, making it a reactive site for nucleophilic attack, leading to the formation of ester groups at the terminal ends of the half-generation dendrimers. These reactions are critical steps in the divergent synthesis of PAMAM dendrimers, allowing for the precise and controlled growth of the dendrimer structure.

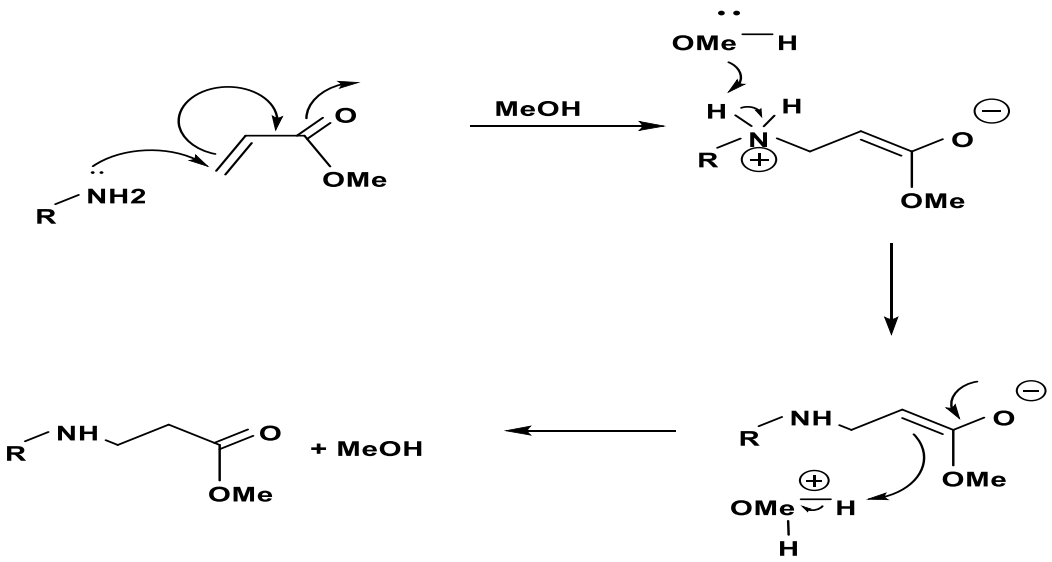

Figure 2.11: Mechanism Reaction for Michael Addition

The second step of a PAMAM dendrimer synthesis is the amidation step. The process was involving the nucleophilic attack from the lone pair of Ethylenediamine's EDA nitrogen to the positively charged carbonyl carbon of the terminal ester groups to generate a tetrahedral intermediate. This is followed by a deprotonation step, which is followed by a collapse of the tetrahedral intermediate, leading to the formation of the amide bond and the release of the methoxy group. The amidation reaction is crucial in extending the dendrimer structure for further growth in PAMAM dendrimer synthesis as it effectively doubles the number of amine groups, which can then be reacted with more methyl acrylate *Figure* 2.12.

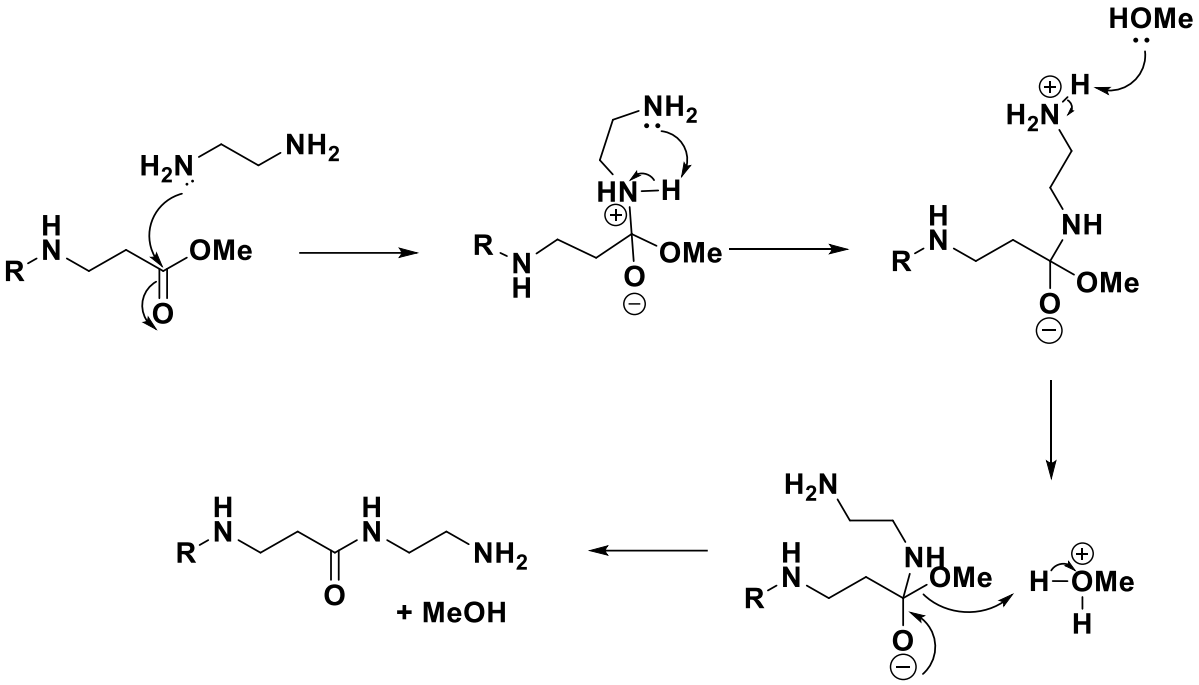

Figure 2.12: The Amidation reaction

2.3.1.2 The Synthesis of 0.5-G Ester Terminated PAMAM dendrimers.

The procedure for the synthesis of the half-generation dendrimers starts by dissolving EDA in methanol, and then adding a slight excess of MA dropwise as illustrated in *Figure* 2.13. The reaction mixture is then stirred at room temperature for 24 hours.

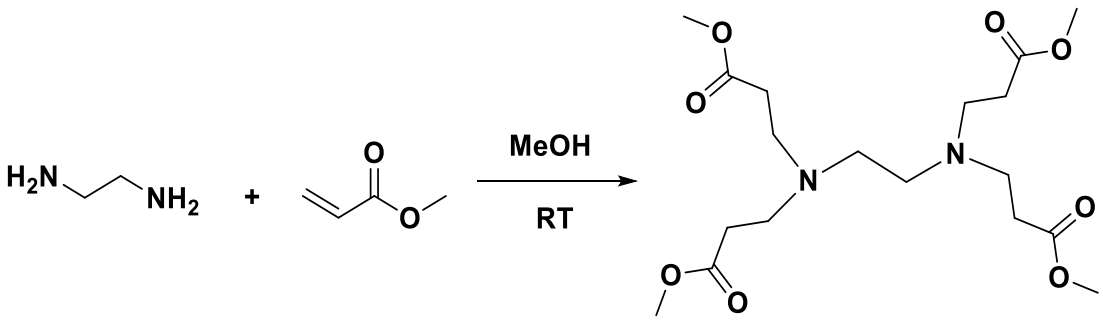

Figure 2.13: The Synthesis of ester Terminated group PAMAM dendrimers.

When the reaction is complete, any excess MA is removed through rotary evaporation (along with the solvent). The successful reaction of MA Methyl acrylate is confirmed by ^{1}H NMR spectroscopy, as the two distinct peaks at 6.15 ppm and 6.37 ppm from the alkene groups are no longer visible in the spectrum. The viscosity of the samples is observed to increase relative to the corresponding t size of the PAMAM dendrimers, along with a gradual darkening of colour.

2.3.1.3 The Synthesis of the Whole Generation of PAMAM Dendrimer (Amine-Terminated Group).

The synthesis of whole-generation dendrimers involves adding a large excess of EDA ethylenediamine to the previously synthesised half-generation dendrimer in methanol. The reaction mixture is then stirred at room temperature for several days *Figure* 2.14. The reaction occurs by the mechanism shown in *Figure* 2.12.

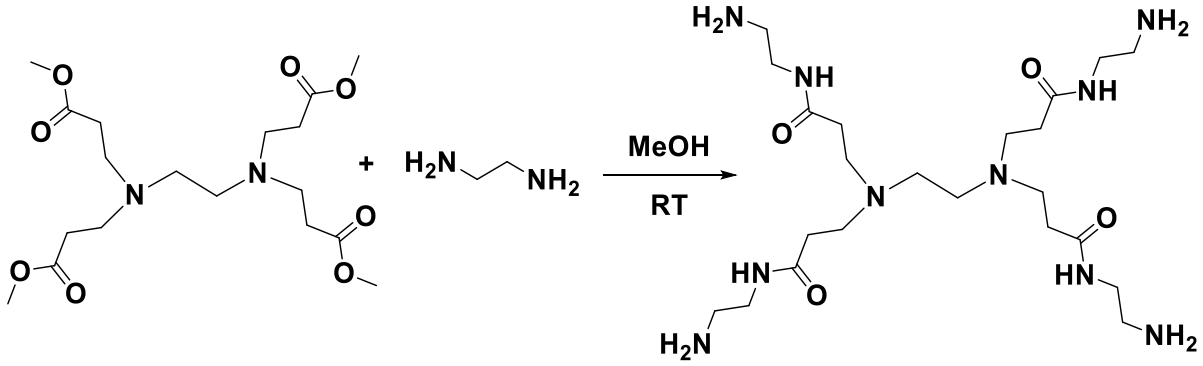

Figure 2.14: The Synthesis of amine-terminated group PAMAM dendrimers.

This step requires a longer duration when compared to the faster 1,4-Michael reaction *Figure* 2.11, and this is one reason why such a large excess of EDA is required. In amidation reactions, a large excess of EDA is often required to ensure the reaction efficiently proceeds towards the desired amide product. This necessity can be

attributed to several key factors, moving the reaction forward by shifting equilibrium, compensating for EDA consumed inside reactions or evaporated, utilising EDA as a solvent, overcoming steric hindrance of substrates, and enhancing the overall reaction rate. The use of excess EDA helps achieve higher yields and faster reactions, as well as accommodates a broader range of reaction conditions. This excess EDA must be removed before the next step, as it can initiate a new dendrimer synthesis of the 0.5 generation dendrimer, which is impossible to remove from any larger dendrimers *Figure* 2.15. EDA can hydrogen bond to the amide-amine groups of the dendrimers, making its removal difficult. Although methanol can compete with EDA for hydrogen bonding, it has a much lower boiling point (65°C 116°C). Therefore, excess EDA is removed by washing the dendrimer with an azeotropic mixture of toluene and methanol (9:1 Ratio), which is removed using rotary evaporation. This process is repeated until the EDA peak is no longer visible in the ^{1}H NMR spectrum.

2.3.1.4 The Purification of PAMAM dendrimer.

Purifying dendrimers is a critical step to ensure the integrity of the final dendrimer. Insufficient removal of EDA can act as a core for the synthesis of smaller, unwanted dendrimer structures during subsequent Michael additions [180], as illustrated in *Figure* 2.15.

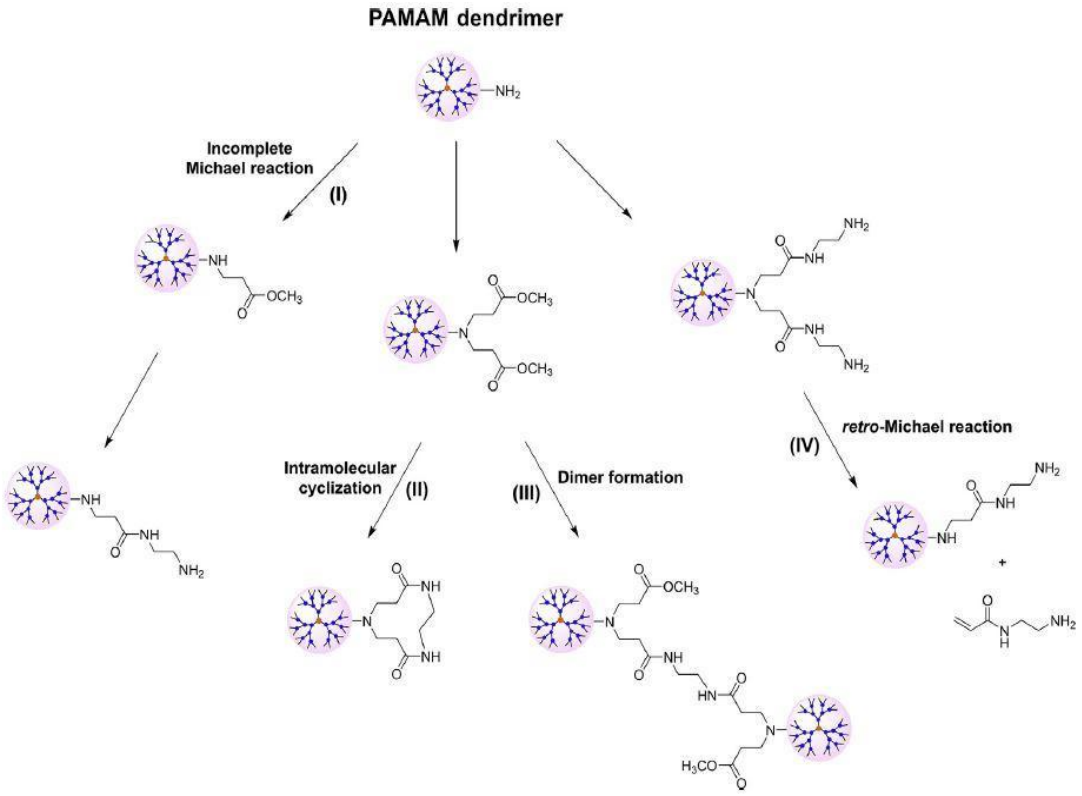

https://www.researchgate.net/figure/Possible-structural-defects-generated-by-the-different-side-reactions-in-PAMAM dendrimer_fig5_333445746

Figure 2.15: Irregular Structures Arising from Side Reactions in PAMAM Dendrimer Synthesis.

2.3.1.5 The Characterisation of half-generation PAMAM Dendrimers (ester-amine terminated group).

PAMAM dendrimers can be characterised using different methods, including mass spectrometry MS and NMR Spectroscopy. The NMR spectrum of the G0.5 dendrimer presents distinct peaks corresponding to various proton environments within the molecule. A singlet at 3.68 ppm indicates the presence of methoxy protons in the half-generation dendrimers. Additionally, there are triplet peaks at 2.79 ppm and 2.48 ppm corresponding to the methylene-proton groups. Furthermore, the core protons of the dendrimer, associated with the central ethylene diamine core, are identified by a peak

at 2.54 ppm. ^{13}C NMR Carbon Nuclear Magnetic Resonance Spectrometry was also used, and a peak corresponding to the terminal ester groups of the G 0.5 was detected in the spectrum. Furthermore, a series of peaks between 32 and 55 ppm, attributed to numerous CH_2 groups, were prevalent in dendrimers with ester terminations. Figure 2.16.

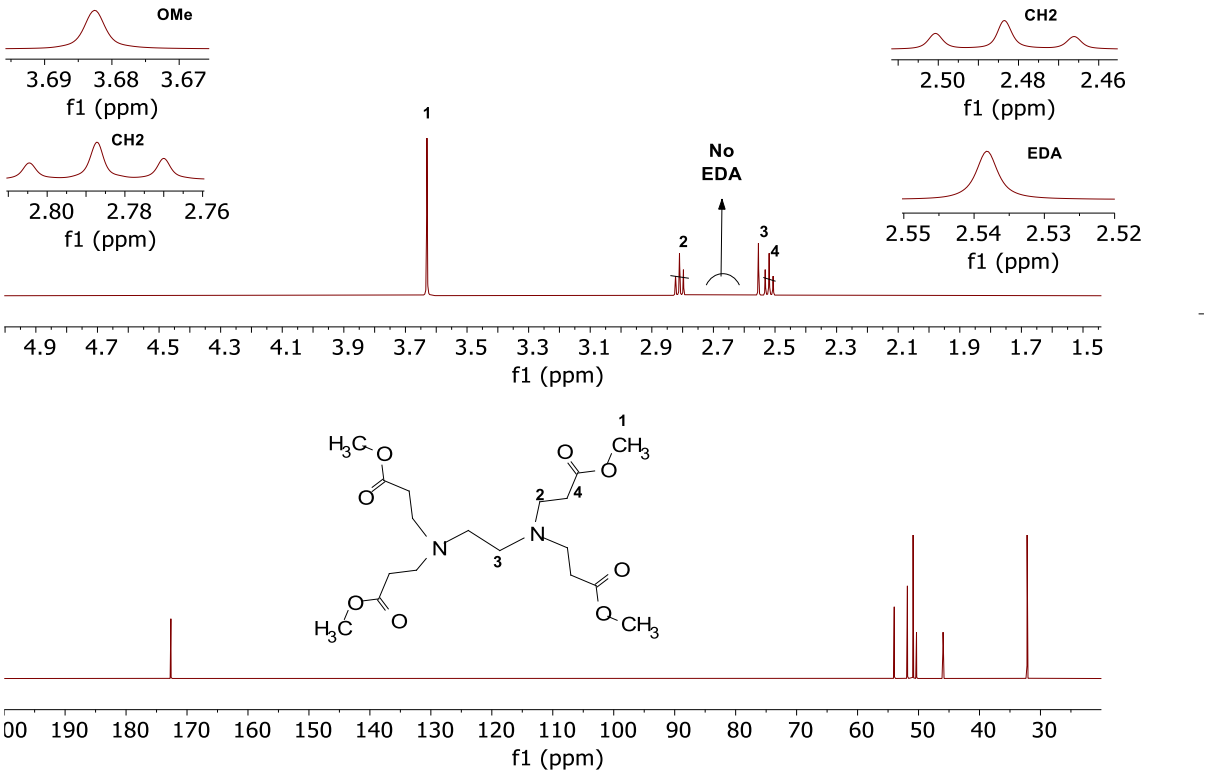

Figure 2.16: ^{1}H-^{13}C NMR spectrum for 0.5 G PAMAM dendrimer in CD3OD.

As dendrimers increase in size, changes in their ^{1}H NMR Proton Nuclear Magnetic Resonance Spectrometry are observed, reflecting the complexity of their structure. The peak corresponding to the terminal methoxy groups remains distinct around 4.83ppm, indicating the amide NH protons. The methoxy singlet remains a distinctive feature in the spectra of half-generation dendrimers, consistently appearing as a sharp singlet peak at 3.68 ppm which is a crucial indicator, confirming the structural integrity

of the half-generation. The monodisperse quality of dendrimers, reflecting their uniformity and exact molecular structure, is best characterised by mass spectrometry. Electron-Spray Mass Spectroscopy is utilised to analyse smaller-generation dendrimers below 1000, but MALDI-TOF-MS (Matrix-Assisted Laser Desorption-Ionization Time-of-Flight Mass Spectroscopy)[66] was better at generating ions for the larger dendrimers Table 2.1, summarises the presented mass measurements of half and full-generation dendrimers using the techniques mentioned above.

Table 2.1: PAMAM dendrimer generation molecular weights ranging from (G0.5 to G3.5) including terminal groups.

Dendrimer Generations	Chemical Formula	T-Group	M.W
0.5 G	$C_{18}H_{32}N_2O_8$	4	404
1.0 G	$C_{22}H_{48}N_{10}O_4$	4	516
1.5 G	$C_{54}H_{96}N_{10}O_{20}$	8	1205
2.0 G	$C_{62}H_{128}N_{26}O_{12}$	8	1429
2.5 G	$C_{126}H_{224}N_{26}O_{44}$	16	2804
3.0 G	$C_{142}H_{288}N_{58}O_{28}$	16	3256
3.5 G	$C_{270}H_{480}N_{58}O_{92}$	32	6004

2.3.1.6 The Synthesis of Hydroxyl Terminated Group PAMAM Dendrimer.

Although the amine and ester dendrimers could be dissolved in water, they were also charged. For example, some of the amines are protonated at neutral pH, and some of the esters can be hydrolysed to carboxylic acids (via dendrimer-assisted autocatalytic hydrolysis) [172]. Charged amines cause haemolysis by disrupting the red blood cell

membrane through interactions with lipids, proteins, or ionic gradients, leading to structural destabilization, osmotic imbalance, oxidative stress, and eventual cell rupture. These effects underline the importance of maintaining the delicate balance of membrane integrity and ionic homeostasis in RBCs [15,181]. Although this is not such a big problem for the ester, it is a significant tricky for the amines, which can cause haemolysis within the body. As such, we needed to convert the terminal groups to a neutral polar functionality. To do this, hydroxyl-terminal groups were added, by reacting the terminal ester groups of the half-generation dendrimers with Tris (hydroxymethyl)aminomethane. The reaction was like the amidation and involved dissolving the half-generation dendrimers in DMSO and adding this dropwise to a DMSO solution containing an excess of TRIS and anhydrous potassium carbonate. The reactions were then stirred at 50°C for 24 hours *Figure 2.17*.

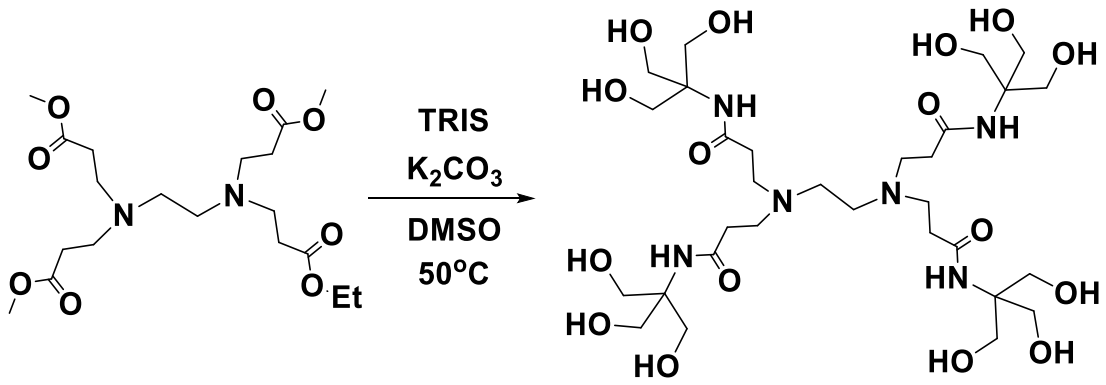

Figure 2.17: The Synthesis of hydroxyl-terminated group PAMAM dendrimers.

The TRIS NH_2 group is a nucleophile that can attack the ester terminal groups in the same way as described for the amidation step. However, the OH groups of the TRIS are not basic enough to enable the same intramolecular deprotonation step that occurs with EDA *Figure* 2.12. For this reason, it was necessary to add a specific base, as shown in *Figure* 2.18. Anhydrous conditions were required to prevent the base-

catalysed hydrolysis of the ester groups. If this occurred, then the successful addition of TRIS would not be possible.

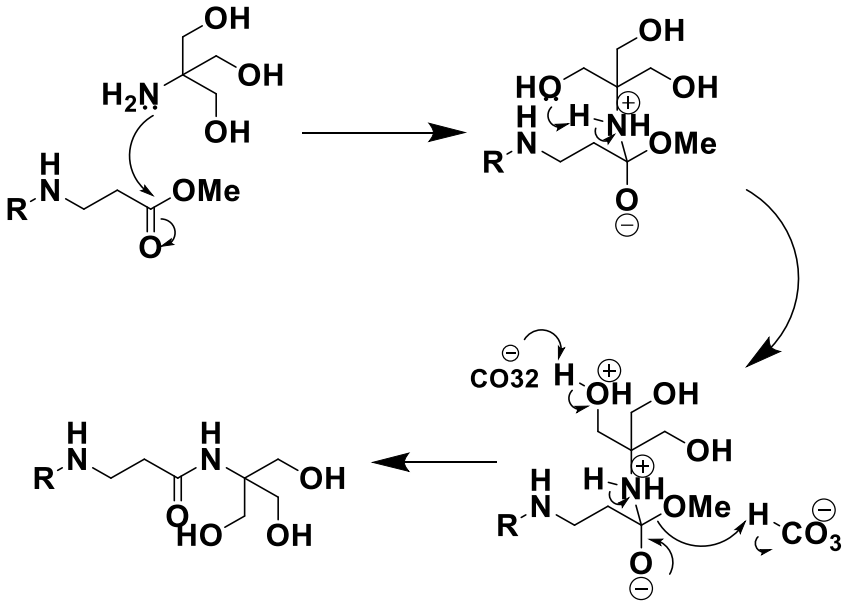

Figure 2.18: *Nucleophilic mechanism tackles ester-terminated group PAMAM dendrimer.*

At the end of the reaction, the mixture was cooled at room temperature and filtered to remove any remaining solid reagents. The solvent was then concentrated via vacuum distillation, with the temperature being maintained at less than 50°C (to prevent retro Michael addition). The product at this stage was a cloudy oil, which was purified by dissolving it in a minimal quantity of water and precipitation using acetone. This purification step was performed twice before being transferred to a vacuum oven, for drying overnight 40°C. The final product was a pale-yellow hygroscopic paste, that immediately turned to an oil upon exposure to air. This protocol was effectively utilized to synthesize OH-terminated dendrimers up to G3.5, with 32 OH end groups.

2.3.1.7 Characterisation of PAMAM Dendrimers OH Terminated Groups.

The characterization of the PAMAM dendrimers OH was carried out using NMR spectroscopy. Confirmation of successful transformation was initially carried out by comparing the ^{1}H NMR spectra of the starting material with the OH dendrimer. to the ^{1}H NMR spectrum of the product no longer possessed the methoxy peak at 3.74 ppm. This was replaced by a new peak at 3.63 ppm, which corresponded to the protons of methylene adjacent to terminated hydroxyl groups. As expected, the integral of the methylene peak was significantly larger than the methoxy peak it replaced. Overall, the ^{1}H data indicates a successful conversion of the terminal groups *Figure* 2.19.

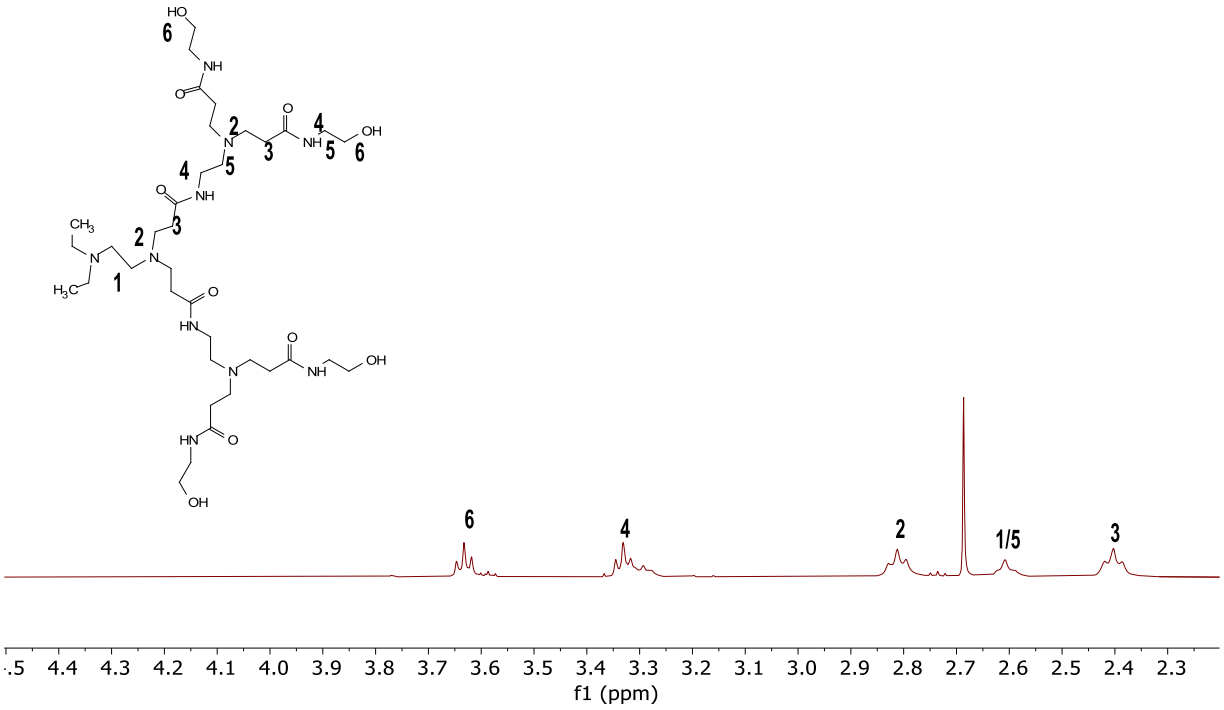

Figure 2.19: The ^{1}H-^{13}C NMR spectrum for G 0.5 dendrimer PAMAM in CD3OD.

This contrasts with the singlet typically observed, implying a complex chemical shift for the NCH_2CH_2N proton 4 in Figure 2.19 due to the proximity and overlap of these two peaks. In the ^{13}C NMR spectrum, a peak at 172 confirmed the presence of the new external amide=O, with a related peak at 173 for the internal amide. The absence of the CH_3 group peak at 52 ppm confirms the successful addition of the ethanolamine groups. Additionally, peaks at 62.0 and 61.5 ppm, were assigned to the carbons closest to the new terminal hydroxyl groups. Further validation was achieved using mass spectrometry, as shown in Table 2.2.

Table 2.2: Hydroxyl-terminated groups PAMAM dendrimer including molecular weights ranging from (G0.5 to G3.5).

Dendrimer Gen	Chemical Formula	OH Group	M-W
G-0.5OH	$C_{18}H_{32}N_2O_8$	4	520
G-1.5OH	$C_{54}H_{96}N_{10}O_{20}$	8	1438
G-2.5OH	$C_{126}H_{224}N_{26}O_{44}$	16	3272
G-3.5OH	$C_{270}H_{480}N_{58}O_{92}$	32	6912

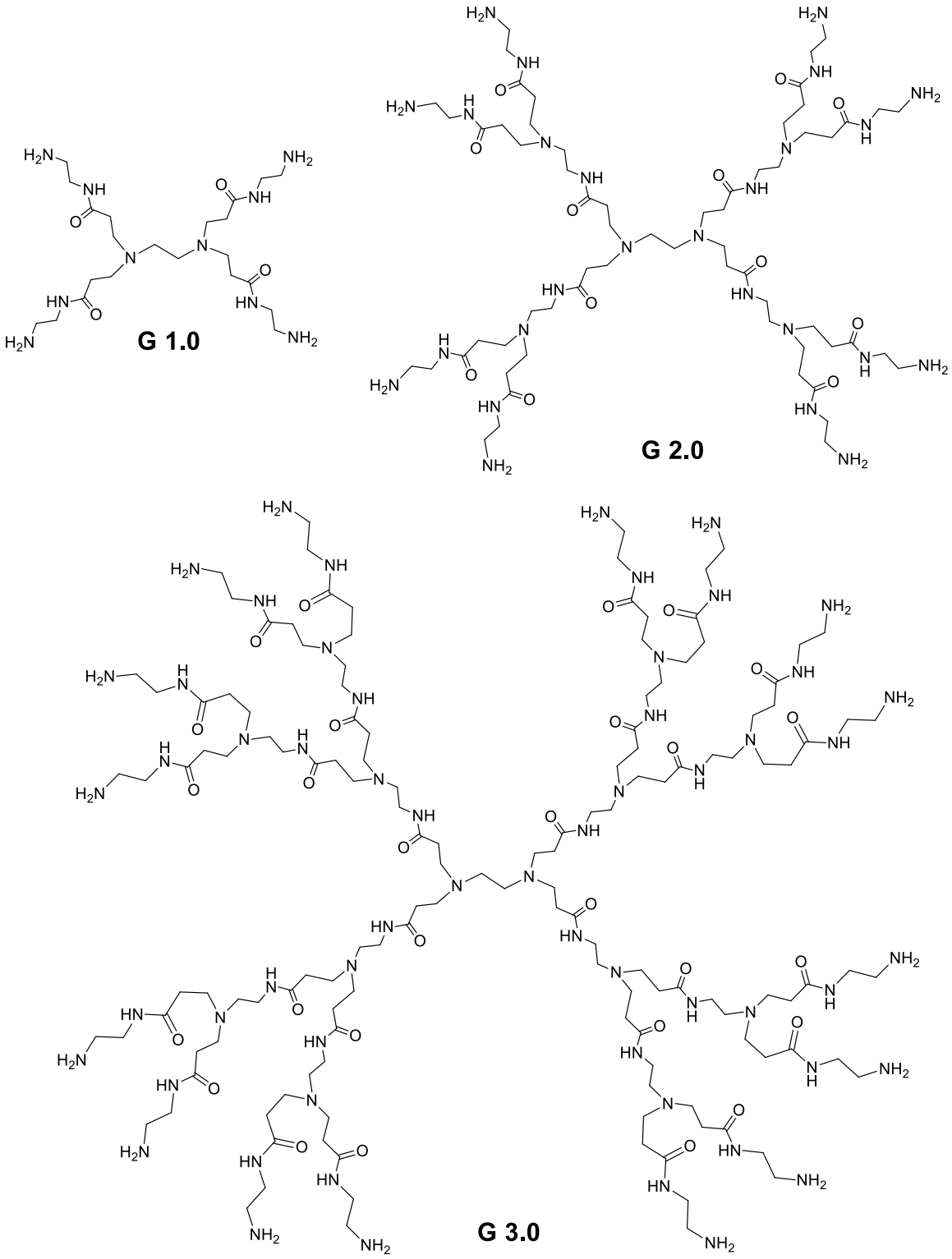

Figure 2.20 The structure of different generations of the whole PAMAM dendrimers.

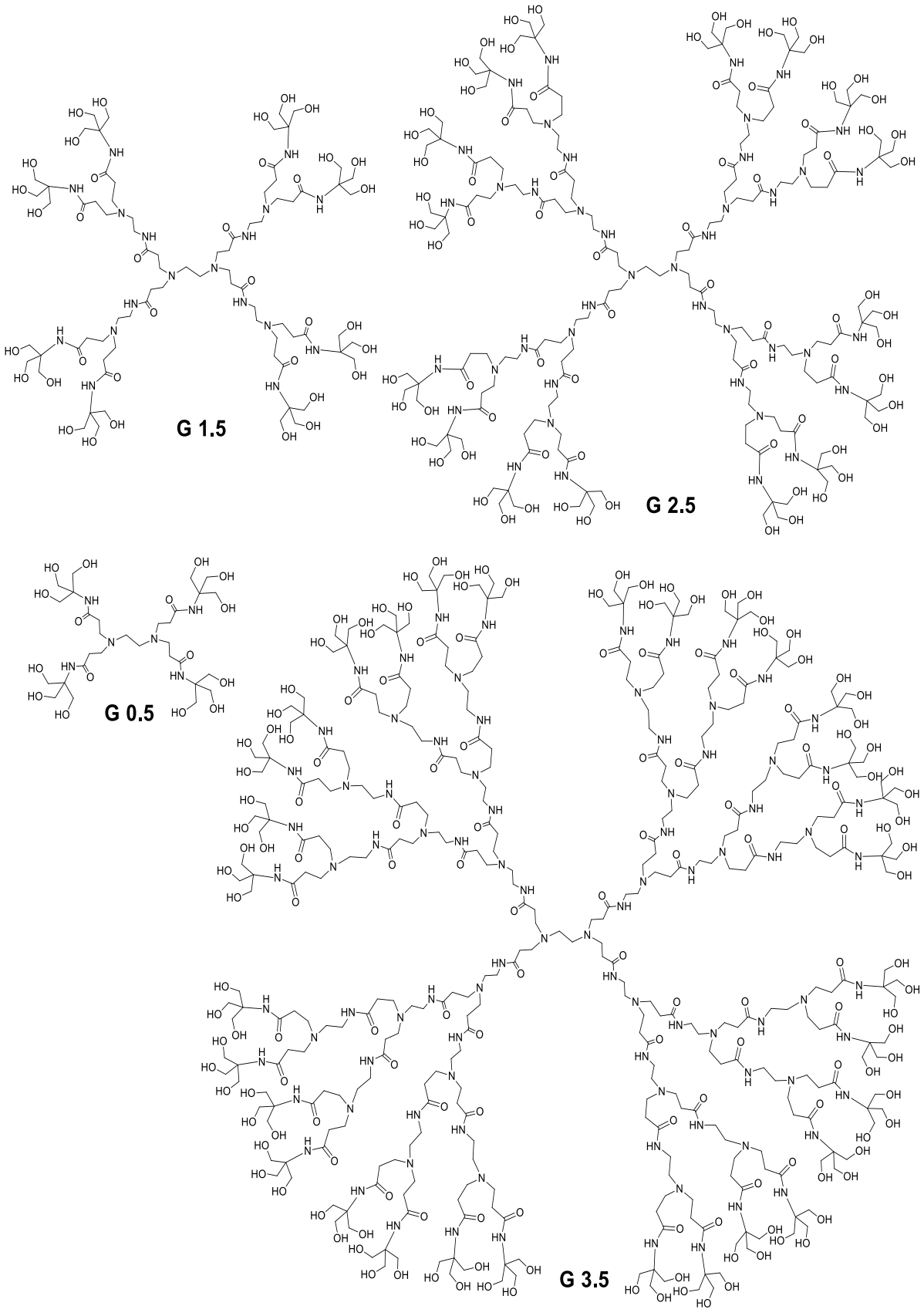

Figure 2.21: The structure of different generations of the neutral PAMAM dendrimers.

2.3.2 The Synthesis of Porphyrins for Encapsulation Within Dendrimers and For Their Oxygen Binding Studies.

Porphyrin is one of the essential components found in natural biological systems. Haemoglobin and chlorophyll are prime examples of these molecules. A unique feature of porphyrins that interests chemists is their ability to recognise molecular structures[181]. This property can be designed to specific needs by modifying its structure and surroundings, as well as selecting an appropriate metal for the porphyrin core. The metal chosen significantly influences the molecular recognition abilities of the porphyrin, which can be used in various fields of chemistry and biology for diverse applications [182].

The primary objective of this chapter is to determine the optimum functionality around the porphyrin and the best metal for binding and encapsulation within a dendrimer host. Specifically, to obtain the best porphyrin for integration into dendritic polymers, to achieve optimum and reversible oxygen binding. We first decided to investigate the simplest porphyrin, the symmetrical tetraphenyl porphyrin TPP.

Tetraphenyl porphyrin TPP is a synthetic porphyrin derivative characterized by its simple chemical structure, featuring a nitrogen-containing macrocyclic porphyrin core with four phenyl groups attached. Its synthesis is also quite easy, typically through a straightforward condensation reaction between pyrrole and benzaldehyde, allowing for high-purity production [183]. TPP can absorb visible light, making it useful in several photochemical applications. TPP's ability to coordinate with metal ions and its stable macrocyclic structure enables it to mimic the catalytic functions of natural heme. Therefore, studying simple TPPs as a model compound, offers insights into the photophysical and coordination characteristics, thereby being a significant compound in both research and practical applications.

TPP is a macrocycle containing 22 π-electrons. These electrons are localised within an aromatic ring, contributing significantly to the molecule's stability. Furthermore, if TPP coordinates with a metal ion, it can change its electronic structure, resulting in obvious changes to its optical properties. The spectroscopic properties of TPP porphyrins are distinctive, typified by their strong UV/Visible absorption, The corresponding UV spectrum is marked by a Soret band around 417 nm. In addition, there are four smaller Q bands located around 512 nm, 550 nm, 585 nm, and 640 nm. FTPP porphyrins are also known for their emission at specific wavelengths. Overall, these spectroscopic properties are useful markers that can be used to monitor successful encapsulation within various systems - including dendrimers [184].

2.3.2.1 The Synthesis of Symmetrical Porphyrins.

Iron-metalated porphyrins are pivotal in various biomolecules, including haems, which are integral for oxygen binding in red blood cells. However, before studying iron porphyrins, we will investigate simpler zinc systems, as these are much easier to synthesise, characterise and study. For example, iron porphyrins are paramagnetic and therefore difficult to characterise and study by NMR. A corresponding zinc system will allow us to make an initial assessment regarding the contribution of metal-to-ligand interactions on porphyrin encapsulation [182].

Porphyrins, both natural and synthetic, are compounds characterised by a macrocyclic structure consisting of four pyrrole units connected by methine bridges. The alterations at the meso-positions of the porphyrin ring result in the formation of porphyrins with symmetric structures as shown in *Figure*: 2.22. Metal complexes of porphyrins are created by replacing the protons attached to the nitrogen atoms in the ring with metal

ions. For metals with higher valency, the metal ion is additionally coordinated to extra ligands, which allows more extended structures and complexes to be synthesised [55].

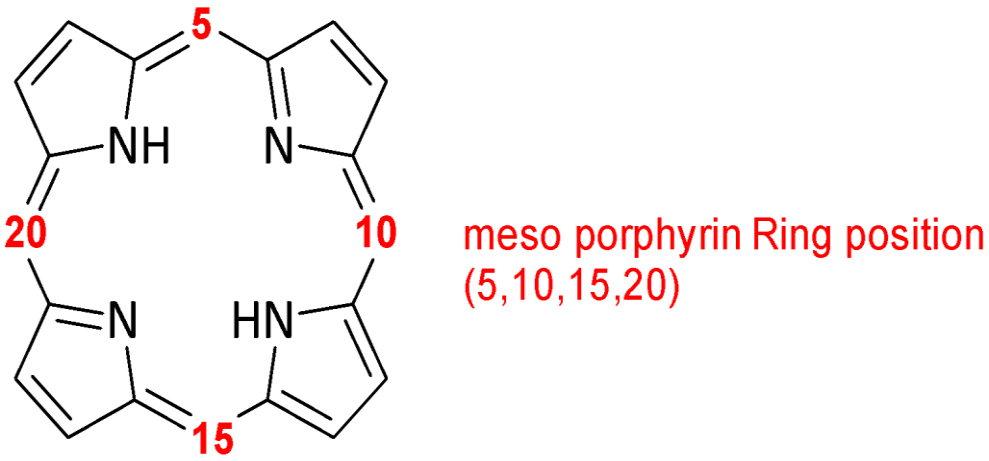

Figure 2.22: porphyrin Structure atom, numbering, and notation.

The first reliable synthesis of porphyrin was reported by Rothemund (1936). The simple method involves a condensation reaction between benzaldehyde and pyrrole at high temperatures. During this process, an intermediate porphyrinogen is formed.

Porphyrinogens are the reduced, colourless precursors to porphyrins, which are brightly coloured, cyclic compounds that play a crucial role in a variety of biological processes, such as oxygen transport (haemoglobin), electron transfer (cytochromes), and photosynthesis (chlorophyll). The transition from a porphyrinogen to a porphyrin involves the oxidation of the porphyrinogen, which typically has four pyrrolic rings linked via methylene bridges (CH_2) in a more saturated state compared to the conjugated system of porphyrins [185].

The synthesis of porphyrins typically begins with the condensation of pyrrole with an aldehyde, such as formaldehyde, to create a series of interconnected pyrrolic rings that lead to a structure closely resembling porphyrinogen [182]. This intermediate is formed through a sequence of steps that construct the tetrapyrrolic framework, utilizing

catalysts or specific conditions to ensure the correct linking of the pyrrole units, resulting in a structure that is not yet fully aromatic and remains colourless. The transition to a porphyrin is achieved through the oxidation of porphyrinogen, where the methylene bridges (-CH_2-) between the pyrrole rings are converted into methine bridges (-CH-), thereby completing the conjugated porphyrin ring system and producing the characteristic coloured, aromatic porphyrin compound [55]. Additionally, many biologically relevant porphyrins include a central metal ion and the insertion of this metal (such as iron in heme or magnesium in chlorophyll) into the porphyrin ring can be carried out at various stages of the synthesis process, depending on the desired outcome and the specific synthesis route employed *Figure* 2.23.

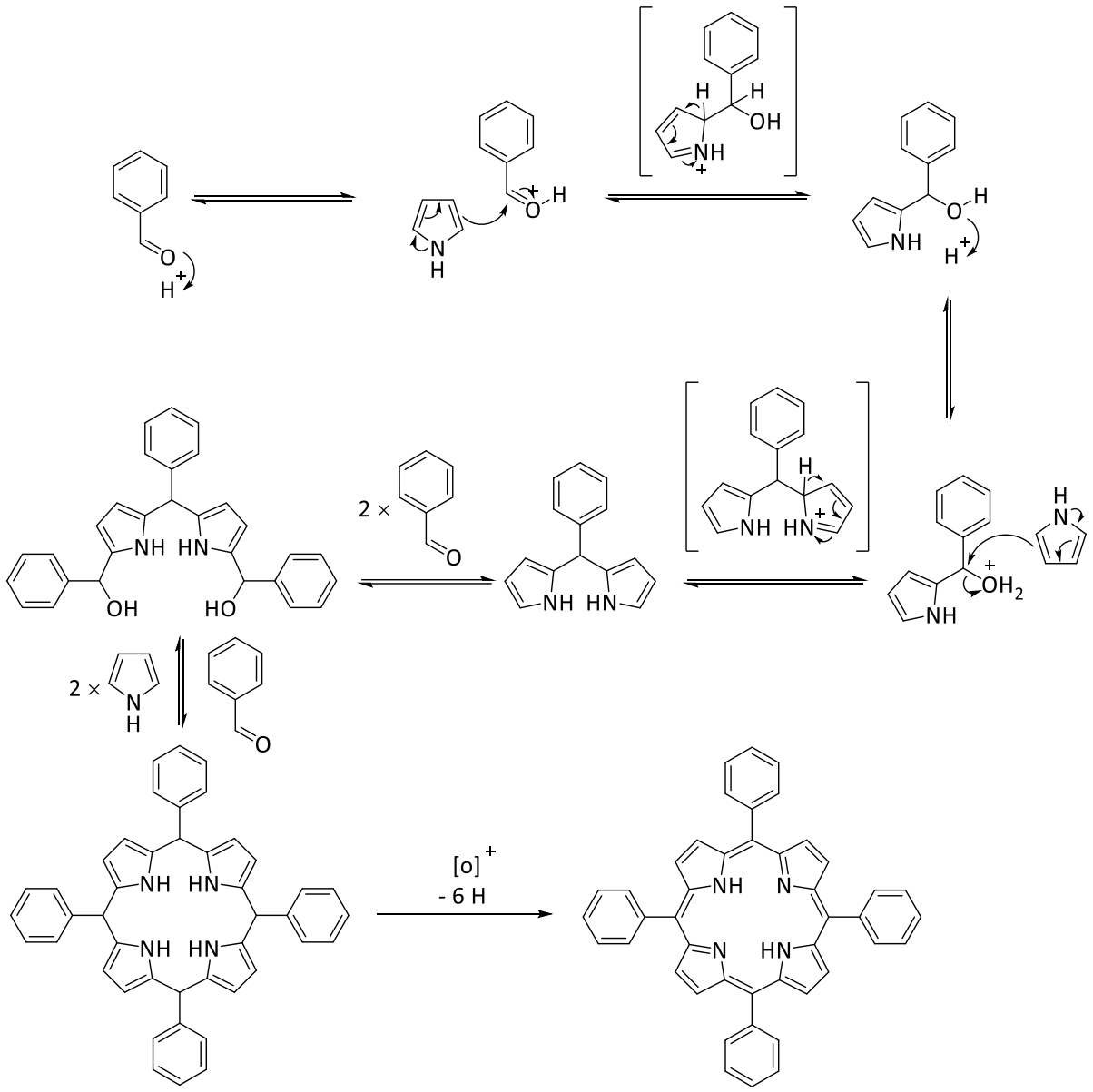

Scheme 2.23: porphyrin formation Mechanism

To convert it into porphyrin, an oxidation step is required, which typically occurs spontaneously when exposed to air. The easy oxidation of the porphyrinogen and the stability of the porphyrin is attributed to its aromatic nature, as porphyrins conform to Huckel's rule of aromaticity [184].

2.3.2.2 The Synthesis of Tetraphenyl porphyrin TPP.

By its simple synthesis, we decided to test Tetraphenyl porphyrin TPP as our first porphyrin system for encapsulation within our dendrimer systems. TPP was synthesised by adding pyrrole to a solution of benzaldehyde in propionic acid and refluxing for 30 minutes. The product was isolated through filtration and purified by sequential washing with hot methanol and then hot water to remove impurities from the final TPP product as shown in *Figure* 2.24.

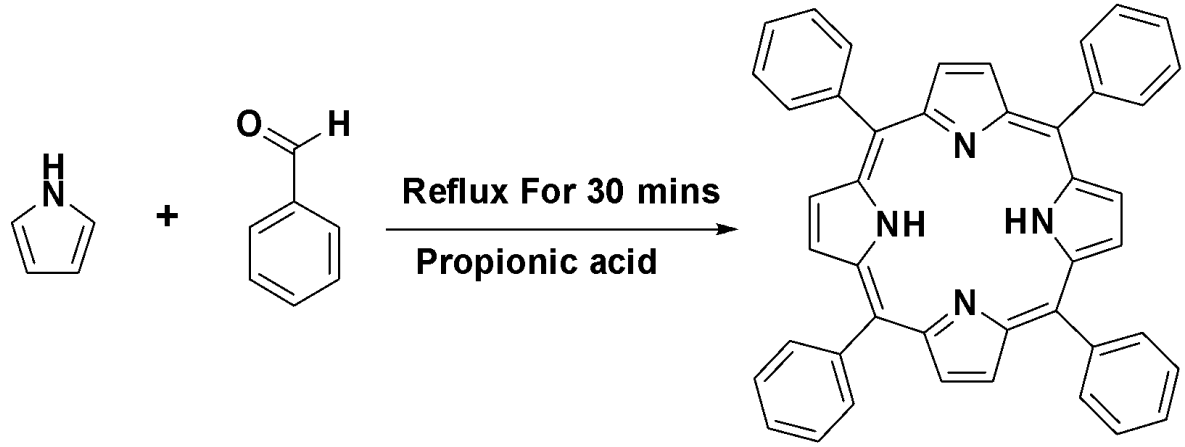

Figure 2.24: Synthesis of tetraphenyl porphyrin (TPP).

The NMR spectra revealed a highly shielded peak at -2.90 ppm, which is characteristic of the NH inner protons of the TPP molecule. This shielding effect is a result of the protons being located within the centre of the aromatic porphyrin ring, thereby experiencing an induced magnetic field that opposes the external field (the NMR field). Additionally, the spectra displayed three distinct peaks: one at 8.94 ppm corresponding to eight β-pyrrolic protons, another at 9.70 ppm for eight protons of MH+ and a third peak at 7.05 ppm associated with the twelve ortho and para-aromatic phenyl protons. UV-Vi's spectroscopy further corroborated the successful synthesis of TPP, as evidenced by the presence of a Soret band at 417 nm, accompanied by four

Q bands located at 512 nm, 550 nm, 585 nm, and 640 nm. Complementing these findings, Electrospray Ionization Mass Spectrometry ES-MS exhibited a molecular ion peak MH^+ at a mass of 615, aligning with the expected molecular weight of TPP. Overall, the combined spectroscopic evidence confirms the successful synthesis of the tetraphenyl porphyrin.

TPP presents solubility challenges for encapsulation due to its hydrophobic nature, leading to poor solubility in aqueous environments and a preference for organic solvents, which may not be suitable for biological applications. TPP's tendency to aggregate can further complicate encapsulation, as can its interactions with encapsulating materials and sensitivity to pH and temperature.

The Twyman research group has highlighted several challenges in encapsulating highly hydrophobic drugs[186], such as low encapsulation efficiency due to poor aqueous solubility, the tendency of these drugs to aggregate or precipitate, and unfavourable interactions with encapsulating materials. These issues can lead to altered release profiles, destabilization of carrier systems, and reduced biological availability. To address these challenges, the group has explored solutions like using surfactants, co-solvents, and lipophilic carriers, as well as modifying the drug molecules themselves. A significant strategy mentioned is the inclusion of a metal within the encapsulation process, which introduces the potential for additional interactions between the metal and internal amines. This approach can enhance the level of encapsulation compared to using the free base TPP, by fostering more stable and specific interactions that can improve the efficiency and stability of the encapsulation process, potentially overcoming the inherent difficulties in encapsulating hydrophobic compounds.

2.3.2.3 The Synthesis of Tetraphenyl Porphyrin, Zinc complex ZnTPP.

To improve the encapsulation efficiency of TPP in dendrimers, zinc was introduced to form Zinc Tetraphenyl Porphyrin ZnTPP. The use of metallated porphyrin should result in an enhanced loading capacity through the additional and strong coordination between the metal and the internal nitrogen within the dendrimer. The strategy to use zinc rather than iron (the desired metal for our intended application), was since Fe is paramagnetic. This would make characterisation and study difficult by NMR. On the other hand, zinc complexes are easy to synthesise and can be studied by NMR. As such, zinc porphyrins would be used as simple “model compounds" for the desired iron porphyrins, enabling us to easily study and quantify any enhancements in loading.

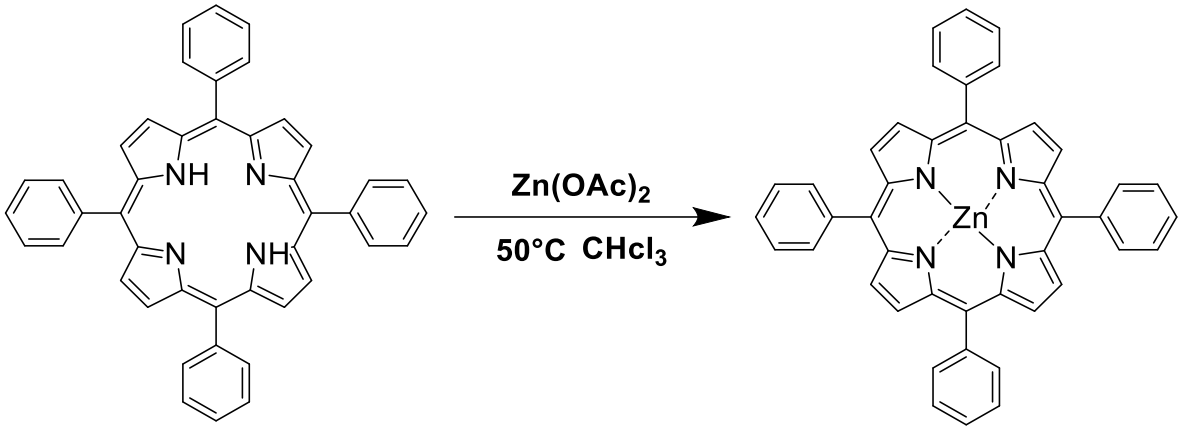

Figure: 2.25 Synthesis of tetraphenyl porphyrin with Zinc (ZnTPP).

Tetraphenyl porphyrin Zinc ZnTPP was successfully synthesised by reacting TPP with zinc acetate in chloroform for an hour as shown in *Figure* 2.25, followed by purification through filtration and rotary evaporation, resulting in a purple-coloured compound. The analysis confirmed the insertion of zinc into TPP For example, ^{1}H NMR spectroscopy showed the absence of the inner porphyrin protons' peak at -2.90 ppm, also the spectra displayed distinct peaks at 8.98 ppm, corresponding to β-pyrrolic protons, and two other peaks at 7.18 ppm and 6.75 ppm, corresponding to the ortho and para-

aromatic phenyl protons. Mass Spectroscopy ES-MS revealed a molecular ion peak at 673, consistent with ZnTPP's molecular weight, and UV-visible spectroscopy indicated the usual Soret band at 423 nm. However, this time, there were only two Q bands, at 550 nm, and 640 nm, reflecting the structural changes after zinc insertion as illustrated in *Figure: 2.26*.

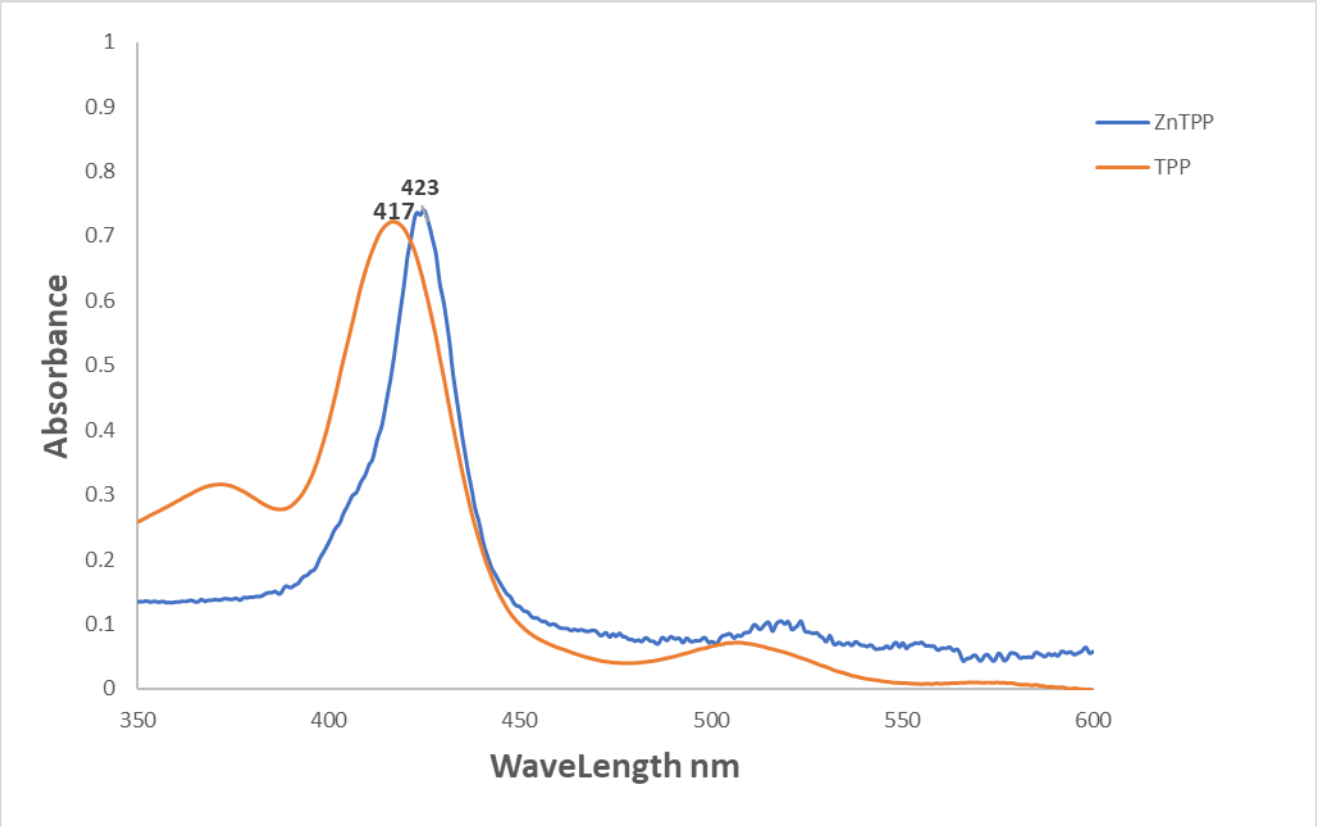

Figure: 2.26; UV- spectroscopy of TPP and ZnTPP in CD_3OD.

TPP was chosen for the encapsulation study as it is a straightforward synthesis and completely insoluble in water. As such, it was expected that the loading of TPP would be low due to its hydrophobic nature, which tends to resist entry into the aqueous environment within the dendrimer cavity.

2.3.2.4 Synthesis of tetraphenyl Porphyrin with Fe^{III} complex $Fe^{III}TPP$.

This step involved dissolving TPP in anhydrous tetrahydrofuran. Afterwards, 2,6-lutidine and ($FeCl_2$) Iron II Chloride were added to the solution and refluxed for four hours. The purpose of reflux was to ensure the complete insertion of iron into the porphyrin core *Figure*: 2.27.

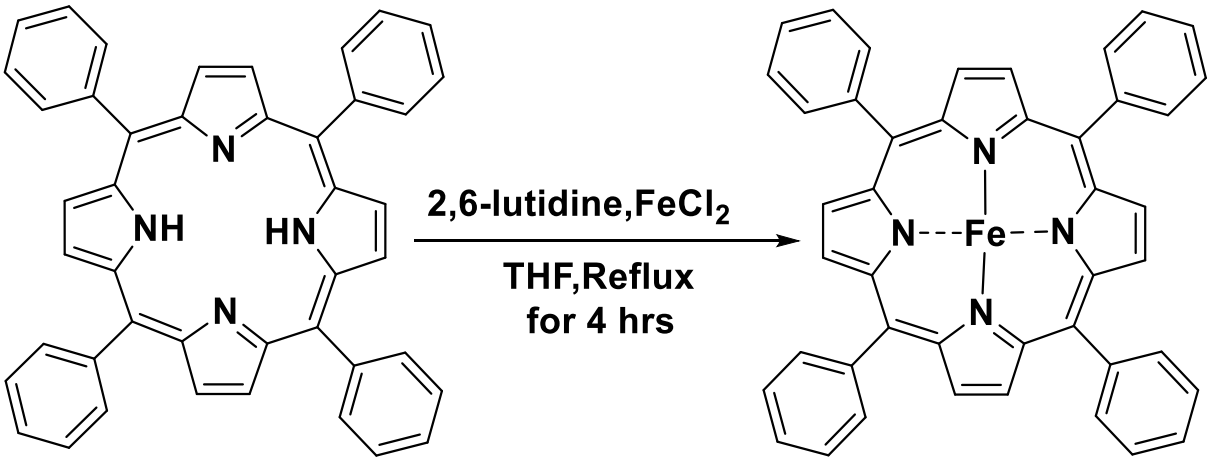

Figure: 2.27: Synthesis of tetraphenyl porphyrin with Fe^{III} complex $Fe^{III}TPP$.

Afterwards, the mixture was allowed to cool to room temperature and stirred for 30 min to reduce the Fe^{II} to the Fe^{III} complex. The solvent was removed using rotary evaporation. The product was then fully washed with 1M HCL. Furthermore, column chromatography was used for purification, Mass spectrometry exhibits a peak at 670, which corresponds to the MH^+ ion. UV-V spectroscopy further confirmed the success of iron insertion, as it revealed a distinct absorption with the Soret band at 417 nm with two Q bands at 550 nm, and 640 nm, reflecting the structural changes after Fe^{III} insertion.

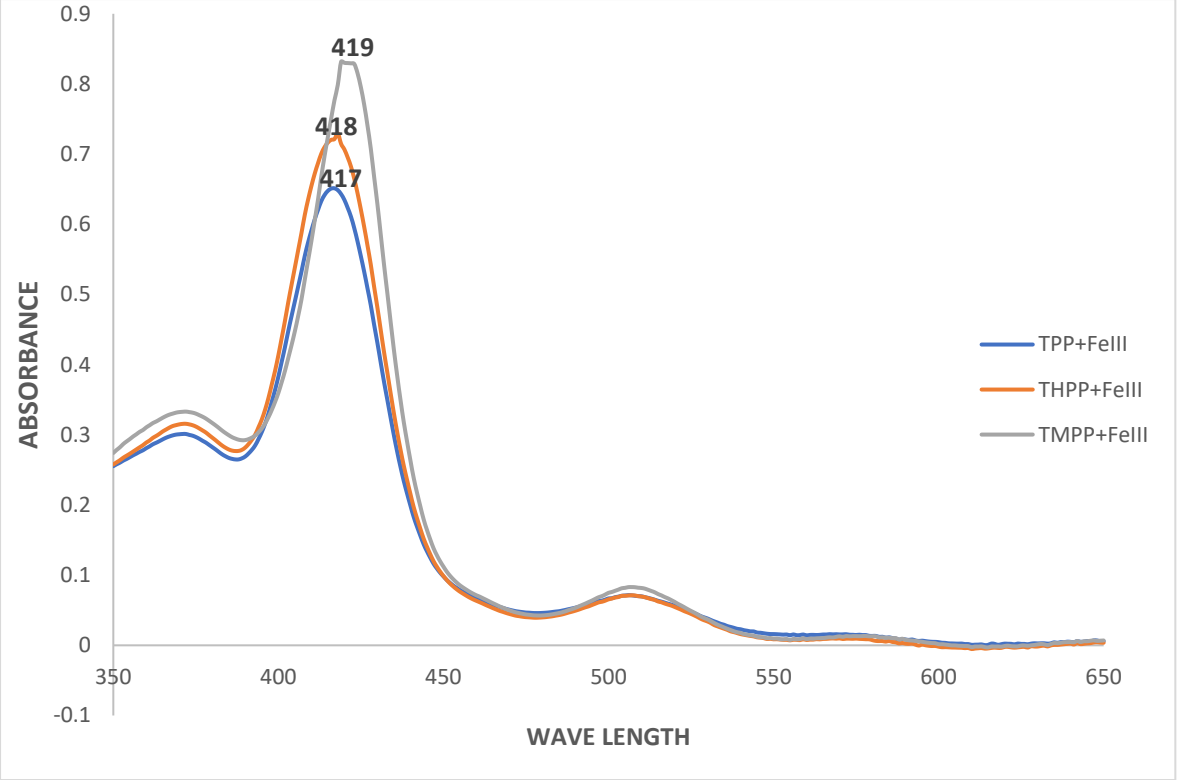

Figure: 2.28; UV- spectroscopy of TPP, TMPP and THPP, Fe^{III} complex in CD_3OD.

The following step involved encapsulating TPP Fe^{III} within the Hydroxyl-terminated PAMAM dendrimers.

2.3.2.5 The Encapsulation process of $TPP^{-}Fe^{III}$ within the PAMAM Dendrimers Hydroxyl Terminated Group.

Beer-Lambert analysis was employed to determine the number of encapsulated porphyrins within the dendrimers that were studied. The encapsulation of Fe^{III}TPP was realized by dissolving the excess amount of porphyrin in methanol MeOH as well as the PAMAM dendrimers separately, resulting in a concentration of $2x10^{-6}$ M. The organic porphyrin solution was then introduced into various aqueous dendrimer solutions involving''8 OH, 16 OH, and 32 OH'' terminated groups of PAMAM dendrimer generations. All mixtures were allowed to stir, forming the porphyrin-dendrimer

complexes. The organic solvent was then removed using rotary evaporation, and an equivalent amount of 7.5 pH phosphate buffer was added. The crude mixture was then filtered to eliminate any unreacted components. Analysis via UV-Vi's spectroscopy revealed the presence of porphyrins, characterized by the intense Soret band at 417 nm and the two weak Q bands at 512 nm and 585 nm Figure: 2.28. The encapsulated porphyrin concentrations within each generation are summarised in Table 2.3.

Table 2.3: Final concentrations of TPP-Fe^{III} encapsulation with the Hydroxyl-terminated PAMAM dendrimer group at 2 x 10^{-6}.

OH, Group	PAMAM conc /M.	Loading	Final conc of Fe^{III} TPP/M
8	2 x 10^{-6}	0.97	9.7 x 10^{-8}
16	2 x 10^{-6}	1.23	1.2 x 10^{-7}
32	2 x 10^{-6}	1.82	1.8 x 10^{-7}

The observed data highlights a reduced efficiency in loading TPP into the dendrimers compared to the THPP Fe^{III} dendrimer complexes, attributable to the hydrophobic nature of TPP. This characteristic restricts the porphyrin's integration into the dendrimer structure. Notably, the dendrimer variant with 32 OH terminal groups demonstrated the highest porphyrin loading capacity. However, the encapsulation efficiency stood at roughly 10%, indicating that out of the available 32 OH-terminated dendrimer molecules, only about three managed to encapsulate a porphyrin unit. This trend was more pronounced in smaller dendrimers, which showed even lower loading capacities. Consequently, it is logical to infer that each dendrimer molecule is likely to

host no more than a single unit of porphyrin, underscoring the limitations imposed by the dendrimer's physical and chemical properties on porphyrin encapsulation.

Due to the hydrophobic nature, large and rigid structure, and its tendency to aggregate which led to the low encapsulation efficiency of TPP within the polymer. These factors lead to poor compatibility and interaction with the dendrimer. Furthermore, the dendrimer’s morphology, including its porosity and structural density, may not be favourable to incorporating bulky TPP molecules. The alternative solvents during the encapsulation process can also affect the distribution and incorporation of TPP if they do not equally dissolve both the polymer and TPP, leading to phase separation. Moreover, optimizing encapsulation efficiency may require selecting compatible polymers, adjusting the encapsulation conditions, and potentially modifying TPP or the polymer to improve their compatibility and interaction.

2.3.2.6 The Synthesis of Tetrakis3,5-(Dimethoxyphenyl) Porphyrin TDMPP.

The synthesis of Tetrakis (3,5-methoxyphenyl) porphyrin TDMPP was conducted in two steps rather than one-step synthesis, the two steps process, the aldehyde group in benzaldehyde derivatives is essential for the condensation with pyrrole to form the porphyrin structure. However, the presence of OH groups in the starting material can influence the reactivity and selectivity of this condensation process. The OH groups can participate in unwanted side reactions or lead to the formation of different by-products, complicating the synthesis. As such, these OH groups would need to be protected. As such, Dimethoxybenzaldehyde was used as the reactive aldehyde. Dimethoxybenzaldehyde is more stable and less reactive than its hydroxy counterpart.

This stability allows for better control over the condensation process, reducing the likelihood of side reactions and improving the yield and purity of the porphyrin product. The methoxy groups can then be removed using boron tribromide as the demethylating agent *Figure* 2.29.

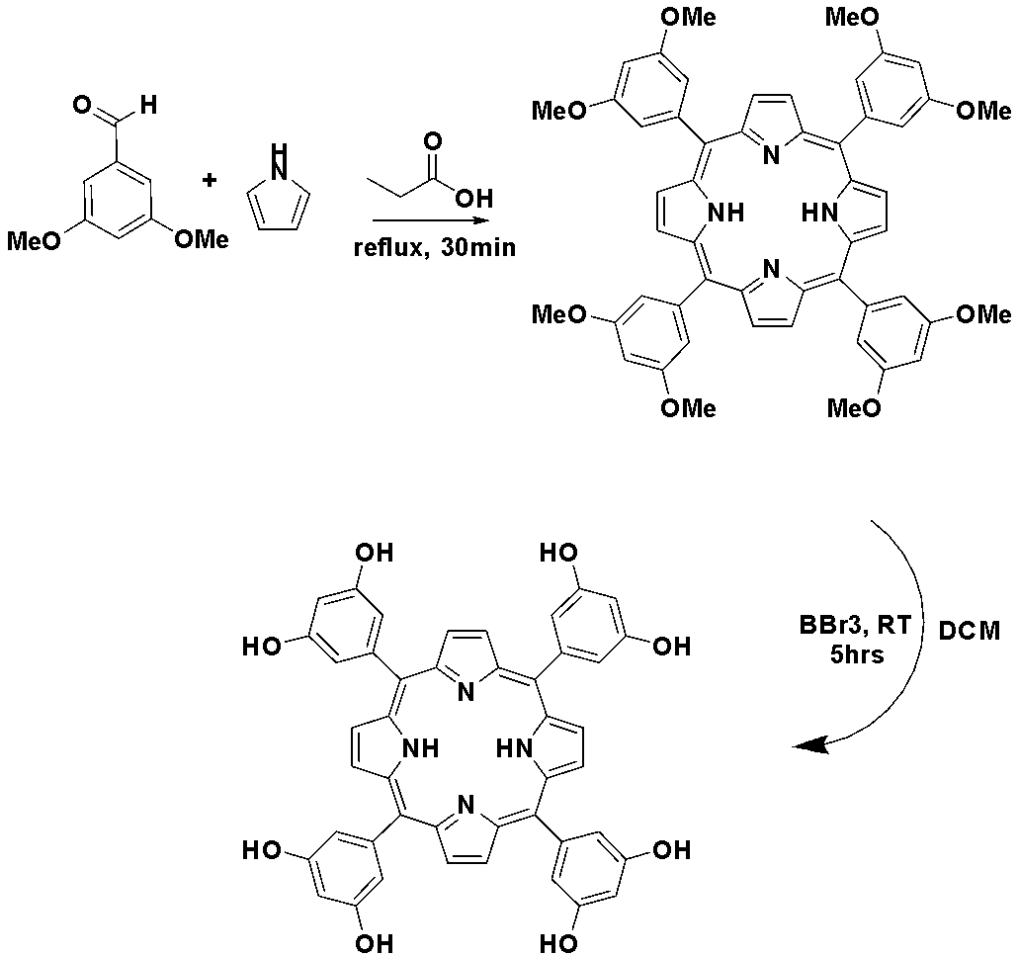

Figure: 2.29 Synthesis of Tetrakis 3,5 (Dihydroxyphenyl Porphyrin) TDHPP.

The dimethoxy porphyrin was synthesised using the same method described above for TPP. Equimolar quantities of tetrakis (3,5-dimethoxybenzaldehyde) TDMPP and pyrrole were combined and subjected to reflux for a duration of 30 minutes. After workup, the successful formation of TDMPP was confirmed through UV/vis absorption spectroscopy. The spectrum of TDMPP exhibited the same characteristic porphyrin

features as described for TPP. This included a Soret band at 419 nm and four Q-bands at 512 nm, 550 nm, 576 nm, and 650 nm. Further confirmation of the methoxy porphyrin structure was obtained through mass spectrometric analysis. The analysis showed a molecular ion peak M^+ at a mass of 882, which is consistent with the expected molecular weight of TDMPP. Additionally, the ^1H NMR spectrum provided further insights into the structure of TDMPP, displaying a large singlet at 3.94 ppm(M^+) corresponding to the methoxy protons and, a singlet peak at 8.95 ppm (MH^+), corresponding to the β-pyrrolic protons, which are characteristic of the porphyrin ring structure. Peaks at 7.38 ppm and 6.99 ppm, are attributed to the ortho- and para-aromatic phenolic protons, respectively, indicating the positions of these protons in the aromatic ring system of the molecule and a peak at -2.99 ppm that is attributed to the NH protons of the porphyrin ring. These spectral features corroborate the successful synthesis and structural integrity of the protected TDMPP. The next step involved the methoxy-protecting groups, to generate the desired hydroxy porphyrin.

2.3.2.7 The Synthesis of Tetrakis-3,5 Dihydroxyphenyl Porphyrin TDHPP.

The preparation of Tetrakis-3,5 Dihydroxyphenyl Porphyrin TDHPP from tetrakis (3,5-dimethoxybenzaldehyde) TDMPP involved a specific demethylation procedure. Initially, TDMPP was dissolved in anhydrous dichloromethane, and the solution was stirred under a nitrogen atmosphere for 10 minutes. Boron-tribromide BBr_3, a potent Lewis acid, was then added dropwise to the solution. This addition caused the green solution, indicating the initiation of the reaction.

The mechanism of this reaction, as illustrated in Scheme: 2.29 above involves the empty orbital of BBr_3 interacting with the lone pair electrons on the methoxy oxygen atoms. This interaction leads to the discharge of a bromide ion, which subsequently attacks the methyl group, resulting in the release of the good-leaving group methyl bromide. The reaction then proceeds through a hydrolysis step, where hydroxyl groups replace the bromide ions. The boron is simultaneously removed as boric acid, yielding the deprotected TDHPP product along with hydrogen bromide.

The reaction was conducted at room temperature, with continuous stirring for approximately 5 hours. The mixture was slowly quenched with water to ensure the reaction was complete and to neutralise any excess boron tribromide by converting it to boric acid H3BO3 an hydrobromic acid HBr, which are less reactive. The slow addition of water is crucial to prevent excessive heat, potentially leading to hazardous conditions. The acidic reaction mixture was then neutralised using a sodium hydrogen carbonate solution and extracted using ethyl acetate. An obvious change in solubility properties initially indicated the crude product's successful synthesis. The starting material TDMPP was soluble in dichloromethane, whereas the final product TDHPP was not. The successful transformation of Tetrakis (3,5-methoxyphenyl)-porphyrin TDMPP to Tetrahydroxy phenyl porphyrin TDHPP was confirmed through ^1H spectroscopic analysis and mass spectroscopy. The ^1H NMR spectrum provided evidence of the demethylation process. This is indicated by the methoxide proton resonance no longer being detectable, which was previously observed at 3.94 ppm in the TDMPP spectrum. The absence of this peak in the TDHPP spectrum signifies the removal of the methoxy groups from the porphyrin ring. The UV absorption spectra of THPP revealed the presence of the Soret band at 418 nm and four distinct Q bands were observed at 512 nm, 550 nm, 576 nm, and 650 nm as shown in Figure; 2.30.

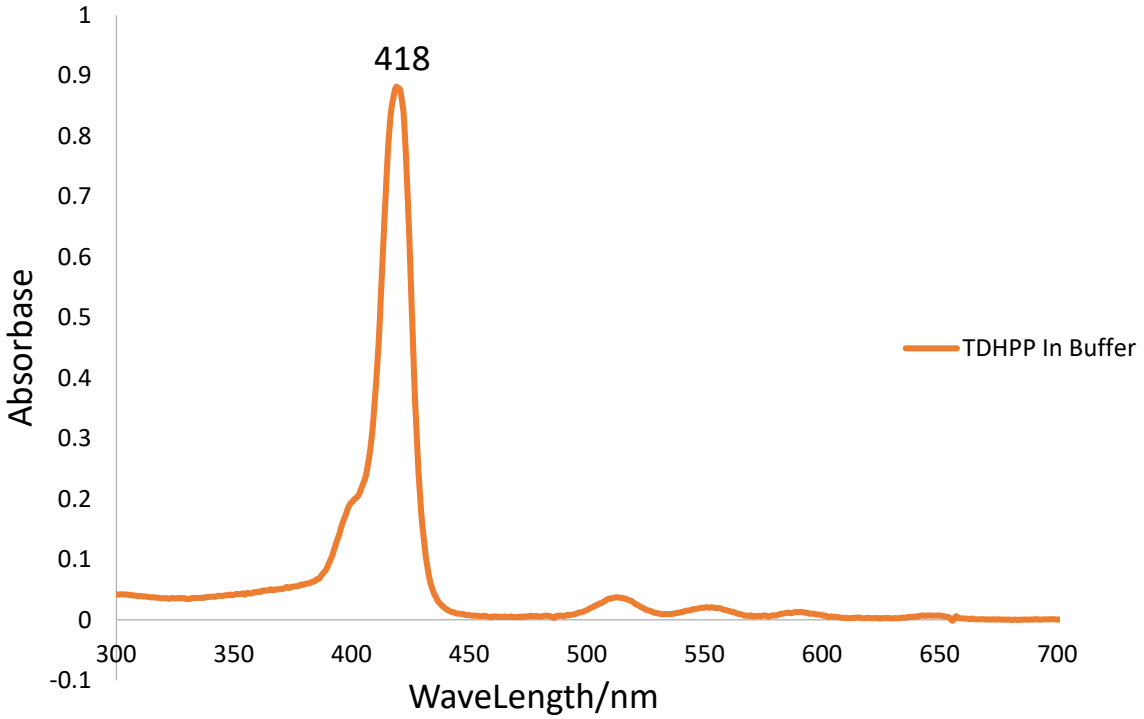

Figure: 2.30; UV- spectroscopy of TDHPP.

TDHPP structure, characterized by the addition of hydroxyl groups, provides polar sites that can enhance solubility and facilitate better interaction with encapsulating agents, such as dendrimers. These OH groups can form hydrogen bonds with the amine groups present in the dendrimer structure, leading to a more stable and efficient encapsulation compared to TPP, which lacks these polar functionalities. The presence of hydroxyl groups in TDHPP not only aids in dispersibility in aqueous environments but also allows for specific orientation and interaction within the encapsulating dendrimer, potentially leading to improved encapsulation efficiencies and more controlled release profiles.

The insertion of zinc into TDHPP to form Zinc-TDHPP complexes is a strategic move aimed at further enhancing the stability, structural integrity, and photophysical

properties of the porphyrin. Zinc's coordination with the porphyrin nitrogen atoms expands the encapsulated system's overall performance by improving reactivity and photostability and holds promise for advancing the porphyrin's applications in fields such as photodynamic therapy.

2.3.2.8 The synthesis and categorisation of zinc-Tetrakis-3,5 Dihydroxyphenyl Porphyrin ZnTDHPP.

The synthesis of Zinc Tetra hydroxy phenyl porphyrin ZnTDHPP was achieved as previously discussed for TPP. The TDHPP was reacted with zinc acetate in a mixture of dichloromethane and methanol. The reaction was stirred for 30 min at ambient temperature. The product was filtered to eliminate any residual, unreacted zinc acetate, and the result was confirmed by ^{1}H NMR, which displayed complete metallisation of the porphyrin macrocycle cavity, indicated by the absence of the peak at 2.99 ppm for the NH protons *Figure* 2.31.

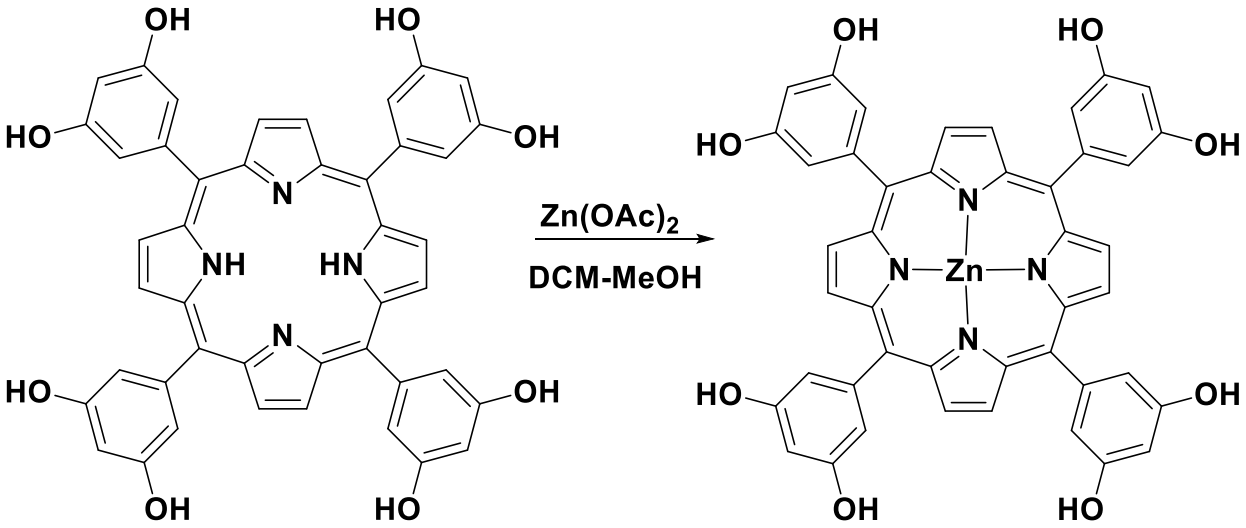

Figure:2.31 The Synthesis of Tetrakis 3,5 Dihydroxyphenyl Zinc complex ZnTDHPP.

The UV-vis spectrum of ZnTDHPP indicated significant differences from its free-base counterpart. The Soret band for ZnTDHPP appeared at 423 nm and shifted from the 418 nm representative to the free base of TDHPP, due to the coordination complex formation between the buffer and zinc metal ions altering the electronic structure affecting UV absorption spectra. Furthermore, ZnTDHPP displayed only two Q bands at 550 and 640 nm, in contrast to the four Q bands in the free-base porphyrin Figure 2.32, a change characteristic to the metalation of the porphyrin is indicative of the successful incorporation of zinc into the porphyrin structure. The following step involved the ZnTDHPP encapsulation within a dendrimer via coordination binding.

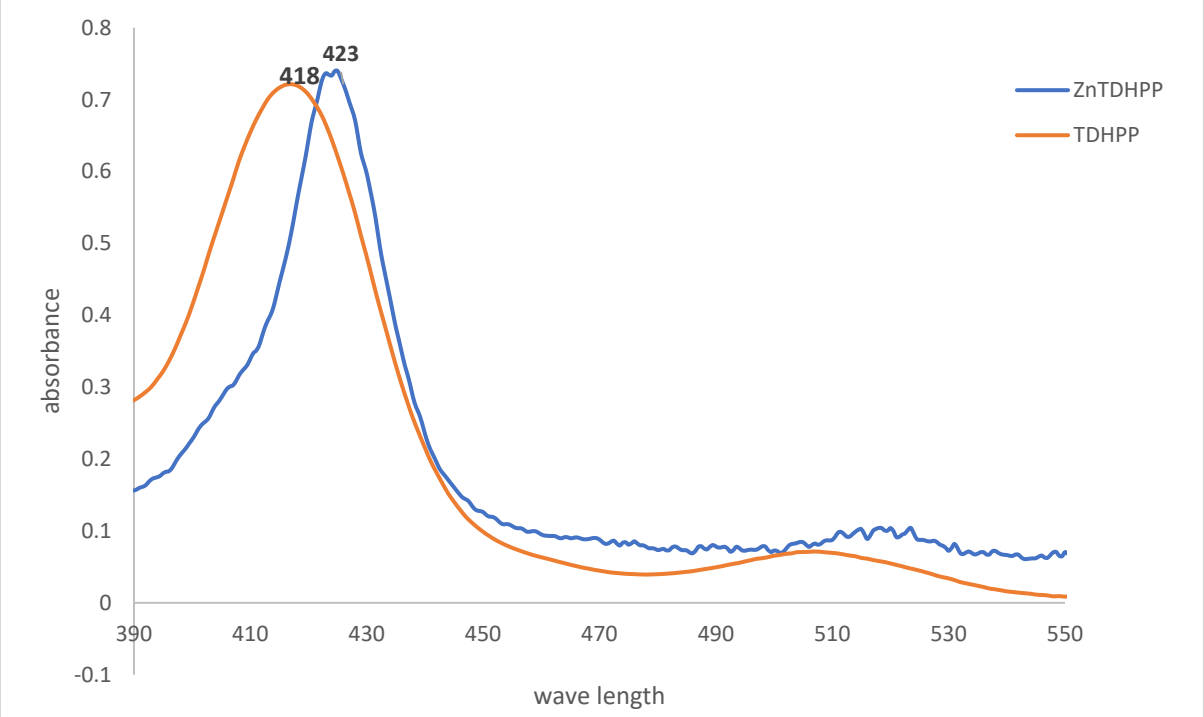

Figure: 2.32; UV- spectroscopy of TDHPP and ZnTDHPP.

2.3.2.9 Zinc porphyrin ZnTDHPP encapsulation within PAMAM dendrimers.

The extinction coefficient for ZnTDHPP was calculated using a Beer-Lambert analysis in a methanol solution, yielding a value of (5,775 dm^{-3} mol^{-1}, cm^{-1}). To avoid problems due to baseline drift (which could change absorptions), the ε coefficient was determined by measuring the change in absorption between 418 nm and 423 nm. To form the dendrimer-porphyrin complex, a methanolic solution of the G1.5, 2.5 and 3.5 OH PAMAM dendrimer and an excess of the porphyrin the methanol was then removed via Rotary evaporation, and a buffer solution (pH 7.4, 0.01M phosphate) was introduced. The volume of buffer used was such that the final dendrimer concentration was $2.1x10^{-6}$M. The successful encapsulation was confirmed using UV/Vi's spectroscopy as illustrated in Figure 2.33.

Table 2.4: ZnTDHPP Encapsulated within different PAMAM dendrimer generations.

Dendrimer/Gen	Total ZnTHPP$1x10^{-4}$ /M	Encap ZnTHPP $1x10^{-4}$ M	Loading
G1.5 OH	0.58	0.55	0.55
G 2.5 OH	1.45	1.40	1.40
G 3.5 OH	1.82	1.75	1.75
Dendrimer-concentration *$1x10^{-4}$* M.			
The Maximum concentration of free ZnTDHPP in buffer = $2.1x10^{-6}$M			

The ZnTDHPP encapsulation within various dendrimers reveals results regarding porphyrin solubility and dendrimer-porphyrin interactions. The ZnTDHPP absorption

peak shifted from 423 nm to 430 nm upon encapsulation, indicating a significant interaction between the metalated porphyrin and the dendrimers. The shift, attended by the presence of two peaks in all samples, suggests a mixture of free and bound porphyrin Figure: 2.33. However, in the case of G2.5 OH and G3.5 OH dendrimers, which exhibit stronger encapsulation capabilities, highlighting the strong coordination between ZnTHPP and the dendrimers' nitrogen atoms. This interaction disturbs the porphyrin's delocalized aromatic structure, modifying its energy states, and significantly enhances ZnTDHPP's solubility compared to TDHPP.

Moreover, solubility and encapsulation efficiency are shown in Table: 2.4 to depend on dendrimer size, with larger dendrimer generations binding more ZnTHPP. Both G2.5 OH and G3.5 OH dendrimers encapsulated about 25% more metalated porphyrin than the free base porphyrin. The G1.5 OH dendrimer, despite its more open structure and fewer coordination sites, encapsulated nearly 50% more metallated porphyrin than its free base equivalent. This unexpected finding could be attributed to the initial low concentration of free base porphyrin in the buffer. The insertion of zinc into THPP enabled an obvious improvement in solubility and underscored the critical role of dendrimer generation and structural characteristics enhancing metallated porphyrin encapsulation.

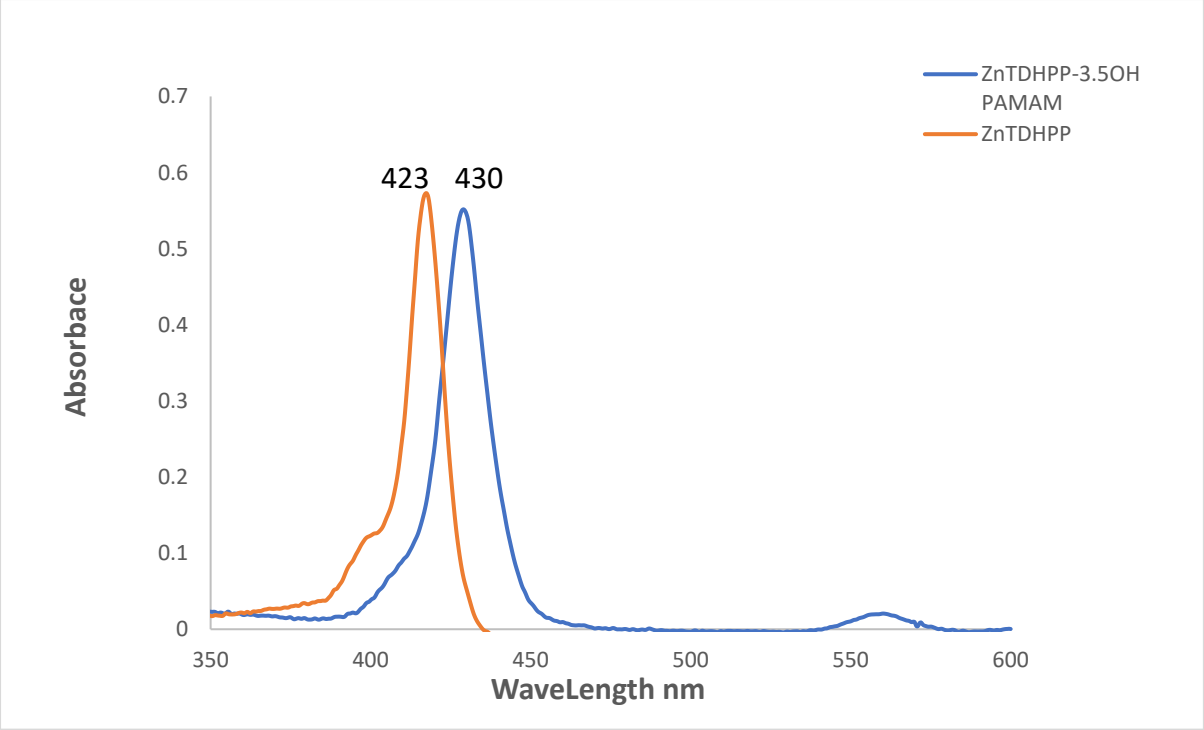

Figure: 2.33; UV- spectroscopy of ZnTDHPP within G3.5 OH PAMAM Dendrimer Complex.

The encapsulation efficiency and solubility improvements in porphyrins, when encapsulated within dendrimers, underscores the influence of inherent solubility characteristics of the encapsulated molecules on the outcomes of dendrimer-based delivery systems. While significant enhancements in solubility were observed for all porphyrins, the actual loading capacity within the dendrimers remained relatively fair, with the largest dendrimer realizing a maximum of nearly two ZnTDHPP molecules per dendrimer. The underlying reason for these differences lies in the intrinsic solubility of the compounds in water or buffer solutions. Porphyrins, with their almost negligible solubility in aqueous environments, experience a dramatic increase in solubility even with low dendrimer loadings, as the dendrimer architecture provides a hydrophilic exterior that facilitates solubility in water.

2.3.2.10 The Synthesis and categorisation of Iron/porphyrin Fe^{III} TDHPP.

The synthesis process involved refluxing TDHPP with 2,6-lutidine and $FeCl_2$ in anhydrous tetrahydrofuran THF at 50°C for three hours, as shown in Scheme 5.8.

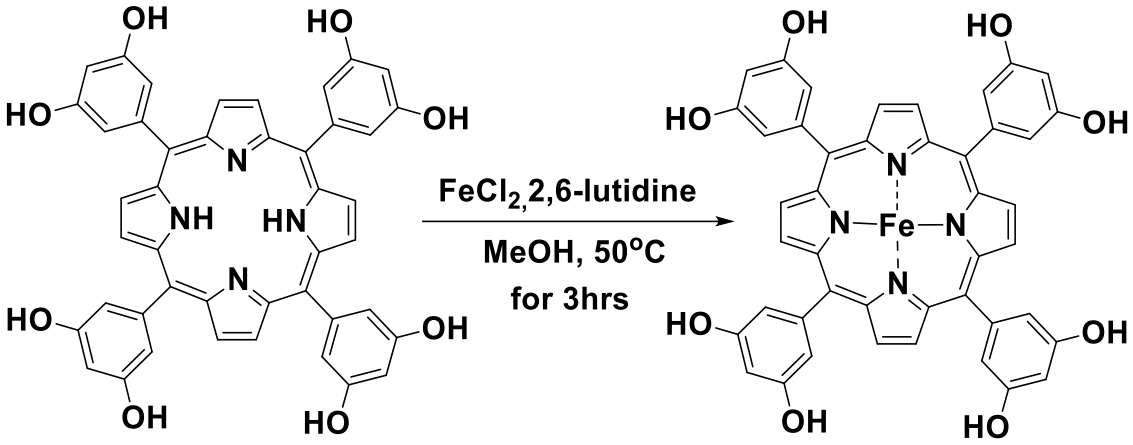

Figure: 2.34 Synthesis of Tetrakis-3,5 Dihydroxyphenyl with (Fe^{III}TDHPP).

Afterwards, the mixture was allowed to cool to room temperature and was exposed to air to oxidise the Fe^{II} into Fe^{III}. Ethyl acetate and water were then added, and the product was extracted. Following this, some solid impurities were removed in the solvent, and these were removed by vacuum filtration. The organic solvent was then removed via rotary evaporation. The resulting product was then purified through short-column chromatography using a 1:1 mixture of methanol and ethyl acetate. Mass spectrometry indicated the presence of a molecular ion peak at 802 Daltons, corresponding to the iron-cored porphyrin complex. The UV-Vis spectrum showed only two Q bands at 512 nm and 550 nm, as presented in Figure 2.14. As expected, the ^1H NMR spectrum consisted of broad e noisy peaks, due to paramagnetic iron. Despite the noise, the spectrum indicated that the metal had been inserted, as evidenced by the absence of the peak at -2.99 ppm Figure: 2.35.

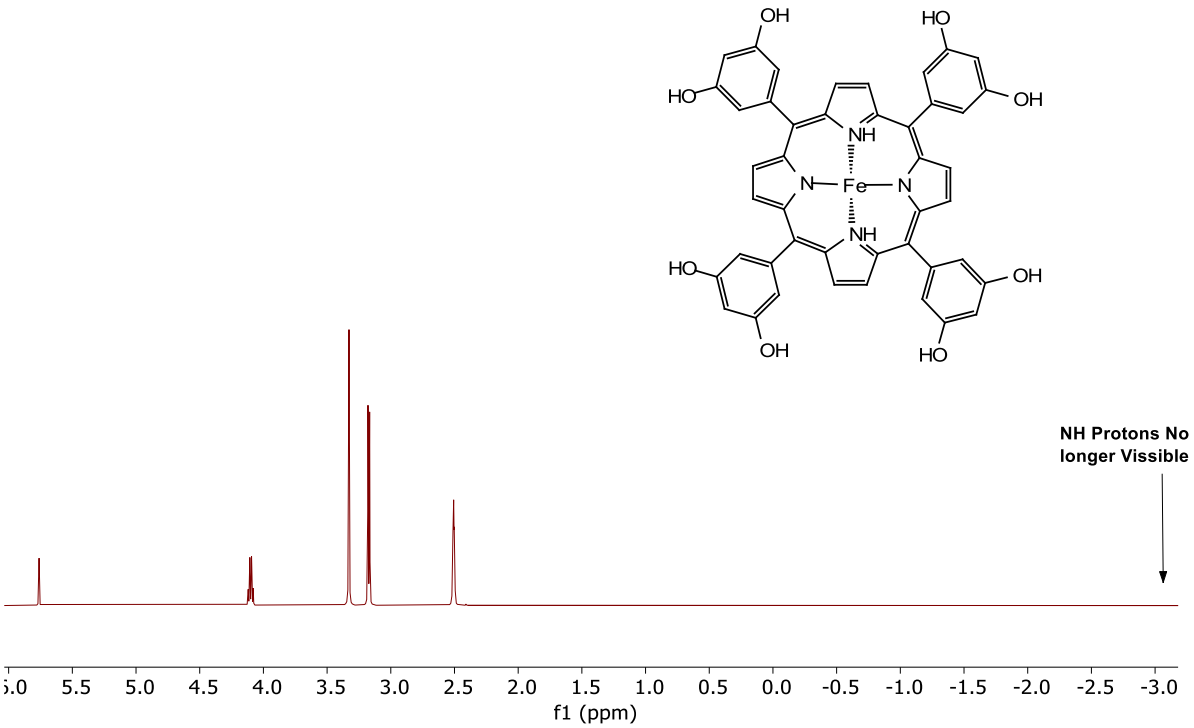

The Figure is Normalised by M Nova

Figure 2.35:The ^{1}H-NMR spectrum for the synthesis of Fe^{III}TDHPP.

2.3.2.11 The encapsulation of Fe-TDHPP within PAMAM dendrimers hydroxyl terminated Group OH.

To study the oxygen-binding properties of Fe-porphyrin, we first need to make a dendrimer-porphyrin complex. Having established that up to two porphyrins can be encapsulated per dendrimer, we needed to limit the number of Fe-porphyrins within the dendrimer. This was necessary to avoid any potential dimerization of the Iron-porphyrin within the dendrimer. As such, the preparation of the PAMAM dendrimer-porphyrin complex used a strict 1:1 ratio (porphyrin to dendrimer). The same co-precipitation technique previously described for encapsulation was used to give final dendrimer solutions with concentrations of $2x10^{-6}$ M for the PAMAM dendrimers with

(8 OH, 16 OH, and 32 OH end groups). UV-Vi's spectroscopy confirmed the presence of porphyrins, with a Soret band around 420 nm, and the two Q bands around 550 and 640 nm, as shown in Figure 2.36.

Table 2.5: final concentrations of encapsulated TDHPP Fe^{III} within PAMAM OH terminal group.

OH, end groups	Dendrimer concentration/M	Encapsulated TDHPP Fe^{III} /M
8 OH	2×10^{-6}	0.54×10^{-5}
16 OH	2×10^{-6}	0.7×10^{-6}
32 OH	2×10^{-6}	1.08×10^{-6}

The encapsulation data above for the porphyrin within different generations of dendrimers indicate a critical relationship between the dendrimer generation size and its capacity to encapsulate porphyrin molecules effectively. With the highest generation dendrimers exhibiting a nearly one-to-one ratio of polymer to porphyrin, it is reasonable to determine that each dendrimer encapsulates approximately one porphyrin molecule. This finding is essential for preventing porphyrin stacking within the dendrimer, which could lead to dimer formation and potentially cooperate following studies by altering the porphyrin's chemical behaviour and its interaction with the dendrimer. The lower-generation dendrimers displayed lower loading capacities, underscoring the significance of dendrimer size in achieving successful and complete encapsulation of guest molecules. This observation highlights the importance of selecting the appropriate dendrimer generation to ensure optimal encapsulation efficiency and stability of the encapsulated porphyrin.

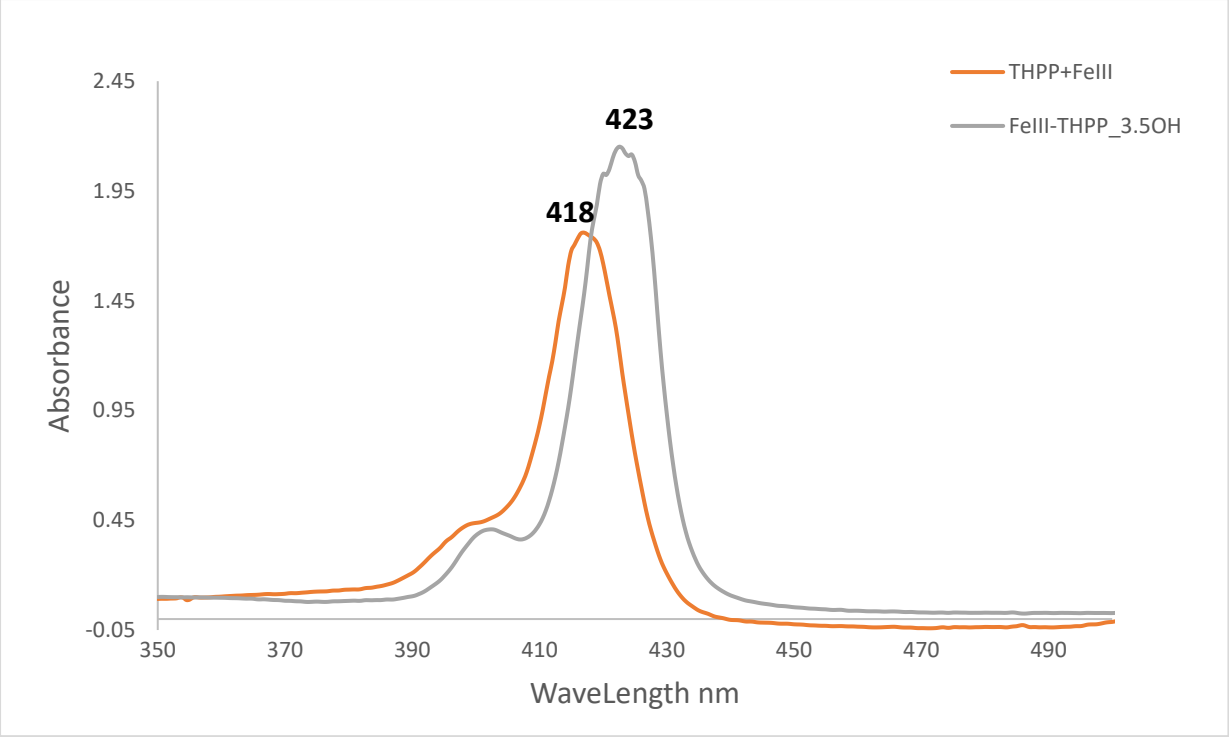

Figure: 2.36; UV- spectroscopy of TDHPP-Fe^{III} within 3.5 OH PAMAM Dendrimer.

The encapsulation process's efficacy is also assisted by the water tolerance of the encapsulated porphyrin, facilitating its entry into the dendrimer in a homogeneous solvent system. However, the same solvent system sets the risk of releasing the porphyrin molecules from the dendrimer, potentially reversing the encapsulation attempt. This accurate balance underscores the importance of carefully choosing a solvent environment that promotes efficient encapsulation while minimizing the risk of disassociation of the porphyrin from the dendrimer *Figure* 2.37.

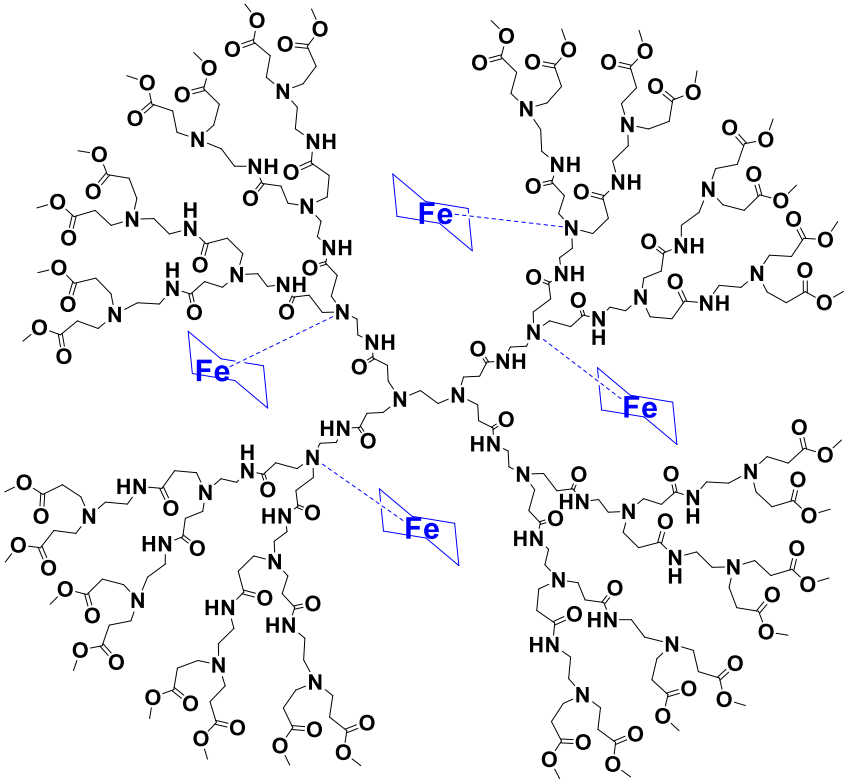

Figure 2.37: The coordination of Fe^{III}TDHPP within 3.5 OH PAMAM Dendrimer.

Following encapsulation, the porphyrin-dendrimer complexes were prepared for iron activation, transitioning from Fe^{III} to Fe^{II}. This step is crucial for the subsequent analysis of iron stability and oxygen-binding studies.

2.3.3 The Oxygen Binding for encapsulating Porphyrin within PAMAM Dendrimer.

Natural haemoglobin acts within an aqueous environment, playing a crucial role in transporting oxygen throughout the human body. Within its structure, each peptide subunit is finely tuned to provide just the right amount of hydrophobicity to the heme unit, facilitating the instant autoxidation of the iron core. These peptide molecules are also essential in preventing the proximity of two heme units, thus preventing dimers

formation and blocking irreversible oxidation, ensuring the solubility of these macromolecules in water.

Previously, the choice of TPP for encapsulation was motivated by its straightforward synthesis and lack of water solubility, facilitating easy iron insertion without interference from adjacent functionalities. However, the expected loading was lower due to TPP's hydrophobic nature, which hindered its entry into the dendrimer's cavity in an aqueous setting. Still, successful encapsulation led to a system with enhanced stability and a prolonged half-life in iron stability studies, assuming each dendrimer contained only a single porphyrin molecule. Preventing porphyrin aggregation within the dendrimer was essential to avoid dimer formation, which could negatively impact subsequent research phases.

Maintaining the stability of an iron core within a water-soluble system during oxygenation stands out as a distinct characteristic of a haemoglobin model. This stability is achieved by encapsulating an iron-core porphyrin within a large PAMAM Dendritic polymer system. Previous discussions have highlighted the potential for customising porphyrin substituents to enhance protection around the active site. Moreover, the technique of encapsulation plays a critical role in ensuring the iron's stability. The incorporation of iron porphyrin into the system provides a more stable structure through a strong and persistent connection between the core and the polymer chains. Despite these progresses, this system was not entirely effective in preventing or slowing down the irreversible oxidation of the iron core during assessments within a water-soluble PAMAM dendrimer system.

Thus, the dendrimer tends to encapsulate a single porphyrin molecule. Preventing the aggregation of porphyrin molecules within the dendrimer was crucial to avoid the

formation of dimers, which could negatively influence future research steps. Additionally, the importance of selecting the appropriate dendrimer size, as it was essential for the systematic and successful encapsulation of the guest molecule. This process was facilitated by the water-soluble nature of the encapsulated porphyrin, which ensured efficient integration of porphyrin into the dendrimer due to the use of a uniform solvent system. However, the same solvent system posed the risk of releasing the porphyrin molecule from the dendrimer, potentially compromising the encapsulation process. Following this, the porphyrin-dendrimer previously prepared coprecipitates underwent a process for the activation of iron from Fe^{III} to Fe^{II}, setting the stage for subsequent examinations of iron stability and oxygen binding capabilities.

2.3.3.1 The encapsulation of Fe^{III}-TDHPP within PAMAM dendrimers OH-terminated Group.

The synthesis, characterisation, and encapsulation of 3,5-TDHPP Fe^{III} were covered in Sections 2.3.2.10 and 2.3.2.11.

2.3.3.2 Iron Stability.

To determine the oxygen binding capability of the encapsulated porphyrins, we proposed to study the stability of a Fe^{II} porphyrin to atmospheric oxygen. This involves measuring the time taken and half-life for a reduced Fe^{II} porphyrin to be oxidised to the Fe^{III} porphyrin. Experiments using the encapsulated system would be compared to the free porphyrin with any differences attributed to the stability provided by encapsulation within the dendrimer. The study first involved reducing the Fe^{III} porphyrin (free or encapsulated) by adding an equimolar amount of sodium dithionite

to a degassed oxygen-free solution under nitrogen. The successful reduction of the inactive Fe^{III} porphyrin was confirmed by UV analysis. The Soret band for Fe^{III} can be observed at approximately 418 nm, this changes to 430 nm when the porphyrin has been reduced to the active Fe^{II} state, Figure 2.38. Following this, a sample of the solution was placed into a sealed quartz cuvette. under nitrogen, the cuvette was then opened to air and the peak for the reduced porphyrin at 430 nm was followed as it decreased over time using UV-Vi's spectroscopy.

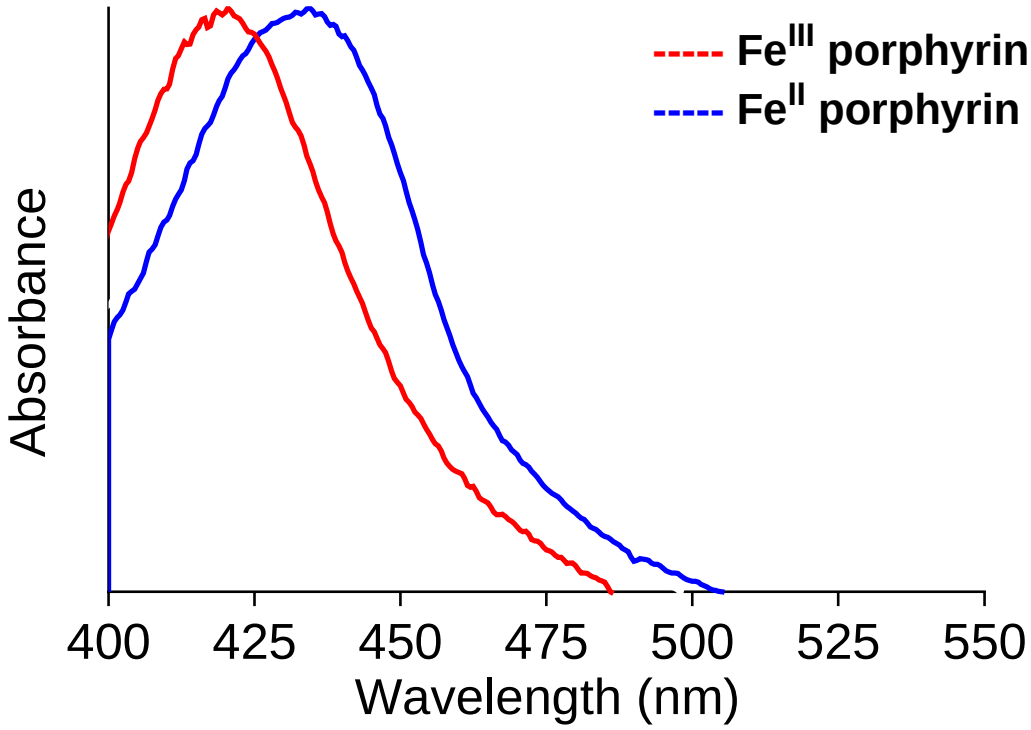

Figure 2.38 *The UV-Vis spectra shift of 3,5TDHPP-Fe-OH PAMAM dendrimer before and after oxygenations.*

After opening the cuvette, the sample started to oxidise, and recordings were taken at 60-second intervals for 30 min. The Absorptions recorded were then plotted against time and the plots were used to calculate a half-life. The plots for the encapsulated porphyrin and free porphyrin are shown in Figures 2.39 and 2.40, respectively.

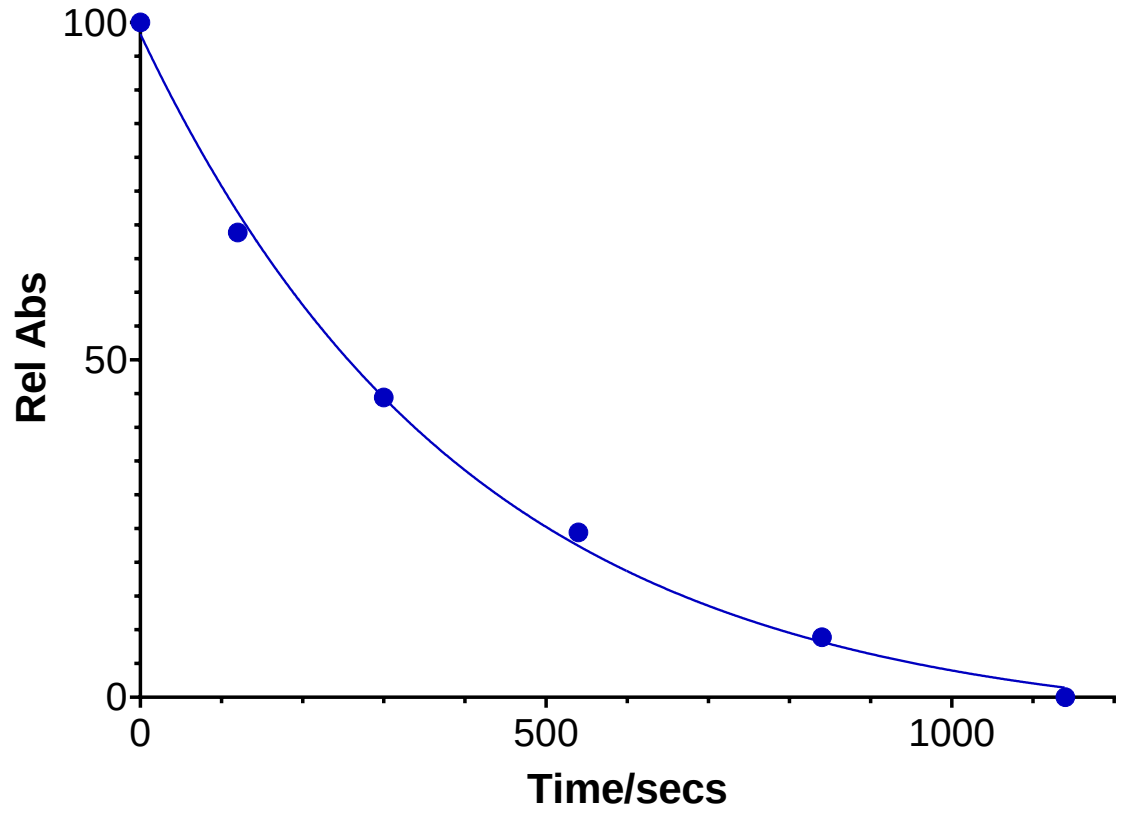

Figure; 2.39: Fe^{II} O_2 stability plot for the Fe^{II}-TDHPP/dendrimer complex. Half-life = 281 seconds.

The graphs demonstrate enhanced stability for the encapsulated 3,5-DHPP Fe^{II} when compared to the free 3,5-TDHPP-Fe^{II}. The increased stability is attributed to the dendritic polymer chains surrounding the porphyrin, which provide steric hindrance, effectively slowing down the degradation of the active Fe^{II} compared to the 3,5-TDHPP Fe^{III} before its full oxidation. Furthermore, when bound within the hydrophobic core of the dendrimer, the usually fast water/proton-driven oxidation of Fe^{II} is also reduced.

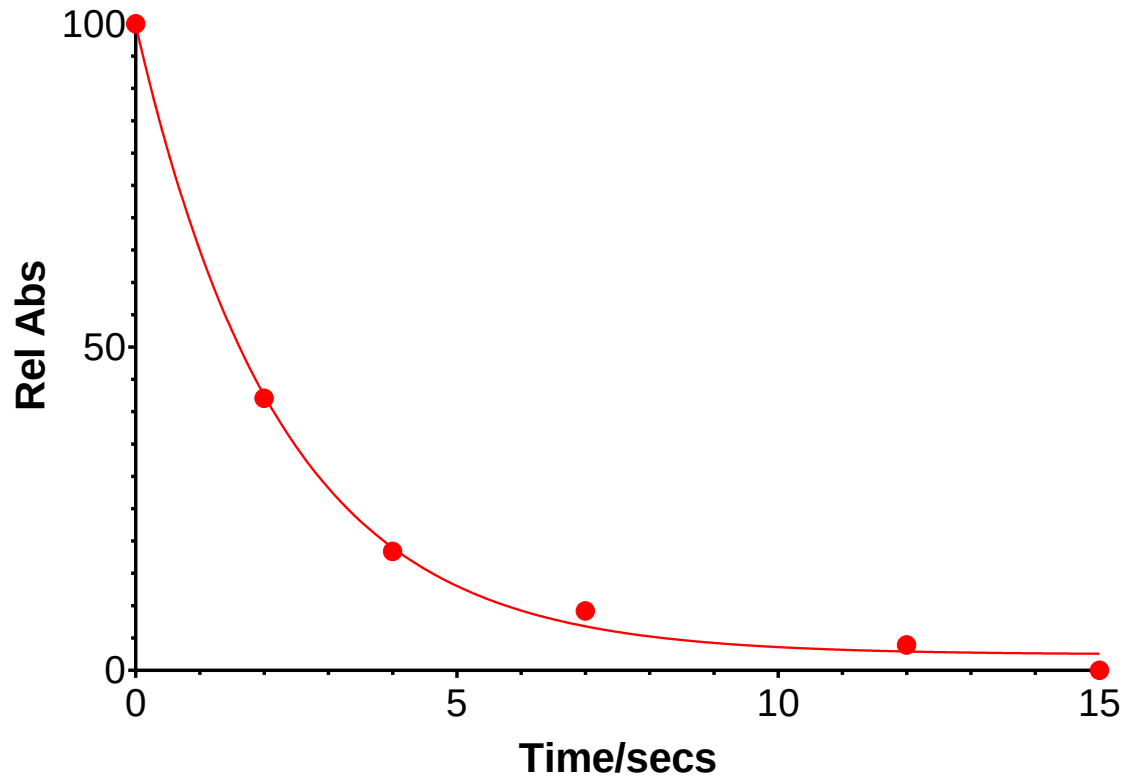

Figure; 2.40: Fe^{II}-O_2 stability plot for the Fe (II)-TDHPP. Half-life = 1.56 seconds.

The experiments were conducted in triplicate and average half-lives were calculated for the encapsulated and free Fe^{II} porphyrins are shown in, Table 2.6, along with the increased stability of the encapsulate system.

Table 2.6: The 3,5. TDHPP Fe^{II} half-life of cored 3.5 OH PAMAM dendrimer against the free 3,5. THPP Fe^{II}.

Complexes	Half-life $T_{/}$sec	Increase of the stability compared to control %
Free 3,5-TDHPP Fe^{II}	1.56	N/A
3,5-TDHPP Fe^{II}	281	180

Overall, the data confirms a significant oxidative stability of iron within the PAMAM dendritic system. Specifically, the encapsulated system is over 150 times more stable than the free porphyrin system. As such, the results demonstrate a clear potential for the encapsulated system to be applied as a biomimetic haemoglobin with a view to application as an artificial blood system. Notwithstanding this positive result, we must acknowledge that the porphyrin host is probably too small to be used clinically. Haemoglobin cannot be used on its own as a blood replacement. Unfortunately, it is small enough to pass through holes in the capillary system and into the tissue, where any oxygen release can be toxic (this is why simple haemoglobin is not a suitable replacement for blood). Haemoglobin in the body is encapsulated within a large blood cell, which is large enough to be retained within the circulatory system. Although this analysis is an oversimplification, any molecules used for artificial blood must be larger than 100-200 nm in diameter. To achieve this, we propose to encapsulate our porphyrin dendrimer within an artificial/synthetic cell. This is described in the following section.

2.3.4 Metalated Porphyrin Fe TDHPP Cored PAMAM Dendrimer Encapsulated non-covalently within the Liposomes.

The previous section of our study highlighted the use of water-soluble dendritic polymers as potential heme mimics. It was found that porphyrin-dendrimer complexes, with their iron cores, demonstrated enhanced stability in terms of iron retention compared to water-soluble hyperbranched polymers previously studied (within our group). The porphyrin/dendrimer host is likely too small for clinical use. While haemoglobin cannot serve as its own for blood replacement due to its ability to pass through capillary holes and potentially cause tissue oxygen toxicity, its encapsulation

within large blood cells prevents this issue by retaining it within the circulatory system. While this overview simplifies that, any molecules intended for artificial blood must exceed 100-200 nm in diameter. To meet these criteria, we suggest encapsulating our porphyrin dendrimer within a synthetic cell, as detailed in the following section.

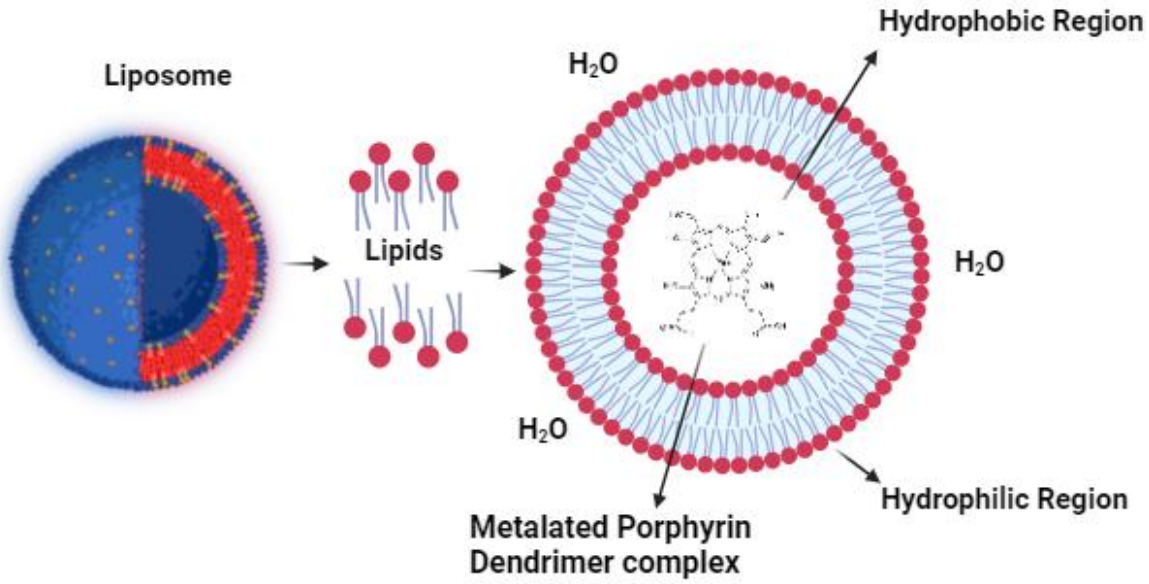

Figure 2.41: Proposed PAMAM dendrimer Encapsulated within the Liposomes.

To achieve our aim of developing a synthetic oxygen-carrying cell, we proposed to synthesise a simple liposome and encapsulate the porphyrin dendrimer complex within its aqueous interior, as shown in Figure 2.41. The liposomes will be constructed using simple phospholipids and their aggregation determined through a combination of DLS dynamic light scattering and (UV-Vis) spectroscopy. Importantly, DLS will also determine the size distribution and stability of the liposomes.

2.3.4.1 The Synthesis and Characterization of Liposomes.

We selected dioleoyl-sn-glycero-3-phosphocholine) DOPC and (1,2-dioleoyl-sn-glycero-3-phosphoethanolamine) DOPE as the lipids for our liposomes *Figure 2.42*.

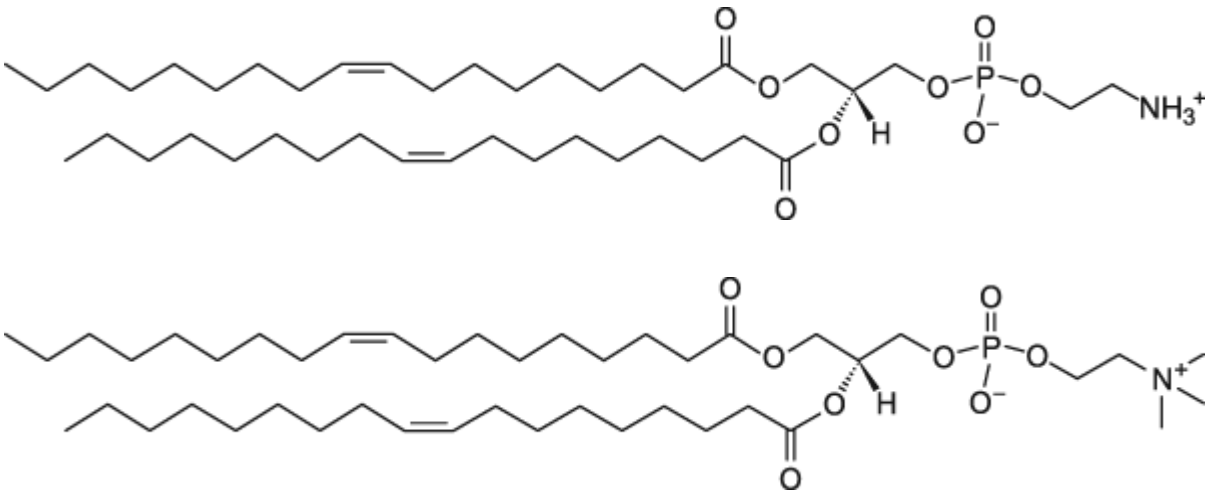

Figure 2.42 The structure of DOPE and DOPC Di-phospholipids.

Our first experiment involved the synthesis of a simple liposome. This would allow us to understand the synthesis and characterisation techniques and inform us concerning the size of any potential liposomes.

DOPC and DOPE Di phospholipids was subsequently produced through extrusion, a well-established technique in liposome preparation. DOPC and DOPE were dissolved in 50 mL of MeOH ensured complete solubilisation of the lipids. The methanol was then removed using a rotary evaporator, to leave a thin film of phospholipids on the walls of the flask. 20 mL of pH 7.4 Tris buffer Tris hydroxymethyl amino methane (0.1 M) was added to the flask, reconstituting the lipids in an aqueous environment, leading them to form bilayer structures spontaneously. At this point, polydisperse liposomes and multilamellar liposomes have been formed. To realise a single, monodisperse

liposome, the suspension was extruded using an ‘’Avanti Mini-Extruder’’ with a pore size of 200 nm. This forces the suspension through the nucleopore membrane. The extrusion process is repeated several times to ensure uniformity in liposome size and structure. After extrusion, a preparative Column was used to remove any non-liposome material, ensuring that the preparation contained the desired mono-dispersed liposomes, Figure 2.43.

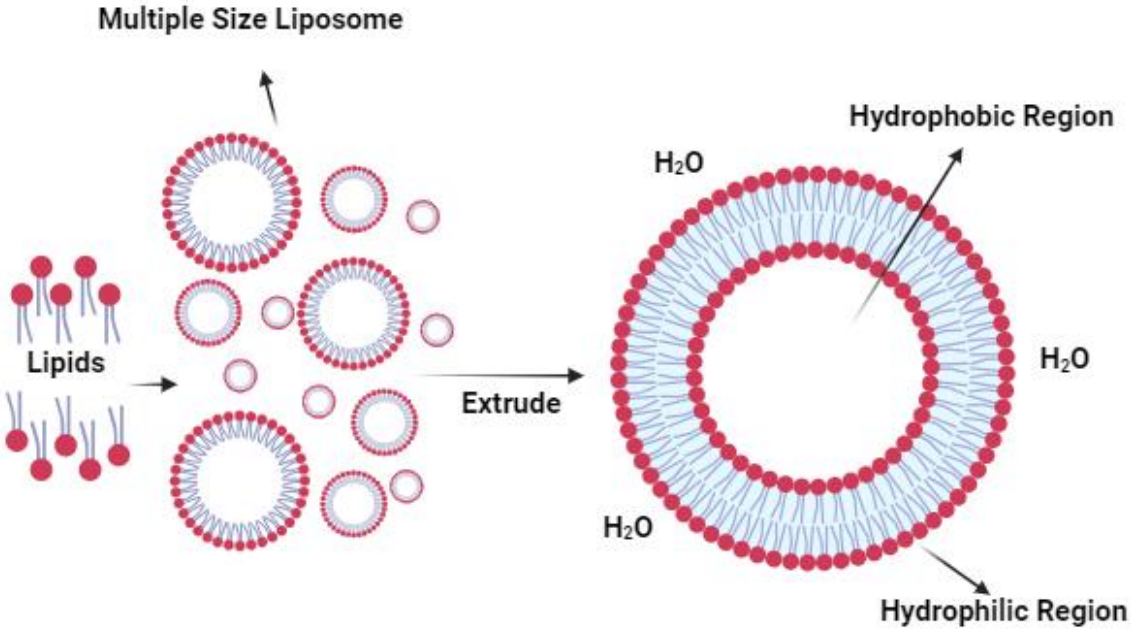

Figure 2.43 The preparation of liposomes from DOPC and DOPE lipids.

The following step was to determine the size of the liposomes, which was done using DLS, which showed mono-dispersed particles with an average diameter of 200 nm, Figure 2.44. This is the perfect size for our porphyrin/dendrimer system, and the resulting liposome should be retained within the circulatory system and any potential toxic effects related to leaching out of veins and into tissue significantly reduced. The

next experiment would repeat the liposome preparation but with the encapsulation of the porphyrin dendrimer complex.

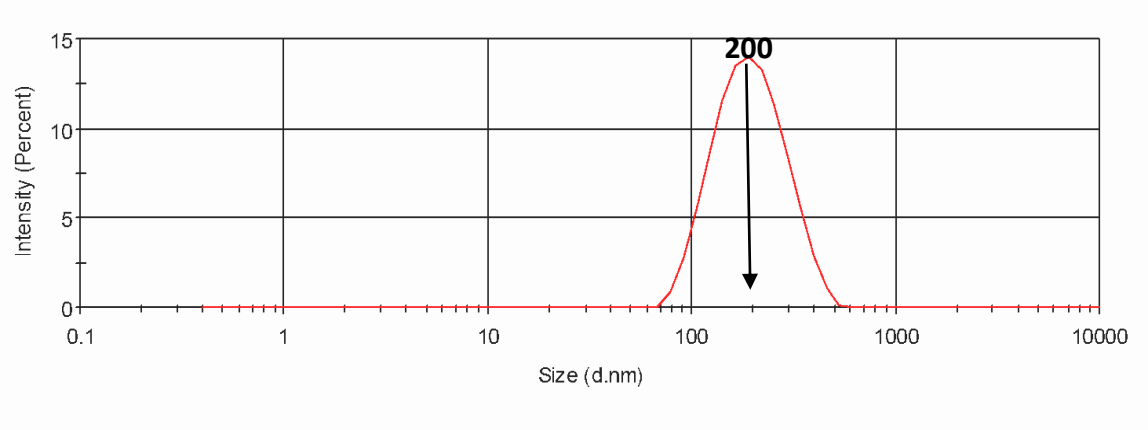

Figure 2.44 The liposome formation determines by DLS.

2.3.4.2 The Encapsulation of 3,5-TDHPP-Zn Cored PAMAM Dendrimer Polymer within Liposome.

Initially, we selected 3,5-THPP-Zn for the complexes, as this would simplify the analysis, as changes in the Soret band can be used to monitor/confirm complexation.

The procedure for encapsulating the Zn-TDHPP-PAMAM dendrimer complex within the liposomes was carried out in two stages. The first involved the synthesis of the porphyrin dendrimer complex, and the second, its encapsulation within the liposome. The initial porphyrin dendrimer complex was carried out using a 1:1 ratio, for the porphyrin and dendrimer, and has already been described in Chapter 5. UV analysis showed a shift in the porphyrin's Soret band, from 418 nm to 420 nm, confirming complexation. The next step involved encapsulation within the liposome with the same procedure described in section 2.3.2.8, by adding a 1:1 ratio of Zn-TDHPP-PAMAM at $1x10^{-4}$ to form a liposome complex.

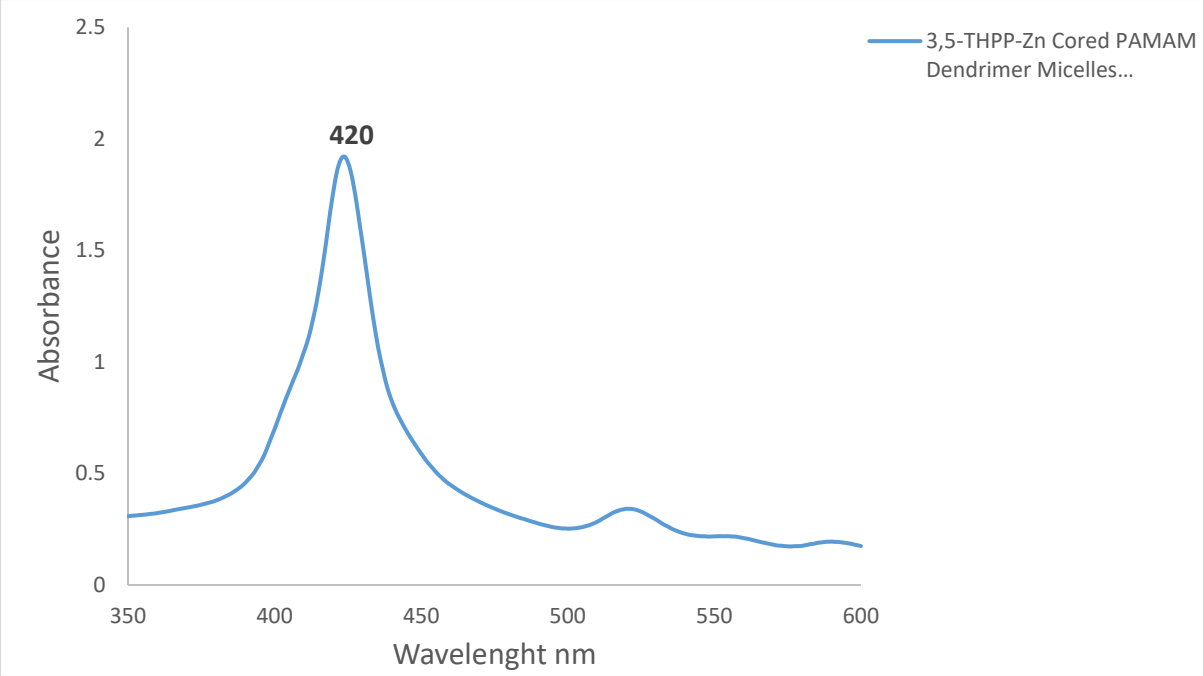

Figure 2.45: 3,5-TDHPP-Zn PAMAM Dendrimer complex encapsulated within liposomes at 3.1x10^{-6}.

The extinction coefficient of 3,5-TDHPP-Fe^{III} is determined to be 57857 M, facilitating the calculation of dendrimer concentrations in the solutions. The addition of the organic 3.5 OH PAMAM dendrimer solution to the micelle solutions is performed slowly, ensuring effective encapsulation.

The successful encapsulation of the PAMAM dendrimer within the micelles is confirmed through UV-Vi's spectroscopy, the spectral confirms the successful integration of the dendrimers into the micelle structures. it is indicated by a Soret band peak at 420nm Figure2.45. The concentrations of the encapsulated PAMAM dendrimers within the micelle system are provided in Table 2.7.

Table 2.7: The final concentrations of 3,5-TDHPP Fe^{III} cored 3.5 OH PAMAM dendrimer OH terminated group encapsulated within micelle systems. ''Liposome concentration is estimated based on the liposome containing approximately 10,000 lipids''[187].

Lipo/Ratio	Dendrimer Conc (M)	Liposome Conc (M)	Final Conc of the complex (M)
1:20	$1x10^{-4}$	$2x10^{-7}$	$3.1x10^{-6}$

The collected data exposed the encapsulation efficiency of dendrimer systems within the micelle structures. Particularly, the micelles were not prepared at a 1:1 molar ratio relative to the dendrimers, which, were prepared with a roughly 20-fold excess in concentration compared to the initial dendrimer. Analysis of the final product concentrations suggested that with every 500 micelles, 15 units typically contained an encapsulated dendrimer. The presence of a considerable number of unoccupied Liposomes was fair enough and more than expected for the subsequent studies. Furthermore, comparing the initial concentrations of dendrimers with their final encapsulated state, revealed that approximately 60% of the introduced dendrimers were successfully encapsulated within the liposome.

2.3.4.3 Iron Stability Analysis.

The preparation process for both the micelle-dendrimer complexes and the micelle-porphyrin complexes corresponded to the encapsulation procedure previously discussed. The control sample was accurately prepared in phosphate buffer pH 7.4, 0.1M, as well as in methanol MeOH, for organic soluble compounds. The details of both the test and the control samples are demonstrated in Table 2.8.

Table 2.8: Final concentrations for the control and the test samples intended for Fe stability.

Compounds	Initial Dendrimer conc/M	Lipid/ Conc	Liposome/ Conc	Final Dendrimer liposome conc/ M	Loading/ Liposome
Free 3,5-TDHPP Fe^{III} in MeOH	N/A		N/A	$6.2x10^{-6}$	
3,5-TDHPP-Fe^{III} cored PAMAM-OH/MeOH	N/A		N/A	$7.2x10^{-6}$	
1:20 Ratio 3,5-TDHPP-Fe^{II}/Liposomes Complex	$1x10^{-4}$	$1x10^{-4}$	$2x10^{-7}$	$3.1x10^{-6}$	15

The successful encapsulation of both test and control samples was verified through UV-Vi's spectroscopy, characterized by a Soret band peak at 420 nm, alongside two weak Q bands.

2.3.4.4 Oxygen Binding Study.

Having demonstrated that the Fe^{III} porphyrin dendrimer complex could be encapsulated efficiently within the liposomes, the next would involve the reduction of the Fe^{III} core, to the active Fe^{II} form, followed by oxygen binding and stability

experiments. As such, a degassed solution of the encapsulated porphyrin dendrimer complex was reacted with a slight excess sodium dithionite $Na_2S_2O_4$. The solution was then stirred under nitrogen gas to facilitate the reduction process. During the reaction period, a milky solution was observed. After 1 hour, a sample was removed by syringe and injected into a sealed UV cuvette filled with nitrogen. Unfortunately, the spectrum obtained was extremely poor and resolved, reproducible peaks were not observed. This was due to the suspension in the sample, which caused scatter and prevented a UV spectrum from being recorded. We suspect that the reducing reagent may have reacted with the lipids and disrupted the liposome. The reaction was attempted several more times, but the same result was obtained, and we were unable to read the UV spectrum. We considered shortening the reaction time, but the formation of the cloudy suspension occurred. At this stage, we were out of time and no further experiments could be carried out.

2.4 Conclusions and future work.

The successful encapsulation of the PAMAM dendrimer within the micelles was confirmed through UV-Vi's spectroscopy, as evidenced by the presence of a Soret band peak at 420 nm. Analysis of the data revealed an encapsulation efficiency of approximately 60%, with 10 to15 dendrimers encapsulated within every 500 liposomes. Despite the excess concentration of dendrimers relative to micelles, the presence of unoccupied micelles did not significantly affect subsequent studies. Moving forward, efforts to reduce the Fe^{III} core to the active Fe^{II} form for oxygen binding experiments were delayed by the suspension in the sample, leading to poor UV spectra due to scatter. Despite attempts to rectify this issue, further experiments were not feasible

within the allotted time frame. Therefore, while successful encapsulation of the dendrimers within the micelles was achieved, challenges in subsequent experiments highlight the need for continued exploration and optimization of experimental techniques.

Future research should explore various strategies for iron reduction, such as utilizing an organic soluble reducing agent if feasible, or exploring alternative techniques like transfer electron processes, for instance, through electrochemistry or specialized chemical species'' Specy chem''.

Chapter 3

3 Drug Delivery

3.1 Introduction.

Drug delivery is a principle of modern pharmacology, encompassing a diverse array of technologies and strategies aimed at optimizing therapeutic outcomes while mitigating adverse effects[188]. With an ever-growing emphasis on improving pharmacokinetic properties, enhancing bioavailability, and achieving precise targeting of pharmacological compounds, the field of drug delivery continues to expand rapidly[189]. This expansion is reflected in the robust growth of the global market for drug delivery technologies, which is projected to continue an upward line. Central to this growth is the imperative for drug delivery systems to adapt to the evolving landscape of biopharmaceutical innovation, ensuring that new compounds can be administered effectively, exhibit enhanced bioavailability, and are precisely targeted, all while minimizing toxicity[190,191].

The quest for more effective drug delivery systems has spurred a broad spectrum of research activities, ranging from the refinement of conventional dosage forms to the development of innovative delivery platforms[192]. These platforms involve a diverse range of technologies, including controlled-release oral formulations, liposomal encapsulation, transdermal patches, and nanocarrier-based delivery systems[191]. Among these, nanotechnology-based drug delivery systems have emerged as particularly promising, offering unique advantages over traditional approaches. Nanoparticle-based systems, such as liposomes, polymeric micelles, dendrimers, and nano capsules, have garnered significant attention for their ability to overcome inherent limitations associated with conventional drug delivery methods[193].

Nanoparticles exhibit a multitude of advantageous properties, including enhanced stability, improved solubility of poorly water-soluble drugs, controlled release kinetics, and precise targeting capabilities[194]. These attributes make them well-suited for delivering a wide range of therapeutics, including small molecules, proteins, peptides, and nucleic acids. Despite their promise, nanoparticle-based drug delivery systems face challenges, such as premature drug release and limited effectiveness in certain contexts. Ongoing research endeavours are focused on addressing these challenges and advancing the clinical translation of nanoparticle-based therapies[195].

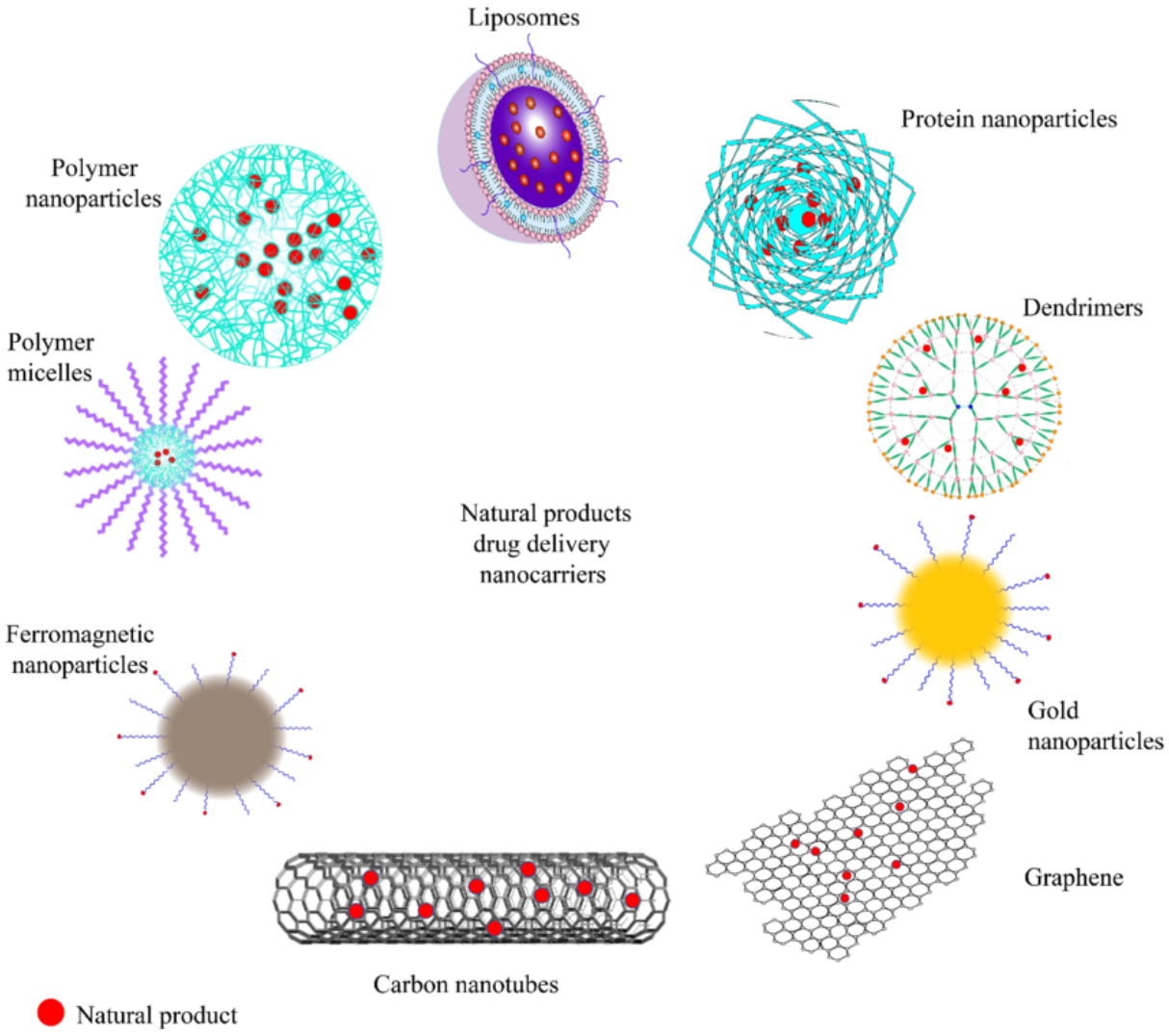

Figure 3.0: Drug delivery with different nanocarriers

Polymers, particularly branched and dendritic structures, have emerged as key players in the field of drug delivery[196]. Offering flexibility and multifunctionality, these polymers hold significant promise for enhancing the efficacy of drug delivery systems. Branched polymers exhibit the ability to engage with multiple ligands simultaneously and offer opportunities for both covalent and non-covalent interactions with drugs[197]. Moreover, the unique structural features of dendrimers present novel possibilities for theragnostic applications, integrating diagnostic and therapeutic functions within a single platform[194,198].

3.2 Aims.

The work described in this chapter was conducted in collaboration with Dr Reyad Elderbag, who conducted the synthesis, encapsulation and stability studies using an equivalent hyperbranched polymer $1x10^{-4}$ M. The results of which would be used for a comparison with the results described in this chapter, to answer the question "*Can a hyperbranched polymer perform as well as a dendrimer for use in drug delivery?*" The release studies, along with all the dendrimer work (including synthesis, encapsulation, stability, and release studies), were carried out by myself.

The primary goal of this work was to evaluate and compare the drug delivery capabilities of dendrimers and hyperbranched polymers HBP. The focus was on determining whether HBP could encapsulate and deliver drugs as effectively as dendrimers. The synthesis of the required dendrimers has already been discussed in Chapter 2. The HBP required for comparison was supplied by Dr Reyad Elderbag[199]. The experimental approach began with dendrimers and a selection of drugs that were only partially soluble in water and were also readily available. This choice allowed for

an initial assessment of any solubility enhancements provided by the dendrimer, followed by experiments to evaluate the stability of the drug within the dendrimer and its release.

3.3 Result and Discussion.

Hydroxyl-terminated PAMAM dendrimers offer significant potential in drug delivery, characterised by their unique, highly branched three-dimensional structure and surface chemistry[173]. The evaluation of their drug delivery capabilities involves assessing their drug loading capacity, which depends on the nature of the drug and the dendrimer's interactions with it[200]. The key aspects include controlled drug release, influenced by the dendrimer's composition and environmental factors like pH and temperature, as well as biocompatibility and toxicity, which are crucial for safe application[201]. The targeting ability can be enhanced by functionalized dendrimers with specific ligands, directing them to desired tissues or cells[202]. Understanding their pharmacokinetics and biodistribution is essential for determining how they are processed in the body. Additionally, the stability and solubility of the drug-dendrimer complex in physiological conditions is vital for effective drug delivery[203]. The potential therapeutic applications of these dendrimers are explored through a combination of chemical synthesis, in-vitro and in-vivo studies, and potential clinical trials, making them a promising area of research in advanced drug delivery systems[204].

3.3.1 Ibuprofen encapsulating within the hydroxyl terminated PAMAM dendrimers OH Group.

Previous research of Twyman groups had demonstrated that hydrophobic acidic guest molecules are particularly suitable for encapsulation within dendrimers if they could also form a simple acid-base ion pair. This additional interaction generated a stronger overall interaction than hydrophobic effects alone. Furthermore, if the drugs possessed sites for hydrogen bonding, then even better overall interactions were possible (than simple hydrophobic effects alone). Significantly, the most effective encapsulation was observed in molecules that combine both acidic properties and hydrogen bonding resources, generating a significant cooperative effect and high encapsulation efficiency.

In this study, Ibuprofen was chosen as the initial test drug due to its availability and structure (acidic and hydrogen bonding regions), making it suitable for studying further interactions with dendrimers. The molecular structure of Ibuprofen includes a carboxylic acid group, which is key for forming salts or hydrogen bonds with dendrimers. This feature is correlated with the Twyman group outcomes, suggesting that Ibuprofen could potentially exhibit efficient encapsulation within dendrimers. In addition, Ibuprofen is UV-active, which is a significant advantage for analytical purposes. Ibuprofen has three peaks in its UV spectrum, and the absorbance peak of Ibuprofen at 273 nm was used to monitor encapsulation and release. A simple Beer-Lambert approach was used to provide a straightforward method to quantify the concentrations of all solutions used *Figure* 3.1.

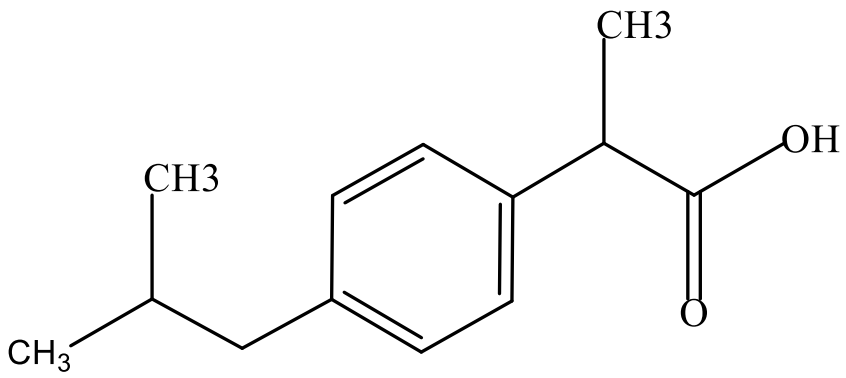

Figure 3.1 The structure of Ibuprofen

However, Ibuprofen is not completely soluble in water, which presents a challenge for analysis. To overcome this, methanol was used as the solvent for the Beer-Lambert analysis. Methanol is similar in polarity to water, but provides a more effective solvent for Ibuprofen, providing an accurate measurement of Ibuprofen's maximum concentration. The extinction coefficient of Ibuprofen in methanol was 95 $dm^3mol^{-1}cm^{-1}$ *Table 3.0*. In the first experiment, the primary objective was to determine the maximum solubility of Ibuprofen in aqueous buffer solution at pH 7.4, 0.01M. The high buffer concentration was required to ensure that the buffer's concentration exceeded the amine concentration present in the largest dendrimers. The largest generation 3.5 OH dendrimer was used. contains 30 amines. Using this value, we can calculate an amine concentration of $3x10^{-3}$ M at a dendrimer concentration of $1x10^{-4}$ M. Therefore, at a buffer concentration of 0.01 M, the amine concentration will not exceed the buffer capacity.

Table 3.0: The extinction coefficient of Zn-TDHPP/Ibuprofen dissolved in methanol.

Drug/s	ε	Maximum solubility/buffer
Zn-TDHPP	5854	$2X10^{-6}$
IBU	95	$1X10^{-4}$

To replicate the future encapsulation experiments, the Ibuprofen was first dissolved in methanol, and then the methanol was evaporated using a Rotary evaporator. Following this, a specific volume of phosphate buffer pH 7.4, 0.01 M was added, such that the Ibuprofen was in excess. The solution was then filtered to remove the undissolved Ibuprofen, and the UV spectrum of the solution was recorded, Figure: 3.2. From Beer-Lambert, the highest viable solubility of Ibuprofen in the buffer was found to be 3.5×10^{-3} M. This value represents the baseline solubility of Ibuprofen in the buffer solution. This value would be used in subsequent experiments where any increase in the solubility of Ibuprofen could be attributed to encapsulation within the dendrimers (referred to as dendrimer-boosted solubility).

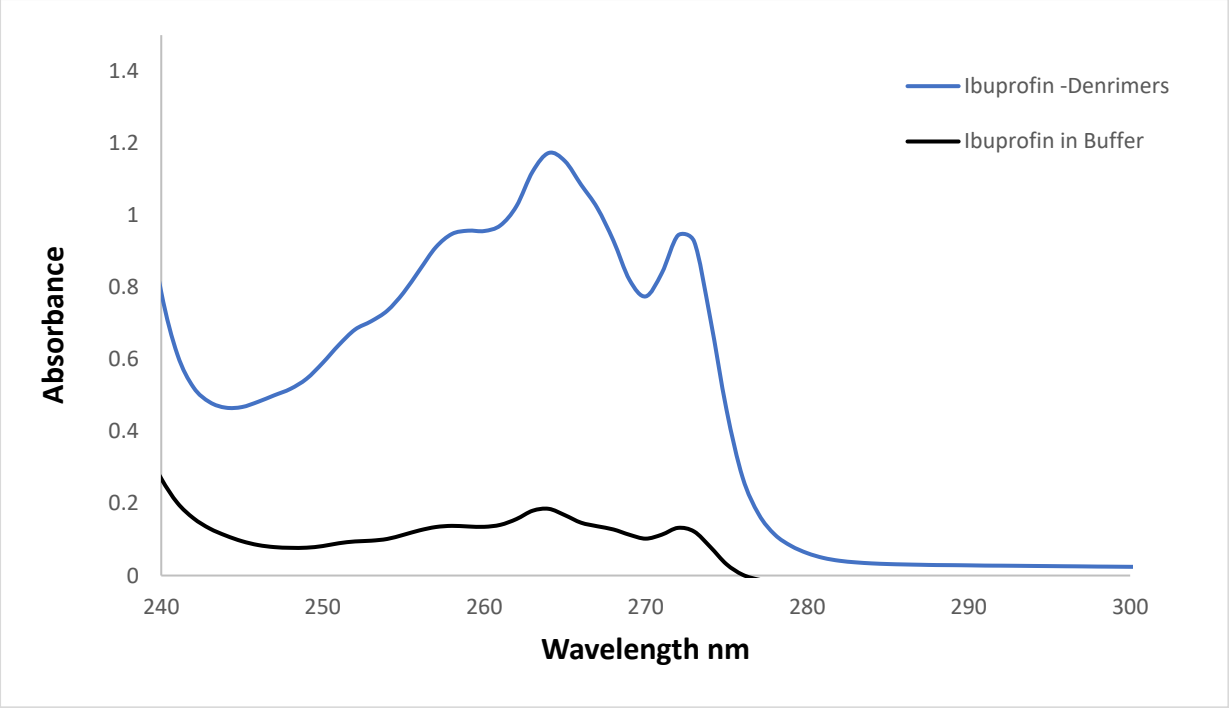

Figure 3.2 UV-Vis of the free ibuprofen solubility Vs the encapsulated Ibuprofen within PAMAM dendrimer at ($1x10^{-4}$) concentration.

The study progressed to evaluating the potential of each dendrimer to enhance Ibuprofen's water solubility. This was achieved by adding excess ibuprofen to a dendrimer solution at a concentration of $1x10^{-4}$ M. To identify any size-dependent effects on drug encapsulation and solubility enhancement, G 1.5, 2.5 and 3.5 dendrimers were studied, with 8 OH, 16 OH, and 32 OH terminal groups, respectively. The specific encapsulation process entailed forming a dendrimer-drug complex via the coprecipitation technique, which involved dissolving Ibuprofen and the dendrimer in methanol. The methanol was then removed using a rotary evaporator to give a co-precipitate of the PAMAM dendrimer and Ibuprofen. Consequently, the co-precipitate was reconstituted in a phosphate buffer pH 7.4, 0.01M, followed by filtration to remove undissolved drugs. The solubilised drug-dendrimer complex's concentration was then determined using UV-vis spectroscopy, employing Beer-Lambert analysis recorded using the delta absorption between 265 to 270 nm this modification to the Beer-

Lambert analysis generated a new extinction coefficient of 95 dm^3, mol^{-1}, cm^{-1}, and was required to mitigate baseline drift. The spectra obtained for all samples are shown in Figure: 3.3.

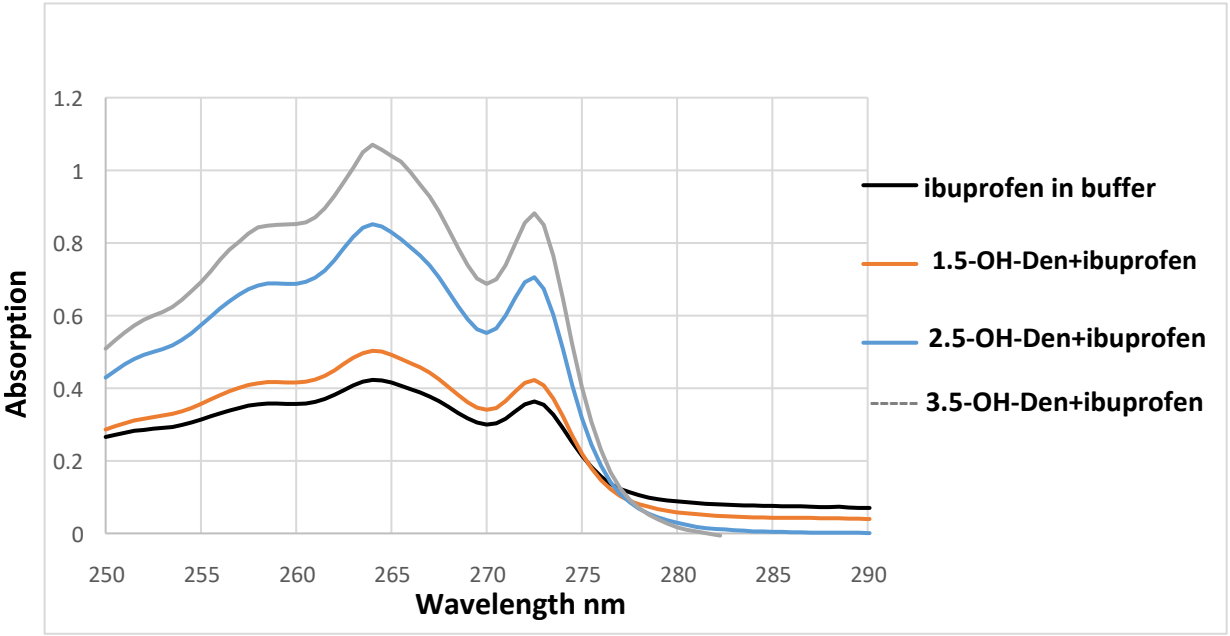

Figure 3.3: UV-Vis of the free ibuprofen Vs the encapsulated Ibuprofen within PAMAM dendrimer at ($1x10^{-4}$) concentration.

The Ibuprofen concentration for each dendrimer is shown in Table 3.1. The maximum concentration of Ibuprofen in the buffer solution was determined as $1x10^{-3}$ M. Using this number, we can calculate the concentration of encapsulated Ibuprofen and determine the loading per mole of Ibuprofen for each dendrimer.

Table 3.0: The concentration of encapsulated Ibuprofen in different OH-terminated PAMAM dendrimer generations.

Den-Gen	ΔABS 424-427	Total/IBU $1x10^{-4}$ M	Encapsulated IBU at $1x10^{-4}$ M	Load/Dendrimer
G1.5 OH	0.013	0.42	0.47	0.47
G2.5 OH	0.035	1.30	1.29	1.29
G3.5 OH	0.039	1.45	1.44	1.44
Maximum concentration of the free Ibuprofen in buffer at $5X10^{-7}$ M				

The effect of dendrimer generation/size on the solubility and encapsulation of Ibuprofen was demonstrated from the results presented in Table 3.1. For instance, the smallest G1.5 OH dendrimer, with 8 hydroxyl OH groups, could encapsulate 4 four molecules of Ibuprofen within its structure. Whereas the larger G2.5 OH dendrimer, with 16 OH groups, could encapsulate 18 molecules of Ibuprofen per dendrimer. However, the number of Ibuprofens encapsulated within the largest G3.5 OH dendrimer was only slightly higher, at just 20twenty per dendrimer. This represented a significantly lower level of encapsulation than expected, despite the doubling in size for the G 3.5 dendrimer Figure3.4.

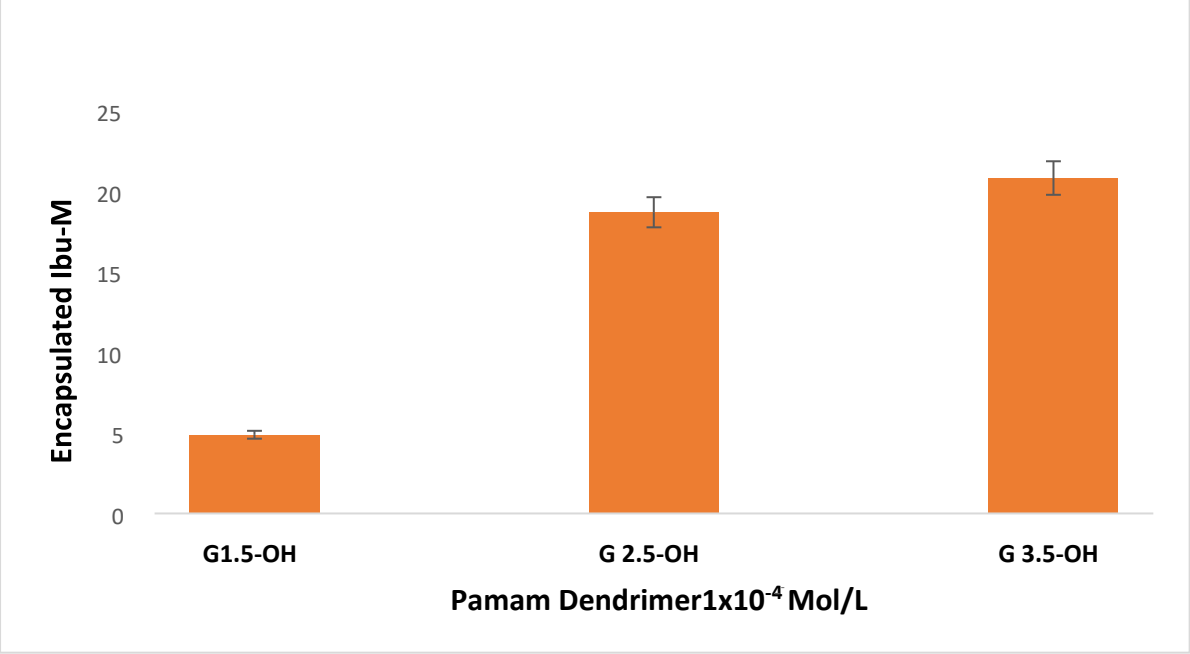

Figure 3.4: The enhancement concentration of encapsulated Ibuprofen within different OH-terminated PAMAM dendrimers.

Overall, the results indicate a significant increase in encapsulated Ibuprofen as we go from G1.5 OH to the G2.5 OH dendrimer, with only a minor increase for the G3.5 OH dendrimer Figure 3.4. The G1.5 OH dendrimer, with its flat-plate-shaped architecture, cannot generate a substantial hydrophobic pocket, and binding is dominated by charge-charge interactions. However, the larger levels of encapsulation for the G2.5 OH and G3.5 OH dendrimers come from their globular spherical configurations, which provide a substantial hydrophobic and H-bonding environment, leading to a marked increase in solubility Ibuprofen encapsulation. The reason for the low level of encapsulation within the G3.5 OH dendrimer was due to an increase in steric crowding within the dendrimer, which limited the space inside. These studies indicated that the G2.5 OH dendrimer was the optimal host for the encapsulation of drugs like Ibuprofen. As such, all future studies will be concentrated on this dendrimer.

The next set of experiments was designed to the relationship between dendrimer concentration and drug encapsulation levels. Specifically, the maximum concentration of encapsulated Ibuprofen was measured at G2.5 OH PAMAM dendrimer concentrations of $1x10^{-3}$,$1x10^{-4}$,$1x10^{-5}$ and $1x10^{-6}$M. It was hypothesised that the encapsulation would increase linearly with dendrimer concentration. The results did not follow this hypothesis, as can be seen from the results shown in Table 3.2.

D/conc	Δ ABS	ε	Total/Ibu $1x10^{-3}$ M	Encap/Ibu $1x10^{-3}$ M	Loading
$1x10^{-6}$	0.095	94	1.0	0.005	5.31
$1x10^{-5}$	0.106	94	1.12	0.12	12.70
$1x10^{-4}$	0.27	94	2.87	1.87	18.71
$1x10^{-3}$	0.5	94	5.31	4.32	4.30

Table 3.2: The Loading of Ibuprofen at different concentrations of PAMAM dendrimers.

Although the data indicates a clear increase in drug encapsulation with increasing dendrimer concentration, the increase is not linear. Initially, the loading of Ibuprofen more than doubled from 5.3 to 12.7, when the dendrimer concentration changed from $1x10^{-6}$ to $1x10^{-5}$ M. As such, we would predict that the loading would again double, as the dendrimer concentration increased to $1x10^{-4}$M. However, the loading of encapsulated ibuprofen only increased by 47%, to 18.71 rather than the 25.40 expected. The problem worsened when the dendrimer concentration was raised to $1x10^{-3}$ M. Based on the initial loading of 5.3 we would expect the loading to be around 50. even taking the previous value of 18.7, we might expect a loading higher than 36. However, at a concentration of $1x10^{-3}$ M, the loading was the lowest recorded in this set of experiments. The data is shown below in Table 3.3 and Figure 3.5.

Table 3.3: The Ibuprofen solubility in G2.5 OH dendrimers concentration between ($1x10^{-3}$and$1x10^{-4}$M). Excess Ibuprofen was used to make the initial complexes.

D/conc	Δ ABS/273-276	ε	Total of IBU/$1x10^{-3}$	Encap /Ibu /$1x10^{-3}$	D/Loading
$1x10^{-4}$	0.27	94	1.80	1.8	18.7
$2.5x10^{4}$	0.32	94	2.60	2.4	24
$5x10^{-4}$	0.325	94	2.92	2.45	24.5
$7.5x10^{4}$	0.33	94	3.31	2.51	25

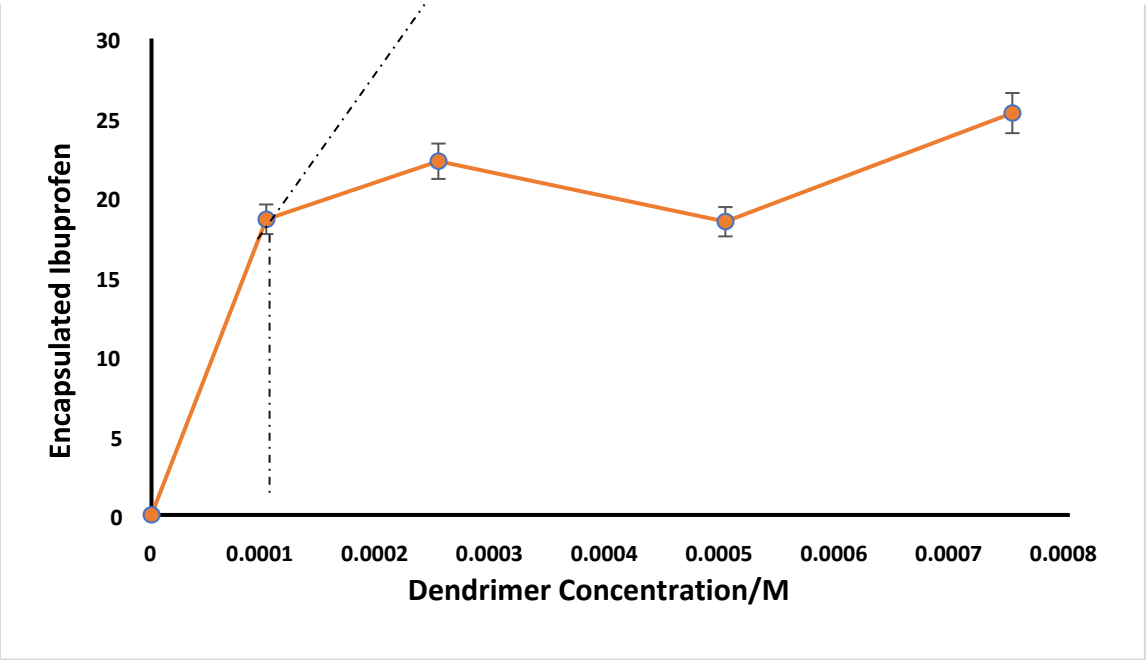

Figure 3.5: The increase in the G2.5 OH dendrimer concentrations affect Ibuprofen solubility.

In the previous experiment using dendrimers of varied sizes/generations, steric crowding of the internal branches accounted for the change in loading. When trying to understand what caused the loading to drop when higher concentrations of the same

dendrimer were used, we also considered a steric argument. However, as the same dendrimer was used in these experiments, an assertion based on internal steric would not make sense. Instead, we considered a premise where the dendrimers might aggregate. That is, the hydrophobic arms of one dendrimer could interact with the arms of other dendrimers. This hydrophobic-driven process could be further improved by hydrogen bonding between the branches of the closest dendrimers. If this occurred, then the space inside each dendrimer would be taken up by the arms of other dendrimers, resulting in a significant drop in the loading/encapsulation of ibuprofen.

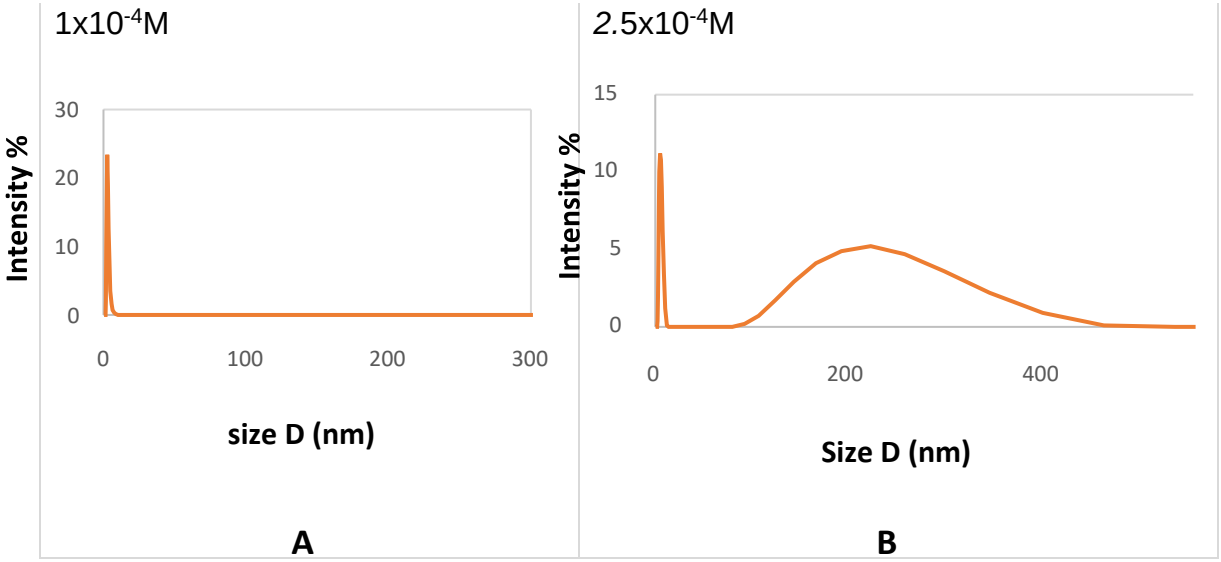

Figure 3.6/A the DLS of G2.5 OH illustrating the non-aggregated OH dendrimer at concentration 1x10^{-4} M. Figure: 3.6/B illustrates the aggregated OH dendrimer at 2.5 x10^{-4} M concentration.

Dynamic Light Scattering DLS was employed to detect the presence of any aggregation of the G 2.5 OH dendrimer as the concentration increased. The DLS data at 1x10^{-4} M showed small molecules with an average diameter of a few nanometres, supporting the expected size of a single unimolecular solvated dendrimer. In contrast, at the higher concentration of 2.5x10^{-4} M, the DLS traces displayed a broad, polydisperse peak with an average diameter of 225 nanometres. This significant difference confirms the formation of large, aggregated dendrimers and provides

compelling evidence that aggregation was indeed responsible for the reduced levels of Ibuprofen loadings/encapsulation. The DLS measurements were performed on the G2.5 16 OH dendrimer at concentrations of $1x10^{-4}$ M and *2*.5 $x10^{-4}$ M. The DLS traces obtained are shown in Figure 3.6.

3.3.2 Ibuprofen stability within the PAMAM dendrimers.

Having established the loading potential of the G 2.5 OH dendrimer and its concentration profile concerning loadings, we needed to establish that encapsulation did not encourage or speed up and degradation of Ibuprofen. This study would consider all the dendrimers synthesised, with a focus on evaluating how the size of the dendrimer could affect the stability of Ibuprofen. As previously described, Ibuprofen-dendrimer complexes at concentrations below the aggregation limit were prepared in a phosphate buffer pH of 7.4 using co-precipitation. method. The resulting complexes were stored at room temperature for 10 days. During this period, UV spectra were recorded at regular intervals, inspecting the difference in absorption intensity between 273 and 276 nm. The outcomes for each dendrimer are summarised in Tables 3.4, and Figure 3.7.

G 1.5-OH/1X10^{-4}M			
Time/Hours	Δ-ABS	ε	Drug-Conc
24H	0.14	94	1.49 X10^{-3}M
48H	0.13	94	1.38 X10^{-3}M

96H	0.11	94	1.2 X10^{-3}M
120H	0.1	94	1.06 X10^{-3}M
144H	0.08	94	8.5 X10^{-3}M
G2.5-OH 1X10^{-4}M			
24H	0.27	94	2.87X10^{-3}M
48H	0.26	94	2.76X10^{-3}M
96H	0.26	94	2.76X10^{-3}M
120H	0.25	94	2.66X10^{-3}M
144H	0.24	94	2.55X10^{-3}M
G3.5-OH/1X10^{-4}M			
Day/time	Δ-ABS	ε	Drug-Conc
24H	0.29	94	3.08 X10^{-3}M
48H	0.27	94	2.87 X10^{-3}M
96H	0.27	94	2.87 X10^{-3}M
120H	0.25	94	2.65 X10^{-3}M
144H	0.24	94	2.55X10^{-3}M

Table: 3.4: Ibuprofen Stability within (G1.5 OH, G2.5 OH and G3.5 OH).

The results indicate that Ibuprofen maintained a reasonable level of stability in all dendrimers studied. However, the G2.5 OH and G3.5 OH dendrimers displayed

slightly higher stability around 90 % over the 10 days than the smaller G1.5 OH system around 10% over the same time. This difference is due to the larger dendrimer's optimised internal structure relative to that of the smaller more open G1.5 OH dendrimer. The structure of the larger dendrimers protects the drug from the external aqueous environment and hydrolysis.

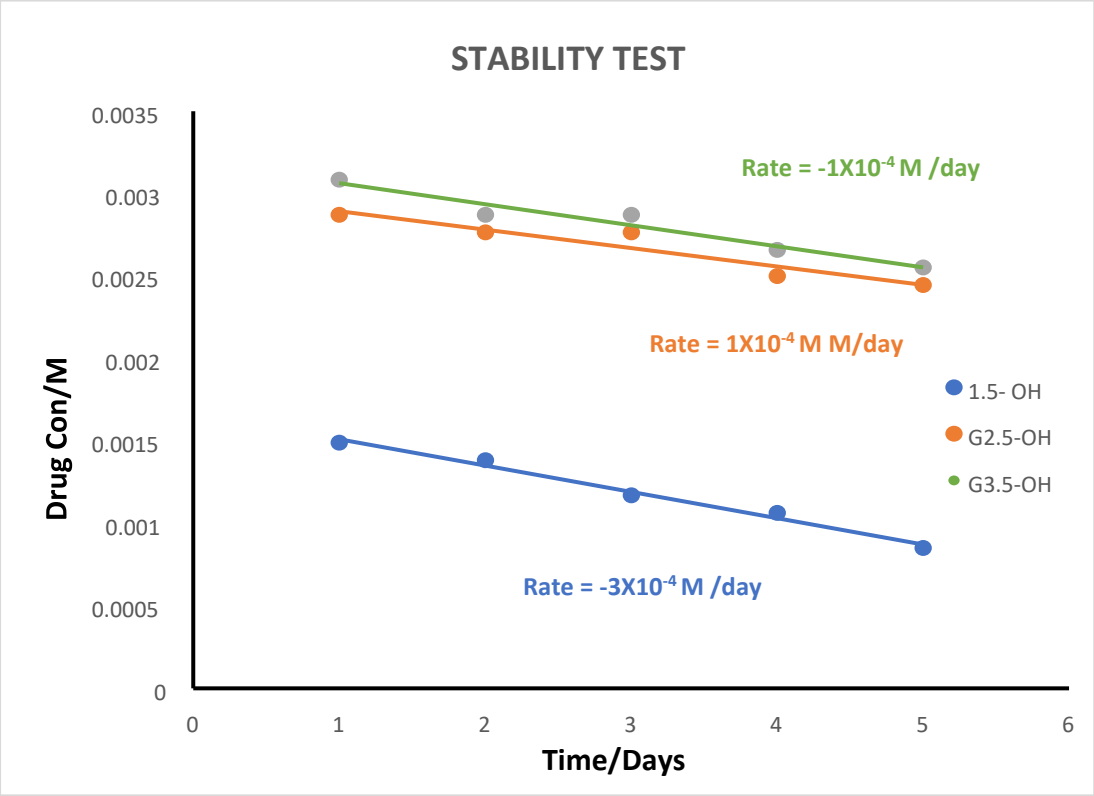

Figure 3.7: The Stability of OH-PAMAM-drug complexes for 10 days.

3.3.3 The release of Ibuprofen from G2.5 OH PAMAM dendrimer Terminated Group.

Having demonstrated excellent levels of encapsulation and stability for the optimised G2.5 OH dendrimer, we need to establish a release profile for the encapsulated Ibuprofen. The therapeutic efficacy will depend on the drug's ability to be effectively released from the dendrimer. The G2.5 OH PAMAM dendrimer emerged as the

optimal choice due to its enhanced drug-loading capacity and stability in primary experiments. Consequently, this generation of the dendrimer was chosen for further experiments aimed at evaluating the release of IBU.

An IBU/dendrimer complex was prepared at a concentration of $1X10^{-4}$ M for the dendrimer and $8x10^{-3}$M for IBU, following the previously discussed coprecipitation method. 6 ml of the complex was then introduced into osmosis tubing with a molecular weight cutoff of 1,000, which was then placed in a beaker containing 200 mL of phosphate buffer. Samples were removed from the dialysis tubes at t=0 and every 24 hours for five days. The samples were analysed using UV spectroscopy and the change in absorption of Ibuprofen's peak nm was recorded. The data is shown in Table 3.5 and shown graphically in Figure 3.8, which was used to estimate a half-life for release.

Table 3.5: The release of Ibuprofen from G2.5 OH PAMAM dendrimer for 5 Days.

Time/Hrs	∆-Abs 273 / 276	Conc/$1X10^{-4}$	Half-life
0	0.803	8.50	34 Hr
24	0.517	5.49	
48	0.329	3.41	
72	0.2305	2.45	
96	0.11	1.17	
120	0	0	
Dendrimer conc at $1x10^{-4}$ M			
IBU Conc at 8.5 $x10^{-3}$ M			

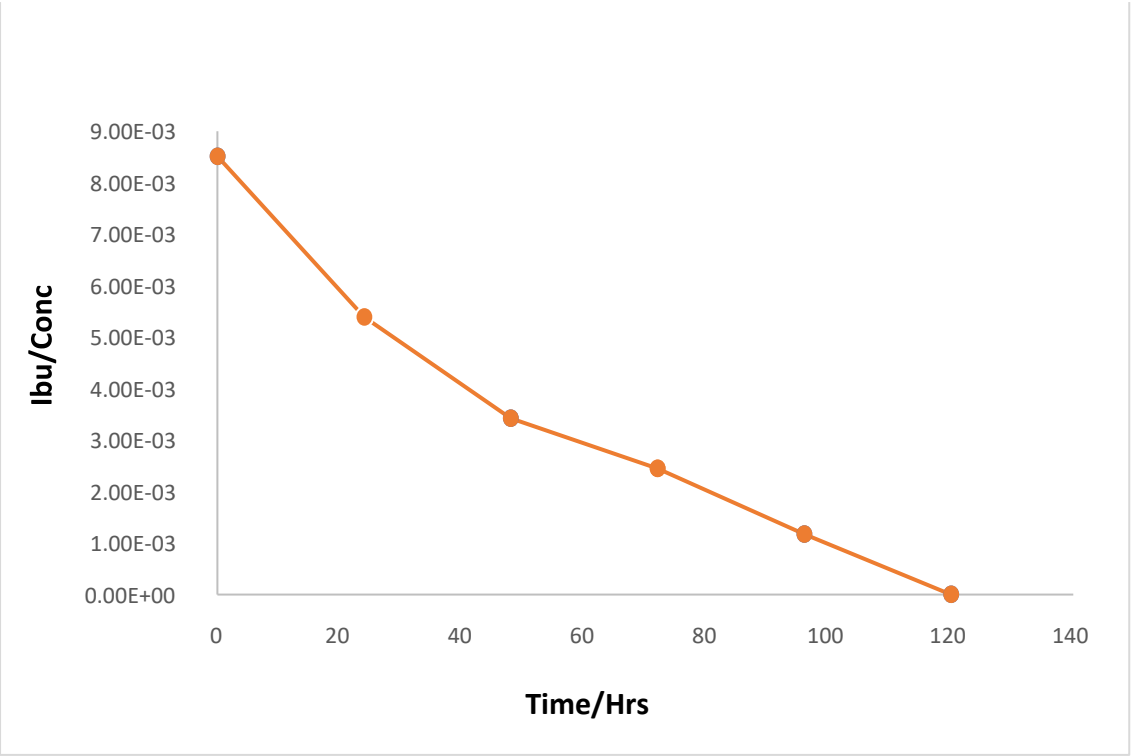

Figure 3.8: The release of Ibuprofen from G2.5 OH PAMAM dendrimer for 5 Days.

The experiment confirms that Ibuprofen can be successfully released from the G2.5 OH dendrimer, highlighting its viability as a potential system for use in drug delivery. Furthermore, the release was slow and occurred over an extended period. A slow-release profile can reduce the frequency of drug administration and aid patient compliance, as well as minimising fluctuations in drug concentration. Furthermore, potential side effects associated with rapid changes in drug levels can be avoided. Overall, such a system can offer significant benefits over a protocol that simply ingests the drug at regular intervals.

Studying Figure: 3.8 in more detail, we observe two phases. Initially, there is a rapid release phase that occurs between t=0 and t=50 hours. This is followed by a slightly slower release phase. Overall, the mechanism of release is a three-phase release process. In the first phase, the free non-encapsulated Ibuprofen present in the

“saturated” aqueous solution can cross the osmosis membrane. This is a rapid process that leads to a reduction in the concentration of free Ibuprofen in the solution. When this occurs, a second phase involving the release of encapsulated Ibuprofen from the dendrimer’s interior occurs as the electrostatic and hydrogen bonding interactions are disrupted. The third phase reflects the first, with the released Ibuprofen crossing the membrane quickly.

The rate of release under physiological conditions might be quicker if the dendrimer-drug interactions can be disrupted more quickly. The most important outcome of these experiments is the confirmation that drugs can be released after encapsulation.

3.3.4 The Stability of ZnTDHPP-PAMAM dendrimer complexes.

The ZnTDHPP encapsulation within various dendrimers specifically G 2.5 OH dendrimer highlights a remarkable interaction between metalloporphyrins and dendritic structures. The G 2.5 OH dendrimer, with its dense branching and terminal hydroxyl groups, provides a favourable environment for encapsulating ZnTDHPP, enhancing its solubility and stability. This encapsulation is facilitated through non-covalent interactions, including hydrophobic interactions within the dendrimer’s internal cavities and coordination between the zinc centre of ZnTHPP and the oxygen atoms of the hydroxyl groups. The G 2.5 OH dendrimer’s ability to effectively encapsulate ZnTDHPP, therefore, not only enhances the drug’s physicochemical properties but also broadens its application in biomedical fields.

This part of the study will explore the effect of dendrimer size on the stability of ZnTDHPP, a porphyrin known for its photosensitivity and role as a photosensitizer in

photodynamic therapy PDT. This experiment was performed in the presence and absence of light to understand how these factors interact to influence the photosensitizer's performance in PDT which is vital for optimizing its therapeutic efficacy and safety. Performing these experiments. This knowledge is crucial for improving treatment outcomes, enhancing patient safety, and guiding the development of new photosensitizers. Dendrimers of all generations were synthesized using the co-precipitation technique, and the resulting samples were stored in dark conditions and transparent glass containers in light conditions at room temperature within a 0.01M pH 7.4 phosphate buffer for 10 days, followed by evaluations every three days to check for precipitation, turbidity, the changes of consistency or losing drug. The extinction coefficient was calculated and determined as (5854dm^3, mol-1, cm-1) *Table; 3,0*. The degradation rate of ZnTDHPP was indirectly determined by tracking the decrease in its concentration over time, using UV-vis spectroscopy. evaluating the peak at 430 nm to determine the rate of degradation under both light and dark conditions. The study illustrates five points of data for each condition over the 10 days, as represented in Figures 3.9 and 3.10 and Tables 3.6 and 3.7.

Table 3.6: The dark storage conditions way of ZnTDHPP Stability within different PAMAM dendrimer generations.

DARK CONDITIONS			
Time/Hrs	1.5 OH $1x10^{-4}$	2.5 OH $1x10^{-4}$M	3.5 OH $1x10^{-4}$M
24H	8.21576	1.77	1.96
48H	7.58378	1.71	1.90
72H	5.68784	1.64	1.83
96H	4.42387	1.52	1.71
120H	3.15991	1.52	1.64

Table 3.7: The light storage conditions of ZnTDHPP Stability within different PAMAM dendrimer generations at 1x10^{-4}M concentrations.

LIGHT CONDITIONS			
Time/Hrs	1.5 OH 1x10^{-4}	2.5 OH 1x10^{-4}M	3.5 OH-1x10^{-4}M
24H	0.82	1.77	1.96
72H	0.695	1.64	1.83
120H	0.515	1.52	1.71
168H	0.375	1.52	1.58
212H	0.255	1.33	1.52

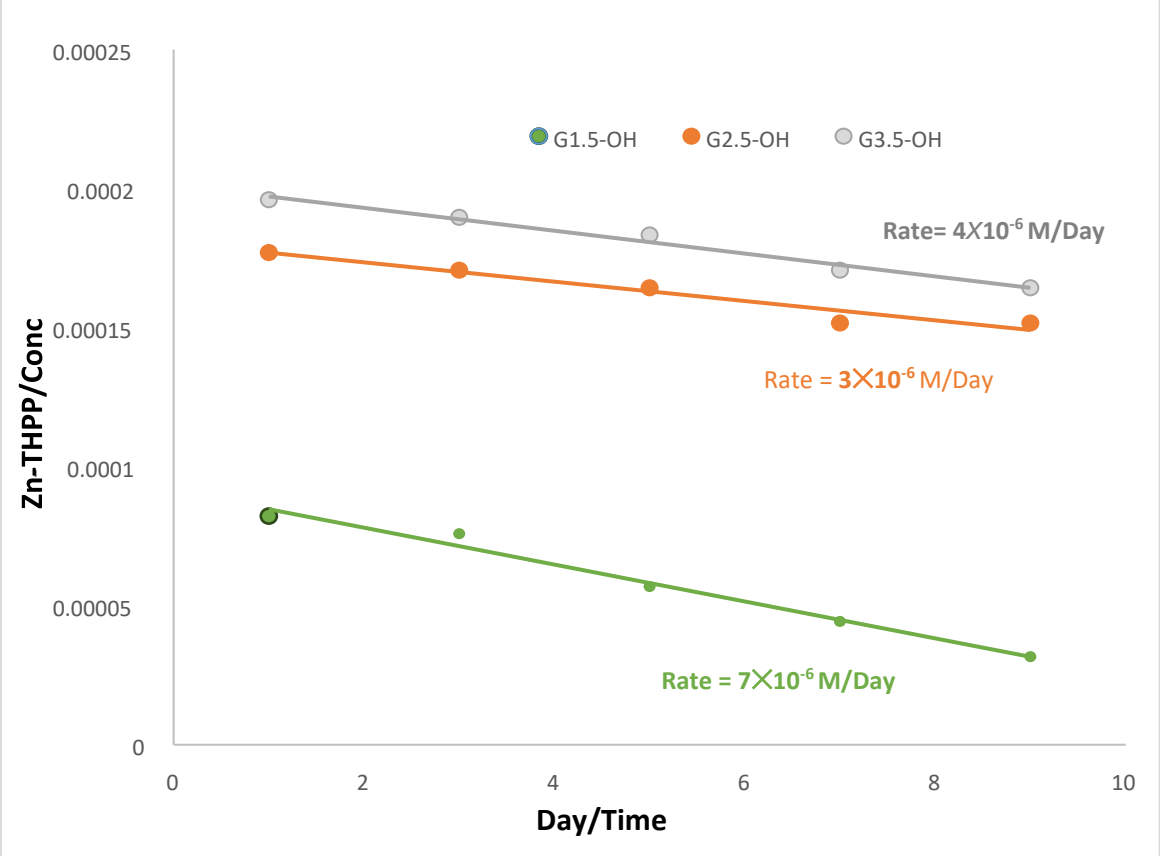

Figure 3.9: The dark storage conditions way of ZnTDHPP Stability within different PAMAM dendrimer generations.

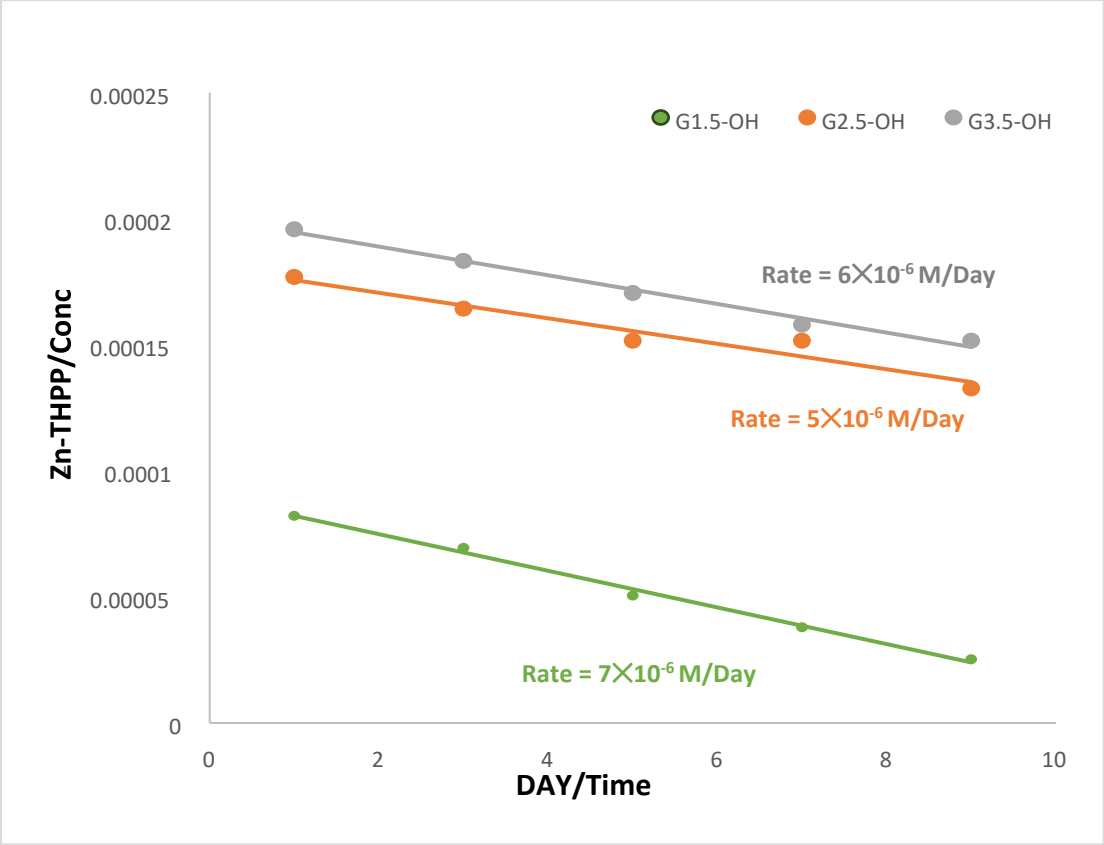

Figure 3.10: The Light storage conditions of ZnTDHPP Stability within different PAMAM dendrimer generations.

The results illustrated in Figure 3.10 reveal that the ZnTDHPP determines a significant level of stability within all dendrimers, with enhanced stability observed in the G2.5 OH and G3.5 OH dendrimers, which were approximately 90% after 10 days. This stability is effective in maximising binding interactions between the drug and the dendrimer. Such an internal configuration promotes more drug-dendrimer interactions, significantly contributing to the enhanced stability of ZnTDHPP within dendrimer generation.

Table 3.8: The degradation rate of ZnTDHPP from PAMAM dendrimers in light and dark conditions.

ZnTHPP Complex	Dark degradation at $1x10^{-6}$ M/day	Light degradation at $1x10^{-6}$ M/day
ZnTDHPP / G1.5OH	7.20	7.60
ZnTDHPP / G2.5OH	3.8	4.52
ZnTDHPP / G3.5OH	4.5	4.91

The results presented in Table 3.8 indicate that ZnTDHPP showed enhanced stability when stored in dark conditions compared to light conditions across all dendrimer generations. This improvement is attributed to the natural photosensitivity of porphyrins, which are liable to the photodegradation process where light exposure compromises the porphyrin's structural integrity and functional properties. In addition, porphyrins are subject to photooxidation, a specific form of photodegradation, where light exposure prompts oxygen molecules to react with the porphyrin, producing free radicals. These radicals can trigger further chain reactions, causing extensive damage to the porphyrin structure. Therefore, storing ZnTDHPP in dark conditions mitigates the degradation processes, protecting the porphyrin's stability and ensuring its efficacy.

3.3.5 The release of ZnTDHPP from the G2.5 OH PAMAM dendrimer.

The PAMAM G2.5 OH dendrimer was identified as the optimal generation for achieving maximum drug loading and stability. As such, this dendrimer would be studied to determine whether encapsulated ZnTDHPP could be released. If so, we will also determine the rate and mechanism of release. The experiment was conducted as previously described for Ibuprofen, using a dendrimer concentration of $1x10^{-4}$ M and a

ZnTDHPP concentration of $8x10^{-4}$ M. 6 mL of the dendrimer/ZnTDHPP complex solution was placed into an osmosis tube with a 1,000 KDa cutoff. The osmosis tube was then sited in a beaker filled with 200 mL of phosphate buffer. To analyse the release of porphyrin from the dendrimer complex, samples were removed from the dialysis tubes at time t=0, and then every 24 hours over five days. The concentration of ZnTHPP in the buffer was determined by the absorbance of the Soret band at 430 nm using UV spectroscopy. The data obtained was visualised in Figure 3.11. providing insights into the release profile of ZnTDHPP from the PAMAM G2.5 OH dendrimer complex under controlled conditions.

Table 3.9: The ZnTDHPP Release from PAMAM dendrimer OH terminated group for five days.

Time/Hrs	∆-Abs 430-433	ZnTHPP$1x10^{-4}$	Release Mol/Hr
0	0.24	7.79	0.25
24H	0.072	3.34	
48H	0.0123	2.4	
72H	0.0032	1.1	
96H	0	0	
Dendrimer conc at $1x10^{-4}$M			
The maximum conc of ZnTDHPP at $7.8x10^{-4}$			

The results presented in Table: 3.9 indicate that the ZnTDHPP can be effectively released from the PAMAM dendrimer over 50 hours. This slow-release mechanism is particularly advantageous for photodynamic therapy PDT, as it would allow the ZnTDHPP complex time to circulate throughout the body, and to accumulate within tumour sites via an enhanced permeability and retention effect EPR. The release time would therefore minimize exposure to normal tissues, reducing the side effects commonly associated with PDT. As with Ibuprofen, the gradual release of ZnTDHPP

is likely influenced by the disruption of the coordination bonds and the electrostatic and hydrogen bonding interactions that initially secured the drug within the dendrimer's structure, due to environmental changes like pH shifts, leading to the drug's release, the electrostatic interactions between the dendrimer's charged groups and the drug can be altered by changes in ionic strength and pH in different biological environments, Hydrogen bonding between the dendrimer and the drug is dynamic and can be disrupted by changes in temperature, solvent composition, or competition from other molecules. Furthermore, there is a possibility that PAMAM dendrimers can undergo slow hydrolysis in the presence of certain enzymes. However, further investigation is necessary to determine the impact of enzymatic activity on dendrimer hydrolysis and ZnTDHPP release in a physiological situation.

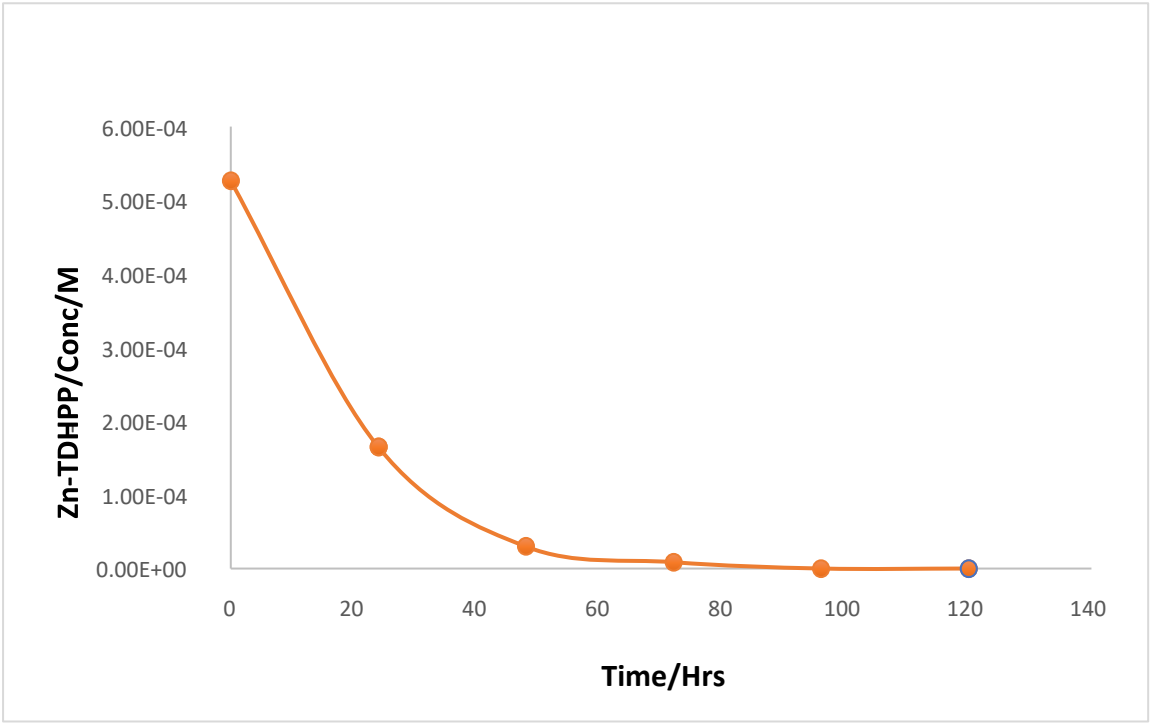

Figure: 3.11: The Zn-TDHPP Release from OH-PAMAM dendrimer for five days.

The release profile of ZnTDHPP from PAMAM dendrimers is characterized by the curved nature of the release pattern, starting with the transport of any non-encapsulated ZnTDHPP through the osmosis membrane from T=0 to T=24 hours. This first phase reduces the concentration of free ZnTDHPP in the solution, creating a concentration gradient that can be filled by releasing encapsulated ZnTDHPP from the dendrimer. This second phase is slow. However, the released ZnTDHPP can now cross the osmosis membrane rapidly, in an identical way to the initial phase. Nevertheless, under physiological conditions interactions within the dendrimer might be weaker and/or the dendrimer degrades rapidly, resulting in a faster release of ZnTDHPP.

3.3.6 The anticancer drug F37 Encapsulated within OH-terminated PAMAM dendrimers.

Building on previous research that investigated and compared the encapsulation capacities of various polymers using Ibuprofen, the current work aims to utilize anticancer drugs, exploring the encapsulation behaviours and efficiencies of dendritic polymers with an anticancer drug, known as F73, which have more complex structures than Ibuprofen. Professor Chen's group has generously provided a quantity of F73 for the study, as structurally identified in *Figure* 3.12.

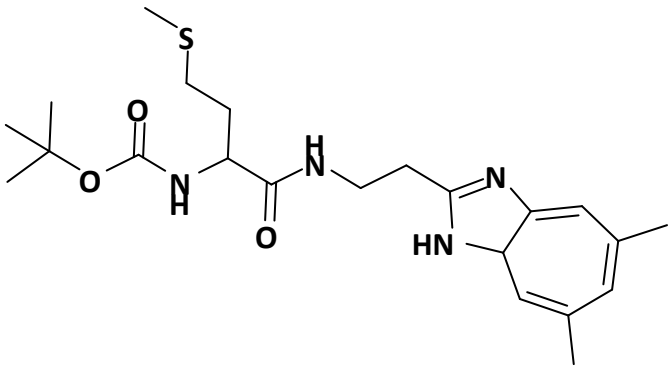

Figure 3.12: The Structure of F73

The F73 compound, officially named ‘’tert-butyl N-(1-[(5,6-dimethyl-^{1}H-1,3benzothiazole-2yl)(methyl]carbamoyl3(methyl-sulfonyl)propyl- carbamate’’, is composed of three primary structural components: a tert-butyloxy carbonyl group that functions as an amino protecting group, a central methionine moiety, and a dimethyl benzimidazole ethylamine group, connected via peptide bonds. Originally developed for dementia treatment, F73 exhibited limited activity in this area but gave a promising efficacy against cancer cells, with IC50 in the nanomolar range, indicating its potential as an anticancer agent. Its mechanism of action involves inhibiting methionine synthase Met-S, an enzyme essential for the metabolic conversion of 5-methyltetrahydrofolate Me-THF to tetrahydrofolate, this process is critical for DNA and RNA synthesis. By inhibiting Met-S, F73 interrupts the transfer of a methyl group from Me-THF to homocysteine, a reaction facilitated by the cobalamin cofactor, which is essential for producing purines and pyrimidines.

On the other hand, F73, like many anticancer agents, presents a significant challenge for drug delivery due to natural hydrophobicity, making a difficult to penetrate cancer cells effectively. To overcome this issue, the research explored both dendrimers and Hyperbranched Polymers HBPs as carriers for encapsulating the hydrophobic F73, intending to enhance its solubility and delivery efficiency. The choice of F73 for this investigation was also influenced by the opportunity to evaluate the efficacy of the drug delivery systems using various cancer cell lines, in collaboration with Dr Nikki Jordan from Sheffield Hallam University. This collaboration will enable a comprehensive evaluation of the encapsulation, release, and delivery capabilities of the Dendrimer and HBP systems. As such, we will be able to address the core research question asked in this part of the thesis: "Are HBPs as effective as dendrimers in terms of drug delivery?".

3.3.7 F73 anticancer drug encapsulated within neutral OH PAMAM dendrimers.

The primary objective was to determine the maximum quantity of the F73 anticancer drug that could be encapsulated in different polymer-based systems *Figure 3.13*. However, unlike Ibuprofen, the scarcity of F73 and the excessive cost required a more analytical approach that avoided the wasteful consumption of the drug (compared to the coprecipitation method that requires the use of excess drugs). Therefore, the encapsulation method was effectively conducted in reverse. That is, we would start by preparing complexes using insignificant amounts of the drug. The amount of drug would then be gradually increased until it was evident that a maximum point had been reached (obvious precipitate after addition of buffer to complex). As such, we started with a 1:1 molar ratio of F73 and dendrimer. The amount of F73 was then doubled in the following steps, gradually increasing until the appearance of an obvious precipitate could be seen. At this point, the polymer's capacity to encapsulate the drug had been exceeded. This incremental method allowed for the efficient use of F73 by carefully titrating the drug amount to determine the maximum encapsulation capacity for the polymer systems.

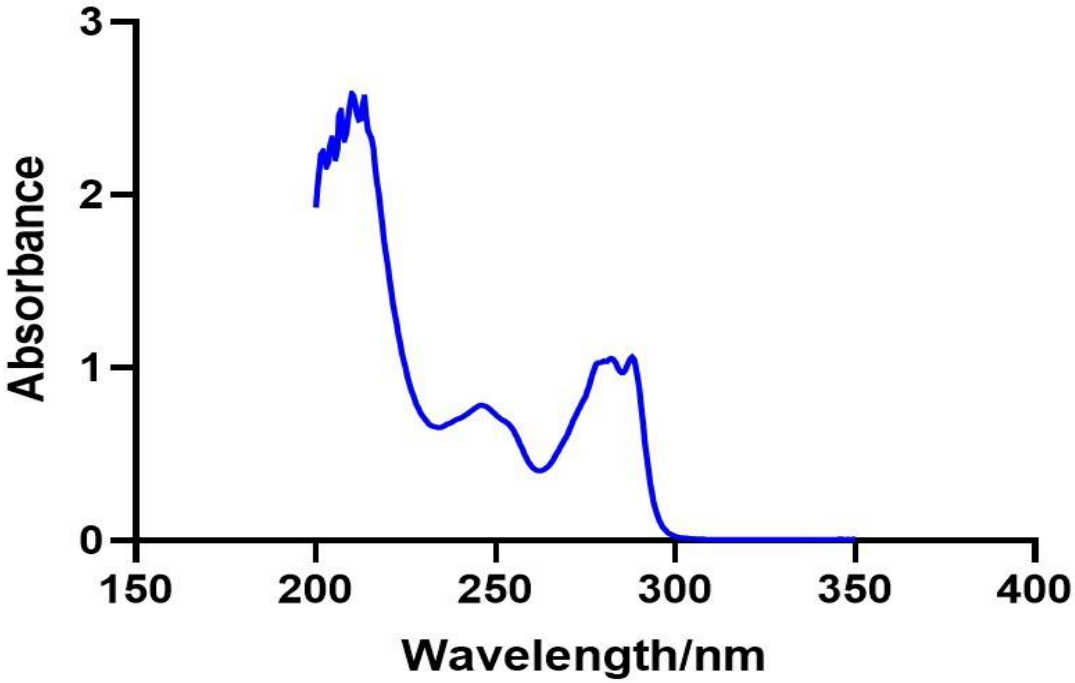

Figure 3.13: The F73 absorbance within a phosphate buffer.

The extinction coefficient 5880/M was obtained using a Beer-Lambert plot, and the maximum absorbance of F73 in a buffer solution was determined as $1x10^{-4}$ M, as shown in Table 3.10.

Drug	ε	Max/solubility in buffer
F73	5880	$3.5x10^{-4}$M

Table 3.10: The Maximum solubility for F73 in Buffer.

The PAMAM dendrimers G1.5 with 8 OH, G2.5 with 16 OH, and G3.5 with 32 OH, were used to evaluate the encapsulation efficiency of the F73 anticancer drug. The maximum concentration of F73 within the dendrimers was determined using the method described above and a dendrimer concentration of $1x10^{-4}$M.

Dendrimer/Gen	Total-F73 $1x10^{-4}$M	Encapsulated F37 $1x10^{-4}$M	Den/Load
G1.5OH	5.40	2.70	2.70
G 2.5OH	8.50	5.0	5.1
G 3.5OH	6	2.90	2.90
The concentration of Dendrimer $1x10^{-4}$M			
The maximum concentration of free/F73 in buffer at $3.5x10^{-4}$M			

Table 3.11: The F73 Encapsulation within different OH terminated PAMAM dendrimers generation.

The encapsulation efficiency of the anticancer drug F73 within different generations of hydroxyl terminated PAMAM dendrimers G1.5 OH, G2.5 OH, and G3.5 OH, had a similar trend to the data obtained using Ibuprofen. That is, the G1.5 OH and G2.5 OH dendrimers demonstrated higher F73 loading compared to the larger G3.5 OH dendrimer. As rationalised for Ibuprofen, the steric crowding in G3.5 dendrimers reduces the available internal space, thereby reducing the level of encapsulation.

Where the G2.5 OH dendrimer could encapsulate 18.7 Ibuprofen molecules, the same dendrimer could only encapsulate 2.5 molecules of the F73, as shown in Table 3.11. There are several reasons for this. One reason for the difference is due to the size of F73, which is much larger than Ibuprofen. Additional factors, including differences in hydrophobicity and the strength or number of secondary interactions between the drug and the dendrimer, may also account for the poor encapsulation efficiency of F73 within the dendrimers.

3.3.8 The Stability of F73 Polymer Complexes within the OH PAMAM dendrimer.

The stability of F73 once encapsulated was evaluated using the same method utilized for Ibuprofen and ZnTDHPP. This involved the extraction of a small sample from the top layer of the solution containing the encapsulated drug each day. The absorbance of the sample was then measured, enabling monitoring of drug concentration within the polymer matrix over time.

Time/Hrs	G1.5 OH $1x10^{-4}$M	G2.5 OH $1x10^{-4}$M	G3.5 OH $1x10^{-4}$M
24H	2.70	5	3
72H	2.50	5	2.80
120H	1.90	4.8	2.70
168H	1.70	4.7	2.50
212H	1.40	4.6	2.40

Table 3.12: The F73 Stability of different OH PAMAM dendrimer generations for 5 days.

The encapsulation levels of F73 within the polymers remained stable over the nine days assessed, Table 3.12 and Figure 3.14. However, for the G1.5 OH /F73 complex, the drug had noticeably lower stability. This is the same as observed for the ZnTDHPP and Ibuprofen. As before, the stability of F73 within higher-generation dendrimers was due to their architectures, which provided a protective environment against external factors, such as hydrolysis. The G1.5 OH dendrimer's structure cannot provide a sufficient hydrophobic environment, which enables hydrolysis leading to loss of drug concentration.

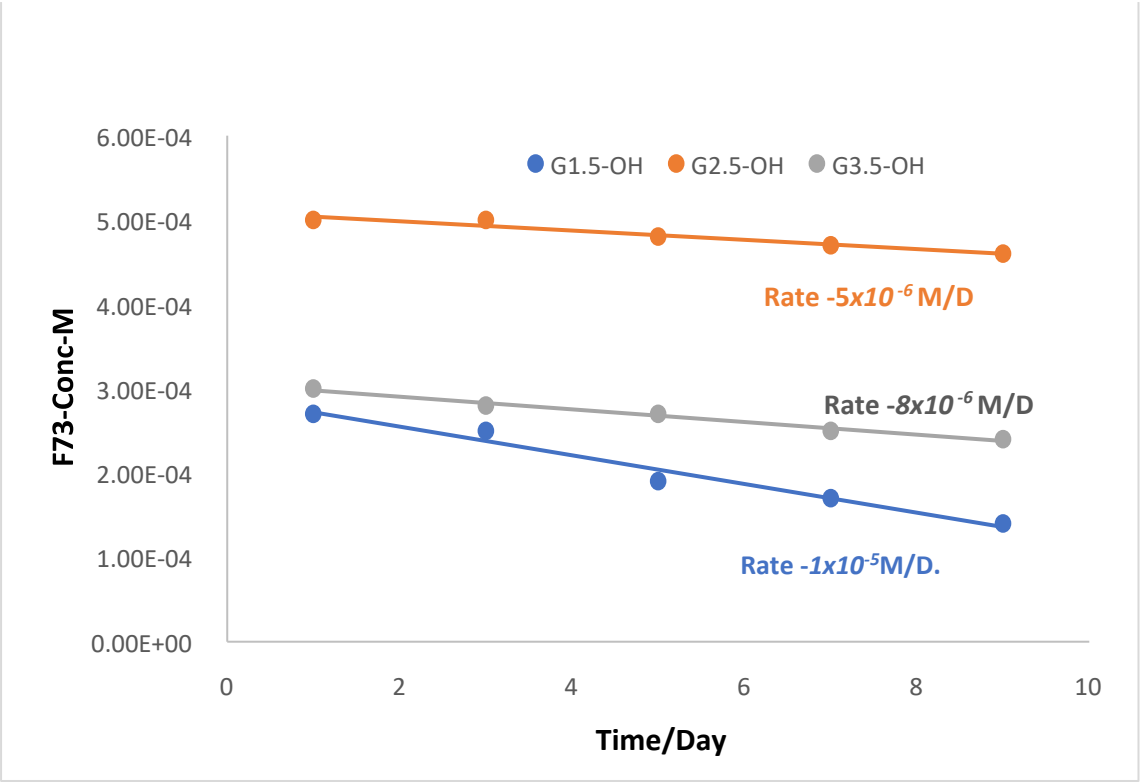

Figure 3.14: The F73 Stability of different OH-PAMAM dendrimer generations for 5 days.

3.3.9 7.4.4 The release process of F73 from G2.5 OH PAMAM dendrimer complex.

As with the previous studies using Ibuprofen and ZnTHPP, it was clear that G2.5 OH was the optimal dendrimer generation for realizing the maximum loading drug and stability for F73. As such, the release studies were conducted using this dendrimer and the same method described above for Ibuprofen and ZnTDHPP. A 6 mL solution of the dendrimer/F73 complex ($1x10^{-4}$M for dendrimer and $9x10^{-4}$M for F73) was placed in an osmosis tube with a molecular weight cutoff of 1KDa, then sited in a beaker filled with 200 mL of a phosphate buffer. Samples were extracted from the dialysis tubes at time zero t=0 and every 24 hours for five days. The concentration of F73 in the buffer was measured using UV spectroscopy to monitor the absorption of the peak at 282 nm. The collected data is listed in Table 3.13 and Figure 3.15.

Time/Hrs	∆-Abs	Conc/1X10^{-4}	Half/Life
0	1.11	1.89	20 / Hrs
48 H	0.7	1.19	
72 H	0.33	0.56	
96 H	0.0	0.0	
Dendrimer conc at 1x10^{-4}M			
ZnTDHPP Conc at 1.9 x10^{-4} M			

Table 3.13. The release process of F73 from G2.5 OH PAMAM generations for 5 days.

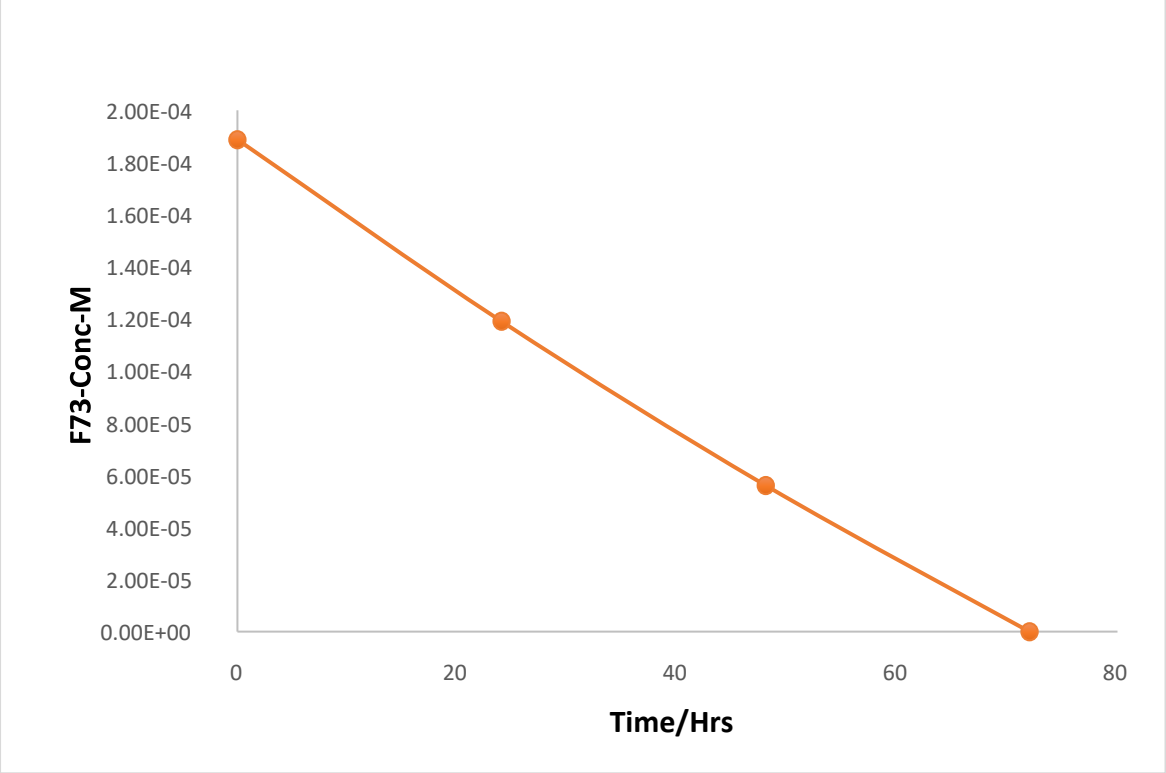

Figure 3.15: The F73 release process from G2.5 OH-PAMAM dendrimer generation for 5 days.

The outcome indicates that the F73 is rapidly released from the PAMAM dendrimer, as proven by the linear graph. The consistent decrease in drug concentration suggests that F73 is released into the bulk solvent as soon as the free F73 in solution diffuses across the membrane. This implies that the release of F73 from the dendrimer occurs much faster than its transport across the membrane. The rapid release also indicates

relatively weak interactions between F73, and the dendrimer compared to those observed with Ibuprofen and Zn-TDHPP. While the dendrimer enhances the solubility of F73, these findings suggest it may not perform as an effective drug carrier for F73.

3.4 Conclusions.

To sum up, a series of PAMAM dendrimers with hydroxyl-functionalized groups were synthesized and evaluated for their ability to encapsulate different hydrophobic drugs. Among these, the G2.5 OH dendrimer with 16 OH terminal groups were identified as the most suitable for drug encapsulation, due to its optimal generation size and structure. The following studies focused on this dendrimer and assessed the effect of dendrimer concentration on encapsulation efficiency using Ibuprofen as a test sample. Converse to the initial hypothesis that encapsulation would scale linearly with dendrimer concentration, a marked deviation from linearity was observed. This was more acute at higher concentrations and was therefore attributed to dendrimer aggregation. It was proposed that aggregation occurred when the internal hydrophobic arms of one dendrimer, interacted with the arms of other dendrimers, through a combination of hydrophobic and hydrogen bonding. This restricts available space within each dendrimer and therefore limits the amount of drug that can be encapsulated. Aggregation was verified by dynamic light scattering DLS, which detected large, aggregated entities with a hydrodynamic radius of 250 nm, at a concentration of $2.5x10^{-4}$M.

The stability of the drugs within the drug/dendrimer complexes was assessed to determine whether the dendrimer affected drug stability. That is, the dendrimer may either protect the drug from degradation (specifically hydrolysis) or assist with any

degradation. For all drugs/dendrimer complexes, the experiments indicated that the G2.5 OH and G3.5 dendrimers were significantly better than the G1.5 OH dendrimer. This enhanced stability can be attributed to its optimised internal structure that promotes an increased number of dendrimer-drug interactions. Furthermore, release studies for Ibuprofen and ZnTDHPP from the G2.5 OH dendrimer showed a slow-release pattern, as represented by the release graphs and a non-constant decrease in drug concentration. Conversely, F73 exhibited a rapid release, characterized by a linear decrease in concentration, indicating a constant release rate, which tells us that release from the dendrimer is faster than transfer across the osmosis membrane. Likely, this occurs because of the high solubility of F73 and the lack of any enhanced interactions between F73 and the dendrimer. Overall, these findings underscore the importance of dendrimer size and concentration in drug delivery systems and highlight the behaviour of different drugs when encapsulated within dendrimers, offering valuable insights for the development of targeted therapeutic applications. The results and experiments discussed here will be compared to the same set of experiments conducted using similar hyperbranched polymers. How they compare will allow us to answer the key question asked at the beginning of this section, specifically, “Can a hyperbranched polymer perform as well as a dendrimer for use in drug delivery?”

Chapter 4

4 The stability Comparison for drugs dendrimer and HBPAMAM complex.

4.1 Introduction.

Extensive research was conducted on hyperbranched polymers (HBPs), including early comparisons with dendrimers. HBPs, a class of highly branched macromolecules with irregular and tree-like structures, have garnered significant interest due to their potential as cost-effective and scalable alternatives to dendrimers in drug delivery applications[205]. It has been suggested that HBPs can achieve comparable drug delivery efficacy to dendrimers while requiring less effort and cost for synthesis and purification[206]. This advantage stems from the simpler synthetic routes for HBPs, often involving single-step polymerization processes, compared to the multi-step and highly controlled synthesis of dendrimers[207].

Despite this potential, most comparative studies between HBPs and dendrimers have not involved direct like-for-like comparisons of specific HBPs and dendrimers[208]. This is a significant limitation, as the encapsulation ability of these materials is heavily influenced by the functionality and connectivity of their repeat units[209,210]. Structural variations, including the presence or absence of specific functional groups capable of interacting with drugs, play a critical role in determining their performance as drug delivery vehicles[30,211].

Aromatic hyperbranched polymers (AHBPs) represent a unique subclass of HBPs that exhibit notable thermal stability, rigidity, and chemical functionality due to their aromatic backbones[212]. These properties make AHBPs attractive for applications in drug delivery, particularly when aromatic interactions, such as π-π stacking or hydrophobic interactions, can be leveraged to enhance drug encapsulation and stability[213]. The aromatic rings in these polymers can also facilitate the incorporation of additional

functional groups to improve their interaction with specific drug molecules, thereby tailoring their encapsulation efficiency and release profiles[214].

In a previous study by the current authors, a PAMAM dendrimer was compared with a hyperbranched polyglycerol, a common non-aromatic HBP. The results showed that the PAMAM dendrimer significantly outperformed the HBP in drug encapsulation. This was attributed to the PAMAM dendrimer's repeat units, which contain amide and amine groups capable of forming hydrogen bonds and acid-base interactions with the drug studied (Ibuprofen). In contrast, the hyperbranched polyglycerol lacked functional groups to interact effectively with the drug, limiting its encapsulation efficiency[215].

However, AHBPs, unlike hyperbranched polyglycerols, possess aromatic structures that could potentially offer better drug interaction capabilities[216]. For instance, their aromatic frameworks may enable stronger interactions with drugs containing aromatic or hydrophobic regions, enhancing encapsulation performance[217]. Moreover, AHBPs can be synthesized with diverse functional groups attached to their aromatic rings, providing opportunities for customization based on the physicochemical properties of the target drug[218]. While these polymers have not yet been widely studied in direct comparison with dendrimers, their unique properties make them promising candidates for advanced drug delivery systems [219].

While HBPs, including AHBPs, offer numerous advantages such as cost-effective synthesis and versatile chemical functionality, the lack of systematic comparisons with dendrimers under standardized conditions remains a key gap in the literature. Future studies focusing on direct comparisons of AHBPs with dendrimers, particularly using drugs that can interact with the aromatic structures of AHBPs, could provide deeper insights into their relative efficacy and potential as drug delivery systems.

4.2 Aims

The primary objective of our research was to conduct a more equitable comparison between hyperbranched polymers HBP and dendrimers, specifically focusing on those with the same functionality and connectivity, and to determine whether dendrimers outperform HBP as drug delivery systems conclusively (the perceived opinion at the start of the project). To achieve this, we needed to identify and synthesise an HBP that mirrored the structural and connectivity characteristics of the OH-terminated PAMAM dendrimer synthesised and discussed in the previous section. We identified a suitable target polymer, and Dr. Reyad Elderbage was responsible for the synthesis.

The HBPAPM structure is shown in Figure 4.1.

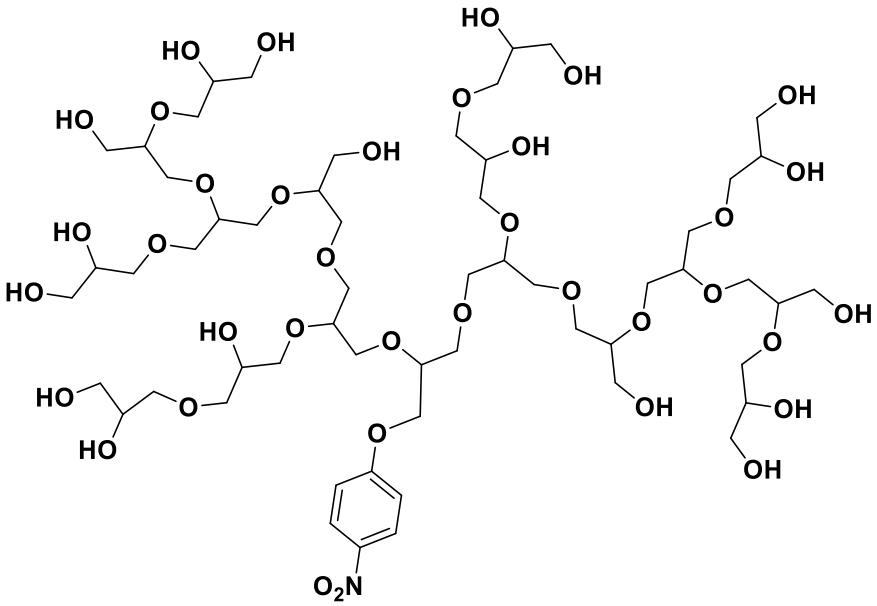

Figure 4.1: Hyperbranched polymer Hydroxy ester-terminated group.

The study would assess the efficacy of HBPs in encapsulating and delivering drugs, and the results compared to those obtained for the dendrimers and discussed in the

previous sections. Initial experiments would involve quantifying drug solubility enhancements via encapsulation within the HBPAMAM. However, the polydisperse nature of the HBPAMAM presents challenges in accurately determining molarity due to the lack of a unique molecular weight [220]. Unlike monodisperse systems where all molecules have identical molecular weights, HBPs are a mixture of molecules with varying molecular weights within the same structure[210]. This heterogeneity makes it difficult to assign a single molecular weight value, leading to uncertainties in molarity calculations. Therefore, in addition to molarity, a mass/volume method was also used to calculate concentrations[221].

Gel permeation chromatography GPC was used to an average molecular weight of the HBPAMAM. However, GPC does not record a molecular weight, but a molecular size [222]. Molecular weights are then assigned relative to those of well-characterised linear polymer calibration standards. Therefore, GPC introduces additional uncertainty in determining the molecular weight of globular molecules such as HBPs. Consequently, GPC tends to underestimate the molecular weight of HBP due to their spherical structures. This uncertainty increases with size/molecular weight. Despite this limitation, GPC analysis in aqueous conditions estimated an average molecular weight of 2500 for the HBPAMAM under investigation[223]. This suggests that the HBPAMAM is relatively small and may not be too far from the actual molecular weight. Furthermore, this molecular weight is like the 2.5 G PAMAM dendrimer, which would be used for the comparative study.

The use of a mass/volume method for concentration is often used by polymer chemists [224]. This method ensures that the same number of monomer units are present in a solution regardless of the polymer's molecular weight, facilitating comparisons of properties across different molecular weights. However, it's crucial to note that this

method requires the polymers to have identical repeat units, which is not the case for the PAMAM dendrimer and HBPAMAM systems under investigation in this study. Nevertheless, despite slight structural variations, the similarities between these systems may allow for a better comparison of properties than the same data obtained using molar concentrations. To facilitate a qualitative comparison between the two systems, we propose to investigate the drug delivery properties of the PAMAM and HBPAMAM using both molarity and mass/volume methods for concentration.

4.3 Result and Discusion.

4.3.1 IBU, ZnTDHPP and F73 Encapsulated within HBPAMAM using molar concentration method.

This aspect of the project was carried out in collaboration with Dr Elderberg and used the same methods previously described in the PAMAM drug delivery chapter presented earlier. The concentrations of HBPAMAM were equivalent to those used in the dendrimer experiments and were established at $1x10^{-4}$ M using both molar concentration and mass/volume methods. The results of which are presented in Table 4.1.

Table 4.1: (IBU. ZnTDHPP and F73) Encapsulated within HBPAMAM by the molar concentration method, $1x10^{-4}$ equivalent.

HBP Concentration	Total of IBU/M	Encapsulated IBU/M	HBP/Load
$1x10^{-4}$ M	2.66 $x10^{-3}$	1.66 $x10^{-3}$	16.51
HBP Concentration	Total of F73/M	Encapsulated F73/M	HBP/Load
$1X10^{-4}$M	0.75	0.41	4
HBP Concentration	Total of ZnTDHPP/M	Encapsulated ZnTDHPP/M	HBP/Load
$1X10^{-4}$M	1.45	1.42	1.42
Ibuprofen concentration $1x10^{-4}$ M			

4.3.2 IBU, ZnTDHPP and F73 Encapsulated within HBPAMAM using Mass/Volume concentrations method.

comparing the encapsulation capabilities of HBPAMAM polymers versus dendrimers using the mass/volume method for concentration determination, a significant difference is observed. The HBPAMAM polymers exhibit a lower loading capacity for all tested drugs compared to the dendrimer-based systems. This variation can be attributed to structural differences between HBPAMAM and dendrimers, specifically in the composition and molecular weight of their repeat units[220].

Table 4.2: The encapsulation of OH terminated HBPAMAM and PAMAM dendrimer at mass/vol concentration equivalent 1X10^{-4} M.

Drug	Dendrimer	HBP
Ibuprofen	1.8x10^{-3} M	9x10^{-4} M
ZnTDHPP	1.7x10^{-4} M	1.2x10^{-4} M
F37	5x10^{-4} M	1.6x10^{-4} M
Mass/volume		

Table 4.2 represents the data that HBPAMAM's repeat units incorporate aromatic groups between each monomer, increasing the molecular weight of these units compared to those of PAMAM dendrimers. Consequently, HBPAMAM has a higher molecular weight per repeat unit 259 than PAMAM 183, approximately 30% higher. This difference means that for an equivalent mass of the carrier system, HBPAMAM polymers have fewer repeat units and, thus, fewer potential encapsulation sites compared to PAMAM dendrimers. As a result, the fewer repeat units in HBPAMAM solutions translate into a reduced capacity for drug encapsulation.

4.3.3 The Stability of the Encapsulated IBU, ZnTDHPP and F73 within HBPAMAM.

The main purpose is to explore how HBPAMAM influences the stability of (IBU. ZnTDHPP and F73) complexes. Utilizing the co-precipitation method, as detailed in Table 4.3, and visually represented in Figures 4.2,3,4 and 5.

Table 4.3: The Stability test of Drugs IBU. ZnTDHPP. and F73 encapsulated within dendrimer and HBPAMAM polymers.

Time/Hrs	IBU dendrimer	IBU/HBP	ZnTDHPP/ dendrimer	ZnTDHPP/ HBP	F73 / dendrimer	F73 / HBP
24 H	$2.87x10^{-3}$ M	$3.1x10^{-3}$ M	$1.77x10^{-4}$ M	$1.4x10^{-4}$ M	$5x10^{-4}$ M	$4x10^{-4}$ M
48 H	$2.77x10^{-3}$ M	$2.87x10^{-3}$ M	$1.71x10^{-4}$ M	$1.32x10^{-4}$ M	$5x10^{-4}$ M	$3.9x10^{-4}$ M
72 H	$2.77x10^{-3}$ M	$2.87x10^{-3}$ M	$1.64x10^{-4}$ M	$1.3x10^{-4}$ M	$4.8x10^{-4}$ M	$3.7x10^{-4}$ M
96 H	$2.66x10^{-3}$ M	$2.66x10^{-3}$ M	$1.52x10^{-4}$ M	$1.28x10^{-4}$ M	$4.7x10^{-4}$ M	$3.5x10^{-4}$ M
120 H	$2.55x10^{-3}$ M	$2.55x10^{-3}$ M	$1.5x10^{-4}$ M	$1.26x10^{-4}$ M	$4.6x10^{-4}$ M	$3.4x10^{-4}$ M

The study's findings demonstrate that all tested drugs maintain prominent levels of stability within both dendrimer and HBPAMAM systems, with approximately 90% stability observed in the G2.5 OH dendrimer complexes and a slight reduction in stability within the HBPAMAM complexes. However, the difference in stability between the two polymer systems is not significant. The stability observed in G2.5 OH dendrimer complexes is due to the dendrimer's optimized internal structure, which facilitates extensive drug-dendrimer interactions, enhancing drug stability. Similarly, the stability in HBPAMAM complexes can be credited to its heavily branched structure, featuring a defined core and multiple branching layers, which effectively protect drugs from degradation. Both systems demonstrate their capability to prevent drug degradation by water, indicating that they serve as effective mediums for preserving the integrity of encapsulated drugs as shown in *Table 4.3*.

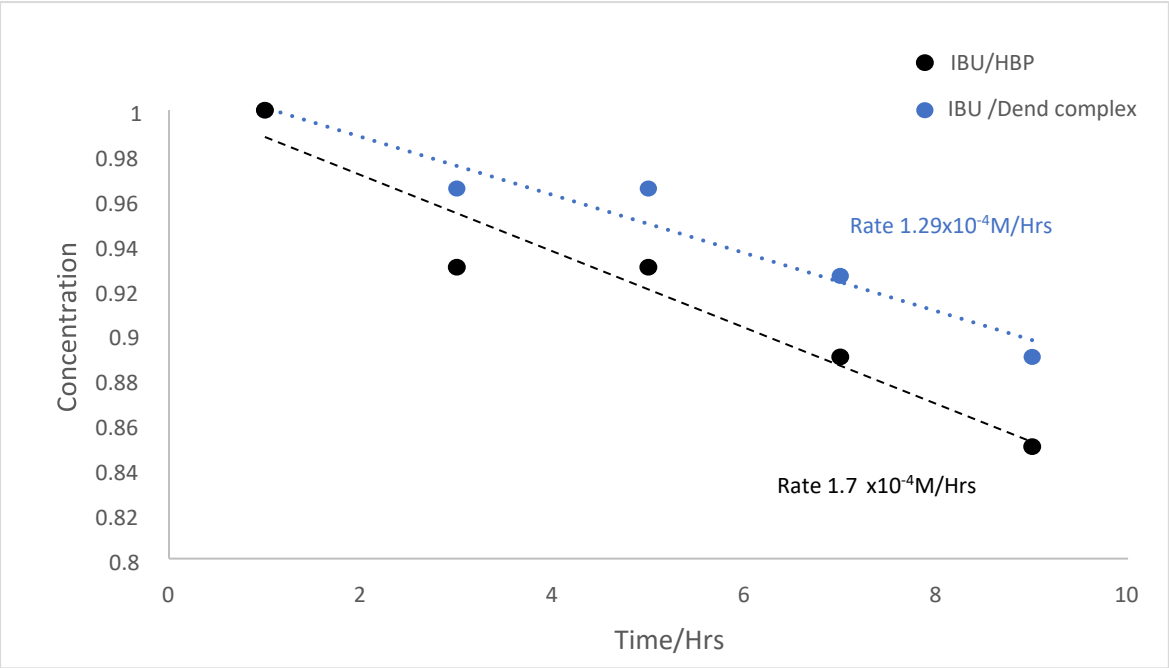

Figure 4.2: The Stability of IBU dendrimer and HBPAMAM polymers Complex.

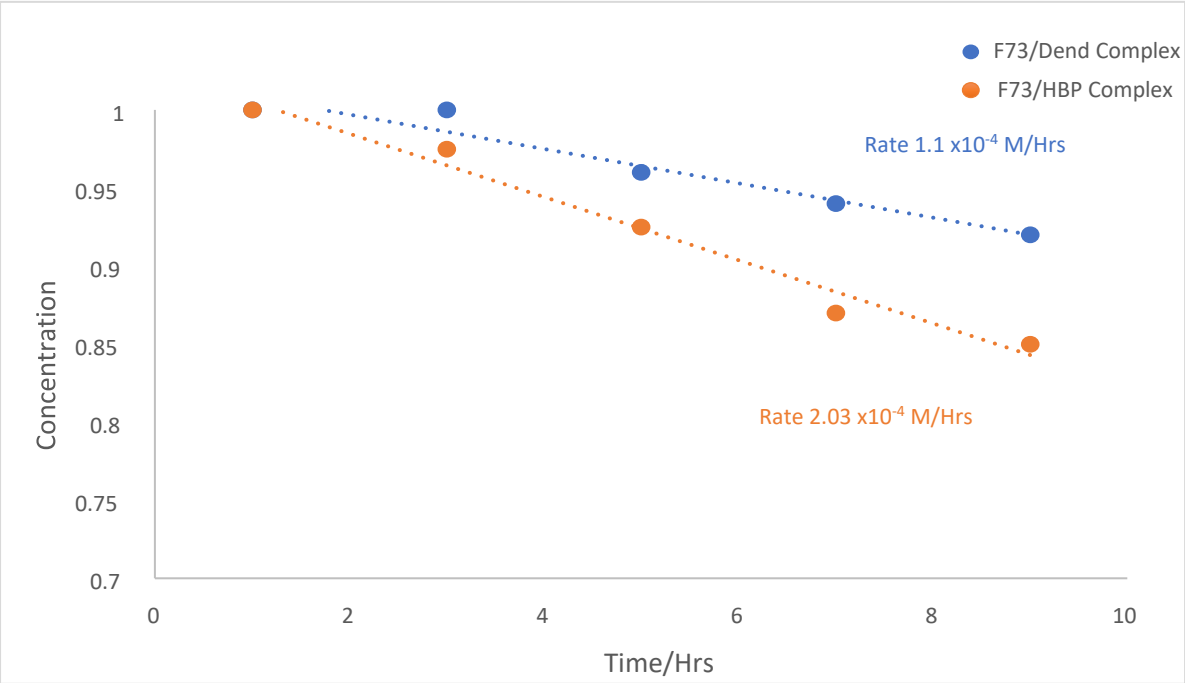

Figure 4.3: The Stability of F73 dendrimer and HBPAMAM polymers Complex.

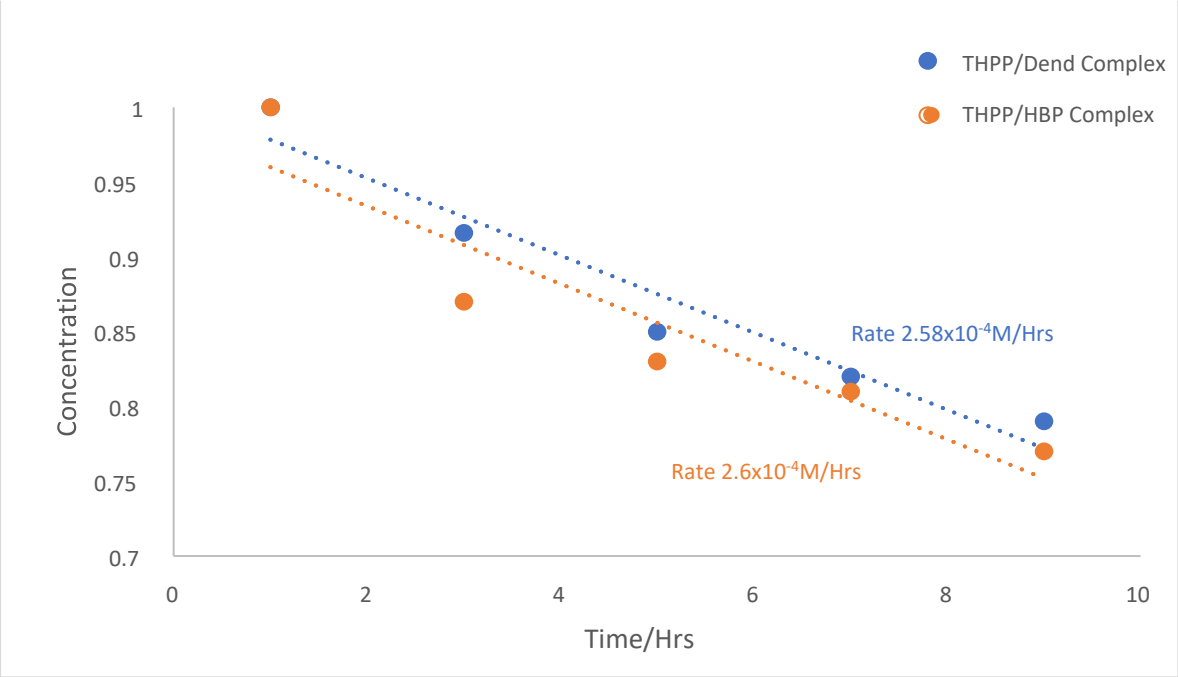

Figure 4.4: Stability of ZnTDHPP dendrimer and HBPAMAM polymers complex in the light states.

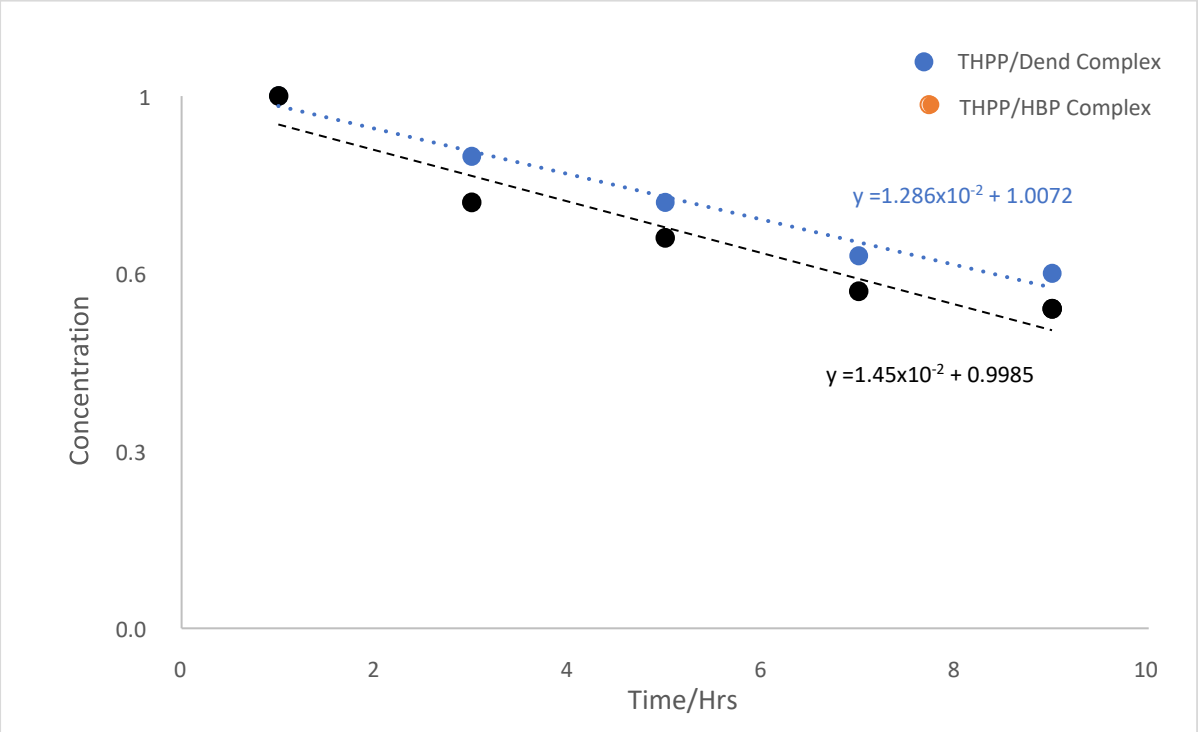

Figure 4.5: Stability of ZnTDHPP dendrimer and HBPAMAM polymers complex in the Dark states.

4.3.4 The release of (IBU. ZnTDHPP and F73) HBPAMAM complex.

The release results of IBU. ZnTHPP and F73 from the complex are demonstrated in the following Table: 4.4 and visually represented in Figures 4.6,7 and 8.

Table 4.4: The release test of Drugs IBU. ZnTDHPP. and F73 from dendrimer and HBPAMAM polymers.

Time/Hrs	IBU dendrimer	IBU/HBP	ZnTDHPP/ dendrimer	ZnTDHPP/ HBP	F73 / dendrimer	F73 / HBP
0 H	$8.5x10^{-3}$ M	$8.4x10^{-3}$M	$7.7x10^{-4}$M	$5.2x10^{-4}$ M	$1.8x10^{-4}$M	$1.7x10^{-4}$ M
24 H	$5.4x10^{-3}$ M	$4.9x10^{-3}$M	$2.3x10^{-4}$M	$1.6x10^{-4}$M	$1.1x10^{-4}$M	$1.07x10^{-4}$ M
48 H	$3.4x10^{-3}$ M	$3.1x10^{-3}$M	$3.9x10^{-5}$M	$2.9x10^{-5}$M	$4.8x10^{-4}$ M	$5.27x10^{-5}$ M
72 H	$2.4x10^{-3}$ M	$1.9x10^{-3}$M	$1.3x10^{-5}$M	8.6 $x10^{6}$M	0	0
96 H	$1.2x10^{-3}$ M	$0.9x10^{-4}$M	0	0	0	0
120 H	0	0	0	0	0	0

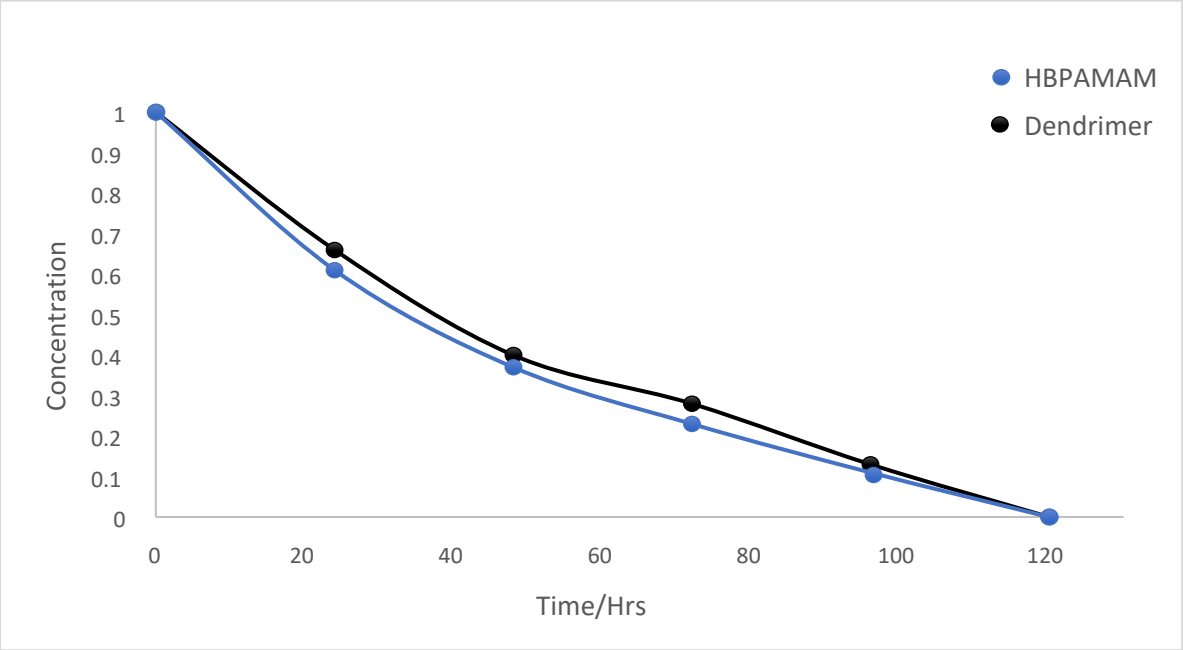

Figure 4.6: IBU Release from HBPAMAM and Dendrimer.

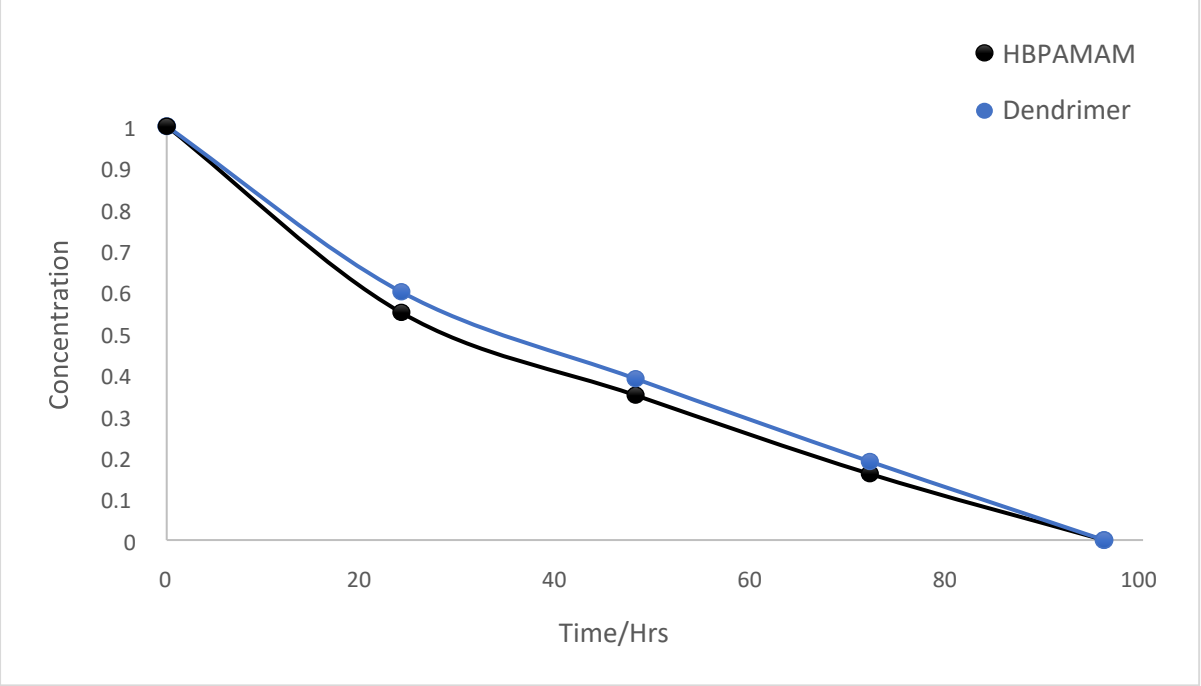

Figure 4.7: ZnTDHPP Release from HBPAMAM and Dendrimer.

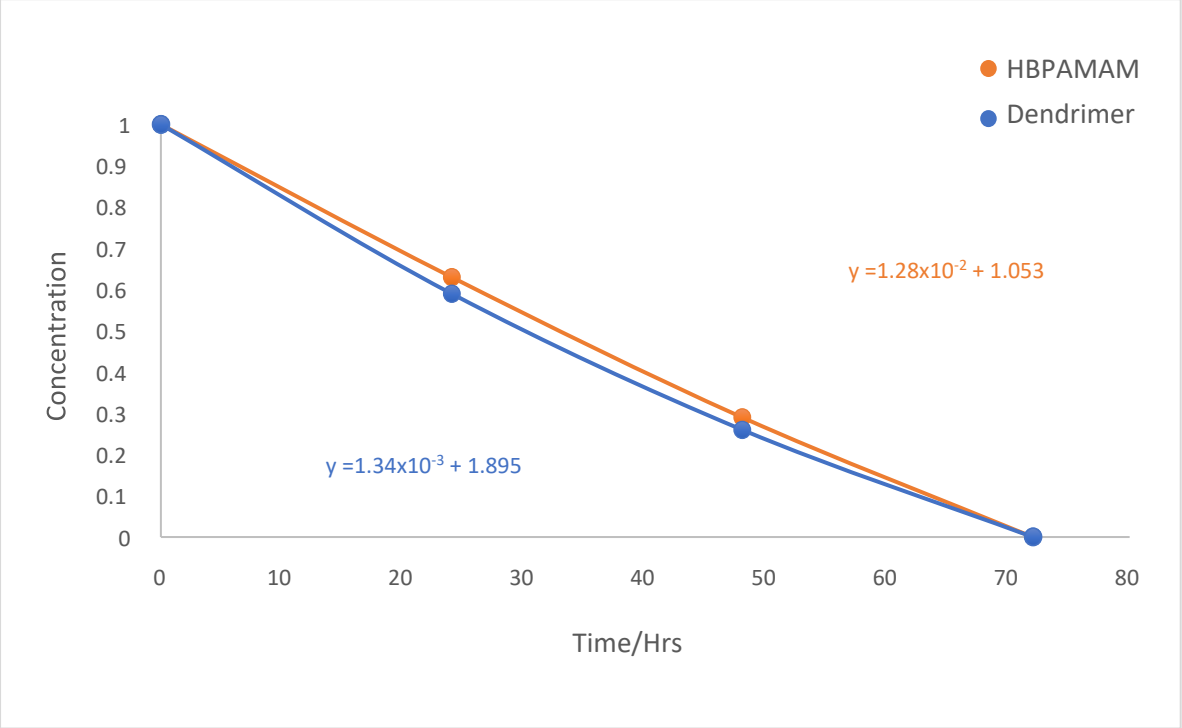

Figure 4.8: F73 Release from HBPAMAM and Dendrimer.

The comparative study of the drugs released from G2.5OH dendrimers and HBPAMAM systems revealed that both polymer types exhibit similar release rates and mechanisms for all tested drugs, indicating insignificant differences in their drug delivery efficiencies. The finding highlights that the simpler and potentially more accessible HBPAMAM system is in parallel with the more complex dendrimer-based system in terms of drug release capabilities. The observed slow-release rate from both systems is advantageous for therapeutic applications, as it allows for a prolonged drug presence in the body. This controlled release is beneficial for maintaining consistent drug levels over time, potentially enhancing treatment efficacy while reducing the risk of side effects. Such a mechanism is particularly valuable for drugs requiring precise dosage control to stay within a therapeutic window, ensuring optimal treatment outcomes with minimal fluctuations in drug concentration.

4.4 Conclusion

In this study, a series of PAMAM dendrimers ranging from generation 0.5 to 3.5 were synthesized through Michael addition and amination steps, and their terminal groups were modified to hydroxyl groups to obtain neutral, water-soluble OH-terminated PAMAM dendrimers. This modification resulted in dendrimers with 8, 16, and 32 OH terminal groups. The investigation then focused on evaluating these dendrimer's ability to encapsulate Ibuprofen, specifically examining the impact of dendrimer size and structure.

Among the tested generations G1.5-OH, G2.5-OH, and G3.5-OH, G2.5-OH emerged as the most effective for Ibuprofen encapsulation, achieving a loading of 18 molecules per dendrimer. Interestingly, despite its larger size, the G3.5 OH dendrimer encapsulated no more Ibuprofen than the G2.5-OH dendrimer, due to its more closely internal structure.

Further experiments at varying dendrimer concentrations revealed a roughly linear increase in Ibuprofen encapsulation up to $1x10^{-4}$ M, beyond which the encapsulation efficiency plateaued. This non-linear relationship at higher concentrations was attributed to dendrimer aggregation, confirmed by Dynamic Light Scattering DLS, which showed a significant size increase at concentrations above $1x10^{-4}$ M.

The study also explored the stability of Ibuprofen within these complexes, with the G2.5 OH dendrimer showing superior stability. This finding suggests that the dendrimer effectively protects the drug from hydrolytic degradation, highlighting the potential of PAMAM dendrimers, especially G2.5 OH, as effective drug delivery schemes. The slow release of Ibuprofen from the dendrimer further confirms a strong interaction between the drug and dendrimer.

Exploring the encapsulation capabilities of PAMAM dendrimers further, the focus shifted towards drugs capable of forming metal-ligand complexes, specifically to assess how metal coordination influences the dendrimers' drug encapsulation efficiency. This investigation focussed on Tetra dihydroxyphenyl porphyrin TDHPP, a compound used clinically as a photosensitizer in photodynamic therapy PDT. Following the synthesis and characterization of TDHPP and its zinc TDHPP complex ZnTDHPP, encapsulation studies were conducted using PAMAM dendrimers of varying generations G1.5 OH, G2.5 OH, and G3.5 OH.

UV spectroscopy revealed successful encapsulation of both porphyrin forms, indicated by a shift in the Soret band wavelength, with THPP shifting from 418 to 425 nm and ZnTHPP from 423 to 430 nm. Particularly, the metalated species demonstrated exceptional improvements in both encapsulation and solubility compared to their non-metalated counterparts. For instance, the G2.5 OH dendrimer showed an increase in encapsulation from 1.29 to 1.75 M equivalents for the free base and metalated porphyrins, respectively. The G3.5 OH dendrimer exhibited a more substantial increase, from 1.44 to 1.96 equivalents.

The enhancement in encapsulation and solubility for the metallated porphyrins was attributed to additional coordination interactions with the terminal OH groups of the dendrimers. While porphyrin loading was lower compared to Ibuprofen, due to the larger molecular size of porphyrins, the relative increase in solubility was much more significant. For instance, while Ibuprofen solubility doubled, metalated porphyrin solubility increased nearly 300 folds. The stability of the metalated porphyrin-dendrimer complexes was evaluated under both light and dark conditions over ten days. Results indicated stable complexes across all tested dendrimer generations, with G2.5 OH demonstrating the highest level of stability. Stability was notably better

in dark conditions, supported by the known sensitivity of porphyrins to photodegradation.

Release studies of ZnTDHPP from dendrimer complexes highlighted their potential for PDT applications, showing a slow release that would allow significant accumulation within tumours for effective treatment.

The research then extended to an anticancer drug, F37, to compare its encapsulation and release profiles with those of Ibuprofen and ZnTDHPP. Although F37 showed improvements in encapsulation and solubility identical to the other drugs, its release from the dendrimers was markedly faster, indicating weaker encapsulation interactions. This rapid release profile suggests that while PAMAM dendrimers are adaptable drug carriers, their effectiveness can vary significantly depending on the linked drug.

The exploration into the drug delivery capabilities of aromatic hyperbranched polymer with hydroxyl groups HBPAMAM aimed to assess its potential as an alternative to more conventional dendrimer systems. Given the challenges associated with the precise molecular weight determination of HBP, the study engaged both conventional molar concentration and mass/volume concentration methods for encapsulation assessments. Despite some differences in results between these methods, the study generally observed enhanced encapsulation using the molar concentration method.

The HBPAMAM demonstrated a significant capacity to encapsulate and enhance the solubility of various hydrophobic drugs, attributed to its hydrophobic environment and internal amine groups. However, deviations from expected linearity in encapsulation efficiency at higher polymer concentrations suggested aggregation issues, potentially limiting free space for drug encapsulation. Stability and release tests across different

drugs revealed a consistent performance, with particularly slow-release rates for Ibuprofen and ZnTDHPP, highlighting the system's suitability for drug delivery applications. Nevertheless, the rapid release of F73 indicated weaker interactions with HBPAMAM, suggesting it may not be as effective for this specific drug.

Comparing the performance of HBPAMAM with hydroxyl terminated PAMAM dendrimers revealed slight advantages for the dendrimer system in terms of encapsulation and solubilization capacities. However, the differences were not significant, indicating that HBP could assist as feasible, cost-effective alternatives to dendrimers for drug delivery. Both systems showed comparable proficiency in encapsulating ZnTDHPP and similar stability and release profiles across all tested drugs.

The outcome shows HBP's potential as a promising drug delivery system, offering a more accessible and reasonable option compared to dendrimers.

4.5 Future work

In our study, we observed that encapsulation of the drug F73 in both the dendrimer and HBP systems enhanced its solubility. However, neither system proved to be an effective drug carrier for F73. This conclusion was supported by the release tests, which revealed a rapid release of F73 from both systems, indicating weak interactions between the drug and the carriers.

The likely reason for this weak interaction lies in the spatial arrangement of H-bonding groups. In the dendrimer and HBP systems, the H-bonding groups are spaced apart, whereas the H-bonding groups in F73 are closely positioned. This structural mismatch limits the strength of the interactions between F73 and the carrier systems. Given these findings, we aim to explore a new drug with delivery challenges that could benefit from encapsulation strategies tailored to address these specific issues.

The inherent polydispersity of HBP presents challenges for regulatory approval and clinical application. A need for improvements in their synthesis and purification to achieve the mono-dispersed characteristics favoured by drug approval agencies. This highlights an area for future research and development to optimize HBPs for wider clinical use.

Chapter 5

5 Work Experiments.

5.1 Chemicals and Reagents

The project employed a range of chemicals and reagents, primarily obtained from commercial vendors, including Sigma-Aldrich. These substances were utilized directly without any further purification processes. Additionally, the dry solvents required for the project were supplied by the Chemistry Department at the University of Sheffield.

5.2 Instruments.

5.2.1 NMR spectroscopy

The project employed sophisticated analytical techniques for the detailed characterization of the chemical compounds being studied. This included the use of ^{1}H NMR and ^{13}C NMR spectroscopy, carried out on a state-of-the-art Bruker AV1400-HD instrument, operating at frequencies of 400 MHz for ^{1}H NMR and 100 MHz for ^{13}C NMR, respectively. Analysis of the NMR spectra was performed using the widely recognized Bruker NMR software, alongside M NOVA. Chemical shifts were reported in parts per million ppm, calibrated against internal solvent signals.

5.2.2 Mass Spectrometry

The project leveraged Mass Spectrometry MS technology to accurately measure the mass of the compounds being studied, utilizing two specialized types of mass spectrometers: Electrospray Ionisation Mass Spectrometry ES-MS and Matrix Assisted Laser Desorption Ionisation Time of Flight MALDI-TOF mass spectrometry. For compounds with a molecular weight under 1000 Daltons, the ES-MS technique was applied, with detailed data acquisition conducted on a Micromass Prospec spectrometer. Conversely, for analysing compounds with a molecular weight above

800 Daltons, the MALDI-TOF method was chosen. This approach involved the use of either dithranol or dihydroxy benzoic acid matrices, employing the advanced Bruker III mass spectrometer. These sophisticated MS techniques enabled highly precise and accurate compound analysis, offering critical insights into their molecular composition and characteristics.

5.2.3 UV-Vis spectroscopy

UV-Vi's absorbance measurements were performed with an Analytik Jena AG Specord S-600 spectrophotometer. The acquired data were processed and analysed using the Win ASPECT software, facilitating an in-depth examination, and understanding of the spectral data collected.

5.2.4 Infrared Spectroscopy IR

The infrared absorption spectra of the compounds were captured using the PerkinElmer Paragon 100 FT-IR device Fourier Transform Infrared Spectrophotometry equipped with the universal ATR Accessory. This setup allowed for precise recording of absorbance peaks to the nearest wavenumber in cm^{1}. For data analysis, the Perkin-Elmer Spectrum software was employed, enabling accurate interpretation of the spectral information.

5.2.5 PH Meter

The pH of the buffer solution was determined using the UEN Way PH Meter 3030. To ensure the accuracy of measurements, the device underwent calibration with standard

buffer solutions of pH 4.0 and pH 10.0, serving as benchmarks for the pH assessments conducted.

5.2.6 Dynamic light scattering DLS.

The hydrodynamic diameter of nanoparticles was measured using the Brookhaven 90Plus Particle Size Analyzer, located in Holtsville, NY, USA. This instrument is equipped with a 35 MW solid-state standard laser, ensuring precise and reliable measurements. For the characterization and analysis of the particle size distribution, Particle Sizing Software version 3.80 was utilized.

5.3 Synthetic and Experimental Procedures.

5.3.1 The synthesis of 0.5 generation PAMAM dendrimer.

In this procedure, ethylene diamine EDA was introduced into a round-bottom flask containing methanol and subjected to stirring. Subsequently, methyl acrylate MA, the monomer essential for dendrimer synthesis, was gradually added to the mixture at 0° over 45 minutes. The reaction mixture was then left to stir overnight at ambient temperature, facilitating full polymerization. Following the completion of the polymerization process, the surplus methyl acrylate and methanol were eliminated through rotary evaporation. Final purification was accomplished using ultra-high vacuum techniques to eradicate any residual solvents, yielding a purified PAMAM dendrimer.

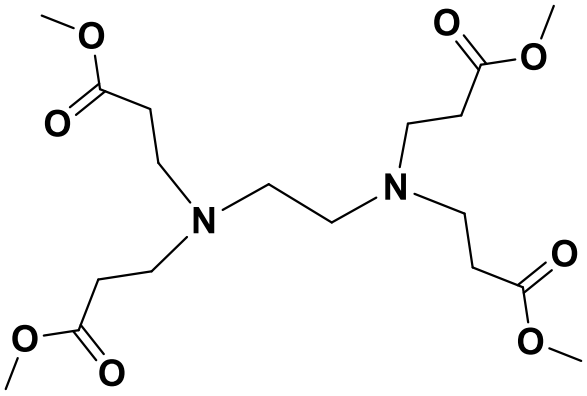

Yield: 17.45g, 88%. ^{1}H NMR. CD_3OD, 400 MHZ δH 3.68 ‘s, 12H, CH3’, 2.78 (t, 8H, $NCH_2CH_2C=O$), 2.53 s, 4H, NCH_2CH_2N, 2.47 (t, 8H, $OC=CH_2$). ^{13}C NMR (CD_3OD, 400 MHZ) δC 172.6, 52.6, 51.7, 48.5, 45.6, 31.9; IR cm^{-1}: 3285 (amide, NH), 2951 (C-H sp3), 1732 ester C=O, 1645 (amide C=O), 1536 (amide, NH bend), 1436 (CH2, bend), 1158, 1337, 1193, 1270 (ester. C-O); MALDI/TOF MS. 405 MH+ (calculated 405/$gmol^{-1}$).

5.3.2 The Synthesis of 1.5 Generation PAMAM dendrimer.

For the synthesis of a G 0.5 dendrimer, a standard protocol was followed, involving a reaction mixture comprising G1.0 dendrimer 2.53 g, 4.86 mmol), methyl acrylate 7.33 g, 0.09 mol, and methanol MeOH, 30 ml. This mixture was stirred at ambient temperature for 24 hours. To remove the excess methyl acrylate, rotary evaporation was conducted under a high vacuum for 4 hours, resulting in a viscous honey-yellow liquid as the product.

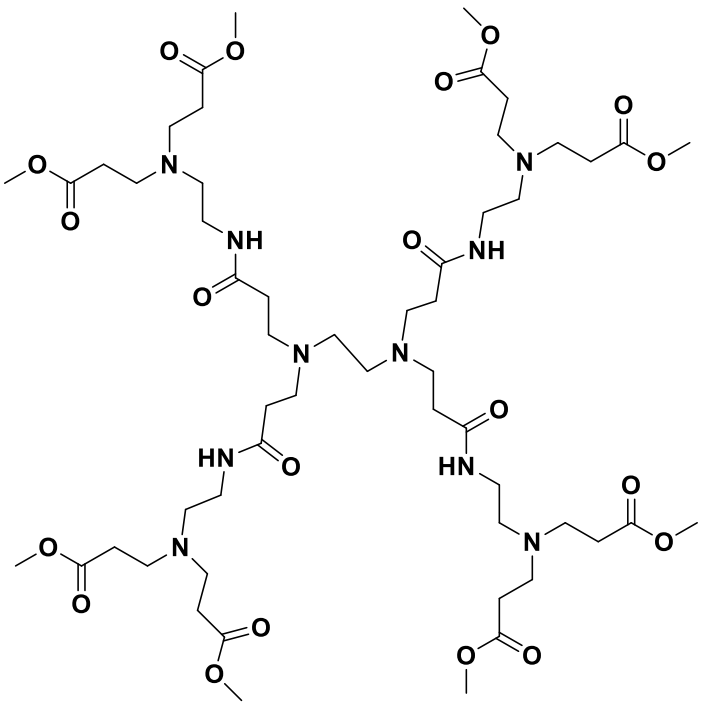

The synthesis of a G 1.5 dendrimer resulted in a yield of 19.19g (89%). The ^{1}H NMR spectrum in CD_3OD at 400 MHz showed signals at δH 4.92 (s, 4H, NH), 3.69 (s, 24H, CH3), 3.38-3.24 m. 24H, $NHCH_2$ + $NHCH_2CH_2CHNCH_2$. and 2.87-2.35 (mm, 44H, NCH_2CH_2N + $NCH_2CH_2C{=}ONH$ + $NHCH_2CH_2N$ + $NCH_2CH_2C{=}OOCH_3$). The ^{13}C NMR spectrum at the same conditions displayed peaks at δC 173.6, 173.3, 52.7, 51.9, 51.1, 49.7, 47.8, 37.8, 33.4, 32.5, and 32.0. The IR spectrum exhibited bands at 3283 cm^{-1} (amide, NH), 2951 cm^{-1}. (CH sp3), 2820 cm^{-1} and 1733 cm^{-1} (ester C=O). 1647 cm^{-1} (amide C=O), 1552 cm-1 (amide. NH bend), 1438 cm-1 (CH2 bend), 1358 cm^{-1}, 1327 cm-1, 1194 cm^{-1}, and 1174 cm^{-1} (ester C-O). The MALDI-TOF MS analysis showed a peak at 1206 (MH+), which is close to the calculated molecular weight of 1206 $gmol^{-1}$.

5.3.3 The Synthesis of 2.5 generation PAMAM dendrimer.

The preparation of a G 0.5 dendrimer followed a standard protocol, utilizing a G 2.0 dendrimer (3.10 g, 2.07 mmol), methyl acrylate (7.06 g, 0.08 mol), and MeOH, 75 ml as starting materials. The mixture was stirred continuously at room temperature for 48

hours. Following this, the surplus methyl acrylate was removed through rotary evaporation under high vacuum conditions for 8 hours, culminating in the production of a viscous deep orange liquid.

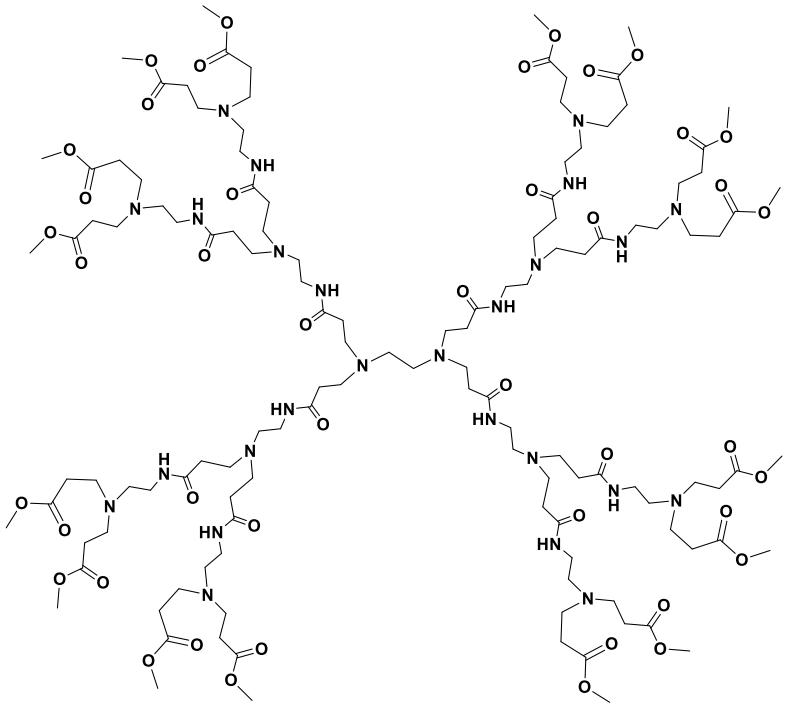

Yield: 4.68g, 75%; ^{1}H NMR, CD_3OD, 400 MHZ, δH 4.91 (s, 12H. NH). 3.78 (s, 48H, CH3), 3.29-3.12 (m, 12H. $NHCH_2CH_2N$), 2.92-2.34 (mm, 152H. $OC=OH_2CH_2N$ + NCH_2CH_2NH + $NHC=OCH_2CH_2N$ + $NHCH_2CH_2N$); ^{13}C NMR (CD_3OD, 400 MHZ) δC 173.3, 173.2, 52.4, 52.1, 50.8, 49.7, 49.1, 47.6, 37.2, 33.2, 32.2; IR (cm-1). 3182 (amide NH), 2964 (C-H sp3), 2829, 1731 (ester C=O), 1643 (amide C=O) 1535 (amide NH bend), 1446 (CH2 bend) 1195, 1177 (ester C-O); MALDI-TOF MS: 2807 (MH+).

5.3.4 The Synthesis of 3.5 generation PAMAM dendrimer.

In the synthesis of a G 0.5 dendrimer, a standard method was followed where a G 3.0 dendrimer (0.84 g, 0.26 mmol) was reacted with methyl acrylate (1.46 g, 0.02 mol) using methanol (MeOH, 30 ml) as the solvent. The mixture was stirred at ambient

temperature for 72 hours. Afterwards, the remaining methyl acrylate was eliminated through rotary evaporation under a high vacuum for 4 hours, resulting in a viscous, deep orange liquid as the final product.

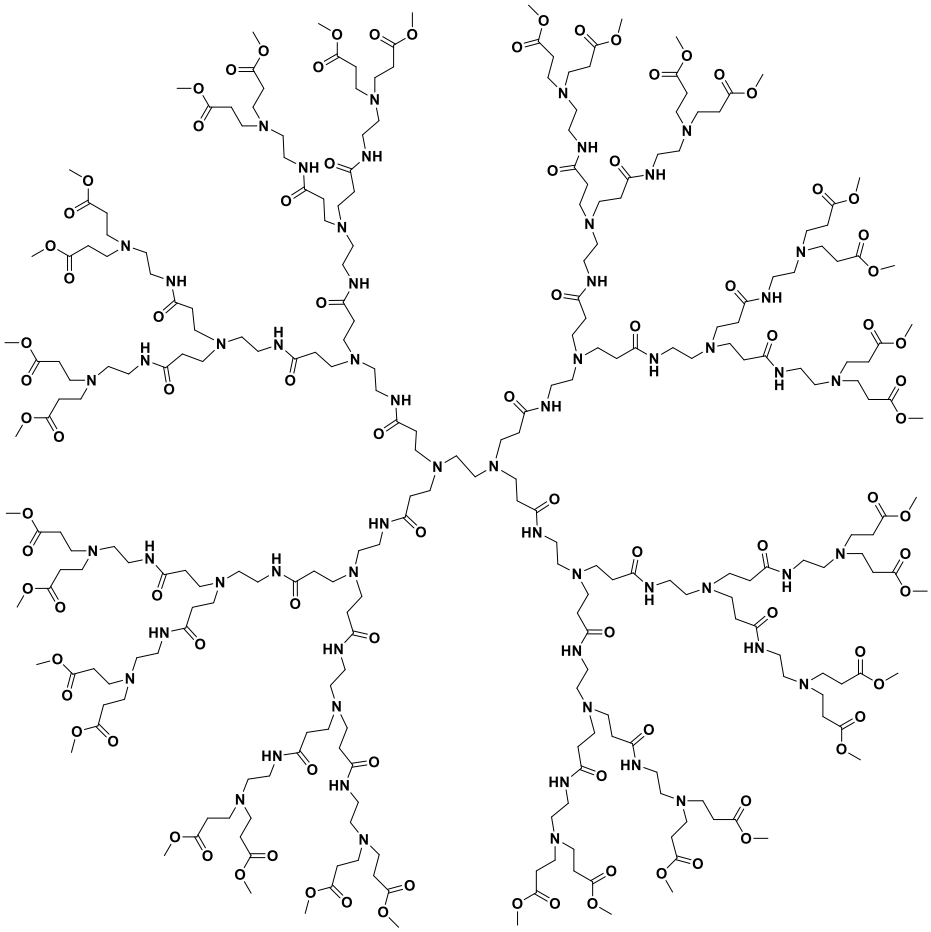

Yield: 1.15g, 68% ^{1}H NMR. CD_3OD, 400 MHZ. δH 4.90 (s, 28H, NH). 3.68 (s, 96H, CH3). 3.39-3.21 (m, 56H, $NHCH_2CH$- 2N), 2.89-2.34 (mm,300H, $NCH_2CH_2C{=}OOCH_3$+ $NCH_2CH_2C{=}ONH$ + NCH_2CH_2N + $NCH_2CH_2C{=}ONH$ + $NHCH_2CH_2N$ + $NCH_2CH_2C{=}OOCH_3$): ^{13}C-NMR (CD_3OD, 400 MHZ) δC 173.3, 173.2, 52.2, 50.6, 49.7, 49.1, 47.6, 37.2, 33.2, 32.2: IR (cm-1): 3275 amide NH. stretch, 2954 (C-H sp3), 2831, 1731 (ester C=O), 1639 (amide C=O), 1536 (amide N-H bend), 1434 CH2, bend. 1360, 1172 ester C-O. 1196, 1041. MALDI/TOF MS: the expected 6011, found 6005 MNa+.

5.3.5 The general procedure for synthesizing whole-generation PAMAM dendrimers.

The synthesis of comprehensive generation PAMAM dendrimers is a methodical process that begins with a core molecule. This method involves the sequential addition of amine-based monomers, utilizing protecting groups to precisely control the reaction dynamics. The dendrimer structure is expanded through repeated cycles of addition and deprotection steps. Terminal groups of the dendrimer are then functionalized to impart desired properties. The final step involves purifying the synthesized dendrimer to obtain a clean product. Throughout this synthesis process, the specific reaction conditions, choice of monomers, selection of protecting groups, and purification methods can be tailored to achieve dendrimers of the desired generation with specific functional modifications.

5.3.6 The Synthesis of G1 generation PAMAM dendrimer

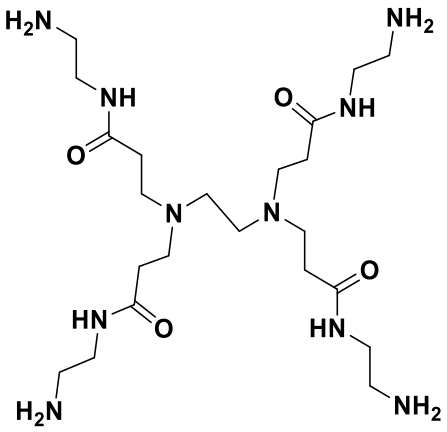

In a round-bottom flask 500 mL, (14.46 g, 0.05 mol) of a G 0.5 PAMAM dendrimer from a prior synthesis was dissolved in 40 mL of methanol. To this solution, (97.78g,1.62 mol) of ethylene diamine EDA was added gradually while maintaining the temperature

at 0°C. The mixture was then stirred at ambient temperature for 5 days. To remove the surplus EDA and methanol, the reaction mixture underwent washing with a 9:1 toluene: methanol azeotropic mixture. This purification step was repeated several times to ensure the complete removal of EDA. Finally, the product was dried under ultra-high vacuum conditions for 5 hours, resulting in a honey-coloured oil. The yield of the product was 12.4 g 0.024 mol, which corresponds to a 75% yield.

5.3.7 Synthesis procedure of 2nd generation PAMAM dendrimer.

In a round bottom flask, a PAMAM dendrimer with 4 amine terminal groups, weighing (5.0 g, 9.71 mmol), was dissolved in 50 mL of methanol. To this, (14.66 g,0.18 mol) of methyl acrylate was added dropwise at a controlled temperature of 0° over 45 minutes. The reaction mixture was then stirred continuously at room temperature for 3 days. Following this period, excess methyl acrylate was removed using a rotary evaporator set at 40°C. The processed PAMAM dendrimer was further dried under ultra-high vacuum conditions for 5 hours, yielding a sticky orange oil. The final yield of the product was 10.2 g, representing 84%.

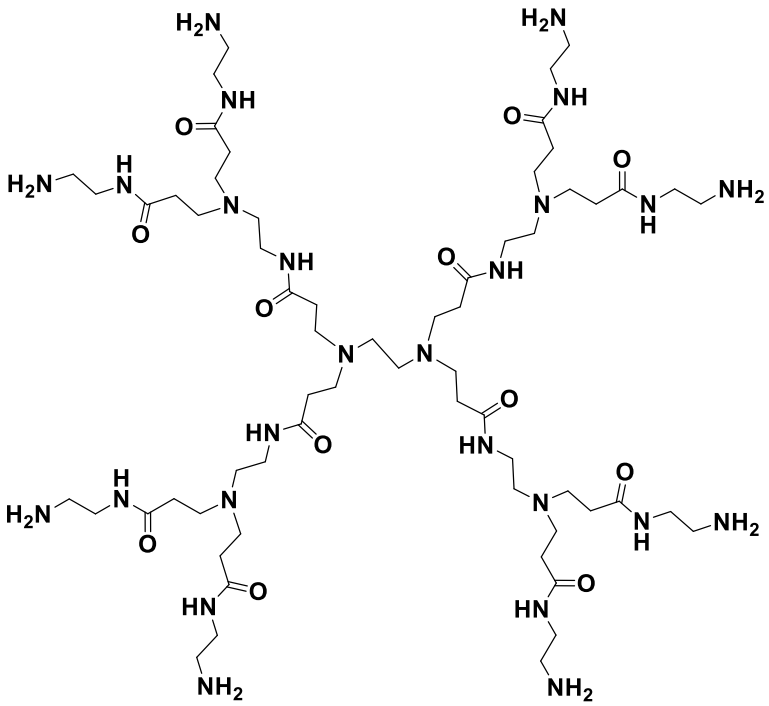

The product was obtained in a yield of 4.43g 85%. The ^{1}H NMR spectrum (CD_3OD at 400 MHz) δH 4.89 (s, 12H, NH) and 3.41-3.22 (m, 48H, $NHCH_2CH_2N$ + $NHCH_2CH_2NH_2$+ $NHCH_2CH_2N$ + $NHCH_2CH_2NH_2$), as well as signals at 2.89-2.30 (mm, 52H, $NCH_2CH_2C{=}O$ + $NCH_2CH_2C{=}O$ + NCH_2CH_2N). The ^{13}C NMR. (CD_3OD at 400 MHz) δC 173.7, 173.1, 51.9, 50.7, 49.5, 48.2, 47.4, 41.2, 40.3, 36.8, and 33.1. The IR spectrum displayed peaks at 3276 cm^{-1} (amide NH), 2939 cm^{-1} (C-H sp3), 1634 cm^{-1} (amide C=O), 1547 cm^{-1} (amide NH bend), 1437 cm^{-1} (CH2 bend). 1322 cm^{-1}, 1195 cm^{-1}, 1120 cm^{-1}, and 1031 cm^{-1}. The MALDI-TOF mass spectrum showed a peak at 1430 (MH+).

5.3.8 The Synthesis procedure of 3rd generation PAMAM dendrimer.

A 2.5 generation PAMAM dendrimer, weighing 2.38g (0.79 mmol), was dissolved in 50 mL of methanol MeOH in a 500 mL round-bottom flask, along with (9.23 g,0.15 mol)

of ethylene diamine EDA. The mixture was stirred continuously at room temperature for 10 days. After this period, 100 mL of an azeotropic mixture of toluene and MeOH in a 9:1 ratio was added to the mixture. The resultant mixture underwent rotary evaporation under a high vacuum for 1 hour. This purification process was performed five times to eliminate any excess EDA and solvent, yielding a highly viscous deep orange liquid as the final product.

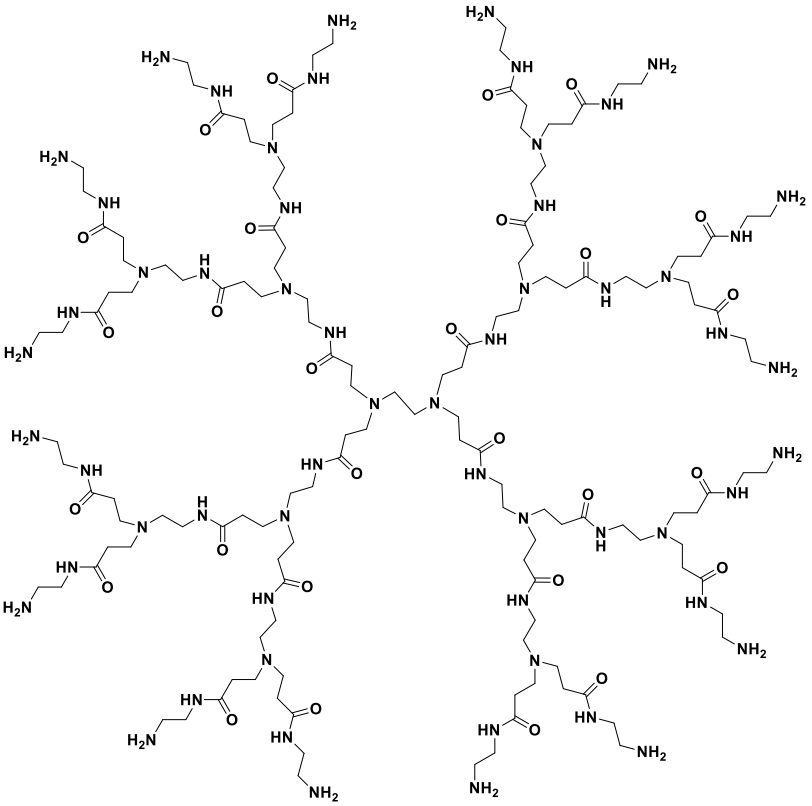

The product was obtained with a yield of 2.29g, a 91% yield. The ^{1}H NMR spectrum CD_3OD at 400 MHz δH 4.91 (singlet, 28H, C=ONH), 3.55-3.19 (multiplet, 112H, $NHCH_2CH_2N$ + $NHCH_2CH_2NH_2$ + $NHCH_2CH_2N$ + NHCH2CH2NH2), and 2.89-2.20 (multiplet, 116H, NCH_2CH_2-C=O + NCH_2CH_2C=O + NCH_2CH_2N). The ^{13}C NMR, CD_3OD at 400 MHz exhibited peaks at δC 173.7, 173.2, 51.8, 49.5, 47.3, 40.9, 40.1, 37.0, 33.4, and 33.2. The IR at 3269 cm^{-1} (amide NH), 2943 cm^{-1} (C-H sp3), 2855 cm^{-}

^{1}, 1633 cm^{-1} (amide C=O), 1547 cm^{-1} (amide N-H bend), 1463 cm^{-1} (CH2 bend), 1331 cm^{-1}, 1157 cm^{-1}, and 1031 cm^{-1}. The MALDI-TOF MS at 3257 (MH+) and 3279 (MNa+).

5.4 The general synthesis procedure for PAMAM dendrimers hydroxyl terminated groups.

The synthesis of the G1.5 PAMAM dendrimer began with its dissolution in DMSO, followed by the addition of a solution of TRIS and anhydrous potassium carbonate K2CO3. The mixture was then filtered to remove any undissolved solid reagents. The filtrate was distilled under reduced pressure at 50°C to remove the solvent, resulting in a thick, opaque oil. This crude product was subsequently dissolved in distilled water and precipitated with acetone, a step that was repeated twice to ensure purity. The final product was dried in a vacuum oven, yielding TRIS-terminated dendrimers as pale yellow, hygroscopic solids.

5.4.1 The synthesis of 1.5G PAMAM Dendrimer Hydroxyl-terminated group.

In this procedure, (0.75g. 0.60mmol) of a G1.5 PAMAM dendrimer was dissolved in 10 ml of anhydrous dimethyl sulfoxide DMSO and then mixed with (0.75g. 6.28mmol) of TRIS solution and (0.77g. 5.29mmol) of K2CO3. The mixture was stirred continuously at a temperature of 50°C for 48 hours. Following the reaction period, the product underwent a comprehensive purification process, ensuring the removal of impurities and unreacted materials to obtain a fully purified product.

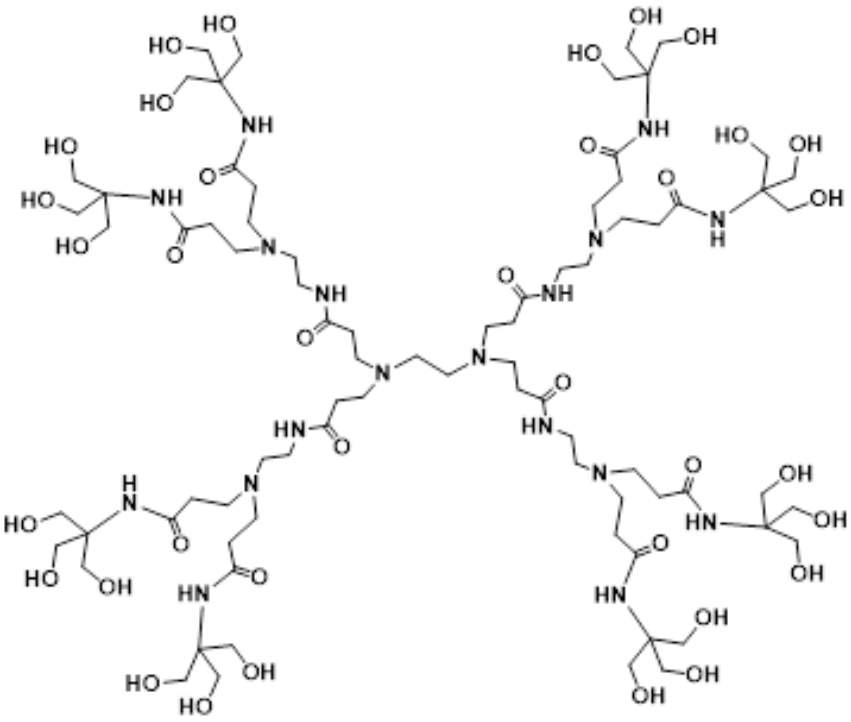

Yield 0.79g, 58%; ^{1}H NMR (D_2O, 400 MHz) δ_H 3.64 (s, 48H, CH_2OH), 3.22 (t, 8H, $NHCH_2CH_2N$), 2.70 m, 24H, NCH_2CH_2CO, 2.52 m, 12H, NCH_2CH_2N + $NHCH_2$, 2.31 (m, 24H, NCH_2CH_2CO); ^{13}C NMR (D_2O, 400 MHz) δ_C 63.0, 62.3, 60.7; IR (cm^{-1}): 3304 (OH), 2945 (C-H sp^3), 1634 (amide C=O), 1556 (amide N-H bend), 1462 (CH_2 bend), 1390, 1248, 1126, 1040, 1021; MALDI-TOF MS: 1957 (MK^+).

5.4.2 The synthesis of 2.5G PAMAM Dendrimer Hydroxyl-terminated group.

In this synthesis, (0.60g. 0.54mmol) of a G1.5 PAMAM dendrimer was initially dissolved in 10 ml of DMSO. This solution was then combined with (0.75g, 6.8mmol) of TRIS solution and (0.88g. 6.29mmol) of K2CO3. The mixture of reactants was stirred at a temperature of 50°C for 48 hours. Following the reaction phase, the resulting product underwent a thorough purification process, ensuring the removal of any impurities or unreacted substances to achieve a fully purified final product.

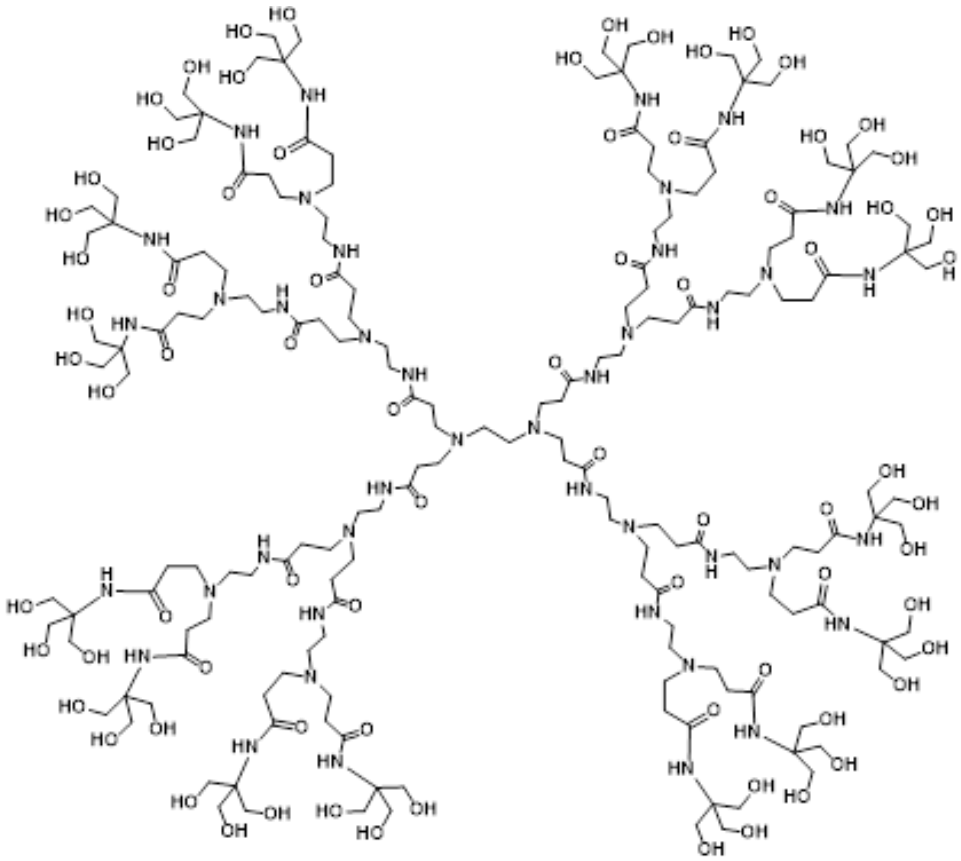

Yield 0.88g, 75%; ^{1}H NMR (D_2O, 400 MH_Z) δ_H 3.64 (s, 96H, CH_2OH), 3.22 (t, 24H, $NHCH_2CH_2N$), 2.71 (m, 56H, NCH_2CH_2CO), 2.52 (m, 28H, NCH_2CH_2N + $NHCH_2$), 2.31 (m, 56H, NCH_2CH_2CO); ^{13}C NMR (D_2O, 400 MH_Z) δ_C 63.0, 62.3, 60.7IR (cm^{-1}). 3306 (OH), 2954 (C-H sp^3), 1635 (amide C=O), 1549 (amide N-H bend), 1460 (CH_2 bend), 1362, 1241, 1137, 1065, 1019; MALDI-TOF MS: anticipated 4243, found 4042 (MH^+).

5.4.3 The synthesis of 3.5 G PAMAM Dendrimer Hydroxyl-terminated group.

In the described reaction, 0.66g (0.59mmol) of a G1.5 PAMAM dendrimer was dissolved in 10 ml DMSO. This was followed by the addition of (0.67g. 6.28mmol) of a TRIS solution and (0.89g. 6.39mmol) of K2CO3 to the dendrimer solution. The mixture of reactants was stirred continuously at a

temperature of 50°C for 48 hours. Following the reaction, the product underwent thorough purification, ensuring the removal of any residual reactants or byproducts to obtain a pure final product.

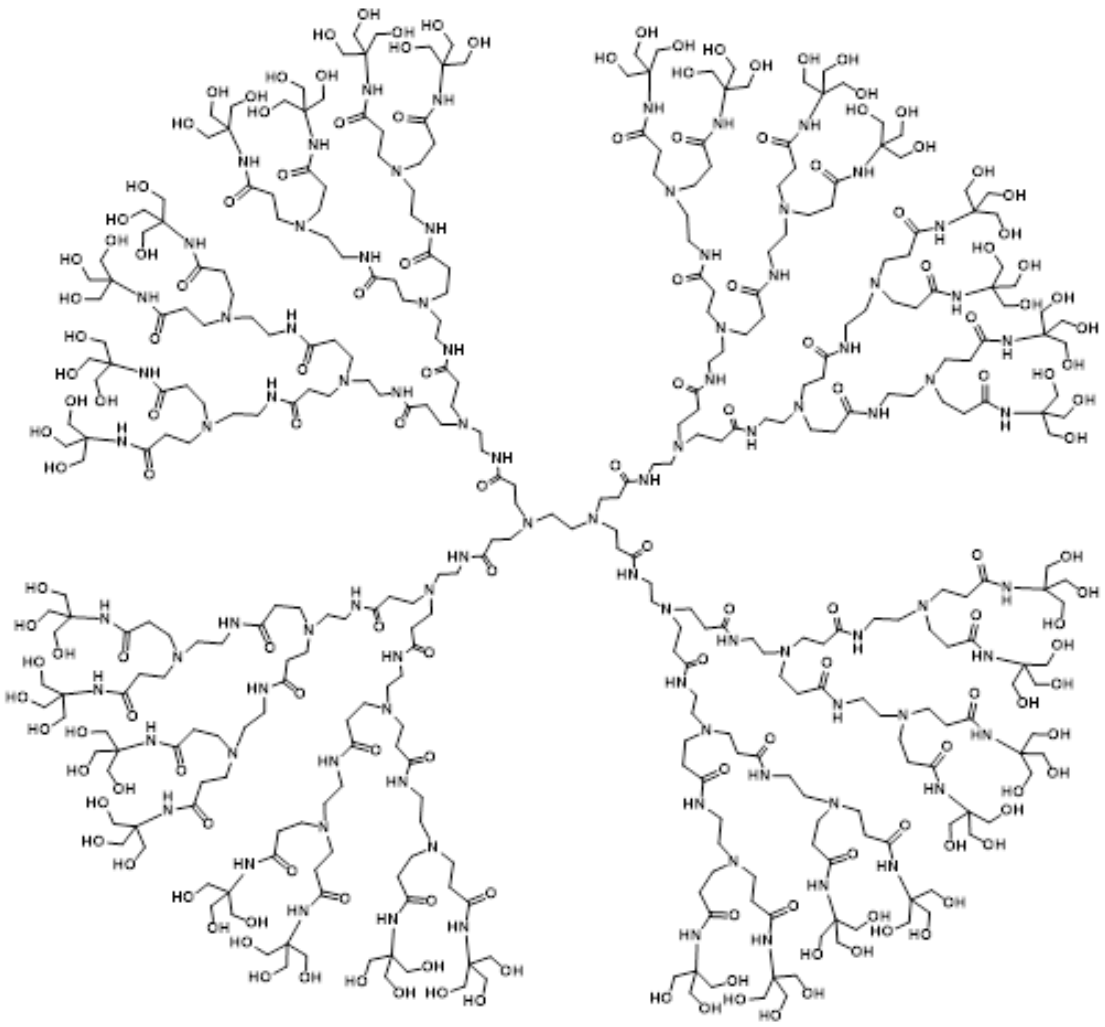

Yield 0.66 g, 65%. ^{1}H NMR (D_2O, 400 MH_Z) δ_H 3.66 (s, 192H, CH_2OH),), 3.22 (t, 56H, $NHCH_2CH_2N$). 2.84 (m, 120H, NCH_2CH_2CO), 2.52 (m, 60H, NCH_2CH_2N + $NHCH_2$), 2.32 (m, 120H, NCH_2CH_2CO). ^{13}C NMR (D_2O, 400 MH_Z) δ_C 63.6, 61.3, 4776; IR (cm-1): 3305 OH, 2936 (C-H sp^3). 1633 (amide C=O. 1548 (amide N-H bend). 1461 (CH_2 bend), 1361, 1246, 1127, 1022; MALDI-TOF MS: expected 8862, found 8286 (MH^+).

5.5 The Synthesis Procedure of 3,5 Tetraphenyl Hydroxy phenyl porphyrin THPP.

5.5.1 Synthesis of Tetraphenyl porphyrin TPP.

In a 500 round-bottom flask containing 250 mL of refluxing propionic acid, freshly distilled pyrrole (7.0 mL. 0.10 mol) and benzaldehyde (10.0 g, 0.094 mol) were introduced, and the mixture was stirred for 30 minutes. After this period, the reaction mixture was allowed to cool to room temperature, then it was filtered under vacuum. The solid product obtained was thoroughly washed with methanol followed by hot distilled water to ensure the removal of any unreacted starting materials or byproducts. This synthetic method is designed to ensure the efficient synthesis of the desired compound, leveraging the reactivity of pyrrole and benzaldehyde in propionic acid as the reaction medium.

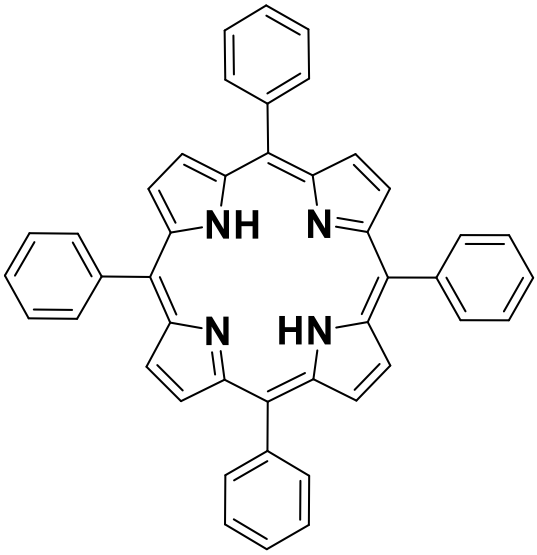

Yield: 1.5g, 19%; ^{1}HNMR (CDCl3. 400 MHZ) δ 8.7, (s, 8H, Pyrrolic – CH), 8.24(8H, dd, Phenylic o-CH), 7.78 (m, 12H), -2.75 (s, 2H, NH) ^{13}C NMR (CDCl3, 400 MHZ) δ ppm 137.1,134.4, 126.5, 120.1; FTIR (cm^{-1}) 3320 (amine N -H stretch), 3013 (aromatic and alkene, C-H stretch), 1675, 1224, 748, 695; UV/absorbance CHCl3 λmax nm. 418, 515.5, 551, 592, 645.

5.5.2 The Synthesis of Zinc Tetraphenyl porphyrin complex, ZnTPP.

500 mg of TPP was first added to a round-bottom flask containing chloroform, and the mixture was stirred until the TPP was completely dissolved. Zinc acetate 1.5g was then introduced to the TPP solution at 50°C. The reaction mixture was stirred for 20 minutes. After the reaction, the mixture was allowed to cool to room temperature and then filtered to remove any unreacted zinc acetate. chloroform solvent was removed using a rotary evaporator, resulting in a purple colour compound.

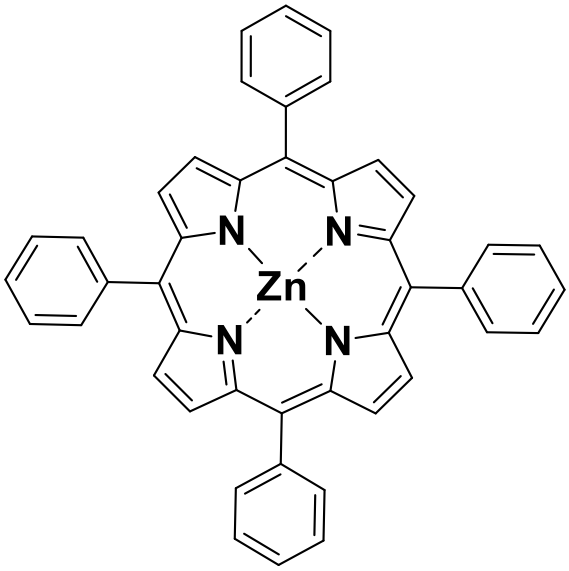

Yield. 52mg, 89%. ^{1}H NMR, (D-CDCl3, 400M Hz). δ 8.86. (s, 8H pyrrolic β-H), 8.35 (d. J, 7.9Hz, 8H phenolic, CH). 7.71(d, J. 8.3 Hz, 12H. phenolic m.p CH). ^{13}C NMR, (D-CDCl3. 400MHz). δ ppm, 150.1, 143.7, 135.6, 142.1, 125.6, 124.7, 122.3. FTIR (cm^{-1}). 2932s, 2845 s, 1364, 1737w, 1137 w. UV-Vis Spectroscopy nm: 418, 546.5, 678-MeOH. ESI/MS. 675 MH^{+}. Calculated at 675 $gmol^{-1}$.

5.5.3 The Synthesis of Iron Tetraphenyl porphyrin complex, FeTPP.

A round-bottom flask equipped with a condenser was initially charged with 550 mg, 0.79 mmol of TPP. Anhydrous tetrahydrofuran THF, 80 mL, 6.43 mmol, 2,6-lutidine 0.70 mL and ferrous chloride $FeCl_2$ were then introduced into the flask via syringe. The reaction mixture was refluxed for 4 hours under a nitrogen atmosphere. After that, the solution was exposed to air while being allowed to cool to room temperature, facilitating oxidation. The unreacted $FeCl_2$ was removed by vacuum filtration. The crude product was then dissolved in (DCM) Dichloromethane and washed with 1M, HCl, followed by distilled water to remove any impurities and unreacted materials. The

purification of the product was accomplished through column chromatography using a solvent system of DCM: MeOH 3:1, resulting in the isolated FeTPP complex.

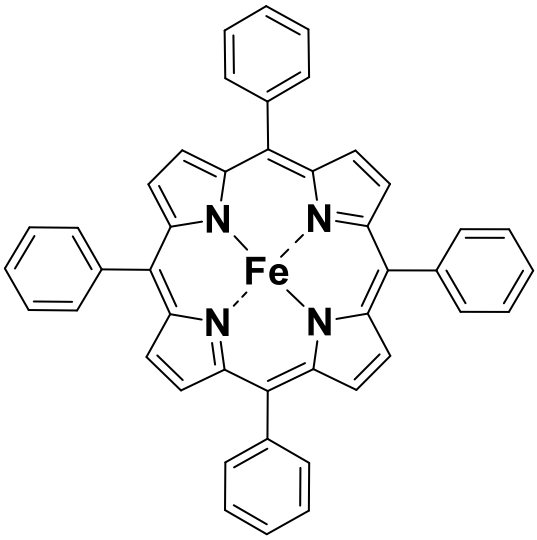

Yield. 0.6g, 80%. IR $cm^{-1.}$ 2819 aromatic, C-H stretch. 1654 (ester, C=O) 118, 1173. (Ester, C-O stretch). 1614, (N-H, bend). 1393, 1476; UV-Vis Absorbance nm. 418 λ_{max} 564.5, 609. CH_2Cl_2. ES-MS: 679 MH^+.

5.5.4 The Synthesis of tetrakis 3,5-dimethoxyphenyl porphyrin TDMPP.

In a round-bottom flask equipped with a condenser, 300 mL of propionic acid was added and brought to reflux. Subsequently, freshly distilled pyrrole (7.74 mL, 40 mmol) and 3,5. dimethoxybenzaldehyde (6.1 g, 40 mmol) were introduced into the refluxing mixture. The reaction was continued under reflux for an additional 30 minutes. Upon completion, the mixture was allowed to cool to room temperature and then filtered to collect the product. The collected solid was thoroughly washed with hot distilled water followed by methanol, resulting in a bright purple product.

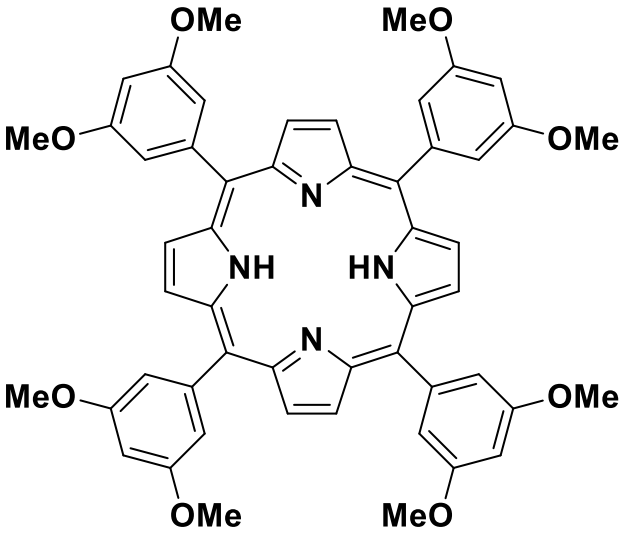

Yield; 1.9g, 21%; ^{1}H NMR, ($CDCl_3$, 400MHz): δ 8.95 (s, 8H, pyrrolic β-H). 7.44 (d, 8H, phenylic *o*-CH), 6.91 (s, 4H, phenylic *p*-CH), 4.02 (s, 24H, phenylic *m*-CH_3). -2.79 (s, 2H, NH). ^{13}CNMR ($CDCl_3$, 400MHz). δ 158.7, 144.1, 119.7, 113.7, 100.2, 55.6 IR Relevant peak (cm^{-1}) 1249 (MeOH); UV/Vis Absorbance nm: 418 (λ_{max}), 516, 552, 591, 650 (CH_2Cl_2). (ES/MS): 854 (MH^+). (Calculated at 854 $gmol^{-1}$).

5.5.5 The Synthesis of 5.10.15.20-tetrakis(3,5-dihydroxyphenyl) porphyrin THPP.

400mg, 0.45 mmol of TMPP and 25 mL of anhydrous dichloromethane DCM were combined in a round-bottom flask and then flushed with nitrogen gas for 10 minutes. Subsequently, (1.15 mL, 11.82 mmol) of BBr_3 was added carefully via a syringe under the nitrogen atmosphere. The reaction mixture was stirred gently at room temperature under a nitrogen for 5 hours. distilled water (1.4 mL, 0.09 mol) was cautiously added over 20 minutes to quench the reaction. The crude product was neutralised with a slight amount of sodium hydrogen carbonate and then extracted using ethyl acetate. Filtration was employed to remove any insoluble impurities, resulting in a distinct

purple organic layer. This solution was then concentrated under reduced pressure using a rotary evaporator, yielding a purple solid product.

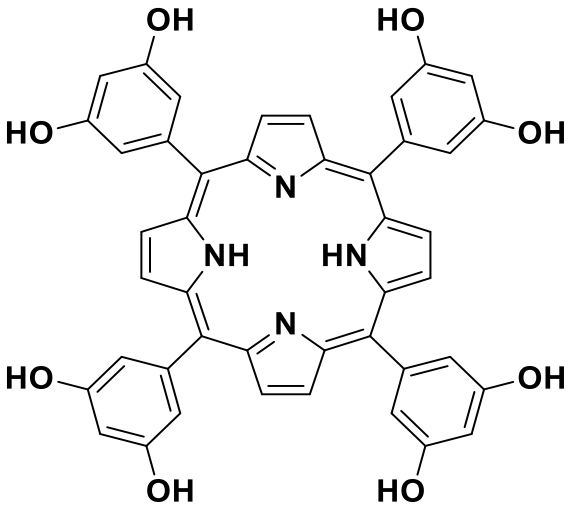

Yield. 350mg, 83%. ^{1}H NMR (CD_3OD. 400MHz). δ 9.07 (s. 8H. pyrrolic β-H) 7.32 (d. 8H. phenylic, *o*-CH), 6.97 (t. 4H. phenylic, *p*-CH). 4.82 (s. 8H. phenylic *m*-OH). 2.14 (s. 2H. NH). ^{13}C NMR (CD_3OD. 400MHz). δ 146.9. 142.58. 120.0, 113.3. 102.1. IR peak, (cm^{-1}) 3438 OH. UV-Vis Absorbance nm 418 λ_{max}. 505, 545, 587, 659 MeOH. ESI-MS. 745 MH^{+}. Calculated 743 $gmol^{-1}$.

5.5.6 The Synthesis of Zn-5.10.15.20-tetrakis(3,5-dihydroxyphenyl) porphyrin Complex ZnTDHPP.

In this procedure, 210mg, 0.023 mmol of THPP was dissolved in 80 mL of DCM in a round-bottom flask. In a separate container, a stoichiometric excess of zinc acetate was dissolved in 5 mL of methanol to ensure a complete reaction. This zinc acetate solution was then added to the THPP solution in the flask. The reaction mixture was heated to reflux at 45 °C and stirred for 1 hour to facilitate the reaction. Afterwards, unreacted zinc acetate was removed by filtration under reduced pressure. The DCM solvent was then removed using a rotary evaporator. The recrystallization was

performed to purify the product, followed by drying of the crystals. This process yielded dark purple crystals of the ZnTHPP complex.

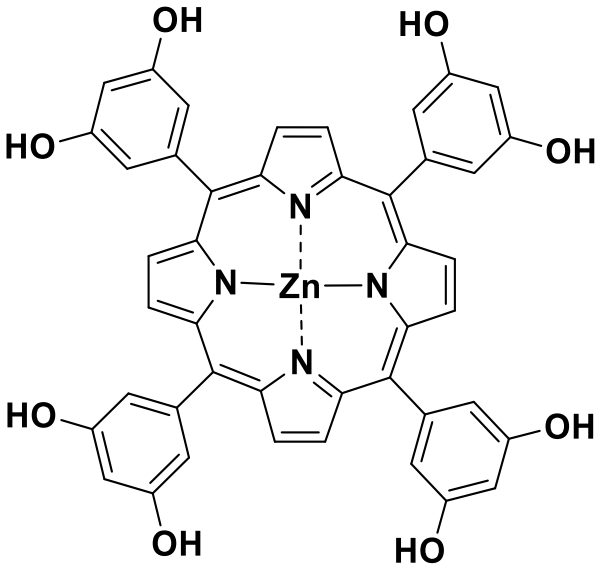

Yield. 200 mg, 94%. ^{1}H NMR. (400 MH., CDCl3) δ 9.88 (d. J-2.9. 8H). 7.39 (d, J-2.5, 8H). 6.82(t, J-2.5, 4H), 4.86 s, 8. ^{13}C NMR; (400 MHz, DMSO). δ 154.4, 153.1, 128, 112, 101. UV -Vis nm 423, ESI-MS 808 $MH^{+\cdot}$ (Calculated at 808 gmol).

5.5.7 The Synthesis of Iron 5.10.15.20-tetrakis(3,5-dihydroxyphenyl) porphyrin Complex FeTDHPP.

A 250 mL round-bottom flask equipped with a condenser was loaded with THPP, 300 mg, 0.40 mmol, 2,6-lutidine, 0.70 mL, 6.05 mmol, and FeCl2, 0.89 g, 7.01 mmol. The components were dissolved in 150 mL of methanol and the mixture was heated to 50°C, with stirring maintained for 3 hours. the mixture was subjected to a rotary evaporator to remove the methanol solvent. A 1:1 mixture of ethyl acetate and water was then added to the flask to facilitate the separation of phases. After vigorous shaking, insoluble impurities were filtered out. the organic layer was then collected

and concentrated. The crude product underwent purification by a silica gel column, a 1:1 mixture of ethyl acetate and methanol as the eluent.

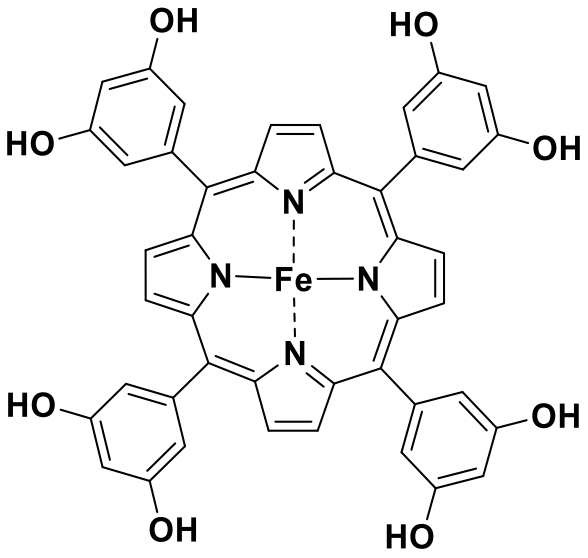

Yield. 235 mg, 70%. ^{1}H NMR. (CD_3OD. 400 MH_Z). δ 11.00, 9.80; UV-Vis nm. 418 λ_{max}. 496, 587 MeOH. ES-MS. 794 MH^+. Calculated at 794 $gmol^{-1}$.

5.6 TDHPP Fe Encapsulation within PAMAM Dendrimer Hydroxyl-terminated group.

5.6.1 Preparation of (0.1 M) TRIS buffer at pH 7.4.

A 12.11g of TRIS was dissolved in 1000 mL of Deionized water. The solution's pH was then adjusted using 0.1M hydrochloric acid HCl until a pH of 7.4.

5.6.2 Beer-Lambert plot of THPP Fe.

To create stock solutions for analysis, 10 mg of THPP-Fe was dissolved in methanol within a volumetric flask, preparing 10 mL of stock solution. Subsequent serial dilutions were performed to realise various concentrations (M) of the solution. The dilutions

were then analysed using UV-Vis spectroscopy, measuring the maximum absorbance at a wavelength of 418 nm. The data obtained from these measurements were utilized to construct Beer-Lambert graphs, plotting concentration against absorbance.

5.6.3 Beer-Lambert plot of TDHPP, Zn-TDHPP.

5.2 mg of TDHPP and 2.1 mg of (Zn-TDHPP were separately dissolved in methanol to prepare 1000 mL solutions in volumetric flasks. The absorbance of these solutions was measured using a UV spectrophotometer at their respective characteristic wavelengths: 418 nm for TDHPP and 423 nm for Zn-TDHPP, with methanol serving as the blank reference, a series of dilutions from the stock solutions were prepared at various concentrations. The dilutions were used to measure absorbance values at the specified wavelengths for each compound. The collected data were utilized to construct Beer-Lambert graphs, plotting the concentration of each solution against its absorbance.

5.6.4 Beer-Lambert plot of IBU.

An excess of Ibuprofen was added to 60 mL of phosphate buffer solution (pH 7.4) in a 100 mL conical flask. The flask was sealed and agitated at 25 °C for 30 minutes. The resulting solution was purified, and the Ibuprofen concentration was measured via UV spectrophotometry.

A stock solution was prepared by dissolving 206 mg of Ibuprofen in methanol in a 100 mL volumetric flask, yielding a concentration of 1×10^{-3} mol/mL. From this stock solution, standard solutions with known concentrations (0.1, 0.3, 0.4, 0.7, and 1 mM) were prepared. The absorbance of Ibuprofen in these solutions was measured using

UV/Vis spectroscopy, and the differences in absorbance (Δ absorbance) were recorded at wavelengths ranging from 273 to 278 nm.

5.7 The encapsulation of TDHTP and Zn-TDHTP within different OH PAMAM dendrimer generations.

PAMAM dendrimers Hydroxyl-terminated group were prepared at a concentration of 1x10^{-}4 M in methanol, separately in 10 mL. The same equivalent amounts of either THPP or ZnTHPP dissolved in methanol were added to form complex solutions with the dendrimers. The methanol solvent was then removed via a rotary evaporator. Subsequently, a 10 mL phosphate buffer solution pH 7.4 and 0.01 M was added to each of the complex solutions, followed by filtration to remove any insoluble matter. The final solutions were analysed using UV/Vi's spectroscopy, measuring the absorbance at 418 nm for the TDHPP complexes and 423 nm for the ZnTDHPP complexes.

6 The encapsulation of Fe-TDHPP within different OH PAMAM dendrimer generations.

PAMAM dendrimers Hydroxyl-terminated group were prepared at a concentration of 2x10^{-6} M in methanol, separately in 10 mL. The same equivalent amounts of either TDHPP or FeTDHPP dissolved in methanol were added to form complex solutions with the dendrimers. The methanol solvent was then removed via a rotary evaporator. Subsequently, a 10 mL phosphate buffer solution pH 7.4 and 0.01 M was added to each of the complex solutions, followed by filtration to remove any insoluble matter. The final solutions were analysed using UV/Vis spectroscopy, measuring the absorbance at 418 nm for the TDHPP complexes and 420 nm for the FeTDHPP complexes.

6.1 The procedure of iron stability and oxygen binding experiments.

porphyrin-polymer sample, a TRIS buffer pH 7.4 was used to get a concentration of $2x10^{-6}$ M. 10 mL The solution was transferred into a rubber-sealed, double-neck round-bottom flask. The solution underwent a cycle of degassing with nitrogen, repeated three times, to ensure an oxygen-free environment. Then, an equal molar amount of aqueous sodium dithionite $Na_2S_2O_4$ solution 0.1 mL, was added to the mixture. The mixture was stirred for 5-10 minutes, after which it was allowed to rest for phase separation to occur. A glass syringe, fitted with a 10 cm needle, was used to extract 1.5 mL of the solution, which was then transferred into a rubber-sealed, nitrogen-flushed quartz cuvette for analysis. UV-Vis spectroscopy was employed to confirm the successful reduction of iron within the sample, monitoring at a wavelength of 430 nm. Subsequently, a time scan at the fixed wavelength of 430 nm was initiated, with continuous stirring under atmospheric air, recording readings every 15 seconds for a total duration of one hour. A similar experimental setup was used for a control sample containing free TDHPP Fe^{III}. Both the test porphyrin-polymer and control samples were analysed following the outlined iron stability experimental procedure to assess their iron stability.

Chapter 6

Reference

1 H. M. Brothers Ii, L. T. Piehler and D. A. Tomalia, *J Chromatogr A*, 1998, 814, 233–246.

2 K. Bacha, C. Chemotti, J. P. Mbakidi, M. Deleu and S. Bouquillon, *Macromol*, 2023, 3, 343–370.

3 E. Abbasi, S. F. Aval, A. Akbarzadeh, M. Milani, H. T. Nasrabadi, S. W. Joo, Y. Hanifehpour, K. Nejati-Koshki and R. Pashaei-Asl, *Nanoscale Res Lett*, 2014, 9, 1–10.

4 C.-C. Peng, M. T. Burke, B. E. Carbia, C. Plummer and A. Chauhan, *J. Controlled Release*, 2012, 162, 152.

5 M. Venturi, S. Serroni, A. Juris, S. Campagna and V. Balzani, in *Dendrimers*, Springer Berlin Heidelberg, 1998, vol. 197, pp. 193–228.

6 A. W. Bosman, H. M. Janssen and E. W. Meijer, *Chem Rev*, 1999, 99, 1665–1688.

7 A. R. Menjoge, R. M. Kannan and D. A. Tomalia, *Drug Discov Today*, 15, 171–185.

8 J. G. Souza, K. Dias, S. A. M. Silva, L. C. D. de Rezende, E. M. Rocha, F. S. Emery and R. F. V Lopez, *J. Controlled Release*, 2015, 200, 115.

9 M. Zenze, A. Daniels and M. Singh, *Pharmaceutics*, DOI:10.3390/pharmaceutics15020398.

10 S. J. Amina and B. Guo, *Int J Nanomedicine*, 2020, 15, 9823–9857.

11 F. Carta, S. M. Osman, D. Vullo, A. Gullotto, J. Y. Winum, Z. AlOthman, E. Masini and C. T. Supuran, *J. Med. Chem.*, 2015, 58, 4039.

12 N. K. Jain and U. Gupta, *Expert Opin Drug Metab Toxicol*, 2008, 4, 1035–1052.

13 D. A. Tomalia, H. Baker, J. Dewald, M. Hall, G. Kallos, S. Martin, J. Roeck, J. Ryder and P. Smith, *Macromolecules*, 1986, 19, 2466–2468.

14 K. M. Kitchens, R. B. Kolhatkar, P. W. Swaan, N. D. Eddington and H. Ghandehari, *Pharm. Res.*, 2006, 23, 2818.

15 W. Wang, W. Xiong, J. Wan, X. Sun, H. Xu and X. Yang, *Nanotechnology*, 2009, 20, e105103.

16 J. M. J. Fréchet and D. A. Tomalia, in *Dendrimers and Other Dendritic Polymers*, John Wiley & Sons, Ltd, 2002, pp. 1–44.

17 C. C. Lee, J. A. MacKay, J. M. Frechet and F. C. Szoka, *Nat Biotechnol. 2005 Dec;23(12):1517-26.*

18 I. Bravo-Osuna, A. Woodward, P. Argueso, I. T. M. Martínez, R. Gómez, F. J. de la Mata, M. M. Navarro, M. Noiray, G. Ponchel and R. Herrero-Vanrell, *Invest. Ophthalmol. Visual Sci.*, 2012, 53, 1845.

19 T. M. Miller and T. X. Neenan, *Chemistry of Materials*, 1990, 2, 346–349.

20 S. J. Amina and B. Guo, *Int J Nanomedicine*, 2020, 15, 9823–9857.

21 H. Yang and W. J. Kao, *J. Biomater. Sci., Polym. Ed.*, 2006, 17, 3.

22 M. Santo and M. A. Fox, *J Phys Org Chem*, 1999, 12, 293–307.

23 H. Yang, P. Tyagi, R. S. Kadam, C. A. Holden and U. B. Kompella, *ACS Nano*, 2012, 6, 7595.

24 S. Hecht and J. M. J. Fréchet, *Angewandte Chemie International Edition*, 2001, 40, 74–91.

25 C. J. Hawker and J. M. J. Frechet, *Macromolecules*, 1990, 23, 4726–4729.

26 U. Boas, J. B. Christensen and P. M. H. Heegaard, *J Mater Chem*, 2006, 3785–3798.

27 H. Yang and C. T. Leffler, *J. Ocul. Pharmacol. Ther.*, 2013, 29, 166.

28 D. A. Tomalia, H. Baker, J. Dewald, M. Hall, G. Kallos, S. Martin, J. Roeck, J. Ryder and P. Smith, *Polym J*, 1985, 17, 117–132.

29 H. Viltres, Y. C. López, C. Leyva, N. K. Gupta, A. G. Naranjo, P. Acevedo–Peña, A. Sanchez-Diaz, J. Bae and K. S. Kim, *J Mol Liq*, 2021, 334, 116017.

30 M. Fana, J. Gallien, B. Srinageshwar, G. L. Dunbar and J. Rossignol, *Int J Nanomedicine*, 2020, 15, 2789–2808.

31 K. Inoue, *Prog Polym Sci*, 2000, 25, 453–571.

32 D. Y. Li, S. W. Li, Y. L. Xie, X. Hua, Y. T. Long, A. Wang and P. N. Liu, *Nat Commun*, 2019, 10, 1–9.

33 O. A. Matthews, A. N. Shipway and J. F. Stoddart, *Prog Polym Sci*, 1998, 23, 1–56.

34 *Development*.

35 F. Rauch, P. Endres, A. Friedrich, D. Sieh, M. Hähnel, I. Krummenacher, H. Braunschweig, M. Finze, L. Ji and T. B. Marder, *Chemistry - A European Journal*, 2020, 26, 12951–12963.

36 S. Mason, *Chemical Evolution: Origin of Elements, Molecules and Living Systems*, Clarendon Press , 1991.

37 D. A. Tomalia, A. M. Naylor and W. A. Goddard, *Angewandte Chemie International Edition in English*, 1990, 29, 138–175.

38 C. Hawker and J. M. J. Frechet, *J Chem Soc Chem Commun*, 1990, 1010–1013.

39 M. Pérez-Ferreiro, A. M. Abelairas, A. Criado, I. J. Gómez and J. Mosquera, *Polymers (Basel)*, DOI:10.3390/polym15224369.

40 C. J. Hawker and J. M. J. Frechet, *J Am Chem Soc*, 1990, 112, 7638–7647.

41 K. R. Tupally, G. R. Kokil, S. S. Thakur, P. Singh and H. S. Parekh, *Controlled Release Systems: Advances in Nanobottles and Active Nanoparticles*, 2015, 48, 259–285.

42 A. Santos, F. Veiga and A. Figueiras, *Dendrimers as pharmaceutical excipients: Synthesis, properties, toxicity and biomedical applications*, 2020, vol. 13.

43 D. A. Tomalia, *Advanced Materials*, 1994, 6, 529–539.

44 J. Singh, K. Jain, N. K. Mehra and N. K. Jain, *Artif Cells Nanomed Biotechnol*, 2016, 44, 1626–1634.

45 J. M. Frechet, *Science (1979)*, 1994, 263, 1710–1715.

46 S. Husain, Y. Abdul, S. Singh, A. Ahmad and M. Husain, *PLoS One*, 2014, 9, e110397.

47 K. Jain, P. Kesharwani, U. Gupta and N. K. Jain, *Int J Pharm*, 2010, 394, 122–142.

48 G. J. de A. A. Soler-Illia, L. Rozes, M. K. Boggiano, C. Sanchez, C.-O. Turrin, A.-M. Caminade and J.-P. Majoral, *Angewandte Chemie International Edition*, 2000, 39, 4249–4254.

49 A. Adronov and J. M. J. Frechet, *Chemical Communications*, 2000, 1701–1710.

50 G. R. Newkome, *Advances in Dendritic Macromolecules*, Jai Press-Elsevier, 1996, vol. 3.

51 Z. Lyu, L. Ding, A. Tintaru and L. Peng, *Acc Chem Res*, 2020, 53, 2936–2949.

52 W. H. De Jong and P. J. A. Borm, *Int J Nanomedicine*, 2008, 3, 133–149.

53 P. J. Farrington, C. J. Hawker, J. M. J. Frechet and M. E. Mackay, *Macromolecules. 1998 Jul 28;31(15):5043-50.*

54 K. Schwartz, M. Tutusaus Luque, M. Rusca and R. Ahlers, 2015, preprint.

55 W. J. Feast and N. M. Stainton, *J Mater Chem*, 1995, 5, 405–411.

56 D. K. Smith and F. Diederich, *Chemistry – A European Journal*, 1998, 4, 1353–1361.

57 J. Singh, K. Jain, N. K. Mehra and N. K. Jain, *Artif Cells Nanomed Biotechnol*, 2016, 44, 1626–1634.

58 Y. H. Kim and O. W. Webster, *J Am Chem Soc*, 1990, 112, 4592–4593.

59 W. F. S. Vaniz, 1976, preprint, https://books.google.com.vn/books?hl=vi&lr=&id=HSnRp1m3DI4C&oi=fnd&pg=PA1&dq=xiphasia+setifer+morphology&ots=FzV5sKOfPQ&sig=SjTHQyHdWbkVwc-F5tmqPBdRoac&redir_esc=y#v=onepage&q=xiphasia setifer&f=false.

60 J. Singh, K. Jain, N. K. Mehra and N. K. Jain, *Artif Cells Nanomed Biotechnol*, 2016, 44, 1626–1634.

61 M. Liu, K. Kono and J. M. J. FrÃ©chet, *Journal of Controlled Release*, 2000, 65, 121–131.

62 L. Zhou, D. H. Russell, M. Zhao and R. M. Crooks, *Macromolecules*, 2001, 34, 3567–3573.

63 F. Aulenta, W. Hayes and S. Rannard, *Eur Polym J*, 2003, 39, 1741–1771.

64 J. S. Fulmore, B. F. Geiger, K. A. Werner, L. L. Talbott and D. C. Jones, *Child Educ*, 2009, 85, 293–299.

65 A. E. Beezer, A. S. H. King, I. K. Martin, J. C. Mitchel, L. J. Twyman and C. F. Wain, *Tetrahedron*, 2003, 59, 3873–3880.

66 J. Peterson, V. Allikmaa, J. Subbi, T. Pehk and M. Lopp, *Eur Polym J*, 2003, 39, 33–42.

67 B. Devarakonda, N. Li and M. de Villiers, *AAPS PharmSciTech*, 2005, 6, E504–E512.

68 C. Yiyun, X. Tongwen and F. Rongqiang, *Eur J Med Chem*, 2005, 40, 1390–1393.

69 A. K. Mandal, *International Journal of Polymeric Materials and Polymeric Biomaterials*, 2021, 70, 287–297.

70 R. Mulller, C. Laschober, W. W. Szymanski and G. Allmaier, *Macromolecules*, 2007, 40, 5599–5605.

71 T. M. S. Chang, *Trends Biotechnol*, 1999, 17, 61–67.

72 H. Sakai, K. Sou, H. Horinouchi, K. Kobayashi and E. Tsuchida, *J Intern Med*, 2008, 263, 4–15.

73 S. Sarkar, *Indian journal of Critical are*, 2008, 12, 140–4.

74 R. Haldar, D. Gupta, S. Chitranshi, M. K. Singh and S. Sachan, *Cardiovasc Hematol Agents Med Chem*, 2019, 17, 11–16.

75 S. Moradi, A. Jahanian-Najafabadi and M. H. Roudkenar, *Clin Med Insights Blood Disord*, 2016, 9, 33–41.

76 G. Iraci and G. G. Toffolo, *Tumori Journal*, 1964, 50, 473–476.

77 L. Kuang, Y. Zhu, Y. Wu, K. Tian, X. Peng, M. Xue, X. Xiang, B. Lau, F. C. Tzang, L. Liu and T. Li, *Front Pharmacol*, 2021, 12, 1–14.

78 J. G. Riess, *Chem Rev*, 2001, 101, 2797–2920.

79 L. Kresie, *Proc (Bayl Univ Med Cent). 2001 Apr;14(2):158-61.*

80 T. Mahambrey, K. Pendry, A. Nee, S. Bonney and P. A. Nee, *Emergency Medicine Journal*, 2013, 30, 9–14.

81 H. W. Kim and A. G. Greenburg, *Artificial Cells, Blood Substitutes, and Biotechnology*, 2006, 34, 537–550.

82 S. I. Kim, S. Yoon, T. M. Kim, J. Y. Cho, H. H. Chung and Y. S. Song, *Gynecol Oncol*, 2021, 162, 72–79.

83 C. Glover and D. L. Twyman, 2013.

84 M. F. Perutz, *Trends Biochem Sci*, 1989, 14, 42–44.

85 P. Kramer Nascimento Jr Vaid, S.U., G C, *Academic Press: Oxford*, 2006, preprint.

86 A. Tinmouth, D. Fergusson, I. C. Yee, P. C. Hébert, A. Investigators and G. the Canadian Critical Care Trials, *Transfusion (Paris)*, 2006, 46, 2014–2027.

87 G. C. Kramer Nascimento Jr, P., Vaid, S.U., in *Blood Substitutes*, ed. R. M. Winslow, Academic Press: Oxford, 1st edn., 2006, pp. 139–151.

88 Blood substitutes and oxygen therapeutics: an overview and current status - PubMed, https://pubmed.ncbi.nlm.nih.gov/12237737/, (accessed 20 December 2024).

89 T. M. Chang, *Trends Biotechnol. 2006 Aug;24(8):372-7. Epub 2006 Jul 11.*

90 L. Williamson, M. Runge, C. Patterson and J.-P. Allain, in *Principles of Molecular Medicine*, Humana Press, 2006, pp. 883–890.

91 J. P. Collman and L. Fu, *Acc Chem Res*, 1999, 32, 455–463.

92 J. G. Riess and J. G. Riess, *Chem Rev*, 2001, 101, 2797–2919.

93 WHO, *Compendium of innovative health technologies*, 2012, 3–76.

94 T. Mahambrey, K. Pendry, A. Nee, S. Bonney and P. A. Nee, *Emergency Medicine Journal*, 2013, 30, 9–14.

95 D. N. Garud S, Derle D, 2013, 4, 180–189.

96 S. Moradi, A. Jahanian-Najafabadi and M. H. Roudkenar, *Clin Med Insights Blood Disord*, 2016, 9, 33–41.

97 F. T. Barbosa, M. J. Juca, A. A. Castro, J. L. Duarte and L. T. Barbosa, *Sao Paulo Med J. 2009 May;127(2):97-100.*

98 W.-D. Jang, K. M. Kamruzzaman Selim, C.-H. Lee and I.-K. Kang, *Prog Polym Sci*, 2009, 34, 1–23.

99 S. Sarkar, .

100 S. J. Urbaniak, *Br Med J*, 1991, 303, 1348–1350.

101 K. Pavenski, E. Saidenberg, M. Lavoie, M. Tokessy and D. R. Branch, DOI:10.1016/j.tmrv.2011.07.003.

102 S. J. Urbaniak, *Br Med J*, 1991, 303, 1348–1350.

103 E. R. Huehns and E. M. Shooter, *J Med Genet*, 1965, 2, 48–90.

104 E. M. Sánchez-Fernández, M. I. García-Moreno, A. I. Arroba, M. Aguilar-Diosdado, J. M. Padrón, R. García-Hernández, F. Gamarro, S. Fustero, J. E. Sánchez-Aparicio, L. Masgrau, J. M. García Fernández and C. Ortiz Mellet, *Eur J Med Chem*, DOI:10.1016/j.ejmech.2019.111604.

105 E. Bissé, A. Hovasse, S. Preisler-Adams, T. Epting, O. Wagner, G. Kögel, A. Van Dorsselaer and C. Schaeffer-Reiss, *J Chromatogr B Analyt Technol Biomed Life Sci*, 2011, 879, 2952–2956.

106 D. J. Weatherall, *J Clin Pathol*, 1974, 1–11.

107 T. Mitsuno, H. Ohyanagi and R. Naito, *Ann Surg*, 1982, 195, 60–69.

108 M. E. Pembrey, P. McWade and D. J. Weatherall, *J Clin Pathol*, 1972, 25, 738–740.

109 D. J. Weatherall, *J Clin Pathol*, 1974, 1–11.

110 M. F. Perutz, M. G. Rossmann, A. F. Cullis, H. Muirhead, G. Will and A. C. T. North, *Nature*, 1960, 185, 416–422.

111 M. Paoli, R. Liddington, J. Tame, A. Wilkinson and G. Dodson, *J Mol Biol*, 1996, 256, 775–792.

112 D. H. Glogar, R. A. Kloner, J. Muller, L. W. V. DeBoer, E. Braunwald and L. C. Clark, *Science (1979)*, 1981, 212, 1439–1441.

113 R. J. Cusimano, K. A. Ashe, I. D. Chin, P. Chi, J. G. Abel, S. V. Lichtenstein and T. A. Salerno, *Ann Thorac Surg*, 1991, 52, 934–938.

114 T. Lambrechts, I. Papantoniou, B. Rice, J. Schrooten, F. P. Luyten and J. M. Aerts, *Cytotherapy*, 2016, 18, 1219–1233.

115 H. G. Breuninger, S. D. Rubenstein, M. R. Wolfson and T. H. Shaffer, *J Pediatr Surg*, 1993, 28, 144–150.

116 J. Baldwin and C. Chothia, *J Mol Biol*, 1979, 129, 175–220.

117 W. Eaton, E. Henry, J. Hofrichter and A. Mozzarelli, *Rendiconti Lincei*, 2006, 17, 147–162.

118 A. Q. Al-Neami, N. S. Shalal and K. H. Rasheed, *IOP Conf Ser Mater Sci Eng*, DOI:10.1088/1757-899X/870/1/012019.

119 T. G. Traylor, N. Koga and L. A. Deardurff, *J Am Chem Soc*, 1985, 107, 6504–6510.

120 T. M. S. Chang, *Artificial Cells, Blood Substitutes, and Biotechnology*, 2012, 40, 197–199.

121 A. I. Alayash, *Nat Biotech*, 1999, 17, 545–549.

122 A. R. Fanelli, E. Antonini and A. Caputo, *Biochim Biophys Acta. 1958 Dec;30(3):608-15.*

123 S. Moradi, A. Jahanian-Najafabadi and M. H. Roudkenar, *Clin Med Insights Blood Disord*, 2016, 9, 33–41.

124 L. Zhang, E. M. E. Andersen, A. Khajo, R. S. Magliozzo and R. L. Koder, *Biochemistry*, 52, 447–455.

125 J. P. Collman, J. I. Brauman and K. S. Suslick, *J Am Chem Soc*, 1975, 97, 7185–7186.

126 K. Shikama, *Coord Chem Rev*, 1988, 83, 73–91.

127 J. P. Collman, R. R. Gagne, C. A. Reed, W. T. Robinson and G. A. Rodley, *Proceedings of the National Academy of Sciences*, 1974, 71, 1326–1329.

128 R. J. Bowman, *Hum Pathol*, 1983, 14, 218–220.

129 C. Rovira and M. Parrinello, *Biophys J*, 2000, 78, 93–100.

130 C. I. Castro and J. C. Briceno, *Artif Organs*, 2010, 34, 622–634.

131 K. Pavenski, E. Saidenberg, M. Lavoie, M. Tokessy and D. R. Branch, DOI:10.1016/j.tmrv.2011.07.003.

132 T. M. S. Chang, *Artificial Cells, Blood Substitutes, and Biotechnology*, 2012, 40, 197–199.

133 K. Huang, W. Yang and Q. Chen, *Int J Mech Sci*, 2015, 103, 127–140.

134 I. Insua and J. Montenegro, *Chem*, 2020, 6, 1652–1682.

135 W. Rudowski, *World J Surg*, 1987, 11, 86–93.

136 J. G. Riess, *Chem Rev*, 2001, 101, 2797–2920.

137 Red blood cell substitutes and artificial blood - ScienceDirect, https://www.sciencedirect.com/science/article/abs/pii/S0046817783800203?via%3Dihub, (accessed 20 December 2024).

138 E. Rideau, R. Dimova, P. Schwille, F. R. Wurm and K. Landfester, *Chem Soc Rev*, 2018, 47, 8572–8610.

139 T. M. S. Chang, *Vox Sang*, 1998, 74, 233–241.

140 E. M. Sánchez-Fernández, M. I. García-Moreno, A. I. Arroba, M. Aguilar-Diosdado, J. M. Padrón, R. García-Hernández, F. Gamarro, S. Fustero, J. E. Sánchez-Aparicio, L. Masgrau, J. M. García Fernández and C. Ortiz Mellet, *Eur J Med Chem*, DOI:10.1016/j.ejmech.2019.111604.

141 H. G. Breuninger, S. D. Rubenstein, M. R. Wolfson and T. H. Shaffer, *J Pediatr Surg*, 1993, 28, 144–150.

142 Y. Jia and A. I. Alayash, *Biochimica et Biophysica Acta (BBA) - Proteins and Proteomics*, 2009, 1794, 1234–1242.

143 J. J. L. L. Brien, .

144 T. Lambrechts, I. Papantoniou, B. Rice, J. Schrooten, F. P. Luyten and J. M. Aerts, *Cytotherapy*, 2016, 18, 1219–1233.

145 C. A. Fraker, A. J. Mendez and C. L. Stabler, *Journal of Physical Chemistry B*, 2011, 115, 10547–10552.

146 L. Zhang, Q. Zhang, Y. Zheng, Z. He, P. Guan, X. He, L. Hui and Y. Dai, *Ind Crops Prod*, 2018, 112, 532–540.

147 C. M. Paleos, D. Tsiourvas and Z. Sideratou, *Mol Pharm*, 2007, 4, 169–188.

148 R. J. Bowman, *Hum Pathol*, 1983, 14, 218–220.

149 L. Latos-Grazynski, R. J. Cheng, G. N. La Mar and A. L. Balch, *J Am Chem Soc*, 1982, 104, 5992–6000.

150 W. J. Wallace, R. A. Houtchens, J. C. Maxwell and W. S. Caughey, *J Biol Chem. 1982 May 10;257(9):4966-77.*

151 J. Almog, J. E. Baldwin and J. Huff, *J Am Chem Soc*, 1975, 97, 227–228.

152 J. Baldwin and P. Perlmutter, in *Host Guest Complex Chemistry III*, Springer Berlin Heidelberg, 1984, vol. 121, pp. 181–220.

153 A. L. Balch, Y. W. Chan, R. J. Cheng, G. N. La Mar, L. Latos-Grazynski and M. W. Renner, *J Am Chem Soc*, 1984, 106, 7779–7785.

154 R. J. Cusimano, K. A. Ashe, I. D. Chin, P. Chi, J. G. Abel, S. V. Lichtenstein and T. A. Salerno, *Ann Thorac Surg*, 1991, 52, 934–938.

155 K. S. Suslick, M. M. Fox and T. R. Reinert, *J Am Chem Soc*, 1984, 106, 4522–4525.

156 J. E. Baldwin, J. H. Cameron, M. J. Crossley, I. J. Dagley, S. R. Hall and T. Klose, *Journal of the Chemical Society, Dalton Transactions*, 1984, 1739–1746.

157 B. Shaanan, *J Mol Biol. 1983 Nov 25;171(1):31-59.*

158 J. Almog, J. E. Baldwin and J. Huff, *J Am Chem Soc*, 1975, 97, 227–228.

159 J. E. Baldwin and J. Huff, *J Am Chem Soc*, 1973, 95, 5757–5759.

160 V. P. Torchilin, T. S. Levchenko, K. R. Whiteman, A. A. Yaroslavov, A. M. Tsatsakis, A. K. Rizos, E. V Michailova and M. I. Shtilman, *Biomaterials*, 2001, 22, 3035–3044.

161 D. Lombardo, M. A. Kiselev, S. Magazù and P. Calandra, *Advances in Condensed Matter Physics*, 2015, 2015, 151683.

162 V. K. Mourya, N. Inamdar, R. B. Nawale and S. S. Kulthe, *Indian Journal of Pharmaceutical Education and Research*, 2011, 45, 128–138.

163 S. Garnier and A. Laschewsky, *Langmuir*, 2006, 22, 4044–4053.

164 S. Ezrahi, E. Tuval and A. Aserin, *Adv Colloid Interface Sci*, 2006, 128–130, 77–102.

165 R. Adams and T. E. Bockstahler, *J Am Chem Soc*, 1952, 74, 5346–5348.

166 R. Schubert, *Methods Enzymol*, 2003, 367, 46–70.

167 D. R. Spahn, *Crit Care*, 1999, 3, R93–R97.

168 G. Rizis, T. G. M. Van De Ven and A. Eisenberg, *ACS Nano*, 2015, 9, 3627–3640.

169 V. P. Torchilin, *Journal of Controlled Release*, 2001, 73, 137–172.

170 A. Giraudeau, H. J. Callot and M. Gross, *Inorg Chem*, 1979, 18, 201–206.

171 Y. L. and P. H. Delphine Schaming, Alain Giraudeau, Laurent Ruhlmann, Clémence Allain, Jian Hao, Yun Xia, Rana Farha, Michel Goldmann, in *Electropolymerization Book*, ed. Ewa-Schab-Balcerzak, InTech, 2011, pp. 52–56.

172 A. Z. dan D. Yusri, *Jurnal Ilmu Pendidikan*, 2020, 7, 809–820.

173 V. K. Panthi, K. E. Fairfull-Smith and N. Islam, *Int J Pharm*, DOI:10.1016/j.ijpharm.2024.124046.

174 D.-H. Chin, J. Del Gaudio, G. N. La Mar and A. L. Balch, *J Am Chem Soc*, 1977, 99, 5486–5488.

175 Z. Makhlouf, A. A. Ali and M. H. Al-Sayah, *Antibiotics*, DOI:10.3390/ANTIBIOTICS12050875.

176 H. Ibaraki, T. Kanazawa, W. Y. Chien, H. Nakaminami, M. Aoki, K. Ozawa, H. Kaneko, Y. Takashima, N. Noguchi and Y. Seta, *J Drug Deliv Sci Technol*, DOI:10.1016/j.jddst.2020.101754.

177 U. Boas, J. B. Christensen and P. M. H. Heegaard, *J Mater Chem*, 2006, 3785–3798.

178 J. Puig-Rigall, C. Fernández-Rubio, J. González-Benito, J. E. Houston, A. Radulescu, P. Nguewa and G. González-Gaitano, *Int J Pharm*, 2020, 578, 119057.

179 K. Nakashima and P. Bahadur, *Adv Colloid Interface Sci*, 2006, 123–126, 75–96.

180 D. G. Mullen, A. Desai, M. A. van Dongen, M. Barash, J. R. Baker Jr. and M. M. Banaszak Holl, *Macromolecules*, 2012, 45, 5316–5320.

181 J. Doskocz, P. Dałek, A. Foryś, B. Trzebicka, M. Przybyło, L. Mesarec, A. Iglič and M. Langner, *Biochim Biophys Acta Biomembr*, DOI:10.1016/j.bbamem.2020.183361.

182 P. Rothemund, *J Am Chem Soc*, 1936, 58, 625–627.

183 R. Schneider, F. Schmitt, C. Frochot, Y. Fort, N. Lourette, F. Guillemin, J. F. Müller and M. Barberi-Heyob, *Bioorg Med Chem*, 2005, 13, 2799–2808.

184 Z. C. Sun, Y. Bin She, Y. Zhou, X. F. Song and K. Li, *Molecules*, 2011, 16, 2960–2970.

185 D. Mauzerall, *J Am Chem Soc*, 1960, 82, 2601–2605.

186 L. J. Twyman and Y. Ge, *Chemical Communications*, 2006, 1658–1660.

187 R. Krishna, M. S. Webb, G. St. Onge and L. D. Mayer, *Journal of Pharmacology and Experimental Therapeutics*, 2001, 298, 1206 LP – 1212.

188 B. Singh, R. Kumar and N. Ahuja, *Critical Reviews™ in Therapeutic Drug Carrier Systems*, 2005, 22, 27–105.

189 M. T. Manzari, Y. Shamay, H. Kiguchi, N. Rosen, M. Scaltriti and D. A. Heller, *Nature Reviews Materials 2021 6:4*, 2021, 6, 351–370.

190 C. Li, J. Wang, Y. Wang, H. Gao, G. Wei, Y. Huang, H. Yu, Y. Gan, Y. Wang, L. Mei, H. Chen, H. Hu, Z. Zhang and Y. Jin, *Acta Pharm Sin B*, 2019, 9, 1145–1162.

191 S. Lv, Y. Wu, K. Cai, H. He, Y. Li, M. Lan, X. Chen, J. Cheng and L. Yin, *J Am Chem Soc*, 2018, 140, 1235–1238.

192 R. Langer, *Science (1979)*, 1990, 249, 1527–1533.

193 S. Adepu, S. Ramakrishna, R. Costa-Pinto and A. L. Oliveira, *Molecules 2021, Vol. 26, Page 5905*, 2021, 26, 5905.

194 M. R. Prausnitz, S. Mitragotri and R. Langer, *Nat Rev Drug Discov*, 2004, 3, 115–124.

195 K. Obata, K. Sugano, R. Saitoh, A. Higashida, Y. Nabuchi, M. Machida and Y. Aso, *Int J Pharm*, 2005, 293, 183–192.

196 C. A. Holden, P. Tyagi, A. Thakur, R. Kadam, G. Jadhav, U. B. Kompella and H. Yang, *Nanomedicine (N. Y., NY, U. S.)*, 2012, 8, 776.

197 G. Di Colo and Y. Zambito, *Eur. J. Pharm. Biopharm.*, 2002, 54, 193.

198 M. R. Prausnitz and R. Langer, *Nat Biotechnol*, 2008, 26, 1261–1268.

199 Reyad Elderbag, .

200 A. Aurelia Chis, C. Dobrea, C. Morgovan, A. M. Arseniu, L. L. Rus, A. Butuca, A. M. Juncan, M. Totan, A. L. Vonica-Tincu, G. Cormos, A. C. Muntean, M. L. Muresan, F. G. Gligor and A. Frum, *Molecules 2020, Vol. 25, Page 3982*, 2020, 25, 3982.

201 Z. Lyu, L. Ding, A. Y. T. Huang, C. L. Kao and L. Peng, *Mater Today Chem*, 2019, 13, 34–48.

202 D. Lombardo and M. A. Kiselev, *Pharmaceutics*, DOI:10.3390/PHARMACEUTICS14030543.

203 K. Madaan, S. Kumar, N. Poonia, V. Lather and D. Pandita, *J Pharm Bioallied Sci*, 2014, 6, 139–150.

204 M. Danaei, M. Dehghankhold, S. Ataei, F. Hasanzadeh Davarani, R. Javanmard, A. Dokhani, S. Khorasani and M. R. Mozafari, *Pharmaceutics*, DOI:10.3390/PHARMACEUTICS10020057.

205 S. Liu, L. Jones and F. X. Gu, *Macromol. Biosci.*, 2012, 12, 608.

206 W. Yao, K. Sun, H. Mu, N. Liang, Y. Liu, C. Yao, R. Liang and A. Wang, *Drug Dev. Ind. Pharm.*, 2010, 36, 1027.

207 D. Nicolosi, S. Cupri, C. Genovese, G. Tempera, R. Mattina and R. Pignatello, *Int J Antimicrob Agents*, 2015, 45, 622–626.

208 J. S. Boateng and A. M. Popescu, *Colloids Surf., B*, 2016, 145, 353.

209 J. Singh, K. Jain, N. K. Mehra and N. K. Jain, *Artif Cells Nanomed Biotechnol*, 2016, 44, 1626–1634.

210 E. Malmström and A. Hult, *Journal of Macromolecular Science, Part C*, 1997, 37, 555–579.

211 M. G. I. I. I. Lancina, S. Singh, U. B. Kompella, S. Husain and H. Yang, *ACS Biomater Sci Eng*, 2017, 3, 1861–1868.

212 B. Malaekeh-Nikouei, B. S. Fazly Bazzaz, E. Mirhadi, A. S. Tajani and B. Khameneh, *J Drug Deliv Sci Technol*, DOI:10.1016/j.jddst.2020.101880.

213 S. L. Shenoy, W. D. Bates, H. L. Frisch and G. E. Wnek, *Polymer (Guildf)*, 2005, 46, 3372.

214 J. Wang, H. He, R. C. Cooper, Q. Gui and H. Yang, *Mol Pharm*, 2019, 16, 1874–1880.

215 S. M. D'Addio, W. Saad, S. M. Ansell, J. J. Squiers, D. H. Adamson, M. Herrera-Alonso, A. R. Wohl, T. R. Hoye, C. W. MacOsko, L. D. Mayer, C. Vauthier and R. K. Prud'homme, *Journal of Controlled Release*, 2012, 162, 208–217.

216 R. Duncan, *Journal of Controlled Release*, 2014, 190, 371–380.

217 J. M. J. Fréchet, C. J. Hawker, I. Gitsov and J. W. Leon, *Journal of Macromolecular Science, Part A*, 1996, 33, 1399–1425.

218 Polymer-drug conjugates: Design principles, emerging synthetic strategies and clinical overview - ScienceDirect, https://www.sciencedirect.com/science/article/abs/pii/S0378517322004185, (accessed 20 December 2024).

219 A. Aurelia Chis, C. Dobrea, C. Morgovan, A. M. Arseniu, L. L. Rus, A. Butuca, A. M. Juncan, M. Totan, A. L. Vonica-Tincu, G. Cormos, A. C. Muntean, M. L. Muresan, F. G. Gligor and A. Frum, *Molecules*, DOI:10.3390/molecules25173982.

220 G. Zu, Y. Kuang, J. Dong, Y. Cao, K. Wang, M. Liu, L. Luo and R. Pei, *J Mater Chem B*, 2017, 5, 5001–5008.

221 A. Javia, J. Vanza, D. Bardoliwala, S. Ghosh, L. A. Misra, M. Patel and H. Thakkar, *Int J Pharm*, 2022, 623, 121863.

222 Y. Tian, M. V. Kuzimenkova, J. Halle, M. Wojdyr, A. Diaz De Zerio Mendaza, P. O. Larsson, C. Müller and I. G. Scheblykin, *Journal of Physical Chemistry Letters*, 2015, 6, 923–927.

223 C. M. Paleos, D. Tsiourvas, Z. Sideratou and L.-A. Tziveleka, *Expert Opin Drug Deliv*, 2010, 7, 1387–1398.

224 B. A. Wolf, *Ind Eng Chem Res*, 2015, 54, 4672–4680.